55/1/2023
ISSN 1338-3523
ISSN 0369-2086

Mineralia Slovaca

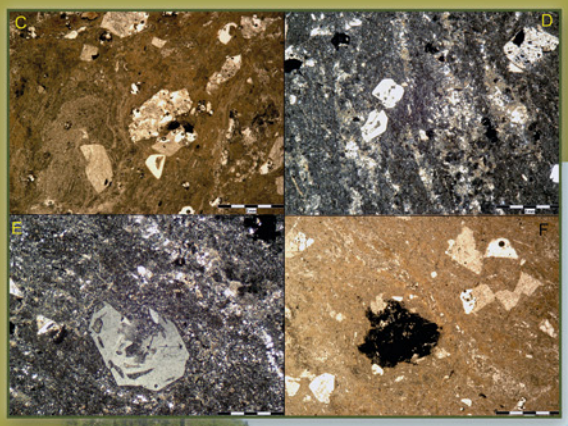

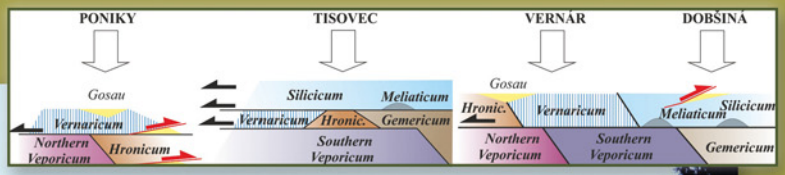

Štátny geologický ústav Dionýza Štúra Bratislava

Mineralia Slovaca

Časopis pre regionálnu a environmentálnu geológiu
a aktivity Slovenskej geologickej spoločnosti a geologických asociácií

Mineralia Slovaca (Web ISSN 1338-3523, ISSN 0369-2086), EV 3534/09, vychádza dvakrát ročne. Vydavateľ a tlač: Štátny geologický ústav Dionýza Štúra, Mlynská dolina 1, 817 04 Bratislava, IČO 31 753 604. Dátum vydania čísla 55/1/2023: júl 2023. Predplatné v roku 2023 vrátane DPH, poštovného a balného pre jednotlivcov 22,00 €, pre členov SGS a geologických asociácií 20,90 €, pre organizácie v SR 31,90 €, pre organizácie v ČR 55,00 €. Cena jednotlivého čísla pri osobnom nákupe v predajniach ŠGÚDŠ v Bratislave a v Košiciach je 6,05 € vrátane DPH. Časopis možno objednať v redakcii a v knižnici regionálneho centra v Košiciach. Adresa redakcie: Štátny geologický ústav D. Štúra – RC Košice (Mineralia Slovaca), Jesenského 8, 040 01 Košice. Telefón: 055/625 00 43; fax: 055/625 00 44, e-mail: mineralia.slovaca@geology.sk, e-mail knižnica: secretary.ke@geology.sk

Mineralia Slovaca (Web ISSN 1338-3523, ISSN 0369-2086) is published twice a year by the State Geological Institute of Dionýz Štúr Bratislava, Slovak Republic. The date of issuing of the number 55/1/2023: July 2023.
Subscription for the whole 2023 calendar year (two numbers of the journal): 66.00 € (Europe), 77.00 € (besides Europe), including VAT, postage and packing cost. Claims for nonreceipt of any issue will be filled gratis.
Order of the Editorial Office: Štátny geologický ústav D. Štúra – RC Košice (Library), Jesenského 8, SK-040 01 Košice, Slovak Republic. Phone: +421/55/625 00 43; fax: +421/55/625 00 44, e-mail: mineralia.slovaca@geology.sk, library: secretary.ke@geology.sk

PÔVODNÉ ČLÁNKY – ORIGINAL PAPERS

COVER: View on the Veľká Stožka Massif from the Teplá dolina valley (Muráň nappe, Western Carpathians; central Slovakia). Geological map of the region is shown in segment located in left down side and detail map in the segment right down. Microscopic documentation of rhyolite from the Veľká Stožka Massif is shown in upper left side and tectonic reconstruction of the Vernaricum nappe, bearing the Veľká Stožka Massif in the frame of Western Carpathian north-vergent nappes, is located upper right. The topic of Vernaricum is presented in article by Hók and Olšavský on p. 3–12 and topic of Permian rhyolite volcanism in the Veľká Stožka Massif in article by Demko et al. on p. 13–26 in this issue. Author of background photo: M. Olšavský

OBÁLKA: Pohľad na masív Veľkej Stožky od Teplej doliny (Muránska planina) – geologickú mapu regiónu zobrazuje segment vľavo dole a detailnú mapu segment vpravo dole. Mikroskopickú dokumentáciu ryolitu z masívu Veľkej Stožky znázorňuje obrázok vľavo hore a tektonickú rekonštrukciu pozície vernárika s masívom Veľkej Stožky v zostave západokarpatských severovergentných príkrovov znázorňuje obrázok vpravo hore. Problematikou vernárika sa zaoberá článok Hóka a Olšavského na str. 3 – 12 a problematikou permského ryolitového vulkanizmu v masíve Veľkej Stožky článok Demka et al. na str. 13 – 26 v tomto čísle časopisu. Autor fotografie v pozadí: M. Olšavský

Mineralia Slovaca, Web ISSN 1338-3523, ISSN 0369-2086, https://doi.org/10.56623/ms.2023.55.1.1
55, 1 (2023), 3 – 12, © Authors 2023. CC BY 4.0

Vernaricum – regional distribution, lithostratigraphy, tectonics and paleogeography

JOZEF HÓK[1] and MÁRIO OLŠAVSKÝ[2]

[1]Department of Geology and Palaeontology, Faculty of Natural Sciences, Comenius University in Bratislava, Mlynská dolina, Ilkovičova 6, 842 15 Bratislava, Slovak Republic; jozef.hok@uniba.sk
[2]State Geological Institute of Dionýz Štúr, Zelená 5, 974 04 Banská Bystrica, Slovak Republic; mario.olsavsky@geology.sk

Abstract: The Vernaricum is the highest partial unit belonging to the Hronic nappe system of the Internal Western Carpathians. The stratigraphic range of the Vernaricum sediments is from the Lower Triassic to the Lower Jurassic. The Permian rhyolites and volcaniclastics are tectonically incorporated into the Lower Triassic sediments. The Vernaricum overlies tectonic units of the Northern Veporicum, Fatricum, lower partial nappes of Hronicum and Southern Veporicum. The Gemeric, Meliatic and Silicic rock complexes are located in the tectonic overburden. The paleogeographic position of the Vernaricum is interpreted between the Veporic and Gemeric zones.

Key words: Internal Western Carpathians, Vernaricum, Hronicum, Veporicum, Gemericum

Graphical abstract

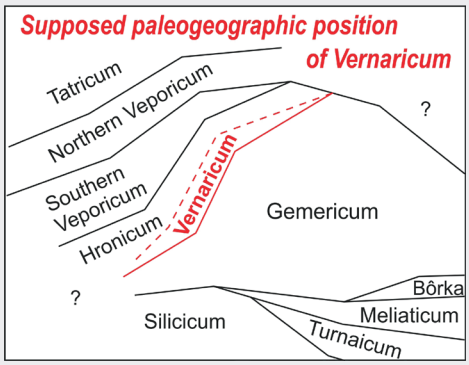

Highlights

- New described lithotectonic unit of Internal Western Carpathians – the Vernaricum – as the highest positioned partial nappe of the Hronic nappe system includes rock sequences of former Vernár nappe, Drienok nappe and lower Muráň nappe with characteristic occurrences of rhyolites and their volcaniclastic material from the pre-Cenozoic basement of the Central Slovakian Neogene volcanites;
- Paleogeographic position of the Vernaricum is assumed between the Hronicum and Gemericum tectonic units.

Introduction

The Vernaricum as a new lithotectonic unit of Internal Western Carpathians was mentioned in work by Hók et al. (2004), but its main attributes including its lithostratigraphy were not defined.

This unit is named after the Vernár village and Vernár nappe (Maheľ, 1986). In the past, the Vernár nappe was interpreted as a part of the Hronicum, as well as Gemericum *ergo* Silicicum. The evolution of opinions on tectonic affiliation of the Vernár nappe and the most complete lithostratigraphic description was consistently presented by Havrila (in Mello et al., 2000b) from the Slovenský raj (Slovak Paradise) area, where the Vernár nappe was supposed to represent a part of Silicicum s.l. Havrila (1997) identifies the Vernár nappe with the Lower Muráň nappe and Drienok nappe, being distinguished by Bystrický (1964) as "*the Drienok series*" and compared with "*facial development of Gemerides in the Muráň plain area*". Most recently, the Drienok nappe, the lower Muráň nappe and the Vernár nappe were considered to be partial nappes of extended Hronicum nappe (Havrila, M. & Havrila, J., 2022; Fig. 2), while the Drienok nappe was understood as a partial nappe of the extensive Považie nappe. The Vernár nappe together with Lower Muráň nappe are presented as partial nappes of Vernaricum in the frame of Hronic nappe system.

Rock complexes, lithostratigraphically corresponding to Middle Triassic dolomites, Szin and Bódvaszilas beds, containing anhydrites and rhyolitic volcaniclastics, resp. "volcaniclastic material of acid origin", were described as a part of pre-Cenozoic basement bedrock in boreholes KOV-33, 39, 40, 41, 42, VŠ-5 and GK-10 (Fig. 1), located in the area of Central Slovakian Neogene volcanites (Vozár in Burian et al., 1968; Vozár, 1969, 1973; Biela, 1978). This rock complex was considered by Vozár (1973) "*to be characteristic of Gemerides as it was described in the Drienok Unit, on the Muránska planina Plain and in the southern part of the Spiš-Gemer Ore Mts*.", i.e. as a part of the Silicic Unit s.l.

Based on above assumptions, it can be concluded that the Vernár nappe, the lower Muráň nappe, the Drienok nappe and the rock complexes in the basement of Central Slovak volcanites represent a part of the same allochthonous tectonic unit, for which we propose the name "Vernaricum". In the following text we define its lithostratigraphy, tectonic location and discuss the paleogeographic position.

Telgárt was assigned to the Lower Triassic of the Vernár nappe (Havrila in Mello et al., 2000b). However, this volcano-sedimentary rock sequence was petrographically, by age and tectonically defined as Permian rhyolite complex (263 ± 3.5 Ma), composed of a cover of rhyolite ignimbrites and central rhyolite extrusions tectonically separated from its surroundings (Demko & Hraško, 2013; Fig. 1), including the Lower Triassic sediments (Bód-

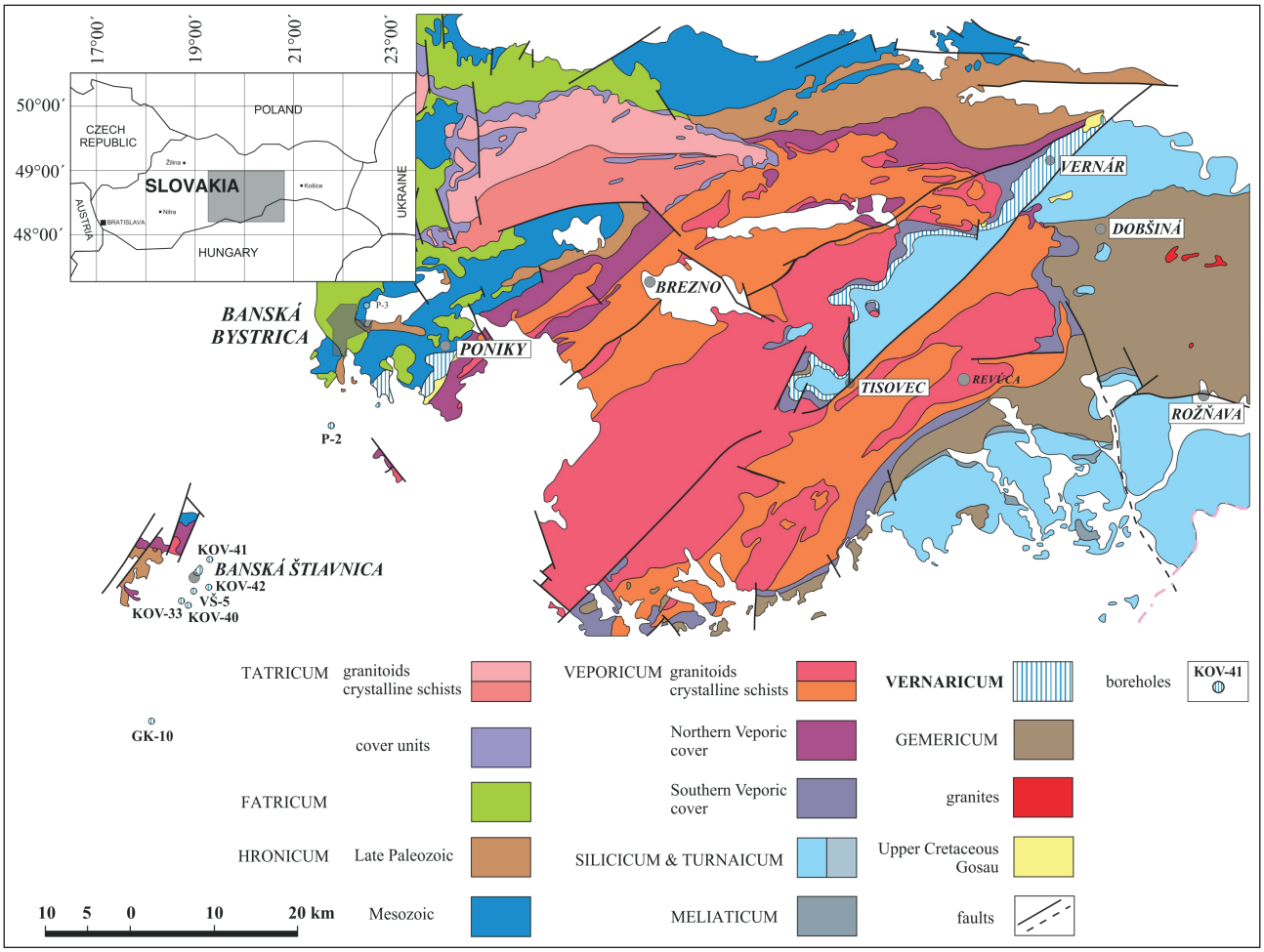

Fig. 1. Simplified tectonic map with occurrences of Vernaricum. Geological map is compiled after maps by Fusán et al. (1987), Biely et al. (1995), Mello et al. (2000a), Polák et al. (2003a).

Lithostratigraphy of Vernaricum

The most extensive and until the most complete sequence of Vernaricum was described from the area of occurrence of the Vernár nappe in the Slovenský raj area (Havrila in Mello et al., 2000b). The rhyolites and rhyolitic volcaniclastics associated with Lower and Middle Triassic sediments were considered as the stratigraphically lowest lithological / lithostratigraphic member. The occurrence of rhyolites and rhyolitic volcaniclastics in the wider vicinity of the Gregová elevation (1168 m a.s.l.) northeast of

vaszilas Beds) and Middle Triassic carbonates (Gutenstein dolomites and limestones). The Permian age of the mentioned rhyolite complex was assumed already by Plašienka (1981). Ondrejka et al. (2018) specified the petrographic classification (A-type rhyolites) and age (263.3 ± 1.9 to 269.5 ± 1.8 Ma) at the localities of occurrence of the so-called lower Murán nappe (*sensu* Havrila, 1997). Dating of monazites from rhyolite at Veľká Stožka (Muránska planina plain) was carried out by R. Demko and reports an age of 281 ± 4.5 Ma (R. Demko, personal communication – November 18, 2019). Rhyolites from the Drienok

area (606 m a.s.l.) west of Poniky locality have the same Permian age (271.0 ± 1.5 and 267.5 ± 1.6 Ma) and are interpreted as tectonically separated bodies in the Drienok nappe (Ondrejka et al., 2022). Despite tectonic position of the rhyolite volcanics and volcaniclastics in relation to the Triassic sediments, these should be considered as an integral part of the Vernaricum (Drienok, Vernár and lower Muráň nappes), because they form a typical lithotectonic horizon and probably represented the substrate on which the Lower Triassic clastics have sedimented.

On the basis of the lithofacies and lithostratigraphic analysis of the Lower Triassic assemblages of the Hronic tectonic unit on the southern slopes of the Low Tatra Mts. and Vernaricum (Drienok, Lower Muráň and Vernár nappes) it is possible to correlate the Lower Triassic sediments in these units with each other (Olšavský, 2004, 2019; Olšavský et al., 2010). For the Lower Triassic lithostratigraphic members of the Vernaricum, it was suggested to use the names Benkov and Šuňava formations, instead of Bódvaszilas and Szin members (Ondrejka et al., 2022). In addition to the mentioned formations, the Hronsek Member was defined (Olšavský et al., 2010) as a separate unit of the uppermost part of the Benkovo Formation and at the same time a correlation horizon between the Franková nappe (Hronicum) and the Drienok nappe (Silicicum s.l.). The Benkovo and Šuňava formations, including the Hronsek Beds, Member represent a unique lithostratigraphic horizon, pointing to the proximality of Vernaricum and Hronicum sedimentary areas in the Lower Triassic period (Figs. 2 and 3).

The Middle Triassic formations of the Drienok nappe in the Poniky area are regularly separated from the Lower Triassic formations by tectonic breccias with a thickness of 30–50 m (Slavkay et al., 1968). As a part of the Middle Triassic assemblages, the Ráztoka Limestones and the Jasenie Limestones (Havrila et al., 2016; Havrila, M. & Havrila, J., 2022), described in the Hronic tectonic unit (Kochanová & Michalík, 1986), are also present in the Drienok nappe. Other Middle Triassic lithostratigraphic members are common both in the Drienok and Vernár nappes (Fig. 3), while it cannot be excluded that the Raming Limestones originally described in Vernár nappe (Havrila in Mello et al., 2000b) could represent Ráztoka Limestones.

The Upper Triassic sediments are known only from the area of occurrence of the Vernár nappe (Mello et al., 2006a, b). The Lunz Formation (Carnian) of dark clayey shales and sandstones represents an important lithostratigraphic member. The Lunz Formation occurs in the tectonic units of the Tatricum, Fatricum, Northern Veporicum, Hronicum and Vernár nappe (Kohút et al., 2018; Havrila et al., 2019). We consider the occurrence of the Lunz Formation and the Reifling Limestones in the southern zone of Veporicum (Aubrecht et al., 2017; Fig. 1) to be unfounded (cf. Havrila et al., 2019; Mello et al., 2000). Grey-black shales, black limestones with cherts and sandstones (Reingraben Shales, "Mürztal" Beds, Julian) are present in the sub-units of Červený Štros and the Gerava unit of the Stratená nappe of Silicicum (or Stratená Group sensu Mello et al., 2000b). Lithostratigraphically similar sediments occur also in the

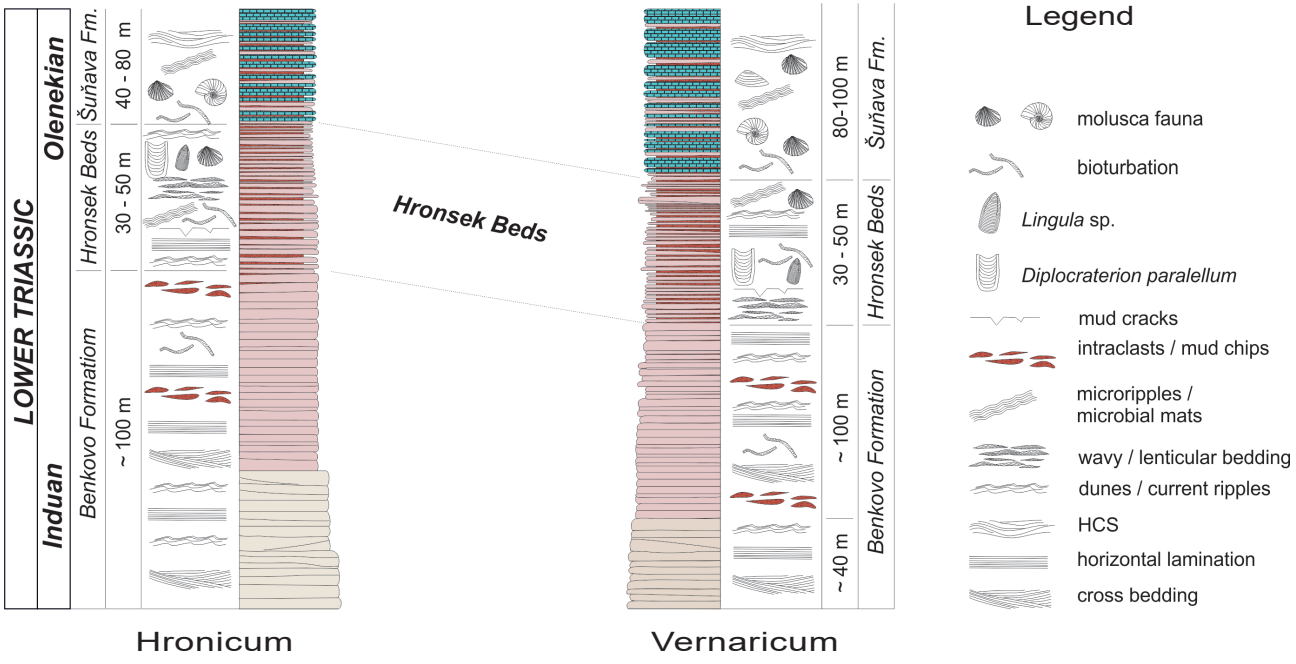

Fig. 2. Correlation of Lower Triassic sediments of the Hronicum and Vernaricum tectonic units.

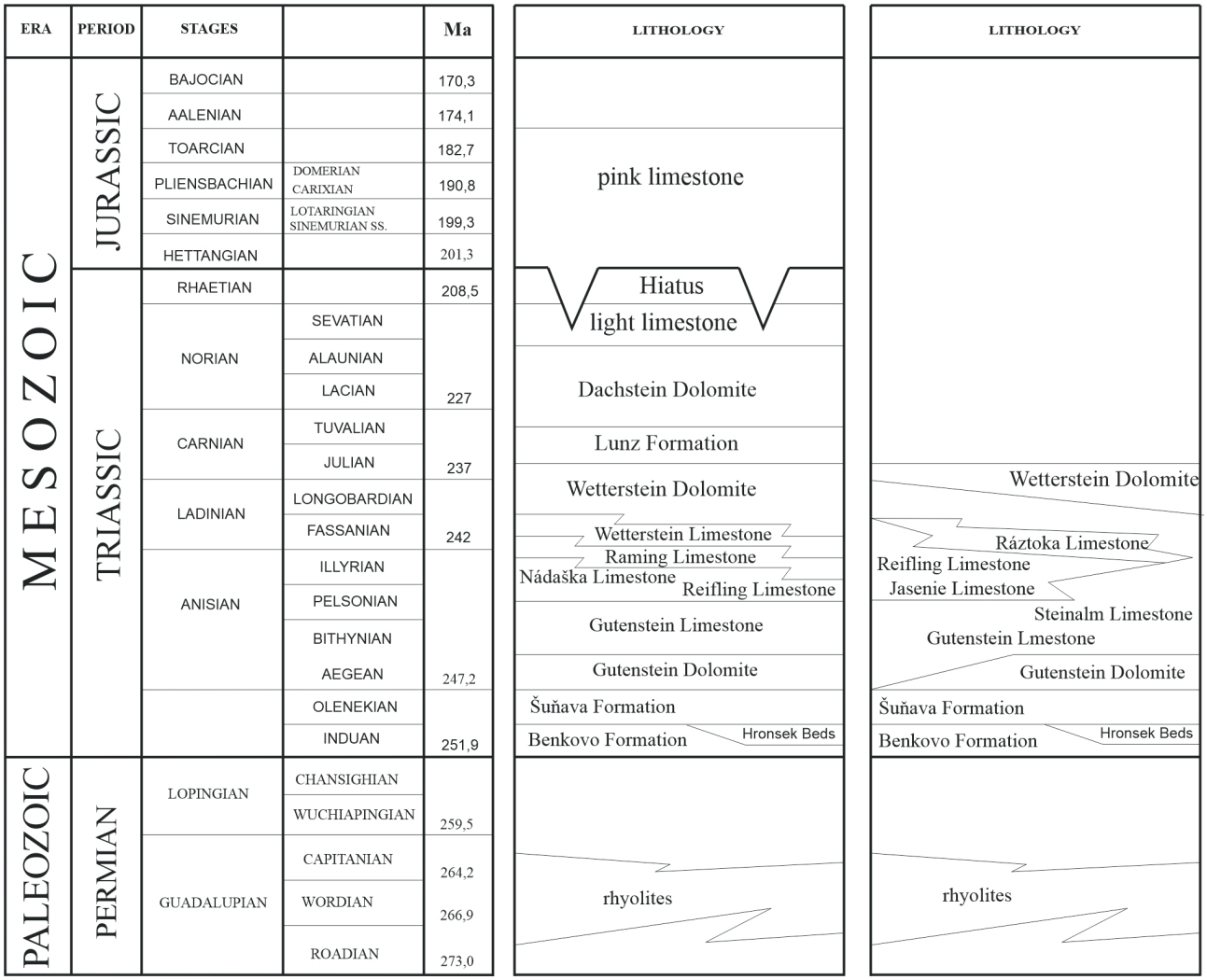

Fig. 3. Lithostratigraphic column of the Vernaricum in the areas of the Vernár nappe (left) and Drienok nappe (right). Permian volcanic bodies are incorporated to Vernaricum tectonically. Compiled according to Havrila (in Mello et al., 2000b), Mello, Vozárová and Polák (in Polák et al., 2003b, modified and supplemented).

Muráň nappe of Silicicum (upper Muráň nappe sensu Havrila, 1997) in the northeastern part of the Muránska planina Plain (Bystrický in Fusán et al., 1963; Geological map of Slovak Republic – https://apl.geology.sk/akt50js/). From the listed lithofacies members of Carnian age, it is possible to unreservedly compare the Lunz Formation from the Vernár nappe (dark shales and sandstones) with the sediments of the Lunz Formation described from the tectonic units of Hronicum, Veporicum, Fatricum and Tatricum. Other lithofacies members (Reingraben Schists, "Mürztal" Beds) are, on the contrary, well correlated with occurrences in Silicicum (Mello et al., 1997a, b). In the area of the Vernár nappe in the Slovenský raj territory, the Dachstein dolomites with light grey and pink limestones (Norian) were described (Havrila in Mello et al., 2000b) in the overlier of the Lunz Formation. In the environment of the latter described limestones the neptunic dikes filled with pink microcrystalline limestones occur (?Liassic). It should be noted that in the Vernár nappe, in contrast to the Stratená Group of Silicicum (sensu Mello et al., 2000b), occurrences of Upper Triassic Aflenz, Hallstatt and Pötschen limestones are absent.

The Lower Triassic lithostratigraphic members (with the exception of tectonically incorporated acid volcanics of the Permian age), the Ráztoky Limestones, Jasenie Limestones and Lunz Formation occurring in the Drienok and Vernár nappes can be parallelized with the tectonic unit of Hronicum.

Tectonic position of the Vernaricum

In the area of Zvolenská kotlina Basin (wider area of Poniky locality; Fig. 1), the Drienok nappe rests on different lithostratigraphic members and at the same time on partial structures / nappes of the Hronicum as well as

the northern Veporicum / Fatricum (Polák et al., 2003a; Olšavský, 2004; Geological map of Slovak Republic https://apl.geology.sk/gm50js/).

At the hypothetical northeastern continuation of the Drienok nappe into the Brusno – Predajná – Bystrá area, three imbricated structures of the Hronicum are present. For these structures, local names of sub-nappes in superposition hierarchization – Bystrá, Svíbová and Okosená nappes – were proposed (Biely, 1963, 1984; Biely et al., 1997). The lithofacial content of partial nappes corresponds to the Biely Váh basin sequence of the Hronicum, similar to the Vernaricum (Biely, 1984; Biely et al., 1997; Havrila, M. & Havrila, J., 2022). In the body of the Svíbová partial nappe, rhyolite ignimbrites of probably Permian age are present between the Malužiná and Benkovo formations (Olšavský & Demko, 2007; Olšavský, 2020). The Stupka Beds were described as the youngest member of the Malužiná Formation in the Svíbová nappe. Their significant component is represented by centimeter- to decimeter-sized rhyolite clasts (Olšavský & Demko, 2007; Olšavský, 2020). In both cases, it is possible to establish a partial lithofacies (Biely Váh Sequence) as well as lithostratigraphic (rhyolite volcanics and rhyolite clastics) affinity with the Drienok nappe, respectively with the Vernaricum. The direct correlation is contradicted by the presence of rock complexes of the Ipoltica Group, and at least by the presence of the Stupka Beds as an integral member of the Malužiná Formation. Another important argument is the tectonic superposition of partial nappes and their lithostratigraphic filling. The Drienok nappe south of Hron river (Zvolenská kotlina Basin *sensu* Mazúr & Lukniš, 1978) clearly appears as the highest structural element tectonically overlying the Marková as well as the Franková partial nappes of the Hronicum (Polák et al., 2003a, b). Structurally, the highest partial nappe north of Hron river (Bystrianske podhorie area sensu Mazúr & Lukniš, 1978) is the Okosená nappe, whose stratigraphic range is Lower to Upper Triassic without the presence of rock complexes typical for Vernaricum or Drienok nappe. A similar situation is also repeated in the superpositionally lowest Bystrany partial nappe of the Hronicum. The Svíbová nappe with the tectonic slice of rhyolites and the Stupka Beds thus occur between two structures where it is not possible to determine their lithostratigraphic relationship with the Vernaricum or Drienok nappe. The lithostratigraphic content of the Svíbová nappe thus indicates only a paleogeographical, but not a tectonic affinity with the Drienok nappe resp. Vernaricum.

The youngest lithostratigraphic member of the Northern Veporicum, which is tectonically overlain by Vernaric sediments, is the Mraznica Formation (Valanginian – Hauterivian). Polymict breccias (Poniky Breccias *sensu* Slavkay & Rohalová, 1993) were described from the area of extension of the Drienok nappe. The Poniky Breccias are stratigraphically, but without biostratigraphic evidences, considered to be Upper Cretaceous–Paleogene sediments (Slavkay & Rohalová, l.c.). They contain Permian to Lower Cretaceous clastics and discordantly overlie the structures of the Northern Veporicum / Fatricum, Hronicum and Drienok nappe (Slavkay et al., 1968; Slavkay & Rohalová, 1993). At the same time, they are tectonically covered by generally south-vergent displaced parts of these tectonic units. According to Slavkay and Rohalová (1993), the most striking thrusting of the Drienok nappe towards the southeast occurs in the area between the elevations of Farbište and Repište in the valley of Suchá Driekyňa and to the W of the road connecting Poniky and Ponická Lehôtka localities, where relics of the Drienok nappe occur from Ľuptákov vrch hill (local name) up to the surroundings of the Žiar elevation point (659 m a.s.l.). The exclusively tectonic character of the breccias is assumed by Polák et al. (2003b). This assumption cannot be accepted when considering the thickness of the breccias, which reaches up to 320 meters (Polák et al., Fig. 13). We assume that the structural reworking of a part of the breccias is a consequence of backthrust displacements (Slavkay et al., 1968; Slavkay, 1971; Olšavský, 2004).

In the pre-Cenozoic bedrock of Central Slovakian Neogene volcanites (Fig. 1), the sediments of Vernaricum were revealed by drilling survey. The Triassic sediments and volcaniclastics are superimposed on the sediments of tectonic units of Southern Veporicum and Hronicum (Vozár, 1973; Hók & Vojko, 2011). In the area of Štiavnica stratovolcano (*sensu* Vass et al., 1988), the occurrence of Lower Triassic sediments near Šobov (Jergištôlňa) was included into the Silicicum s.l. (Konečný et al., 1998). In view of the North Veporic affiliation of the pre-Cenozoic bedrock in the wider area of the Sklené Teplice horst (Konečný et al., 1998; Hók & Vojko, 2011; Hók et al., 2013) and the geometry of the spatial spread of tectonic units in the boreholes as well as in the geological map (Fig. 1) it is more likely that the Lower Triassic assemblage belongs rather to the Drienok nappe or to Vernaricum.

The Lower Carboniferous sediments with carbonates (Ochtiná Formation) as well as sediments that are lithologically close to Hámor Formation and occur in the overburden of the Ochtiná Formation (Plašienka & Soták, 2001) were identified in the footwall of the Muráň nappe in the Furmanec valley (NW of Tisovec town, Fig. 1). This sedimentary complex, named as Furmanec unit (Furmanec sub-unit *sensu* Plašienka and Soták, 2001), occurs in the overlier of Southern Veporic sediments. According to other authors (Demko & Olšavský, 2005), the Upper Carboniferous (non-carbonate) members in the Slávča valley (approx. 5 km to northeast of the Furmanec unit occurrence) as well as in the Furmanec valley, correspond – together with vein bodies of sub-ophytic basalts of the Permian age – to the lithology of the Nižná

Boca Formation. In this case, the volcano-sedimentary complex of the Nižná Boca Hronic assemblage would emerge in the tectonic overburden of the rock complexes of the Southern Veporicum, which would also be located in the tectonic footwall of the Furmanec unit (Demko & Olšavský, 2005). Due to the fact that the lower Muráň unit of Gemericum (Demko and Olšavský, 2005) should be located in the footwall of the Silicic nappe (upper Muráň nappe). The arrangement of tectonic units in the southern part of the Muránska planina plain (Tisovec area) is then as follows: Southern Veporicum → Hronicum → Vernaricum → Gemericum → Meliaticum → Silicicum (Fig. 4).

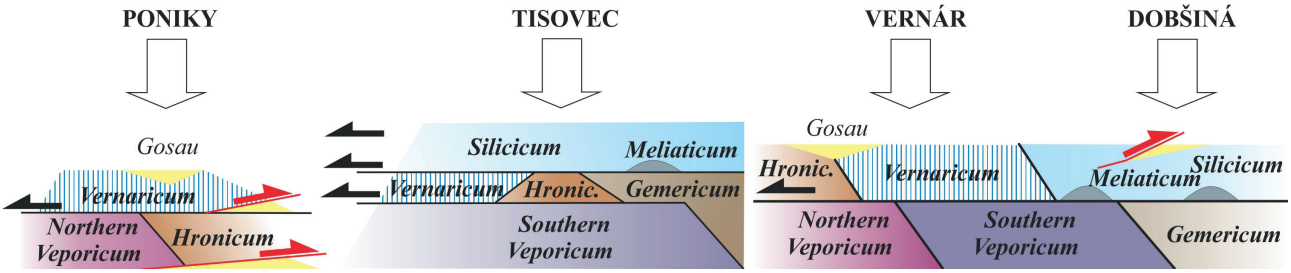

Fig. 4. Simplified situation of the tectonic position of the Vernaricum in individual areas of its occurrence (see Fig. 1). Black arrows indicate north-vergent displacements of tectonic units, red arrows indicate south-vergent displacements of tectonic units.

nappe occurs in the immediate tectonic underlier of the upper Muráň nappe included in Silicicum s.s. (Havrila, 1997) and in northeast direction from the Furmanec and the Slávča valleys immediately tectonically overlies the rocks of the Southern Veporicum, the Lower Muráň nappe (Vernaricum) is found in a structural superposition above the sediments and volcanics of the Nižná Boca Formation (Fig. 4).

From a nearby area (elevation point Magnet, 964 m a.s.l.), Bacsó and Valko (1969 ex Vojtko, 2000) described in the borehole TV-10 a set of metamorphosed black graphitic and siliceous phyllites with evaporites, situated in the underlier of Triassic silicic limestones (of upper Muráň nappe sensu Havrila, 1997). The metamorphosed rock complex is considered to be a part of the tectonic unit of Meliaticum (Vojtko, 2000). At the same time, a Lower Triassic rock sequence (Bodvaszilas and Szin beds) with rhyolite pyroclastics in the basal part of the Bodvaszilas Formation as well as the complex of Middle and Upper Triassic limestones in the stratigraphic range Aegean to Cordevolian conditionally correlated with the Turnaicum tectonic unit or the Drienok nappe, were described in this area (Vojtko, 2000). From the point of view of the present body of knowledge, the Triassic rock complex with rhyolite pyroclastics can be assigned to the Lower Muráň nappe or Vernaricum (Havrila, 1997). In the area of the Furmanec valley and elevation Magnet (964 m a.s.l.), the rock complexes of the southern Veporicum, Gemericum (Furmanec partial unit sensu Plašienka & Soták, 2001), the lower Muráň nappe (Havrila, 1997), Meliaticum (Vojtko, 2000) and Silicicum (upper Muráň nappe sensu Havrila, 1997) occur in tectonic superposition. In the Slávča and Furmanec valleys, the sediments and volcanics of the Nižná Boca Formation of Hronicum and the Furmanec

In the Slovenský raj area (Vernár area; Fig. 1) the situation is more complicated. The Vernár nappe here should rest on the sediments of the Southern Veporicum and Hronicum, but at the same time in the tectonic footwall of Silicicum (Mello et al., 2000a; Geological map of Slovak Republic – https://apl.geology.sk/gm50js/). The results of reambulatory geological mapping (Madarás and Ivanička, 2001) show that the slice of Carboniferous sediments located between the Southern Veporicum (https://apl.geology.sk/gm50js/) and Vernaricum belongs to the Slatviná Formation (Southern Veporicum) and not to the Hronicum tectonic unit as was primarily assumed (Mello et al., 2000a). The principal argument for such decision was primarily the structural record. Kováčik (2012), however, assumes that the entire complex of Carboniferous sediments with volcanics belongs to the tectonic unit of the Hronicum, displaced on the sediments of the Southern Veporicum, protruding from under the rock complexes of the Hronicum in tectonic windows, while the author (l.c.) considers the structural record in both units to be comparable. From the point of view of the tectonic location of the Vernár nappe, the tectonic arrangement of the rock zone between the Vernár nappe and the rocks of Southern Veporicum (Madarás & Ivanička, 2001; Kováčik, 2012) is irrelevant, because the Vernár nappe tectonically overlies the rock complexes of the Hronicum and the Southern Veporicum and, due to its tectonic position, it is in a situation similar to the one in the area of Tisovec. the Vernaricum (Vernár nappe) tectonically covers the Southern Veporikum as well as the Hronicum, and the Vernaricum itself is overlain by Meliaticum and Silicicum (Fig. 4; Geological map of Slovak Republic – https://apl.geology.sk/gm50js/).

Southwest of Betlanovce village, the ?Upper Cretaceous to ?Paleocene sediments (in each case sediments younger than the Campanian and older than the Lower Eocene) cover the tectonic contact of the Hronicum and the Vernár nappe (l.c.; Figs. 1 and 4). These sediments contain clasts derived from tectonic units of Veporicum, Gemericum, Hronicum, as well as Meliaticum and Silicicum (Havrila, Filo, Mello in Mello et al., 2000a, b). The Upper Cretaceous sediments of the Gosau Group, situated under the south-vergent back-thrust displacements, are present in the area north of Dobšiná. Similarly, the geological setting of Upper Cretaceous to Paleogene sediments is complicated by south-vergent displacements in the Poniky area (Slavkay et al., 1968; Slavkay, 1971; Slavkay & Rohalová, 1993). The south-vergent displacements are probably related to the exhumation of the Tatric crystalline basement of the Nízke Tatry Mts. during the Upper Eocene (Králiková et al., 2016).

In the area of the Zvolenská kotlina Basin, the Drienok nappe covers the Northern Veporicum / Fatricum and Hronicum and represents the highest tectonic unit in this area of its occurrence (Fig. 4). The Vernár nappe (Vernaricum) in the Slovenský raj area rests in a tectonic position on the Betlanovce partial nappe / the slice of Hronicum (Mello et al., 2000a, b). From the Gľac partial nappe and the Červený Štros Group of the Stratená nappe, the Vernáricum is separated along the entire contact by the Muráň fault, but southwest of Hrabušice village (the Píla area) the Stratená nappe (the Červený Štros Group) is displaced on Vernár nappe (Vernaricum).

Paleogeographic position of Vernaricum

The present spatial arrangement of tectonic units in individual areas of the Vernaricum occurrence is expressed in Fig. 4. The immediate tectonic contact of the Vernaricum with the tectonic unit of the Northern Veporicum and Hronicum is observable in the area of Poniky (Zvolenská kotlina Basin), where the Vernaricum (Drienok nappe) represents the highest tectonic unit. In the area of Central Slovakian Neogene volcanites, occurrences of Vernaricum were recorded mostly in boreholes and overlap the tectonic contact of the Northern and Southern Veporicum (Hók & Vojtko, 2011). In the Slovenský raj area, the direct tectonic underlier of Vernaricum (Vernár nappe) is the Southern Veporicum and Hronicum. The direct tectonic overlier of Vernaricum is represented by Silicicum. In the area of the Muránska planina Plain (the Lower Muráň nappe) the tectonic underlier of Vernaricum is formed of units of Southern Veporicum and Hronicum. The Vernaric tectonic overlier is formed again by Silicicum (Upper Muráň nappe).

Silicicum in the entire range of its occurrence has Vernaricum in its tectonic underlier only in areas of Slovenský raj and the Muránska planina Plain. As a separate tectonic unit, Silicicum was displaced onto already structured basement of Veporicum, Hronicum, Vernaricum and Gemericum in the Upper Cretaceous period (Plašienka, 2018). Of the last mentioned tectonic units, Gemericum is found in the highest structural position under Silicicum. Taking into account the movement of tectonic units generally from the southeast to the northwest (in today's geographical coordinates, cf. Plašienka, 1999, 2018; Csontos & Vörös, 2004; Hók et al., 1995), the paleogeographical position of the Vernaricum lies between the Hronicum and Gemericum, while Vernaricum represents the structurally highest element of the Hronic system of nappes (Havrila, M. & Havrila, J., 2022).

Permian volcanism in the Hronicum is represented by tholeiitic basalts, andesites and their volcaniclastics, originating in the extensional tectonic regime, which conditioned the riftogenesis of the continental margin or forearc resp. backarc basin formation within the continental crust (Vozár et al., 2015). The presence of a continental type of crust is indicated by the occurrence of crystalline rocks (crystalline schists and granitoids) at the base of the Nižná Boca assemblage of the Ipoltica Group of Hronicum on the northern slopes of the Nízke Tatry (Low Tatra) Mts. (Andrusov, 1936; Vozárová & Vozár, 1979). The same is true on the northern side of the Nízke Tatry Mts. in the area of Okrúhly vrch (Olšavský, unpublished data) as well as on the southern slopes of the Nízke Tatry Mts. (Olšavský & Demko, 2007; Olšavský, 2020), however, acidic varieties of volcanics (rhyolites and rhyolite ignimbrites and Stupka Beds) have also been detected in the structure of the Hronicum, indicating the lithological affinity of the Permian acidic volcanics of Hronicum and Vernaricum (Olšavský, 2020).

Another aspect in deciphering the paleogeographic position of the Vernaricum is represented by lithostratigraphic members that are part of Vernaricum but also occur in other tectonic units. These include the Benkovo and Šuňava formations together with the Hronsek Beds (Lower Triassic; Olšavský et al., 2010; Olšavský, 2019), Ráztoky and Jasenovo Limestones (Havrila et al., 2016; Havrila, M. & Havrila, J., 2022), but also other lithofacies of Triassic limestones (see Fig. 2) and the Lunz Formation (Upper Triassic; Havrila in Mello., 2000b), which are lithostratigraphically identical to the occurrences in the tectonic unit of Hronicum and in the given lithological, facies and stratigraphic configuration they do not occur elsewhere. Vernaricum can be considered as a part of the Hronicum tectonic unit (cf. Havrila, M. & Havrila, J., l.c.). Presently, it crops out in the highest structural position within the partial nappes of the Hronicum. Vernaricum belongs to internal zone of the Hronicum paleogeographic area, which stretched between Veporicum and Gemericum.

Conclusion

Vernaricum is defined as the structurally highest unit or partial nappe of Hronicum in the stratigraphic range of Lower Triassic to Lower Jurassic. A typical lithotype accompanying Vernaricum is represented by rhyolites and rhyolitic volcaniclastic, being tectonically incorporated to Lower Triassic sediments. These probably formed the substrate of the Triassic lithostratigraphy of Vernaricum (Fig. 3). The Vernaricum includes the tectonic units, in the past referred to the Vernár nappe (Maheľ, 1986), the Drienok Series (Bystrický, 1964) or the Drienok nappe (Polák et al., 2003), as well as the Lower Muráň nappe (Havrila, 1997). The structurally individualized occurrences, referred as the Vernár nappe, the Lower Muráň nappe, the Drienok nappe and occurrences in the footwall of the Central Slovakian Neogene volcanites (Fig. 1), were in the past considered to be a part of the Gemericum s.l. (*e.g.* Bystrický, 1964; Vozár, 1973), Silicicum (e.g. Andrusov & Samuel, 1983; Mello et al., 2000) or Hronicum (e.g. Kettner, 1937; Havrila, M. & Havrila, J., 2022). The Vernaricum tectonically overlies the units of the Northern Veporicum / Fatricum, Southern Veporicum and Hronicum, and at the same time it is situated in the tectonic underlier of Gemericum, Meliaticum and Silicicum (Figs. 1 and 4). The tectonic individualization of the Vernaricum can be dated to the Lower Cretaceous period. The presumed paleogeographic position of Vernaricum (in today's geographical coordinates) was located on the internal / southern edge of the Hronic sedimentary basin.

Acknowledgement

The authors of the article are grateful for financial support by VEGA 1/0346/20, APVV-17-0170 and APVV-21-0281 grants. At the same time, they express their thanks to Dr. Milan Havrila, without whom this publication would not have been created. Thanks are extended to reviewers B. Kronome and Z. Németh (ŠGÚDŠ) for valuable comments and suggestions, improving the primary manuscript.

References

Andrusov, D. & Samuel, O. (eds.), 1983: Stratigrafický slovník Západných Karpát 1, A – K. *Bratislava, Geol. Úst. D. Štúra, 5–440.*

Andrusov, D., 1936: Subtatranské příkrovy Západních Karpát. *Carpatica (Praha), 1–50.*

Aubrecht, R., Sýkora, M., Uher, P., Li., X.-H., Yang, Y.-H., Putiš, M. & Plašienka, D., 2017: Provenance of the Lunz Formation (Carnian) in the Western Carpathians, Slovakia: Heavy mineral study and in situ LA-ICP-MS U-Pb detrital zircon dating. *Palaeogeogr. Palaeoclimatol. Palaeoecol., 471, 233–253.*

Bacsó, Z. & Valko, P., 1969: Final report and calculation of resouces, the l[st] part: Horehronie valley from locality Tisovec-Hnušťa investigation, raw material Fe, state 1. XI. 1968. Geologický prieskum Spišská Nová Ves – GS Rožňava. *Manuscript. Bratislava, archive St. Geol. Inst. D. Štúr, 200 p.*

Biely, A., 1963: Beitrag zum kenntnis des inneren baues der Choč-einheit. *Geol. Práce, Zpr., 28, 69–78.*

Biely, A., 1984: Tektonická stavba územia horehronského podolia medzi Slovenskou Ľupčou a Breznom. *Manuscript. Bratislava*, *archive St. Geol. Inst. D. Štúr (arch n. AP 7218).*

Biely, A., Bezák, V., Elečko, M., Kaličiak, M., Konečný, V., Lexa, J., Mello, J., Nemčok, J., Potfaj, M., Rakús, M., Vass, D., Vozár, J. & Vozárová, A., 1995: Geologická mapa Slovenskej republiky. M = 1 : 500 000. *Bratislava, Min. život. prostr., GS SR.*

Biely, A. & Bezák, V. (eds.), Bujnovský, A., Vozárová, A., Klinec, A., Miko, O., Halouzka, R., Vozár, J., Beňuška, P., Hanzel, V., Kubeš, P., Liščák, P., Lukáčik, E., Maglay, J., Molák, B., Pulec, M., Putiš, M. & Slavkay, M., 1997: Vysvetlivky ku geologickej mape Nízkych Tatier 1 : 50 000. *Bratislava, Geol. Úst. D. Štúra, 232 p.*

Burian, J., Konečný, V., Krist, E., Lexa, J. & Vozár, J., 1968: Regionálny ložiskový výskum neovulkanitov, oblasť Banská Štiavnica. *Manuscript. Bratislava, archive St. Geol. Inst. D. Štúr*.

Bystrický, J., 1964: Stratigrafia a vývin triasu série Drienka. *Zpr. geol. Výzk. v r. 1963, Časť 2, 94–96.*

Csontos, L. & Vörös, A., 2004: Mesozoic plate tectonic reconstruction of the Carpathian region. *Palaeogeogr. Palaeoclimatol. Palaeoecol., 210, 1–56.*

Demko, R. & Olšavský, M., 2005: Petrography and geochemistry of subvolcanic basalt bodies among the Upper Carboniferous sediments from the underlier of Muráň Mesozoic sequences (Slávča and Furmanec valleys, West Carpathians). *Slovak Geol. Mag., 11, 2–3, 143–153.*

Demko, R. & Hraško, Ľ., 2013: Ryolitové teleso Gregová pri Telgárte. *Miner. Slov., 45, 161–174.*

Fusán, O., Bystrický, J., Franko, O., Chmelík, F., Ilavský, J., Kamenický, L., Kullman, E., Lukniš, M. & Matějka, A., 1963: Vysvetlivky k prehľadnej geologickej mape ČSSR 1 : 200 000, M – 34 – XXVII, list Vysoké Tatry. *Bratislava, Geofond, 5–123.*

Fusán, O., Biely, A., Ibrmajer, J., Plančár, J. & Rozložník, L., 1987: Podložie terciéru Vnútorných Západných Karpát. *Bratislava, Geol. Úst. D. Štúra, 1–103*.

Geologická mapa Slovenska M 1 : 50 000 [online], 2013: *Bratislava, Št. Geol. Úst. D. Štúra, http://apl.geology.sk/gm50js*.

Havrila, M., 1997: Vzťah hronika a silicika. Čiastková záverečná správa. Geodynamický vývoj Západných Karpát – II. etapa. Manuscript. *Bratislava, archive St. Geol. Inst. D. Štúr.*

Havrila, J., Boorová, D. & Havrila, M., 2016: Ráztocký vápenec štureckej faciálnej oblasti hronika. *Geol. Práce, Spr., 129, 35–54*.

Havrila, M., Boorová, D. & Havrila, J., 2019: Paleogeografická schéma depozičného priestoru sedimentov reingrabenského a lunzského eventu (centrálne Západné Karpaty): rešerš, poznámky, dierkavce [Paleogeographic scheme of the Reingraben and Lunz event sediments deposition area (Central Western Carpathians): research, notes, foraminifers]. *Geol. Práce, Spr., 134, 3–32.*

Havrila, M. & Havrila, J., 2022: Paleogeografické rozšírenie gaderského a ráztockého vápenca (vrchný pelsón – ilýr, hronikum, Západné Karpaty): rešerš. [Paleogeographical extension of Gader a Ráztoka Limestones (Upper Pelsonian – Illyrian, Hronicum, Western Carpathians): review]. *Geol. Práce, Spr., 138, 3–28.*

Hók, J. & Vojtko, R., 2011: Interpretácia pohorelskej línie v podloží stredoslovenských neovulkanitov (Západné Karpaty). *Acta Geol. Slov., 3, 1, 13–19.*

Hók, J., Havrila, M., Rakús, M., Vojtko, R. & Kráľ, J., 2004: Nappe Contact as a Tool of Paleotectonic Reconstruction (Inner Western Carpathians a Case of Study). *Geolines, 17, 39–40.*

Hók, J., Kováč, P. & Rakús, M., 1995: Výsledky štruktúrneho výskumu vnútorných Karpát a ich interpretácia. *Miner. Slov., 27, 4, 231–235.*

Hók, J., Pelech, O. & Slobodová, Z., 2013: Kinematic analysis of the Veporicum and Hronicum rock complexes within the Sklené Teplice pre-Neovolcanic horst basement (Central Slovakia Neogene volcanic field). *Acta Geol. Slov., 5, 2, 129–134*.

Hók, J., Pelech, O., Teťák, F., Németh, Z. & Nagy, A., 2019: Outline of the geology of Slovakia (W. Carpathians). *Miner. Slov., 51, 31–60.*

Kettner, R., 1937: Geologické poměry okolí Vernáru na Slovensku. *Rozpr. Čes. Akad. Věd Umění, Tř. II, 47, 8, 1–11*.

Kohút, M., Hofmann, M., Havrila, M., Linnemann, U. & Havrila, J., 2018: Tracking an upper limit of the Carnian Crisis" and/or Carnian stage in the Western Carpathians (Slovakia). *Int. J. Earth Sci. (Geol. Rdsch.) (Berlin – Heidelberg), 107, 1, 321– 335.*

Kochanová, M. & Michalík, J., 1986: Stratigraphy and microfauna of the Zámostie limestones (upper pelsonian – lower illyrian) of the Choč nappe at the southern slopes of the Nízke Tatry Mts. (West Carpathians). *Geol. Zbor. Geol. carpath., 37, 4, 501–531.*

Konečný, V. (ed.), Lexa, J., Halouzka, R., Hók, J., Vozár, J., Dublan, L., Nagy, A., Šimon, L., Havrila, M., Ivanička, J., Hojstričová, V., Mihaliková, A., Vozárová, A., Konečný, P., Kováčiková, M., Fiľo, M., Marcin, D., Klukanová, A., Liščák, P. & Žáková, E., 1998: Vysvetlivky ku geologickej mape Štiavnických vrchov a Pohronského Inovca (Štiavnický stratovulkán) I. diel. *Bratislava, GS SR.*

Kováčik, M., 2012: Geologická stavba a metamorfóza vulkanicko-sedimentárneho pásma na severovýchodnom úpätí Kráľovej hole. *Miner. Slov., 44, 241–256.*

Králiková, S., Vojtko, R., Hók, J., Fügenschuh, B. & Kováč, M., 2016: Low-temperature constraints on the Alpine thermal evolution of the Western Carpathian basement rock complexes. *J. struct. Geol., 91, 144–160.*

Madarás, J. & Ivanička, J., 2001: Tektonická pozícia mladopaleozoických-mezozoických komplexov hornín na východných svahoch Kráľovej hole v Nízkych Tatrách. *Miner. Slov., 33, 1, 15–28.*

Maheľ, M., 1986: Geologická stavba československých Karpát – Paleoalpínske jednotky. *Bratislava, Veda, pp. 503.*

Mazúr, E. & Lukniš, M., 1978: Regionálne geomorfologické členenie Slovenskej socialistickej republiky. *Geogr. Čas., 30, 2, 101–125.*

Mello, J., Filo, I., Havrila, M., Ivanička, J., Madarás, J., Németh, Z., Polák, M., Pristaš, J., Vozár, J., Koša, E. & Jacko, S. jr., 2000a: Geologická mapa Slovenského raja, Galmusu a Hornádskej kotliny (M 1 : 50 000). *Bratislava, Min. život. prostr., Št. Geol. Úst. D. Štúra.*

Mello, J., Elečko, M., Pristaš, J., Reichwalder, P., Snopko, L., Vass, D., Vozárová, A., Gaál, Ľ., Hanzel, V., Hók, J., Kováč, P., Slavkay, M. & Steiner, A., 1997a: Geologická mapa Slovenského krasu 1 : 50 000. *Bratislava, GS SR.*

Mello, J., Elečko, M., Pristaš, J., Reichwalder, P., Snopko, L., Vass, D., Vozárová, A., Gaál, Ľ., Hanzel, V., Hók, J., Kováč, P., Slavkay, M. & Steiner, A., 1997b: Vysvetlivky ku geologickej mape Slovenského krasu 1 : 50 000. *Bratislava, GS SR, Vyd. D. Štúra, 7–244.*

Mello, J., Filo, I., Havrila, M., Ivan, P., Ivanička, J., Madarás, J., Németh, Z., Polák, M., Pristaš, J., Vozár, J., Vozárová, A., Liščák, P., Kubeš, P., Scherer, S., Siráňová, Z., Szalaiová, V. & Žáková, E., 2000b: Vysvetlivky ku geologickej mape Slovenského raja, Galmusu a Hornádskej kotliny 1 : 50 000. *Bratislava, Št. Geol. Úst. D. Štúra, 7–299*.

Olšavský, M., 2004: Pozícia drienockého príkrovu k podložným tektonickým jednotkám a jeho spodnotriasový vývoj. *Miner. Slov., 36, 2, 77–86.*

Olšavský, M., 2019: Litostratigrafia spodnotriasových súvrství Západných Karpát. Rigorózna práca. *Manuscript. Bratislava, archive Kat. geol. paleont. PriF Univ. Komen., pp. 122.*

Olšavský, M., 2020: Litostratigrafia malužinského súvrstvia z oblasti Bystrej (svíbovský čiastkový príkrov, Nízke Tatry). *Geol. Práce, Spr., 136, 59–72.*

Olšavský, M. & Demko, R., 2007: Mladšie paleozoikum Hronika na SZ svahoch Nízkych Tatier. Čiastk. správa k záver. správe geologickej úlohy: Aktualizácia geologickej stavby problémových území Slovenska v mierke 1 : 50 000. *Manuscript. Bratislava, archive St. Geol. Inst. D. Štúr (arch. n. 91 733-43), pp. 95.*

Olšavský, M., Šimo, V. & Golej, M., 2010: Hronsecké vrstvy: korelačný člen medzi silicikom s. l. (drienocký príkrov) a hronikom (frankovský príkrov; Západné Karpaty). *Miner. Slov., 42, 407–418.*

Ondrejka, M., Vojtko, R., Putiš, M., Chew, D. M., Olšavský, M., Uher, P., Nemec, O., Drakou, F., Molnárová, A. & Spišiak, J., 2022: Permian A-type rhyolites of the Drienok Nappe, Inner Western Carpathians, Slovakia: Tectonic setting from in-situ zircon U-Pb-LA-ICP-MS dating. *Geol. Carpath., 73, 2, 123–136. https://doi.org/10.31577/GeolCarp.73.2.2.*

Ondrejka, M., Li, X.-H., Vojtko, R., Putiš, M., Uher, P. & Sobocký, T., 2018: Permian A-type rhyolites of the Muráň Nappe, Inner Western Carpathians, Slovakia: in-situ zircon U-Pb SIMS ages and tectonic setting. *Geol. Carpath., 69, 2, 187–198. doi: 10.1515/geoca-2018–0011.*

Plašienka, D., 1981: Tektonické postavenie niektorých metamorfovaných mezozoických sérií veporika. Kandidátska dizertačná práca. *Manuscript. Bratislava, archive St. Geol. Inst. D. Štúr (arch. n. AP8662), 153 p.*

Plašienka, D., 1999: Tektonochronológia a paleotektonický model jursko-kriedového vývoja centrálnych Západných Karpát. *Bratislava, Veda. Vyd. Slov. Akad. Vied, 9–125.*

Plašienka, D., 2018: Continuity and episodicity in the early Alpine tectonic evolution of the Western Carpathians:

How large-scale processes are expressed by the orogenic architecture and rock record data. *Tectonics, 37. https://doi.org/10.1029/2017TC004779.*

Plašienka, D. & Soták, J., 2001: Stratigrafické a tektonické postavenie karbónskych sedimentov v doline Furmanca (Muránska planina). *Miner. Slov., 33, 1, 29–44.*

Polák, M., Filo, I., Havrila, M., Bezák, V., Kohút, M., Kováč, P., Vozár, J., Mello, J., Maglay, J., Elečko, M., Olšavský, M., Pristaš, J., Siman, P., Bučeк, S., Hók, J., Rakús, M., Lexa, J. & Šimon, L., 2003a: Geologická mapa Starohorských vrchov, Čierťaže a severnej časti Zvolenskej kotliny 1 : 50 000. *Bratislava, Št. Geol. Úst. D. Štúra*.

Polák, M., Filo, I., Havrila, M., Bezák, V., Kohút, M., Kováč, P., Vozár, J., Mello, J., Maglay, J., Elečko, M., Vozárová, A., Olšavský, M., Siman, P., Bučeк, S., Siráňová, Z., Hók, J., Rakús, M., Lexa, J., Šimon, L., Pristaš, J., Kubeš, P., Zakovič, M., Liščák, P., Žáková, E., Boorová, D. & Veněková, H., 2003b: Vysvetlivky ku geologickej mape Starohorských vrchov, Čierťaže a severnej časti Zvolenskej kotliny 1 : 50 000. *Bratislava,* Št*. Geol. Úst. D.* Štúra*, pp. 218.*

Slavkay, M. & Rohalová, M., 1993: Karbonátové brekcie pri Ponikách, ich litologický a tektonický význam. *Západ. Karpaty, Sér. Geol., 17, 39–50.*

Slavkay, M., Tomko, I., Lukaj, M. & Barkáč, Z., 1968: Poniky, Pb rudy. Záverečná správa a výpočet zásob VP, so stavom k 30. 11. 1968. *Manuscript. Spišská Nová Ves, archive Geol. Priesk., pp. 387.*

Slavkay, M., 1971: Ložiská polymetalických rúd pri Ponikách. *Miner. Slov., 2, 81–213.*

Vojtko, R., 2000: Are there tectonic units derived from the Meliata-Hallstatt trough incorporated into the tectonic structure of the Tisovec Karst ? (Muráň karstic plateau, Slovakia). *Slovak Geol. Mag., 6, 4, 335–346.*

Vozár, J., 1969: Vulkanoklastický materiál v mezozoiku v podloží neovulkanitov južne od Banskej Štiavnice. *Geol. Práce, Spr., 48, 47–52.*

Vozár, J., 1973: Petrograficko-litologická charakteristika chočskej jednotky a gemeridného mezozoika v podloží neovulkanitov severne od Levíc. *Zbor. geol. Vied, Západ. Karpaty, 18, 183–214.*

Vozár, J., Spišiak, J., Vozárová, A., Bazarnik, J. & Kráľ, J., 2015: Geochemistry and Sr, Nd isotopic composition of the Hronic Upper Paleozoic basic rocks (Western Carpathians, Slovakia). *Geol. Carpath., 66, 1, 3–17. doi: 10.1515/geoca-2015-0007.*

Vozárová, A. & Vozár, J., 1979: Kryštalinikum v bazálnej časti chočského príkrovu. *Geol. Práce, Spr., 72, 195–198.*

Vernárikum – rozšírenie, litostratigrafia, tektonika a paleogeografia

Vernárikum je definované ako štruktúrne najvrchnejšia jednotka alebo čiastkový príkrov príkrovového systému hronika. Tektonické jednotky zaradené do vernárika sa označovali ako séria Drienka (Bystrický, 1964), vernársky príkrov (Maheľ, 1986) a spodný muránsky príkrov (Havrila, 1997), pričom Havrila (l. c.) koreloval spodný muránsky príkrov s drienockým príkrovom, resp. sériou Drienka (*sensu* Bystrický, 1964). Zároveň boli drienocký príkrov, vernársky príkrov a spodný muránsky príkrov považované za súčasť tektonických jednotiek gemerika (napr. Bystrický, 1964; Vozár, 1973), silicika (napr. Andrusov a Samuel, 1983; Mello et al., 2000) alebo hronika (Kettner, 1937).

Stratigrafický rozsah vernárika je spodný trias až spodná jura (obr. 3). Typickými asociujúcimi litotypmi sú permské ryolity a ryolitové vulkanoklastiká, tektonicky začlenené do sedimentov spodného triasu (Demko a Hraško, 2013; Ondrejka et al., 2018, 2022). Príkrovové premiestnenie vernárika možno datovať do obdobia spodnej kriedy. Vernárikum prikrýva tektonické jednotky severného veporika/fatrika, hronika a južného veporika. V jeho štruktúrnom nadloží sa nachádza gemerikum, meliatikum a silicikum (obr. 1 a 4). Predpokladaná paleogeografická pozícia vernárika sa nachádzala v priestore medzi veporikom a gemerikom.

Doručené / Received: 6. 6. 2023
Prijaté na publikovanie / Accepted: 30. 6. 2023

Mineralia Slovaca, Web ISSN 1338-3523, ISSN 0369-2086, https://doi.org/10.56623/ms.2023.55.1.2
55, 1 (2023), 13 – 26, © Authors 2023. CC BY 4.0

Electron microprobe dating of monazites from rhyolites of the Veľká Stožka Massif (Muráň nappe, Western Carpathians) – implications for the Permian volcanic evolution in Internal Western Carpathians

RASTISLAV DEMKO[1], BALÁZS KRONOME[1], MÁRIO OLŠAVSKÝ[2] and ONDREJ PELECH[1]

[1]State Geological Institute of Dionýz Štúr, Mlynská dolina 1, SK-817 04 Bratislava 11;
rastislav.demko@geology.sk
[2]State Geological Institute of Dionýz Štúr, Zelená 5, SK-974 04 Banská Bystrica

Abstract: New results of field research, as well as petrographical and geochronological studies are presented in the form of a geological map, tectonostratigraphic scheme and new magmatic age data of monazite crystallization from the rhyolite body located on SW slopes of the Veľká Stožka Massif, Dudlavka Valley (Muráň Plateau). The rhyolite bodies in the Veľká Stožka area are tectonically incorporated into the Lower Triassic formations at the base of the Muráň nappe. The electron microprobe dating of monazites yields magmatic / volcanic age 281 ± 4.5 Ma (Artinskian – Kungurian), which complements geochronological data from the same rhyolite body below the Veľká Stožka Massif, as well as other rhyolite bodies from Telgárt, Poniky and Tisovec, which, originally erupted in a Permian volcanically active fault zone (VAFZ) geodynamical setting. The comparison of geochronological data 281 ± 4.5 Ma and 269.5 ± 1.8 Ma from the studied locality suggest a geodynamic evolution, where not only one, but several separate volcanic eruption phases acted in the original domain of rhyolitic volcanism. The geochronological correlation of the rhyolite bodies in the Upper Hron Valley, active in time span 281–263 Ma, allowed to identify a volcanic hiatus between 280–271 Ma. Such eruptional pause correlates very well with other volcanic provinces such as Harnobis volcanogenic horizon of the North Veporic realm, the Petrova hora and Novoveská Huta Fm. of the Northern Gemericum, which erupted during hiatus of VAFZ and their activities have ended in during recovering rhyolite eruptions in VAFZ. Reactivation of rhyolitic volcanic activity in VAFZ 271–263 Ma is a result of paleostress reorganisation in Pangea lithosphere. The revealed paleovolcanic relationships highlight interconnection of paleotectonic and paleovolcanic events in the known paleotectonic units of Internal Western Carpathians during Permian.

Key words: EPMA, monazite magmatic age, Permian volcanic evolution, Muráň nappe

Graphical abstract

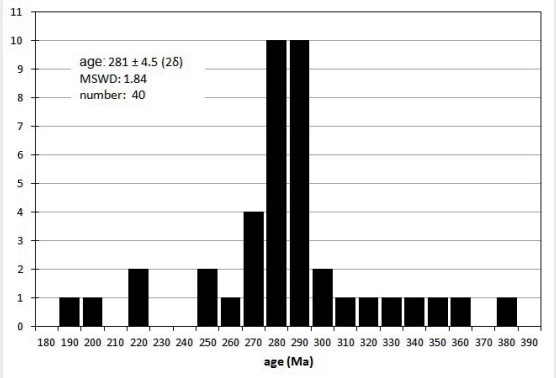

Highlights

- Dating of monazites from two samples gives a new magmatic age 281 ± 4.5 Ma (Artinskian – Kungurian) of the rhyolite eruption
- Permian rhyolitic bodies of the Internal Western Carpathians were generated and erupted along volcanically active fault zones (VAFZ)
- At least two different eruption phases can be recognized in the VAFZ: an older (ca. 281–280 Ma) and a younger (starting at ca 271–263 Ma) phase
- Reactivation of rhyolitic volcanic activity in VAFZ 271–263 Ma is a result of changed paleostress in Pangea lithosphere.

Introduction

The products of Permian acidic magmatic activity in the Internal Western Carpathians (volcanic detritus, rhyolite or granitic rocks) occur in several tectonic units. They are mostly connected with their coeval sedimentary complexes (Hronicum, Tatricum, Veporicum, Gemericum), but some of them, namely the rhyolite bodies Gregová near Telgárt, Veľká Stožka in the Muráň nappe, rhyolite bodies in the area of Poniky (usually assigned into Silicicum s.l., e.g. Plašienka et al., 1997) are tectonically amputated from their original environment and incorporated into geologically younger Lower Triassic sedimentary formations.

The presence of Permian rhyolites in the Internal Western Carpathians were already known since the 19th century (Stur, 1868; Oppenheimer, 1931; Kovářík, 1955; Grenar & Kotásek, 1956; Biely, 1956; Náprstek, 1958; Zorkovský, 1959a, b; Losert, 1963; Slavkay, 1965, 1971, 1981; Kravjanský, 1961, 1964, 1966; Kravjanský et al., 1966; Kusák, 1967; Rozložník et al., 1974; Orlický & Slavkay, 1979; etc.). Their study has a long geological tradition and has produced several lithostratigraphic correlations (see Havrila in Mello et al., 2000, p. 94), which results almost regularly consider them as Lower Triassic with an exception of some works that also considered the Permian age (Kusák, 1967, p. 37–42; Maheľ, 1986, p. 153; Plašienka, 1981).

Permian fault zones associated with active volcanism are a product of late Hercynian or even older tectonic processes and are not genetically bound to given Alpine tectonic units and their paleosedimentary environment. According to the character of the rhyolitic complexes, genetically bound to volcanically active fault zones (VAFZ), the paleovolcanic relation of these complexes to the hosting Alpine structural units remains problematic.

Some of mentioned tectonic models used the disputed rhyolitic rocks as a marker for assignment of whole sequences into overlying Mesozoic rocks (see Havrila, 1997; Hók et al., 2004). Due to our intention to avoid geological bias in the subdivision and definition of tectonic units (Hronicum, Vernaricum, Silicicum, etc.; for a recent discussion on this issue see, e.g., Hók & Olšavský, 2023), in the following text we will refer to the VAFZ of the Internal Western Carpathians.

The presented paper is focusing on the body of rhyolitic rocks on the western slopes of the Veľká Stožka Massif, Muráň Plateau, as one of the typical occurrences of Permian rhyolitic complexes tectonically incorporated into younger Triassic sedimentary formations.

Geological setting

The occurrence of the studied rhyolitic body in the Veľká Stožka Massif at the base of the Muráň nappe was for the first time reported during geological mapping by Kovářík (1955) and referred to as the *"Werfenian with melaphyres"*. The rocks were later petrographically characterized by Zorkovský (1959a, b). The position of the rhyolites in the studied area was usually described as an integral part of the Lower Triassic sequence (Slavkay, 1965; Bystrický in Slavkay et al., 1968, p. 61; Slavkay, 1971, 1981; Havrila in Mello et al., 2000, p. 94). More recent works have dealt with other aspects of the rhyolites (Uher et al., 2002; Ondrejka, 2004; Ondrejka et al., 2007). The Permian age of the rhyolites at the base of the Muráň nappe was proven by geochronological methods in the area of Gregová hill near Telgárt (Demko & Hraško, 2013) and from the vicinity of Tisovec and Veľká Stožka (Ondrejka et al., 2018). More recently, rhyolites in the Drienok nappe, which is usually correlated with the Muráň nappe, were also analysed (Ondrejka et al., 2022).

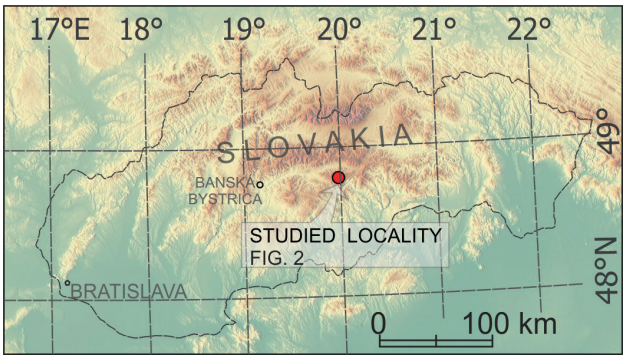

Fig. 1. Location of studied locality in the territory of Slovakia.

The studied area of the Veľká Stožka Massif is located within the Vepor Belt (Klinec, 1976; Vass et al., 1988; Vojtko et al., 2000). The wider area is composed of the (South) Veporic crystalline basement, with locally preserved Triassic sedimentary cover and overlying allochthonous Triassic sedimentary rocks of the Muráň nappe (Kronome et al., 2019; Figs. 1–2). The Veporic crystalline basement rocks are represented by granites and migmatites of the so-called Kráľova hoľa Complex (Klinec, 1966). The South Veporic cover rocks are mostly metamorphosed quartzites and phyllites, with locally preserved metamorphosed and often tectonized crystalline limestones, locally reworked into rauhwackes (Figs. 2–3). The Veporic rocks are overthrust by the Muráň nappe built mostly of Mesozoic carbonates. The basal décollement zone of the Muráň nappe is characterized by imbricated tectonic slices of Lower Triassic rocks with pink and grey rhyolites which are the main subject of this paper. The hanging wall of rhyolites is represented by Lower Triassic red/variegated sandy shales of the Hronsek Beds (upper part of the Benkovo Formation sensu Olšavský et al., 2010) and orange to yellow fine grained sandy marls of the Šuňava Formation. The Middle Triassic part of overlying sequence is composed of Anisian Gutenstein limestones and dolomites, Steinalm, Raming and Ráztoka limestones. The highest part of the Veľká Stožka Massif is formed of light grey Ladinian Wetterstein limestones (Kronome et al., 2019; Figs. 2–3).

Overall, three rhyolite bodies are located on the northern and western slopes of the Veľká Stožka Massif (Fig. 2). We were able to verify two of the bodies south of Závadka nad Hronom during our geological mapping:

1. Larger elongated body in the Dudlavka Valley, SE slopes of the Veľká Stožka Massif (48.768428° N, 19.946801° E) which is analysed in this paper;

2. Smaller body above the cottages on the western slope of the Veľká Stožka Massif; the rhyolite body is not exposed, its material is present only as a rock debris, not suitable for further analysis due to its low quality and volume;
3. The third rhyolite body was not visualized in the published map of the region (Klinec, 1976). Its presence was mentioned by Uher et al. (2002) and Ondrejka et al. (2015) at the end of Teplá dolina Valley, where it was not verified during the geological mapping.

Methods

Rhyolite rock samples were studied microscopically applying polarizing microscope for the purpose of basic petrographic description and obtaining data enabling the reconstruction of solidification during syn- to post-eruptive history. Subsequently, the samples were analysed using an electron microanalyzer "EPMA" in the Laboratory of electron microanalysis at the Dionýz Štúr State Geological Institute in Bratislava, cooperation with the analyst RNDr. Viera Kollárová, PhD.

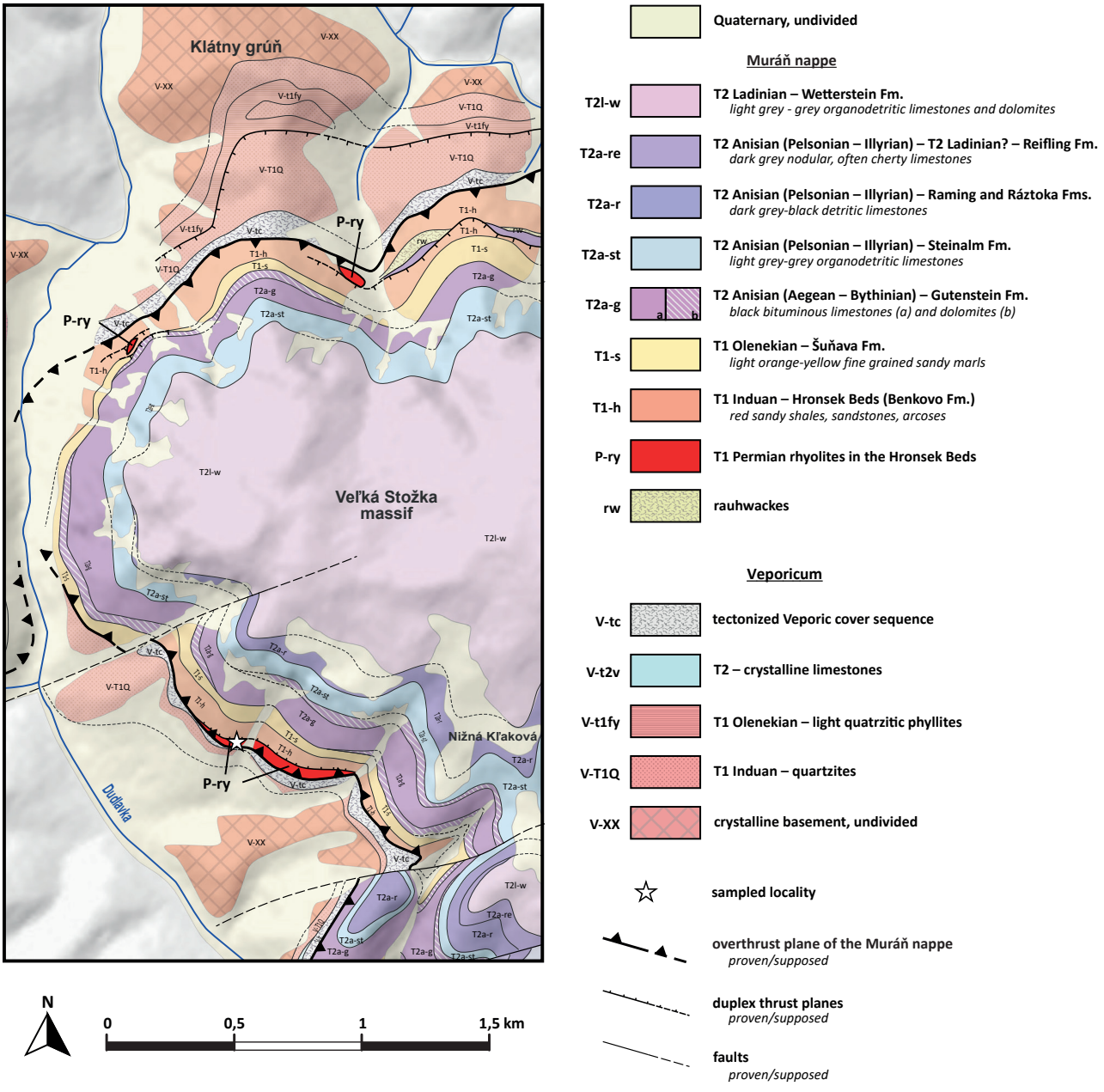

Fig. 2. Geological map of the studied area of the Veľká Stožka Massif (Kronome et al., 2019, modified). Permian rhyolites are marked by red colour. Location of the studied samples from the Dudlavka valley (48.768428° N, 19.946801° E).

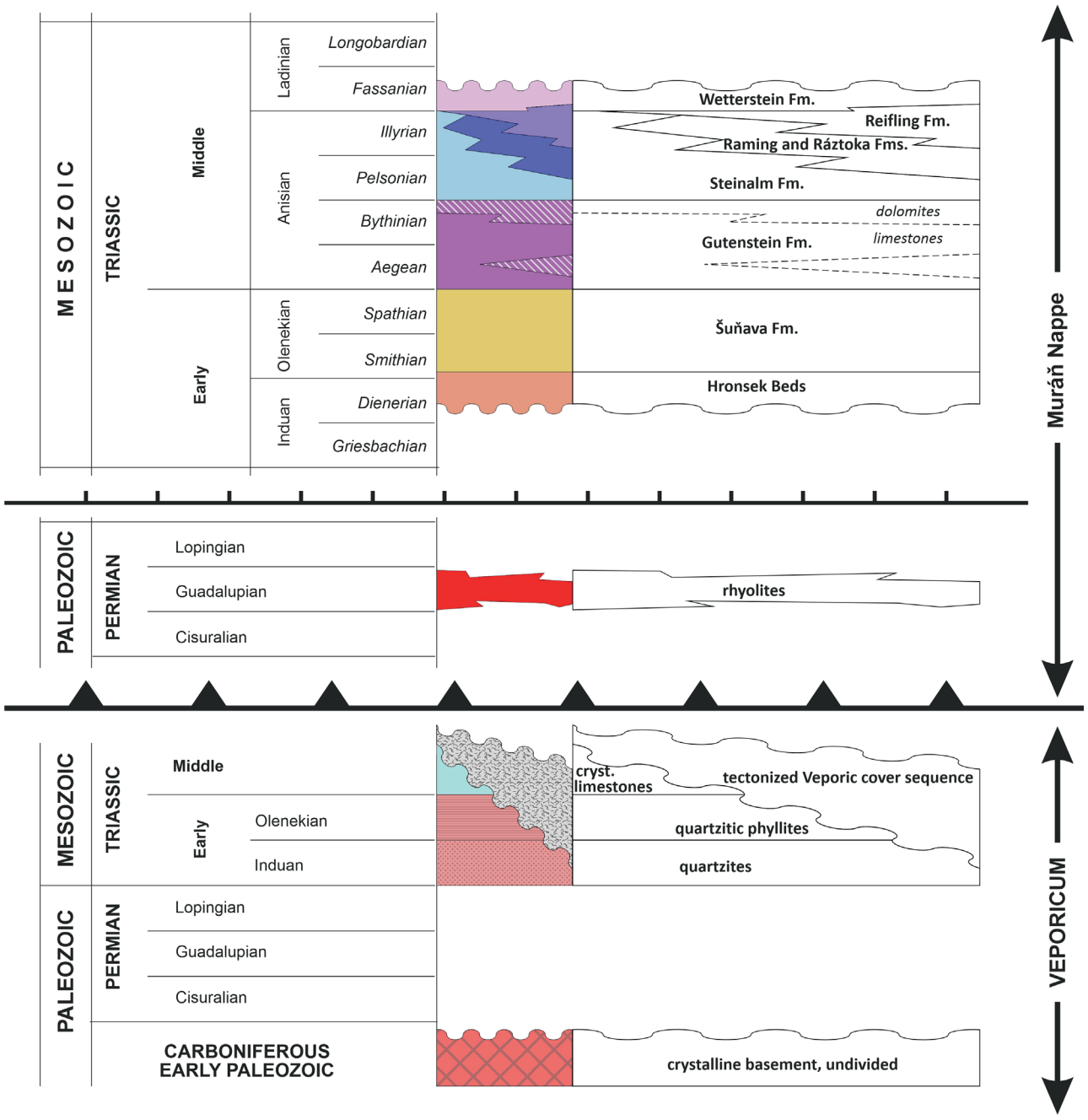

Fig. 3. Lithotectonic scheme of the studied area of the Veľká Stožka section, showing the relations of the South Veporic complexes and the Muráň nappe, including the rhyolite body tectonically incorporated into the base of the nappe. The thickness of the rhyolite body does not exceed 15–20 m.

Analyses of monazite crystals for geochronological dating purposes were done by Cameca SX-100 electron microanalyzer at analytical conditions of 15 kV accelerating voltage, analytical current of 80–150 nA, with 165 s a measurement time for Pb, Th, U, Y analysis and 25 s for other elements, and 3–5 μm defocused electron beam.

The principles of measuring method, analytical conditions and the method of result processing are presented in the work of Konečný et al. (2018). Individual magmatic ages for every measurement were calculated by methods described in Montel et al. (1996, 2017). The MONDAT program (P. Konečný) was used for the final software processing. The electron microanalyser was calibrated using the following standards and spectral lines shown in parentheses: Pb-PbS (Mα, LPeT), U-UO_2 (Mβ, LPeT), Th-ThO_2 (Mα, LPeT), Y-YPO_4 (Lα, LPeT), Ce-

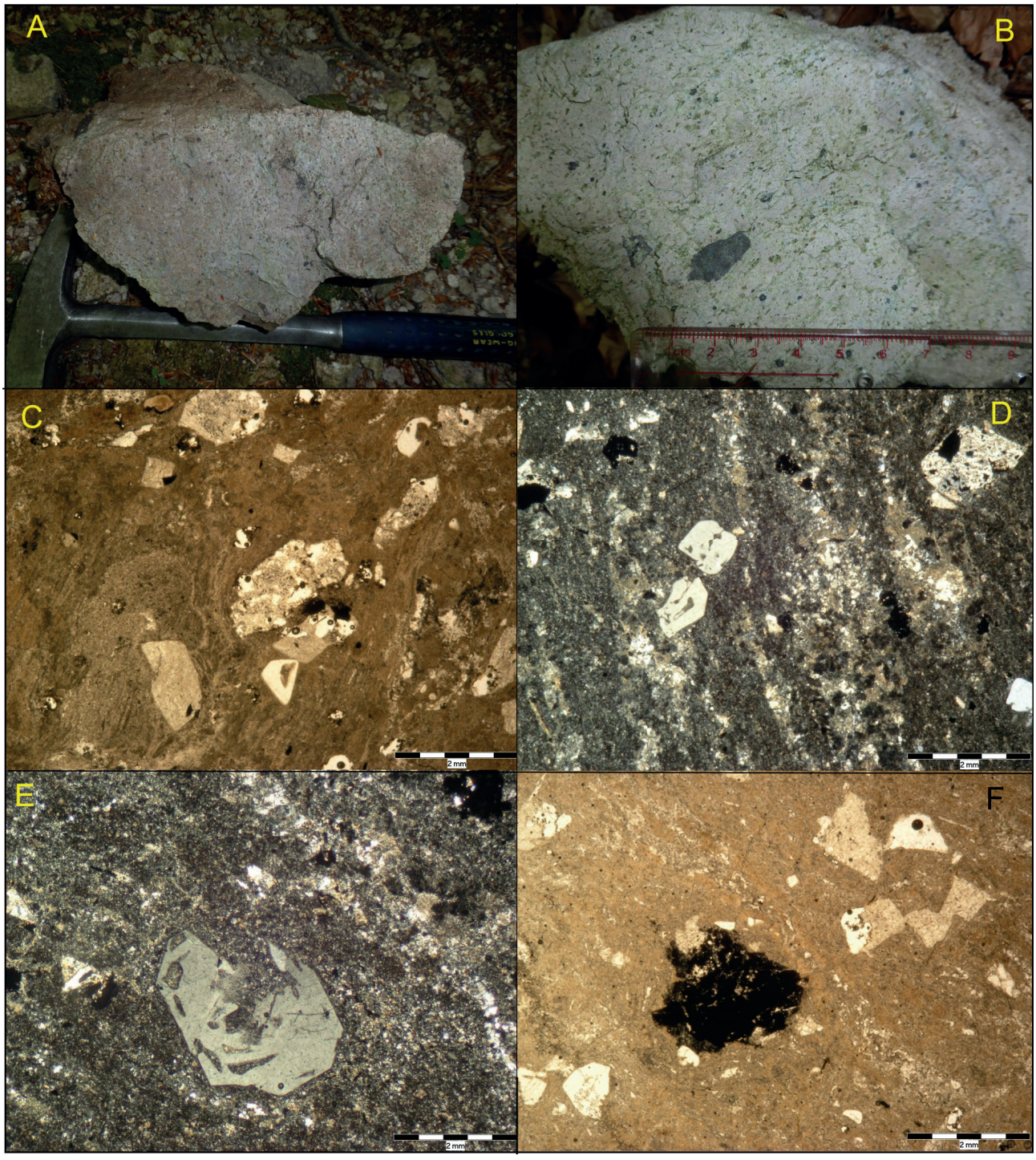

Fig. 4. Macroscopic and microscopic documentation of rhyolite rock samples from the Veľká Stožka Massif used for the geochronological study of chemical U-Th-Pb dating of monazites. A – rhyolite rock with reddish-white stripes created a fluidal structure; B – light rhyolitic rock with small microxenoliths of older rhyolite; C – porphyric rhyolite with phenocryst association formed by altered feldspar and magmatically corroded quartz. Red fluidal matrix and synvolcanic alteration of phenocrysts are typical features of extrusive and some subvolcanic rhyolite bodies (transmitted light); D – porphyric rhyolite with phenocrysts of corroded quartz, K-feldspar and Fe-Ti oxides. The allotriomorphic matrix with fluidic texture contains a parallel network of cracks as a result of shear deformation during the flow of a highly viscous rhyolitic magma. The crack network is filled by a low-temperature association of quartz and sericite; E – phenocryst of magmatically corroded quartz with partial transition to a skeletal habit as a consequence of intense thermodynamic parameters oscillation controlling SiO_2 saturation (crossed pollars); F – porphyritic rhyolite with phenocrysts of altered feldspar and quartz. The dark aggregate of Fe-Ti oxides in the central part is product of opacitization of mafic minerals, probably amphibole.

$CePO_4$ (Lα, LliF), La-$LaPO_4$ (Lα, LliF), Gd-$GdPO_4$ (Lα, LliF), Yb-$YbPO_4$, (Lα, LliF), Sm-$SmPO_4$ (Lβ, LliF), Pr-$PrPO_4$ (Lβ, LliF), Er-$ErPO_4$ (Lβ, LliF), Nd-$NdPO_4$ (Lβ, LliF), Lu-$LuPO_4$ (Lβ, LliF), Ho-$HoPO_4$ (Lβ, LliF), Dy-$DyPO_4$ (Lβ, LliF), Tb-$TbPO_4$ (Lα, LliF), Al-Al_2O_3 (Kα, TAP), wollastonite for Si and Ca (Kα, TAP), apatite for P (Kα, LPET).

Results

Petrography of analysed rhyolite rocks

The rhyolite rock samples are macroscopically porphyritic of mottled and striped structures with typical alternating reddish and light zones. In part of samples, microxenoliths of different structures occur (Fig. 4B). The phenocryst mineral association consists of feldspars, magmatically corroded β-quartz and Fe-Ti oxides (Fig. 4D, E, F). Part of the Fe-Ti oxides replaces the original mafic minerals, probably amphiboles (Fig. 4F). Intense alteration is manifested by feldspars sericitization, which are transformed into a mixture of light mica aggregate mixed with quartz and albite. The matrix has fluidal and holocrystalline allotriomorphic texture preceded into axiolitic, graphic, micropoikilitic to granophyric development.

The matrix is deformed locally by invasion of parallel network of deformation ruptures, which were originated as a result of cracks opening during shear deformation of the viscous rhyolitic magma stressed during flowing.

The opening cracks were cemented by low-temperature quartz and clay minerals during deformation accompanied by synvolcanic subsolidus alteration (Fig. 4D, E).

The observed interactions between association of magmatic minerals, mechanism of synvolcanic alteration linked to stage of highly viscous magma flowing, indicate a dynamic alteration associated with final stages of solidification, ductile deformation and controlled decompression devolatilization, i.e. conditions associated with eruptions of rhyolite extrusions or solidification of subvolcanic bodies. The intense alteration of the rhyolite body, which results in the decomposition of magmatic feldspars and the cementation of a matrix deformed in ductile conditions, is clearly related to the processes of the final stage of rhyolite solidification associated with devolatilization and eruptive emplacement of rhyolite. Rhyolites do not contain any signs associated with metamorphism, as a result of burial of the rhyolite body accompanied by with progressive increase in temperature and pressure.

Monazite dating

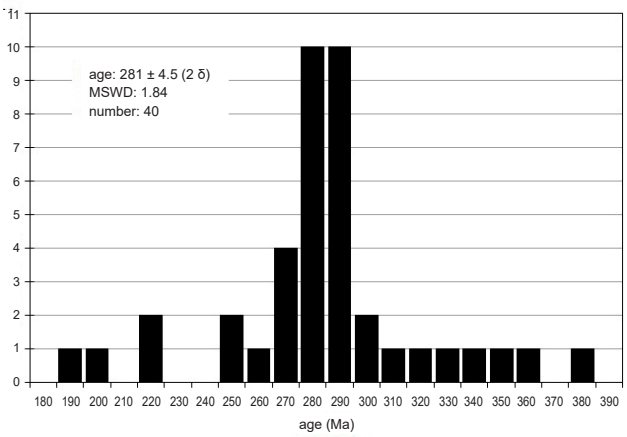

Fig. 5. Histogram of calculated ages for individual analyses of monazite crystals from rhyolite rock samples from Veľká Stožka. The weighted average of the calculated ages gives result of monazite magmatic crystallization in time 281 ± 4.5 Ma. The calculated ages create a sharp central maximum of 280–290 Ma, where the arithmetic mean (280 Ma) = median (280), based on which the result is considered correct.

Microprobe EPMA study of monazites identified small subhedral monazite crystals up to 20 μm in size in two rhyolite samples. Analytical data corrected for interference together with calculated ages for individual analyses are processed using the MONDAT ver. 5.5 program (P. Konečný) and listed in Tab. 1. Statistical processing of 40 measured analyses in the form of a weighted average for two separately analysed samples RY-01 and RY-02 gives the age of the rhyolite eruption of 281 ± 4.5 Ma. The identified crystallization age of the accessory monazite crystals corresponds to the magmatic age, which is practically identical to eruption age. Statistically processed results from individual measurements are presented in the form of a histogram in Fig. 5, where showed results are grouped into a sharp central maximum, corresponding to the interval of 280–290 Ma, where arithmetic mean (280 Ma) = median (280 Ma). The determined magmatic age of monazite crystallization, or age of rhyolite magma eruption 281 ± 4.5 Ma is partially different from 269.5 ± 1.8 Ma magmatic age, obtained by precise in-situ SIMS analysis of zircon crystals from the rhyolites of Veľká Stožka (Ondrejka et al., 2018). A partial 11 Ma difference between magmatic ages obtained by two different methods may not have analytical significance, since the identical age of 280 Ma is also captured by a separate analysis of euhedral core of an older zircon by U-Pb in-situ SIMS analysis No. 8 (Ondrejka et al., 2018). Considering practically ideal distribution with a sharp central maximum of 280–290 Ma, see Fig. 5, we assume a statistically identified age of 281 ± 4.5 Ma as correct and real.

Tab. 1

Th-U-Pb-Y data of measured monazite crystals, corrections for analytical interferences and magmatic ages, calculated by equations listed in Montel et al. (1996).

Grey boxes indicate samples after reduction for low analysed thorium and high absolute age deviation.
A reduced statistical set of analyses (n = 30) gives the same age of 281 ± 4.7 million years.

Analysis	Th	U	Pb	Y	Th corr	U corr	Pb corr	Th ± 2δ	U ± 2δ	Pb ± 2δ	Age Ma	Abs. dev.
mnz2-1	1.191	0.053	0.020	0.562	1.168	0.039	0.012	0.020	0.011	0.005	212.1	-69.0
mnz3-1	1.640	0.078	0.027	0.392	1.607	0.058	0.021	0.023	0.012	0.005	256.1	-24.9
mnz4-2	3.068	0.082	0.046	0.097	3.007	0.048	0.040	0.032	0.012	0.005	280.3	-0.7
mnz5-1	0.681	0.056	0.029	1.824	0.667	0.047	0.010	0.017	0.011	0.005	271.0	-10.0
mnz6-1	0.851	0.079	0.030	1.214	0.834	0.068	0.016	0.018	0.011	0.005	347.2	66.1
mnz7-1	6.890	0.247	0.103	0.538	6.752	0.168	0.089	0.054	0.012	0.006	273.0	-8.0
mnz7-2	6.831	0.220	0.101	0.540	6.694	0.142	0.086	0.054	0.012	0.006	270.4	-10.6
mnz8-1	1.920	0.042	0.022	0.228	1.882	0.022	0.016	0.025	0.011	0.005	184.3	-96.8
mnz9-1	5.423	0.132	0.085	0.599	5.315	0.072	0.072	0.046	0.012	0.006	289.8	8.8
mnz10-1	1.409	0.029	0.020	0.269	1.381	0.014	0.014	0.022	0.011	0.005	219.7	-61.3
mnz11-1	1.236	0.051	0.016	0.208	1.211	0.037	0.011	0.021	0.011	0.005	191.8	-89.2
mnz11-2	0.667	0.041	0.017	0.346	0.654	0.033	0.012	0.016	0.011	0.005	338.3	57.2
mnz12-1	2.876	0.086	0.047	0.511	2.819	0.054	0.037	0.030	0.011	0.005	280.2	-0.8
mnz12-2	2.450	0.068	0.049	0.468	2.401	0.041	0.040	0.028	0.011	0.005	353.3	72.2
mnz12-3	3.651	0.102	0.052	0.534	3.578	0.061	0.042	0.035	0.012	0.005	247.4	-33.6
mnz13-1	3.376	0.185	0.070	1.049	3.308	0.145	0.055	0.034	0.012	0.006	324.8	43.8
mnz14-1	1.887	0.123	0.040	1.420	1.849	0.100	0.024	0.025	0.012	0.005	246.7	-34.3
mnz15-1	1.425	0.051	0.031	0.280	1.396	0.035	0.025	0.022	0.011	0.005	375.4	94.3
mnz16-1	1.437	0.034	0.022	0.061	1.408	0.019	0.018	0.021	0.011	0.005	279.9	-1.1
mnz17-1	5.087	0.110	0.076	0.434	4.985	0.054	0.064	0.043	0.011	0.005	279.8	-1.2
mnz17-2	5.078	0.107	0.074	0.467	4.976	0.051	0.063	0.043	0.012	0.005	273.5	-7.6
mnz17-3	3.946	0.098	0.061	0.585	3.867	0.054	0.050	0.037	0.012	0.005	276.2	-4.8
mnz17-4	4.041	0.092	0.059	0.405	3.960	0.048	0.049	0.038	0.012	0.005	266.5	-14.5
mnz17-5	3.962	0.102	0.064	0.660	3.882	0.058	0.052	0.037	0.012	0.006	284.3	3.2
mnz18-1	4.182	0.112	0.064	0.640	4.099	0.066	0.052	0.038	0.011	0.005	268.5	-12.5
mnz18-2	4.810	0.125	0.074	0.567	4.714	0.072	0.062	0.042	0.012	0.005	279.1	-1.9
mnz18-3	4.266	0.102	0.067	0.459	4.180	0.056	0.056	0.038	0.011	0.005	287.9	6.9
mnz18-4	4.129	0.134	0.071	0.958	4.046	0.088	0.056	0.038	0.012	0.005	289.0	8.0
mnz18-5	3.918	0.089	0.058	0.425	3.839	0.046	0.049	0.036	0.011	0.005	272.7	-8.3
mnz18-6	3.976	0.094	0.069	0.556	3.897	0.050	0.058	0.037	0.011	0.005	319.8	38.8
mnz19-1	6.751	0.168	0.102	0.524	6.615	0.093	0.088	0.054	0.012	0.006	283.9	2.8
mnz19-2	6.729	0.178	0.104	0.510	6.595	0.103	0.090	0.053	0.012	0.006	291.9	10.9
mnz19-3	6.657	0.173	0.104	0.540	6.524	0.099	0.090	0.053	0.012	0.006	294.2	13.2
mnz19-4	6.746	0.177	0.102	0.526	6.611	0.102	0.088	0.053	0.012	0.006	282.4	1.4
mnz20-1	4.148	0.100	0.064	0.510	4.065	0.055	0.053	0.038	0.012	0.006	280.8	-0.3
mnz21-1	4.279	0.097	0.065	0.402	4.193	0.050	0.055	0.039	0.012	0.006	282.0	0.9
mnz21-2	4.266	0.104	0.064	0.429	4.181	0.057	0.053	0.038	0.011	0.005	274.4	-6.6
mnz21-3	5.170	0.131	0.074	0.445	5.066	0.073	0.062	0.044	0.012	0.005	263.2	-17.9
mnz22-1	4.010	0.095	0.060	0.511	3.930	0.051	0.049	0.037	0.011	0.005	267.1	-13.9
mnz22-2	3.682	0.103	0.063	0.561	3.608	0.062	0.052	0.035	0.012	0.005	304.6	23.6

Discussion – Permian magmatic activity in the area of the Internal Western Carpathians

Based on results of previous research, focused on the Gregová rhyolite extrusion near Telgárt village and identification of its Permian age, it was assumed that allmost all rhyolite bodies in Silicicum (sensu Plašienka et al., 1997), previously considered as Triassic, may be of Permian age (Demko & Hraško, 2013). This assumption was later confirmed by Ondrejka et al. (2018, 2022). The originally raised questions (Demko & Hraško, 2013), whether it is a single massive rhyolite province active in one time period and later tectonically fragmented, or a rhyolite volcanism active during a longer time with migrating activity in time and space, can be answered using the synthesis of new geochronological data (Fig. 6).

A set of Permian rhyolite bodies (Gregová, Veľká Stožka, Poniky), which are located in the Upper Hron Valley assigned to the Silicicum (sensu Plašienka et al., 1997) are tectonically amputated from their basement and incorporated into a complex of Lower Triassic sediments at the base of these nappes (Demko & Hraško, 2013; Ondrejka et al., 2018, 2022). A comparison of geochronological data (Demko & Hraško, 2013; Ondrejka et al., 2018, 2022 and Demko et al., this work) shows a separate age of each body, in chronological sequence Veľká Stožka (281 ± 4.5) → Poniky, Piesky (271 ± 1.5) → Veľká Stožka, (269.5 ± 1.8) → Poniky, Žiarec (267 ± 1.6) → Tisovec-Rejkovo (266.6 ± 2.4) → Gregová (263 ± 3.5; 263.3 ± 1.9), while in the rhyolite body on the western slopes below Veľká Stožka Massif, two age-separate volcanic pulses are identified (this work). The situation indicates a rhyolitic volcanic activity in the wide time span between 281–263 Ma, which took place in the form of separate volcanic pulses migrating in time and space. In the present tectonic structure rhyolite bodies are tectonically amputated from their sedimentary and volcanic environment. Tectonic and erosional activity caused their volume reduction, when mainly the rigid cores of extrusive bodies were preserved. Traces of pyroclastic volcanic activity remained preserved only to a limited extent. These are relics of ignimbrites at the Gregová hill (Demko & Hraško, 2013) and relics of lithoclastic and lapilli tuffs at the Poniky area (Slavkay, 1965, 1981). Migrating eruptions of rhyolite magmas in the period 281–263 Ma in the geochronological synthesis (Fig. 6) show hiatus or cessation of magmatic activity (after 280 Ma) for a time span 9 Ma between 280–271 Ma. This cessation in volcanic activity (280–271 Ma) was followed by next incoming separate magmatic episodes 271 → 269 → 267 → 263 Ma. The identified magmatic hiatus is fundamental for the understanding of wider magmatic and volcanic events and relationships in the realm of the Permian magmatic provinces in the Internal Western Carpathians.

Activity of rhyolitic volcanic centres in the studied area of VAFZ is synchronous in time with andesite volcanic activity (267 Ma) of the Čierna hora Mts. (Vozárová et al., 2021), acid volcanism 268–267 Ma was recorded in the Rožňava Fm. in the Southern Gemericum (Vozárová et al., 2009), basic volcanism of Veporicum (267 Ma) in the Tribeč Mts. (Vozárová et al., 2020), acid volcanism in the Infratatricum 267–262 Ma (Putiš et al., 2016) and also with basic magmatic activity in the Tatric unit in time 260 Ma (Pelech et al., 2017) and 263 Ma (Spišiak et al., 2018). Time-synchronous volcanic activity is assumed in the space of the Permian sedimentary area of the Hronicum unit (Vozár, 1977; Vozárová & Vozár, 1988). The termination of magmatic activity in the VAFZ in the Internal Western Carpathians (263 Ma) is highlighted by the production of basaltic lavas recorded in the Permian of Tribeč Mts. (Vozárová et al., 2020) and intrusive activity of S-type granites placed in Gemericum domain 265 Ma (Poller et al., 2000), 265–263 Ma (Kohút & Stein, 2005) and 263 Ma (Finger et al., 2003). The magmatic activity in the VAFZ overlaps in time interval between 281–263 Ma with the magmatic activity of several units of the Internal Western Carpathians, but their synchronicity and petrogenetic causality may be purely coincidental. It is precisely in these contexts that the magmatic hiatus of volcanic activity in the VAFZ of the Internal Western Carpathians appears to be fundamentally important. It is marginally synchronous with the volcanic activity of the Northern Gemericum, namely rhyolite tuff 278 Ma (Rojkovič & Konečný, 2005) and zircon detritus 281–276 Ma (Vozárová et al., 2019), 275–272 Ma andesite-rhyolite volcanism occurred in Petrova hora Fm. (Vozárová et al., 2012) and the most important dacite-trachyandesite volcanism of the Northern Veporic 279–273 Ma was recorded in the Harnobis volcanogenic horizon of Brusno Fm. – 279–273 Ma (Vozárová et al., 2016). The sharp, time-limited concurrence of volcanic activity in original space of the Harnobis volcanogenic horizon accompanied by cessation of magmatic activity in VAFZ, discussed in this work is most probably not coincidental.

The specific paleovolcanic situation can be explained by the wider geodynamic relationship between terrains of the Internal Western Carpathians during the Permian, when the dacite-trachyandesite volcanic activity (279–273 Ma) of the Harnobis volcanogenic horizon (Vozárová et al., 2016) reflected the release of tectonic stress in the continental crust of the Northern Veporic domain, where the adjacent continental crust remained in tectonic stress shadow.

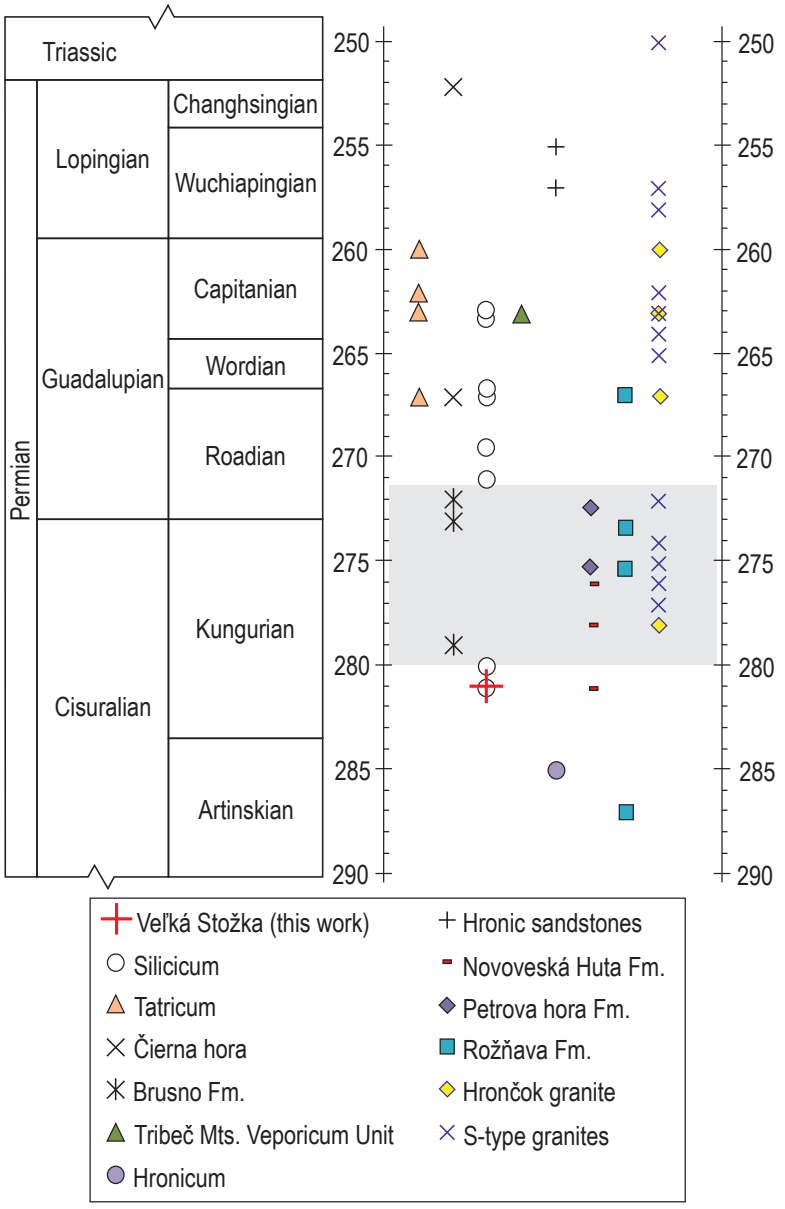

Fig. 6. Graphically presented synthesis of geochronological results of magmatic events in the Permian of Tatricum, Veporicum and Gemericum of the Internal Western Carpathians. The grey marked area is determined by the magmatic hiatus identified by the absence of geochronological data from VAFZ rhyolite volcanism between 280–271 Ma (based on data by Demko & Hraško, 2013; Ondrejka et al., 2018, 2021, 2022 and Demko et al., this study). The sources used in the synthesis from Tatricum (Putiš et al., 2016; Pelech et al., 2017; Spišiak et al., 2018), Veporicum (Čierna hora Mts.: Vozárová et al., 2021; Tribeč Mts.: Vozárová et al., 2020; Harnobis volcanogenic horizon: Vozárová et al., 2016), Hronicum (Vozár, 1977; Vozár et al., 2015; Vozárová & Vozár, 1988; Vozárová et al., 2014; Demko & Olšavský, 2007; Demko & Olšavský, 2007); Northern Gemericum (Vozárová et al., 2019; Novoveská Huta Fm.: Rojkovič & Konečný, 2005; Petrova hora Fm.: Vozárová et al., 2012); Southern Gemericum (Rožňava Fm.: Vozárová et al., 2009). Data sources from Veporic Hrončok granite (Cambel et al., 1977; Kotov et al., 1996; Ondrejka et al., 2021; Finger et al., 2003; Putiš et al., 2000) and Gemeric S-type granites (Finger & Broska, 1999; Poller et al., 2000; Finger et al., 2003; Kohút & Stein, 2005; Radvanec et al., 2009; Kubiš & Broska, 2010; Villaseñor et al., 2021).

The termination of geodynamic stress compensation (for example, by subduction termination gradually changing into collision) in the area of the Northern Veporic domain caused a tectonic stress migrating to more southern zones, where it is evidenced by the initiation of pulsating volcanic activity in the VAFZ (from 271 Ma). The discussed VAFZ volcanic activity between 271–263 Ma are clearly results of stress compensation from area of wedged terrain continental blocs to free space along deep seated crust-mantle fault zones as a result of the relaxation of the transferred stress. In other words, centers of rhyolitic volcanic activity in VAFZ during the Permian in the realm of the Internal Western Carpathians were located in the fault zones of the continental crust, along which stress relaxation took place. The presented tectonic processes of a transpressional-transtensional tectonics induced melting of the mantle, whose magmas intruded the continental crust and created discussed rhyolite magmas by anatectic and fractionation mechanisms. Current paleomagmatic reconstructions based on correlations of Permian magmatic activity link the discussed Permian "Silicic" rhyolitic volcanism (sensu Ondrejka et al., 2018, 2021, 2022) with intrusions of mantle magmas into the continental crust, where they induced melting of quartz-feldspar rocks to form rhyolitic magmas in the extensional tectonic regime as part of the "disintegration of the Pangea supercontinent during the Permian – Triassic period" (Ondrejka et al., l. c.).

Our different view on tectono-magmatic processes associated with the formation of rhyolite magmas in the VAFZ is the active participation of transpressional-transtensional tectonics, in contrast to the extension supported concept by the aforementioned authors. The centres of volcanic activity in domain of rhyolite volcanism were definitely located on the VAFZ, because the faults provide ideal structures for transport of acidic magmas to the Earth's surface. However, we favour transpressional-transtensional tectonic processes (as opposed to extensional tectonics), since no basic eruptive rocks are observed with rhyolites in VAFZ. Active

extension destabilizes crustal filter allowing blocking of intruded mantle magmas into continental crust, reduces volume of crustal rocks anatexis and practically supports straight eruptions of basalts to Earth's surface, which were not observed. We observe exactly opposite situation of what was discussed, namely due to the petrographic and compositional homogeneity of VAFZ rhyolitic rocks without basic rocks in association in time and space (Veľká Stožka, Gregová, Tisovec, Poniky).

Conclusions

- The rhyolite body located on the SW slope of Veľká Stožka Massif is one of several examples of Permian rhyolites tectonically displaced and incorporated into the younger Triassic sedimentary formations at the base of the Muráň nappe.
- Electron microprobe dating of monazite crystals from Veľká Stožka rhyolite body provides new information on the Permian age of rhyolitic volcanism.
- The presented geochronological result 281 ± 4.5 Ma complements previous in-situ zircon U-Pb SIMS age 269.5 ± 1.5 Ma of Ondrejka et al. (2018) and suggests not a single rhyolite eruption in the original volcanic area but several eruptional pulses repeating in time.
- According to geochronological data from similar tectonically amputated rhyolitic bodies of VAFZ (Volcanically Active Fault Zones; Gregová, Veľká Stožka, Poniky, Tisovec) a hiatus is observed in eruptive activity between 280–271 Ma.
- Using actual geochronological data of the Permian volcanic rocks in the tectonic units of the Internal Western Carpathians, we suggest important correlation of eruptive events between observed hiatus of VAFZ rhyolitic group and the Permian volcanic activity in the Harnobis volcanogenic horizon of the Northern Veporicum (279–273 Ma; Vozárová et al., 2016), Permian volcanism in the Northern Gemeric Petrova hora Fm. (275–272 Ma; Vozárová et al., 2012) and Novoveská Huta Fm. (281–276 Ma; Rojkovič & Konečný, 2005; Vozárová et al., 2019).
- The cessation of Permian eruptive activity in the present day Northern Veporic and/or Northern Gemeric area as well as the resuming of the interrupted rhyolitic volcanism in the VAFZ suggest change, reorganisation and transfer of tectonic stress during the Permian in Internal Western Carpathian before 272/271 Ma.

Acknowledgement

This research was supported by the project of the Ministry of Environment of Slovak Republic no. 17 13 Research of geological structure and compilation of geological maps in problematic areas of the Slovak Republic – Topic: A – 01/14 Geological structure of the Muránska planina Plateu. Special thanks are dedicated to RNDr. Viera Kollárová, PhD., for the analytical assistance and help with monazite measurements. Authors express their thanks to Jozef Hók and Martin Ondrejka (Comenius University in Bratislava) for their valuable comments.

References

Biely, A., 1956: Zpráva o základnom geologickom výskume severovýchodných svahov Kráľovej Holi. *Manuscript. Bratislava, archive St. Geol. Inst. D. Štúr*.

Cambel, B., Shcherbak, N. P., Kamenický, L., Bartnicky, J. N. & Veselský, J., 1977: Nekatorye svedeniya po geochronologii kristallinikuma Zapadnich Karpat na osnove dannych U-Th-Pb metoda. *Geol. Zbor. Geol. carpath., 28, 243–259.*

Demko, R. & Olšavský, M., 2007: Otázka ryolitového detritu v malužinskom súvrství. *Miner. Slov., 39, 4, Geovest., 8–9.*

Demko, R. & Hraško, L., 2013: Ryolitové teleso Gregová pri Telgárte. *Miner. Slov., 45, 4, 161–174.*

Finger, F. & Broska, I., 1999: The Gemeric S-type granites in southeastern Slovakia: Late Paleozoic or Alpine intrusions? Evidence from electron-microprobe dating of monazite. *Schweiz. Mineral. Petrogr. Mitt., 79, 439–443.*

Finger, F., Broska, I., Haunschmid, B., Hraško, Ľ., Kohút, M., Krenn, E., Petrík, I., Riegler, G. & Uher, P., 2003: Electron microprobe dating of monazites from Western Carpathian basement granitoids: plutonic evidence for an important Permian rifting event subsequent to Variscan crustal anatexis. *Int. J. Earth Sci., 92, 86–98. https://doi.org/10.1007/s00531-002-0300-0.*

Grenar, A. & Kotásek, J., 1956: Výskyt křemitých porfyrů vewerfenu Chočského příkrovu na SSZ od Ponik. *Geol. Práce, Zpr., 8, 187–188.*

Havrila, M., 1997: Vzťah hronika a silicika. *Manuscript. Bratislava, archive St. Geol. Inst. D. Štúr, 31 p.*

Hók, J. & Olšavský, M., 2023: Vernaricum – extension, litostratigraphy, tectonics and paleogeography. *Miner. Slov., 55, 1.*

Hók, J., Havrila, M., Rakús, M., Vojtko, R. & Kráľ, J., 2004: Nappe contact as a tool for paleotectonic reconstruction (Inner Western Carpathians a case of study). *Geolines, 17, 39–40.*

Klinec, A., 1966: K problémom stavby a vzniku veporského kryštalinika. *Zbor. geol. Vied, Západ. Karpaty, 6, 7–27.*

Klinec, A. (ed.), 1976: Geologická mapa Slovenského rudohoria a Nízkych Tatier 1 : 50 000. *Bratislava, Geol. Úst. D.* Štúra.

Kohút, M. & Stein, H., 2005: Re-Os molybdenite dating of granite related Sn-W-Mo mineralization at Hnilec, Gemeric Superunit, Slovakia. *Mineral. petrogr., 85, 117–129. https://doi.org/10.1007/ s00710-005-0082-8.*

Konečný, P., Kusiak, M. A. & Dunkley, D. J., 2018: Improving U-Th-Pb electron microprobe dating using monazite age references. *Chem. Geol., 484, 22–35. https://doi.org/10.1016/j.chemgeo.2018.02.014.*

Kotov, A. V., Miko, O., Putiš, M., Korikovsky, S. P., Salnikova, Y. V., Kovach, V. P., Yakovleva, S. Z., Bereznaya, N. G., Kráľ, J. & Krist, E., 1996: U/Pb dating of zircons of postorogenic acid metavolcanics: a record of Permian-Triassic taphrogeny of the West-Carpathian basement. *Geol. Carpath., 47, 73–79.*

Kováříк, J., 1955: Geologie západních okrajů Muráňské plošiny. Diplomová práca. *Manuscript. Bratislava, archive St. Geol. Inst. D. Štúr (arch. n. 19270), 76 p.*

Kravjanský, I., 1961: Dielčia záverečná správa o vyhľadávacom prieskume a výpočet zásob, lokalita: Poniky-Drienok sever, surovina: Pb, Zn, Cu rudy a vápenec, vyhľadávací prieskum, stav k 1.1.1961. *Manuscript. Bratislava, archive St. Geol. Inst. D. Štúr (arch. n. 55199).*

Kravjanský, I., 1964: Prieskumné práce na okolí Poník. *Zpr. geol. Výzk. v r. 1963, 2, Slovensko, 98–100.*

Kravjanský, I., 1966: Poniky – surovina: Pb-Zn rudy, vyhľadávací prieskum, ročná správa o geologicko-prieskumných prácach za rok 1965. *Manuscript. Bratislava, archive St. Geol. Inst. D. Štúr (arch. n. 16895_3).*

Kravjanský, I., Slavkay, M. & Barkáč, Z., 1966: Stav preskúmanosti na ložisku Drienok a problémy riešenia k 1. 5. 1966. *Manuscript. Bratislava, archive St. Geol. Inst. D. Štúr (arch. n. 98367), 77 p.*

Kronome, B., Boorová, D., Buček, S., Olšavský, M., Sentpetery, M., Pelech, O., Maglay, J. & Vlačiky, M., 2019: Geologická stavba Muránskej planiny. Názov geologickej úlohy: Výskum geologickej stavby a zostavenie geologických máp v problematických územiach Slovenskej republiky. *Manuscript. Bratislava, archive St. Geol. Inst. D. Štúr, 134 p.*

Kubiš, M. & Broska, I., 2010: The granite system near Betliar village (Gemeric Superunit, Western Carpathians): evolution of a composite silicic reservoir. *J. Geosci., 55, 131–148. https://doi.org/10. 3190/jgeosci.066.*

Kusák, B., 1967: Geologicko-petrografické pomery územia medzi Šumiacom a Vernárom. Mastersthesis. *Manuscript. Bratislava, archive St. Geol. Inst. D. Štúr (arch. n. 18422), 74 p.*

Losert, J., 1963: Geologie a petrografie západní části ľubietovské zóny a přilehlého subtatrika. *Rozpr. Čs. Akad. Věd, 73, 12, 3–91.*

Maheľ, M., 1986: Geologická stavba československých Karpát. Paleoalpínske jednotky I. *Bratislava, Veda, vyd. Sov. Akad. Vied, 503 p.*

Mello, J. (ed.), Filo, I., Havrila, M., Ivan, P., Ivanička, J., Madarás, J., Németh, Z., Polák, M., Pristaš, J., Vozár, J., Vozárová, A., Liščák, P., Kubeš, P., Scherer, S., Siráňová, Z., Szalaiová, V. & Žáková, E., 2000: Vysvetlivky ku geologickej mape Slovenského raja, Galmusu a Hornádskej kotliny 1 : 50 000. *Bratislava, Št. Geol. Úst. D. Štúra, 303 p.*

Montel, J.-M., Foret, S., Veschambre, M., Nicollet, Ch. & Provost, A., 1996: Electron microprobe dating of monazite. *Chem. Geol., 131, 37–53. https://doi.org/10.1016/0009-2541(96)00024-1.*

Montel, J.-M., Kato, T., Enami, M., Cocherie, A., Finger, F., Williams, M. & Jercinovic, M., 2017: Electron-microprobe dating of monazite: The story. *Chem.Geol., 484. https://doi.org/10.1016/j.chemgeo.2017.11.001.*

Náprstek, V., 1958: Výsledky geologického mapovaní mezi Slovenskou Ľupčou a Poniky. *Geol. Práce, Zpr., 14, 134–138.*

Olšavský, M. & Demko, R., 2007: Mladšie paleozoikum Hronika na SZ svahoch Nízkych Tatier. Čiastk. správa k záver. správe geologickej úlohy: Aktualizácia geologickej stavby problémových území Slovenska v mierke 1 : 50 000. *Manuscript. Bratislava, archive St. Geol. Inst. D. Štúr (arch. n. 91 733-43), 95 p.*

Olšavský, M., Šimo, V. & Golej, M., 2010: Hronsecké vrstvy: korelačný člen medzi silicikom s. l. (drienocký príkrov) a hronikom (frankovský príkrov, Západné Karpaty). *Miner. Slov., 42, 407–418.*

Ondrejka, M., 2004: A-type rhyolites of the Silicic Superunit in the Permian-Triassic continental rifting in the Western Carpathians: geochemistry, mineralogy, petrology. PhD thesis. *Manuscript, Bratislava, archive Comenius Univ., 129 p.*

Ondrejka, M., Uher, P., Pršek, J. & Ozdín, D., 2007: Arsenian monazite-(Ce) and xenotime-(Y), REE arsenates and carbonates from the Tisovec-Rejkovo rhyolite, Western Carpathians, Slovakia: Composition and substitutions in the (REE,Y)XO 4 system (X = P, As, Si, Nb, S). *Lithos, 95, 116–129. https://doi.org/10.1016/j.lithos.2006.07.019.*

Ondrejka, M., Broska, I. & Uher, P., 2015: The late magmatic to subsolidus T-fO2 evolution of the Lower Triassic A-type rhyolites (Silicic Superunit, Western Carpathians, Slovakia): Fe-Ti oxythermometry and petrological implications. *Acta Geol. Slov., 7, 51–61.*

Ondrejka, M., Li, X.-H., Vojtko, R., Putiš, M., Uher, P. & Sobocký, T., 2018: Permian A-type rhyolites of the Muráň Nappe, Inner Western Carpathians, Slovakia: in-situ zircon U-Pb SIMS ages and tectonic setting. *Geol. Carpath., 69, 2, 187–198. https://doi.org/10.1515/geoca-2018-0011.*

Ondrejka, M., Uher, P., Putiš, M., Kohút, M., Broska, I., Larionov, A., Bojar, A.-V. & Sobocký, T., 2021: Permian Atype granites of the Western Carpathians and Transdanubian regions: products of the Pangea supercontinent breakup. *Int. J. Earth Sci., 110, 6, 2133–2155. https://doi.org/10.1007/s00531-021-02064-2.*

Ondrejka, M., Vojtko, R., Putiš, M., Chew, D., Olšavský, M., Uher, P., Nemec, O., Drakou, F., Molnárová, A. & Spišiak, J., 2022: Permian A-type rhyolites of the Drienok Nappe, Inner Western Carpathians, Slovakia: Tectonic setting from in-situ zircon U-Pb LA-ICP-MS dating. *Geol. Carpath., 73, 2, 123–136. https://doi.org/10.31577/GeolCarp.73.2.2.*

Oppenheimer, J., 1931: Die geologischen Verhältnisse der Bahn Červená Skala – Margecany. *Věst. St. geol. Úst., 7, 417–422.*

Orlický, O. & Slavkay, M., 1979: Paleomagnetický výskum kampilských paleovulkanitov príkrovu Drienok. *Miner. Slov., 11, 5, 439–451.*

Pelech, O, Vozárová, A., Uher, P., Petrík, I., Plašienka, D., Šarinová, K. & Rodionov, N., 2017: Late Permian volcanic dykes in the crystalline basement of the Považský Inovec Mts. (Western Carpathians): U-Th-Pb zircon SHRIMP and

monazite chemical dating. *Geol. Carpath., 68, 530–542. https://doi.org/10.1515/geoca-2017-0035.*

Plašienka, D., 1981: Tektonické postavenie niektorých metamorfovaných mezozoických sérií veporika. Kandidátska dizertačná práca. *Manuscript. Bratislava, archive St. Geol. Inst. D. Štúr, 153 p.*

Plašienka, D., Grecula, P., Putiš, M., Kováč, M. & Hovorka, D., 1997: Evolution and structure of the Western Carpathians: an overview. In: Grecula, P., Hovorka, D. & Putiš, M. (eds.): Geological evolution of the Western Carpathians. *Bratislava, Miner. Slov., Monogr., 1–24.*

Poller, U., Broska, I., Finger, F., Uher, P. & Janák, M., 2000: Permian age of Gemeric granites constrained by single zircon and EMPA monazite dating. *Miner. Slov., 32, 189–190.*

Putiš, M., Kotov, A. B., Uher, P., Salnikova, E. & Korikovsky, S. P., 2000: Triassic age of the Hrončok pre-orogenic A-type granite related to continental rifting: a new result of U-Pb isotope dating (Western Carpathians). *Geol. Carpath., 51, 59–66.*

Putiš, M., Li, J., Ružička, P., Ling, X. & Nemec, O., 2016: U/Pb SIMS zircon dating of a rhyolite intercalation in Permian siliciclastics as well as a rhyodacite dyke in micaschists (Infratatricum, W. Carpathians). *Miner, Slov., 48, 99–108.*

Radvanec, M., Konečný, P., Ondrejka, M., Putiš, M., Uher, P. & Németh, Z., 2009: The Gemeric granites as an indicator of the crustal extension abovethe Late-Variscan subductionzone and during the Early Alpine riftogenesis (Western Carpathians): an interpretation from the monazite and zircon ages dated by CHIME and SHRIMP methods. *Miner. Slov., 41, 381–394 (In Slovak with English summary).*

Rojkovič, I. & Konečný, P., 2005: Th-U-Pb dating of monazite from the Cretaceous uranium vein mineralization in the Permian rocks of the Western Carpathians. *Geol. Carpath., 56, 493–502.*

Rozložník, O., Tomko, I. & Bartalský, J., 1974: SGR – sádrovec – VP so stavom 1. 1. 1974, záverečná správa a výpočet zásob, lokality: Pusté Pole, Bohúňovo. *Manuscript. Bratislava, archive St. Geol. Inst. D. Štúr (arch. n. 33478), 295 p.*

Slavkay, M., 1965: Vulkanogenné horniny mezozoika na okolí Ponik. *Čas. Mineral. Geol., 10, 249–259.*

Slavkay, M., 1971: Ložiská polymetalických rúd pri Ponikách. *Miner. Slov., 3, 11, 181–213.*

Slavkay, M., 1981: Paleovulkanity a zrudnenie v spodnom triase príkrovu Drienka. In: Bajaník, Š. & Hovorka, D. (eds.): Paleovulkanizmus Západných Karpát. *Bratislava, Geol. Úst. D. Štúra, 137–144.*

Slavkay, M., Tomko, I., Lukaj, M. & Barkáč, M., 1968: Poniky Pb-Zn rudy. Záverečná správa z etapy vyhľadávacieho prieskumu a výpočet zásob so stavom k 30. XI. 1968. *Manuscript. Bratislava, archive St. Geol. Inst. D. Štúr (arch. n. 22903).*

Spišiak, J., Vetráková, L., Chew, D., Ferenc, Š., Mikuš, T., Šimonová, V. & Bačík, P., 2018: Petrology and dating of the Permian lamprophyres from the Malá Fatra Mts. (Western Carpathians, Slovakia). *Geol. Carpath., 69, 453–466. 10.1515/geoca-2018-0026.*

Stur, D., 1868: Bericht über die geologische Aufnahme im oberen Waag und Gran-Thale. *Jb. K.-Kön. geol. Reichsanst., 18, 337–426.*

Uher, P., Ondrejka, M., Spišiak, J., Broska, I. & Putiš, M., 2002: Lower Triassic potassium-rich rhyolites of the Silicic Unit, Western Carpathians, Slovakia: geochemistry, mineralogy and geneticaspects. *Geol. Carpath., 53, 1, 27–36.*

Vass, D., Began, A., Gross, P., Kahan, Š., Krystek, I., Köhler, E., Lexa, J., Nemčok, J., Ružička, M. & Vaškovský, I., 1988: Regionálne geologické členenie Západných Karpát a severných výbežkov Panónskej panvy na území ČSSR. Mapa 1 : 500 000. *Bratislava, Geol. Úst. D.* Štúra.

Vojtko, R., Hók, J., Kováč, P., Madarás, J. & Filová, I., 2000: Geological structure and tectonic evolution of the Southern Veporicum. *Slovak Geol. Mag., 6, 2–3, 287–292.*

Villaseñor, G., Catlos, E. J., Broska, I., Kohút, M., Hraško, Ľ., Aguilera, K., Etzel, T., Kyle, J. R. & Stockli, D. F., 2021: Evidence for widespread mid-Permian magmatic activity related to rifting following the Variscan orogeny (Western Carpathians). *Lithos, 390–391. https://doi.org/10.1016/j.lithos.2021.106083.*

Vozár, J., 1977: Magmatic rocks of tholeitic series in the Permian of the Choč Nappe of the Western Carpathians. *Miner. Slov., 9, 4, 241–258.*

Vozár, J., Spišiak, J., Vozárová, A., Bazarnik, J. & Kráľ, J., 2015: Geochemistry and Sr, Nd isotopic composition of the Hronic Upper Paleozoic basic rocks (Western Carpathians, Slovakia). *Geol. Carpath., 66, 3–17. https://doi.org/10.1515/geoca-2015-0007.*

Vozárová, A. & Vozár, J., 1988: Late Paleozoic in West Carpathians. *Bratislava, Geol. Inst. D. Štúr, 314 p.*

Vozárová, A., Šmelko, M. & Paderin, I., 2009: Permian single crystal U-Pb zircon age of the Roznava Formation volcanites (Southern Gemeric Unit, Western Carpathians, Slovakia). *Geol. Carpath., 60. 439–448. https://doi.org/10.2478/v10096-009-0032-1.*

Vozárová, A., Šmelko, M., Paderin I. & Larionov, A., 2012: Permian volcanics in the Northern Gemericum and Bôrka Nappe system: U-Pb zircon dating and the implications for geodynamic evolution (Western Carpathians, Slovakia). *Geol. Carpath., 63, 3, 191–200. https://doi.org/10.2478/v10096-012-0016-4.*

Vozárová, A., Konečný, P., Vďačný, M., Vozár, J. & Šarinová, K., 2014: Provenance of Permian Malužiná Formation sandstones (Hronicum, Western Carpathians): evidence from monazite geochronology. *Geol. Carpath., 65, 5, 329–338. https://doi.org/10.2478/geoca-2014-0023.*

Vozárová, A., Rodionov, N., Vozár, J., Lepekhina, E. & Šarinová, K., 2016: U-Pb zircon ages from Permian volcanic rocks and tonalite of the Northern Veporicum (Western Carpathians). *J. Geosci., 61, 221–237. https://doi.org/10.3190/jgeosci.215.*

Vozárová, A., Šarinová, K., Laurinc, D., Lepekhina, E., Vozár, J., Rodionov, N. & Lvov, P., 2019: Exhumation history of the Variscan suture: Constrains on the detrital zircon geochronology from Carboniferous-Permian sandstones (Northern Gemericum; Western Carpathians).

Geol. Carpath., 70, 512–530. https://doi.org/10.2478/geoca-2019-0030.

Vozárová, A., Šarinová, K., Rodionov, N. & Vozár, J., 2020: Zircon U-Pb geochronology from Permian rocks of the Tribeč Mts. (Western Carpathians, Slovakia). *Geol. Carpath., 71, 274–287. https://doi.org/10.31577/GeolCarp.71.3.6.*

Vozárová, A., Rodionov, N., Šarinová, K. & Vozár, J., 2021: U-Pb zircon ages from Permian volcanites of the Čierna Hora Mts. (Western Carpathians, Slovakia): Regional tectonic implications. *Geol. Carpath., 72. https://doi.org/10.31577/GeolCarp.72.5.1.*

Zorkovský, B., 1959a: Zpráva o petrograficko-chemickom štúdiu melafýrov, vystupujúcich vo verféne v okolí Veľkej Stošky na západnom okraji Muráňskej planiny. *Geol. Práce, Zpr., 16, 193–197.*

Zorkovský, B., 1959b: Zpráva o petrograficko-chemickom štúdiu melafýrov, vystupujúcich vo verféne severne od Švermova (bývalý Telgárt). *Geol. Práce, Zpr., 16, 199–203.*

Datovanie monazitu z masívu Veľkej Stožky (muránsky príkrov, Západné Karpaty) – význam pre poznanie vývoja permského vulkanizmu Vnútorných Západných Karpát

Produkty permskej acidnej magmatickej činnosti Vnútorných Západných Karpát (ryolity, granitoidy alebo vulkanický detrit) sa nachádzajú vo viacerých tektonických jednotkách. Aj keď sú väčšinou viazané na ich súveké sedimentárne komplexy (hronikum, tatrikum, veporikum, gemerikum), niektoré z nich, konkrétne ryolitové telesá Gregová pri Telgárte, telesá vo svahoch pod Veľkou Stožkou na Muránskej planine a ryolitové telesá v oblasti Poník (zvyčajne zaraďované do silicika s. l.; napr. Plašienka et al., 1997), sú tektonicky amputované z pôvodného prostredia a začlenené do geologicky mladších sedimentárnych útvarov spodného triasu.

Skúmané územie masívu Veľkej Stožky sa nachádza vo veporskom pásme (Klinec, 1976; Vass et al., 1988; Vojtko et al., 2000). Širšie územie je tvorené (juho)veporským kryštalinickým fundamentom s lokálne zachovaným triasovým sedimentárnym obalom a nadložnými mezozoickými komplexmi muránskeho príkrovu (Kronome et al., 2019; obr. 1 – 2). Veporské kryštalinikum zastupujú granitoidy a migmatity tzv. kráľovohoľského komplexu. Prekrývajú ho prevažne metamorfované kvarcity a fylity, lokálne sa zachovali metamorfované a tektonizované kryštalické vápence, lokálne prepracované na rauvaky (obr. 2 – 3). Veporikum tektonicky prekrýva muránsky príkrov. Bázu muránskeho príkrovu tvoria na mnohých miestach imbrikované tektonické šupiny. Tvoria ich obvykle spodnotriasové súvrstvia, miestami s tektonicky inkorporovanými ružovými a sivými ryolitmi, ktoré sú hlavným predmetom tejto práce. Nadložie ryolitov zastupujú prevažne spodnotriasové pestré piesčité bridlice hronseckých vrstiev (vrchná časť benkovského súvrstvia, sensu Olšavský et al., 2010) a pestré bridlice a piesčité vápence šuňavského súvrstvia. Strednotriasovú časť sledu na tejto lokalite tvoria gutensteinské vápence a dolomity, steinalmské, raminské a ráztocké vápence. Najvyššiu časť masívu Veľkej Stožky tvoria svetlosivé ladinské wettersteinské vápence (Kronome et al., 2019; obr. 2 – 3).

Ryolitové horniny v masíve Veľkej Stožky sú tektonicky amputované zo svojho pôvodného geologického prostredia. Mikrosondové U-Th-Pb datovanie monazitových kryštálov ryolitových hornín zo svahov masívu Veľkej Stožky na Muránskej planine poskytlo magmatický vek 281 ± 4,5 mil. rokov, ktorý je prakticky totožný s vekom ryolitovej erupcie. Identifikovaný permský vek guadalup je podobný ako zistený vek ďalších ryolitových telies – Gregová pri Telgárte (Demko a Hraško, 2013; Ondrejka et al., 2018), Tisovec-Rejkovo, Poniky-Piesky, Poniky-Žiarec alebo Veľká Stožka (Ondrejka et al., 2018; Ondrejka et al., 2022). Porovnanie geochronologických údajov (Demko a Hraško, 2013; Ondrejka et al., 2018; Ondrejka et al., 2022 a táto práca) ukazuje samostatný vek každého telesa v chronologickej postupnosti Veľká Stožka (281 ± 4,5) → Poniky-Piesky (271 ± 1,5) → Veľká Stožka, (269,5 ± 1,8) → Poniky-Žiarec (267 ± 1,6) → Tisovec-Rejkovo (266,6 ± 2,4) → Gregová (263 ± 3,5; 263,3 ± 1,9), pričom v prípade ryolitového telesa v masíve Veľkej Stožky sú identifikované dva vekovo samostatné vulkanické pulzy, konkrétne 281 ± 4,5 mil. r. a 269,5 ± 1,8 mil. r. Situácia ukazuje na širokú vulkanickú aktivitu ryolitového vulkanizmu v rozpätí 281 – 263 mil. r.

Tektonická a erozívna činnosť spôsobila objemovú redukciu ryolitových telies, z ktorých ostali zachované predovšetkým rigidné jadrá extruzívnych telies. Stopy po pyroklastickej vulkanickej aktivite sa zachovali len obmedzene (Telgárt, Poniky). Migrujúce erupcie ryolitových magiem v období 281 – 263 mil. r. ukazujú na hiát vulka-

nickej aktivity v období medzi 280 – 271 mil. r. v trvaní 9 mil. r., ktorý je synchrónny s vulkanickou aktivitou severogemerickej jednotky – ryolitový tuf 278 mil. r. (Rojkovič a Konečný, 2005) a zirkónový detrit 281 – 276 mil. r. (Vozárová et al., 2019), s andezitovo-ryolitovým vulkanizmom petrovohorskej formácie 275 – 272 mil. r. (Vozárová et al., 2012), a predovšetkým s dacitovo-trachyandezitovým vulkanizmom severného veporika 279 – 273 mil. r., ktorý je zaznamenaný vo vulkanogénnom horizonte Harnobisu (Vozárová et al., 2016).

Ryolitové horniny sú produktom extruzívnej erupčnej aktivity situovanej na hlboko založených zlomoch transpresno-transtenznej tektonickej povahy „VAFZ“, ktoré po reaktivácii slúžili na kompenzáciu tektonického napätia zmeneného v období od 271 mil. r., t. j. po skončení vulkanickej aktivity budúceho severného veporika a severného gemerika.

Doručené / Received: 4. 6. 2023
Prijaté na publikovanie / Accepted: 30. 6. 2023

Mineralia Slovaca, Web ISSN 1338-3523, ISSN 0369-2086, https://doi.org/10.56623/ms.2023.55.1.3
55, 1 (2023), 27 – 52, © Authors 2023. CC BY 4.0

The Brehov volcanogenic and stratabound base metal and gold deposit (Eastern Slovakia): Position and genetic relations in the Internal Carpathian–Alpine Cenozoic metallogenetic belt

ZOLTÁN BACSÓ

Branisková 10, SK-040 01 Košice, Slovakia; ybacso@gmail.com
Former address: Geologický prieskum, š. p., Werferova 1, SK-040 00 Košice, Slovakia

Abstract: The Brehov ore deposit, near the village of Brehov, is located in the East Slovakian Basin 15 km south-east of the Trebišov town. A progressive development of Middle Badenian to Middle Sarmatian sedimentation and volcanism in the Brehov hydrothermally mineralized area is manifested in the article. The volcanogenic, stratabound, polymetallic (Zn, Pb, Cu) and gold sulphide deposit within the Brehov–Sirník interpreted resurgent caldera occurs in the volcanosedimentary sequence. Mineralization in the deposit, consisting of the fine-grained aggregate of sulphides, is interpreted to be of shallow water origin. It is placed mostly in the rhyodacite volcaniclastics and partly in calcareous claystone, altered and brecciated. Three types of ores – the stringer (keiko), yellow and black ore – were distinguished near the Brehov village on the basis of ore composition, being formed by successive mineralization stages. The stringer ore, consisting of the sulphide minerals, dominates in the quartz-dioritic (siliceous) rocks. The yellow ore is represented primarily by pyrite, but contains also minor chalcopyrite and quartz. The black ore is an intimate mixture of sphalerite, galena, sometimes barite and minor pyrite and chalcopyrite. Tetrahedrite and marcasite occur sporadically. The ore in all cases is fine-grained. The ore bodies are almost everywhere enclosed by clay, composed of montmorillonite, sericite and chlorite. The ore bearing fluids were probably colloids of hydrothermal origin. Textures are considered to indicate that the colloids replaced the country rocks, rather than merely filled open spaces in the rhyodacite pyroclastics and epiclastics. Despite the precious metals (mostly gold) are economically important commodity in many Kuroko type deposits, in the Brehov ore deposit they occur in volumetrically minor amounts. Visible gold is present as inclusions of native gold in major sulphide minerals, whereas silver occurs in Ag-sulphides and sulphosalts, e.g. tetrahedrite and ferberite.
The location of important Neogene magmatic, as well as metallogenetic structures in the "Boundary Zone" between the Western and Eastern Carpathians, in the Brehov–Zemplín area, is controlled by the orthogonal deep penetrative regional faults – lineaments. They are interpreted as the surface expression of deep-crustal and mantle rooted trans-lithospheric structures, which have been periodically reactivated as pure-shear regional faults during individual orogenic cycles, forming discontinuities long several tens, hundreds, or even thousands of kilometers.
In regions of subduction-related magmatism, the Kuroko type volcanogenic stratabound sulphide and gold ore deposits, like Brehov in Eastern Slovakia, may be generated along these lineaments, because the discontinuities allow the ascent of relatively evolved magmas and fluids from the deep-crustal magma reservoirs. However, the lineament intersections can focus this activity under appropriate lithospheric stress conditions only where a magma supplies exist – as was demonstrated in the case of the Brehov ore deposit, represented by an extended quartz diorite-porphyry stock body related sills and dikes (like in Cenozoic rifted back arc basin between Western and Eastern Carpathians).
The Brehov ore deposit occurs in the crossing of the Ondava submeridional lineament zone with the Komárovce–Brehov subequatorial lineament, which developed in weakened zone of Mesozoic Meliata suture zone after Neo-Tethys Ocean. The resurgent elevation of the Brehov–Sirník caldera is developed on this crossing.

Graphical abstract

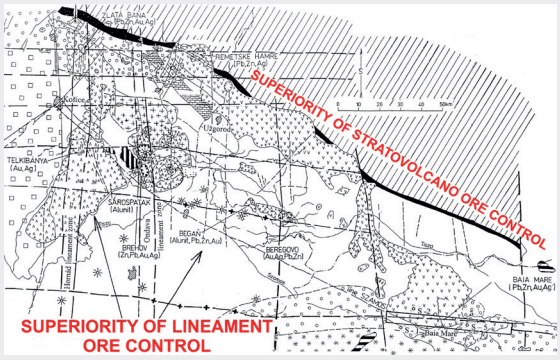

Highlights

- The Brehov deposit mineralization is interpreted as Kuroko genetic type
- Role in magma and fluid transport is attributed to regional trans-crustal discontinuities (lineaments) of subequatorial and submeridional course, and especially their crossings

1 Introduction

In the beginning of the 1980s, the "Border Zone" segment between Western and Eastern Carpathians (Figs. 1 and 2) was considered to be an insignificant metallogenetic unit of the Internal Carpathian–Alpine Cenozoic metallogenetic belt. The discovery of the Kuroko type submarine volcanogenic Zn-Pb-Cu sulphide and gold deposit Brehov had started a new exploration period, which continued until the 1998, after the Brehov type ore prices have decreased.

In the Brehov submarine ore structure (Fig. 7), following stages of evolution have been recognized:

1. Origin of the Brehov–Sirník caldera as a result of the Middle Badenian acidic-rhyodacite explosive volcanism and its filling with rhyodacite type volcanosedimentary complex.
2. Denudation and emplacement of a quartz-diorite porphyry intrusion (15.4 ± 0.4; 15.1 ± 0.1 Ma; Lang et al., 1994), with development of the Kuroko type semimassive, matrix- breccia Zn-Pb-Cu-Au-Ag mineralization in the volcanosedimentary complex (main concordant-stratabound part of the deposit), as well as in the form of veinlets and disseminations in subvolcanic quartz-diorite bodies (discordant part of the deposit). Simultaneously with the intrusion of magmatic bodies, as a consequence of this intrusion, the uplift of resurgent horst ore structure took place.
3. Origin of the fresh and strongly argillized lava flows and extrusive bodies of pyroxene andesite near the villages of Brehov, Sirník and Hraň of ages 14.7 ± 1.1 and 14.1 ± 0.5 Ma for andesite extrusive body from the Veľký Vrch hill (272.2 m a.s.l.) near the village of Brehov (Lang et al., 1994).
4. Silicified and adularized rhyodacite extrusive bodies and lava flows developed directly in the Brehov ore deposit (11.8 ± 0.2 Ma, l.c.). Formation of volcanic exhalation mineralization.

Based on our observations and experiences with the Carpathian Neogene metallogenetic belt, its volcanic rock structures and ore deposits are principally connected with the deeply seated tectonic zones (lineaments). These trans-crustal discontinuities, and in particular their intersections, may provide high-permeability channels for ascent of deeply derived magmas and fluids. Optimum conditions for magma penetration were provided when these structures formed at regional extension or transtension (Mayo, 1958; Kutina, 1980; O'Driscoll, 1981, 1985, 1986; Richards, 2000; Richards et al., 2001).

When tracing the course of lineaments, the earlier ophiolites (suture zones) may represent an essential tool for the location of the younger lineaments, because they are related with the zones of earlier continental breakup and even after collision and closure of oceanic spaces they still represent trans-crustal discontinuities, which can be essential for the Cenozoic magmatic and metallogenetic processes.

In the Internal Carpathian-Alpine Cenozoic metallogenetic belt the discontinuous bodies of Mesozoic ophiolites (ca 150 Ma) exclusively follow the subequatorial lineament zones. The Alpine-Himalayan Mesozoic ophiolite belt (ca 150 Ma) was ascertained by Ishiwatari (1985) and Dilek and Furnes (2014).

In the "Border Zone" metallogenetic segment between W. Carpathians and E. Carpathians, besides the Brehov–Zemplín Neogene ore sector, there is well known a group of ore fields with partly subaerial and partly submarine nature. They include the Zlatá Baňa ore sector, the Begaň–Beregovo–Kvasovo ore sector and submarine influences are known also from the Telkibánya, mostly subaerial ore sector. The above mentioned Neogene ore sectors possess a number of characteristics that are, in part, typical for Kuroko type deposits and in part resemble volcanogenic epithermal base and gold deposits.

The Cenozoic magmatism and metallogeny in the area between towns of Banská Štiavnica (Slovakia) and Baia Mare (Romania) are preferably conditioned by subequatorial and complementary submeridional lineaments. Other – so-called "normal faults", which reach a depth of 10–40 kilometers from the surface, have only secondary, or very small influence for Cenozoic magmatism and metallogeny in the Internal Carpathian–Alpine Cenozoic metallogenetic belt.

Remark: In this article, the hierarchy and terminology of metallogenetic units is used after Popescu and Neascu (2010).

2 Regional geological setting, description of principal lineaments

The Brehov–Zemplín metallogenetic sector is located in Eastern Slovakia, 46–54 kilometers south-east from the town of Košice. The Brehov ore deposit is a part of the Internal Carpathian–Alpine Cenozoic metallogenetic belt (Fig. 1; sensu Heinrich & Neubauer, 2002; slight modified by Bacsó, 2014), which consists of six regional segments:

1. The Western Alps – Brusson segment;
2. The Eastern Alps – Hohe Tauern segment;
3. The Western Carpathians segment;
4. The "Border Zone" segment between Western and Eastern Carpathians;
5. The Eastern Carpathians segment;
6. The Apuseni Mountains segment.

Concerning the Brehov ore deposit, three segments of above listed metallogenetic belt are important: The Western Carpathians segment; the "Border Zone" segment between W. Carpathians and E. Carpathians; and the Eastern Carpathians segment (Figs 1, 2 and 3).

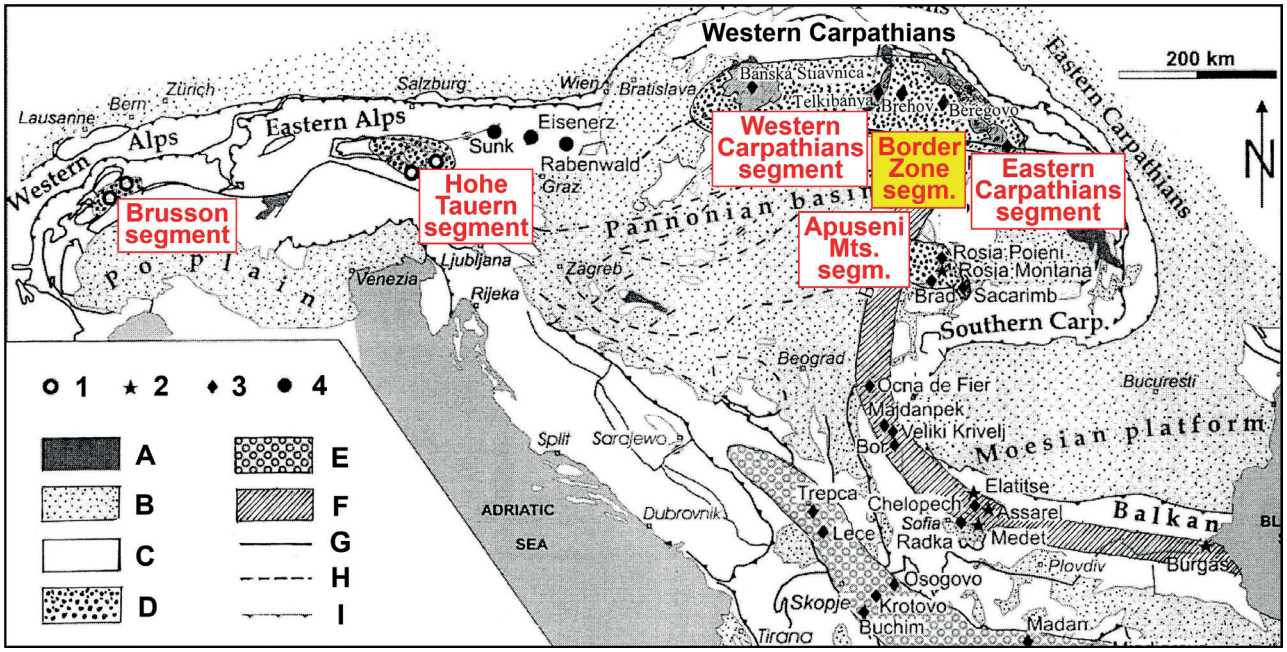

Fig. 1. Simplified tectonic map displaying distribution of six major segments of Internal Carpathian–Alpine Cenozoic metallogenetic belt within the Alpine-Balkan-Carpathian-Dinaride (ABCD) region (slightly modified after Heinrich and Heubauer, 2002, by Bacsó, 2014). Ore deposits: 1 – Orogenic Au; 2 – Porphyry Cu-Mo-Au; 3 – Polymetallic Pb-Zn-Ag-Au ores – e.g. skarn, low-sulphidation polymetallic vein and carbonate mineralization, high-sulphidation massive sulphide; 4 – metamorphogenic mineralization (siderite, magnesite, talc). Lithotectonic and metallogenic explanations: A – Neogene volcanic and plutonic rocks; B – Oligocene–Neogene basins; C – Alpine-Balkan-Carpathian-Dinaride orogenic zones (sensu Heinrich and Heubauer, 2002); D – Internal Carpathian–Alpine Cenozoic metallogenetic belt; E – Oligocene-Miocene Serbomacedonian Rhodope metallogenetic belt; F – Late Cretaceous (Apuseni–Balkan) Banatite magmatic-metallogenetic belt ("Banatite belt" sensu l.c.); G – Major strike-slip fault; H – Inferred fault; I – Major thrust.

From the nearer perspective the Brehov ore deposit lies in the center of the "Border Zone" segment between W. Carpathians and E. Carpathians and areally extends westward, including the submeridional Hornád lineament zone. Eastward the "Border Zone" segment extends up to Chust town submeridional lineament, included. The northern boundary of the "Border Zone" segment is represented by the tectonic line of the Pieniny Klippen Belt, while the southern boundary includes the Recsk–Baia Mare subequatorial lineament (Fig. 2).

The "Border Zone" metallogenetic segment consists of principal metallogenetic sectors encompassing following ore fields:

a) The Brehov–Zemplín metallogenetic sector encompasses the Brehov base metal and gold ore field and the Zemplín base metal ore field;
b) The Telkibánya metallogenetic sector in Hungary encompasses the Telkibánya gold and silver ore field;
c) The Zlatá Baňa metallogenetic sector encompasses three ore fields: The Zlatá Baňa base metal and gold ore field, the Dubník mercury ore field, and the Dubník precious opal field;
d) The Begaň–Beregovo–Kvasovo metallogenetic sector in Ukraine encompasses three ore fields: The Muzievo gold, silver and base metal ore field, the Kvasovo gold, silver and base metal ore field and the Begaň barite, alunite and base metal ore field.

All metallogenetic sectors are located within the Prešov–Kráľovský Chlmec graben and all ore deposits are developed on the intersections of the submeridional and subequatorial lineaments (Figs. 2 and 3).

The neighbouring Brehov submarine ore deposit and Zemplín submarine base metal ore structure form the **Brehov–Zemplín fully submarine base and gold metal metallogenetic sector** (Figs. 3, 5a, 5b and 11), located on the submeridional Ondava lineament zone, form satellite ore structure to the ore deposits on the Hornád lineament zone, as well as to Telkibánya metallogenetic sector located west, and to the Zlatá Baňa metallogenetic sector located north-west (Figs. 3, 5a, b).

Despite of the regional-geological similarities between the principal volcanogenic deposits of the "Border Zone" metallogenetic segment between the W. Carpathians and E. Carpathians, there exist also distinct local differences. First of all, the Telkibánya and Zlatá Baňa metallogenetic sectors occur in the central volcanic zones of middle sized stratovolcanoes, while the Brehov–Zemplín metallogenetic sector is connected only with smaller and very simple volcanic edifices (not with stratovolcanoes).

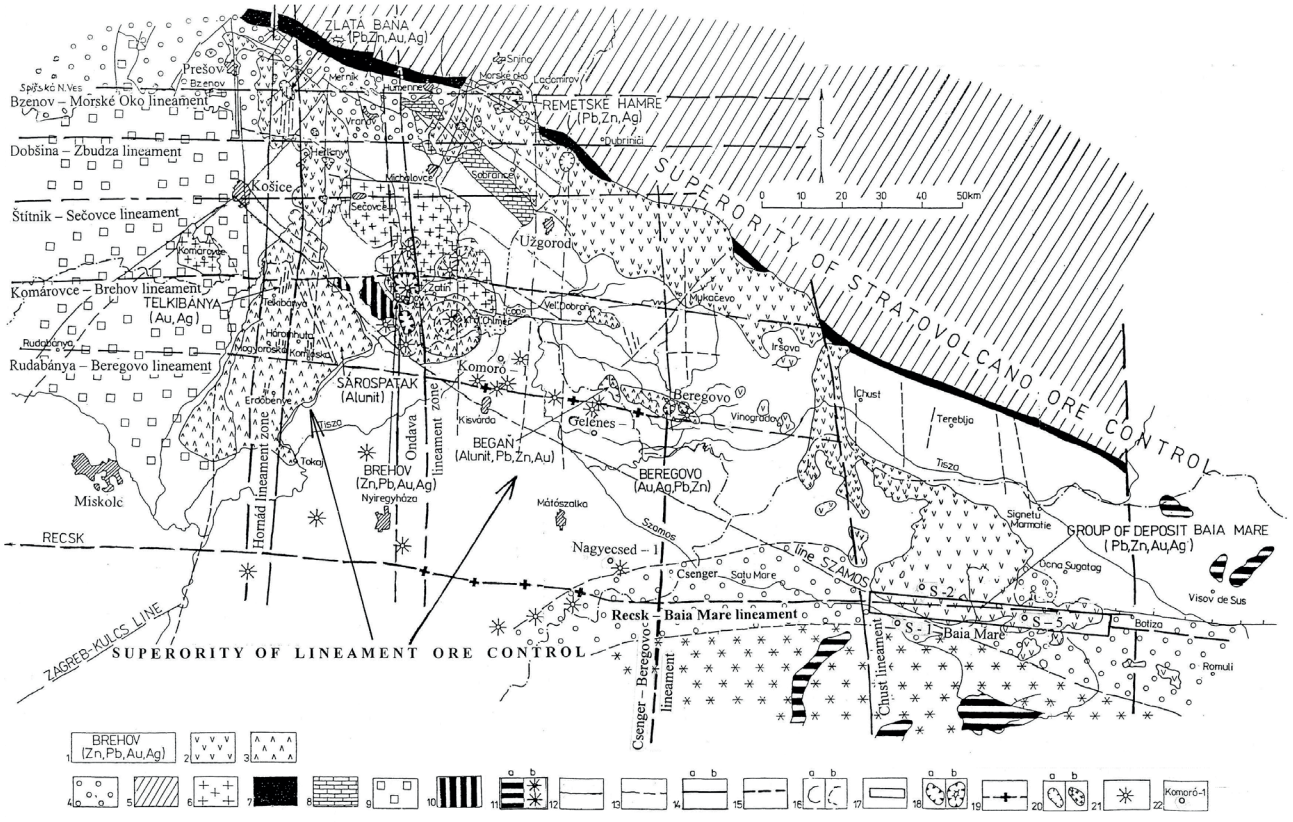

Fig. 2. Deep fault structures of the "Border Zone" segment between Western and Eastern Carpathians and the Eastern Carpathian Segment and their relation to magmatism and Neogene ore mineralizations. Geological interpretation of geological and geophysical data by Bacsó, 2014). 1 – principal ore deposit and ore occurrence; 2 – andesitic and rhyodacitic volcanics, Upper Badenian to Pannonian; 3 – rhyodacitic and andesitic volcanics, Upper Badenian–Sarmatian; 4 – Late Cretaceous and Paleogene sediments of the Internal Carpathians; 5 – Cretaceous and Paleogene sediments of the Outer Carpathians; 6 – ophiolite complex; 7 – Mesozoic and Paleogene sediments of the Klippen Belt; 8 – Mesozoic sediments of the Krížna nappe, Internal Western Carpathians; 9 – Paleozoic and Mesozoic sediments of Internal Western Carpathians; 10 – Late Paleozoic and Mesozoic sediments of Internal Carpathians ("Zemplín Island"); 11 – crystalline complexes of Northern Transylvania: a) on surface, b) covered with younger sediments; 12 – shallow faults; 13 – assumed shallow faults; 14 – interpreted lineaments; 15 – assumed lineaments; 16 – geological boundaries: a) proved, b) assumed; 17 – big group of Neogene ore deposits near city Baia Mare; 18 – submarine caldera: a) without central elevation, b) with central elevation; 19 – gravity anomaly in the lower crust (upwarping Neogene magmatics); 20 – subaerial central volcanic zone of stratovolcano: a) in form of eroded crater, b) in form of eroded caldera; 21 – buried volcanic structure; 22 – deep drillhole.

Despite the Telkibánya and Zlatá Baňa metallogenetic sectors are located in the same Hornád submeridional lineament zone, they are genetically very different. Telkibánya ore field represents a subaerial, epithermal, low-sulfidation precious metal deposit, with excellent developed classical long-vein ore structures, while the Zlatá Baňa ore field represents only partly subaerial and partly submarine ore structure, where only in very rudimentary conditions short and small ore vein developed. For the essential part of the Zlatá Baňa base and gold metal ore deposit the **ore mineralized tectonic zones** are characteristic and not classical vein type structures (Tőzsér, 1972; Kaličiak & Ďuďa, 1980; Burian et al., 1985; Divinec et al., 1988).

The relations between the Brehov–Zemplín submarine metallogenetic sector and the Beregovo partly submarine and partly subaerial metallogenetic sector are very complicated. The Beregovo metallogenetic sector is developed not only on the intersection of different submeridional and subequatorial lineaments, but the pre-Neogene basement is very different, too. The Brehov–Zemplín Neogene metallogenetic sector lies on the Zemplín Paleozoic-Mesozoic block, while the Begaň–Beregovo–Kvasovo Neogene metallogenetic sector is developed in the Krichevo Mezozoic-Paleogene elevation with ophiolites. In the Brehov–Zemplín metallogenetic sector there are essentially present the bimodal (rhyodacite, quartz diorite porphyry, andesite) Neogene magmatics, while in the Begaň–Beregovo–Kvasovo metallogenetic sector there are present only rhyolite-rhyodacite unimodal Neogene magmatics (Vityk & Krouse, 1994; Biruk & Skakun, 2000).

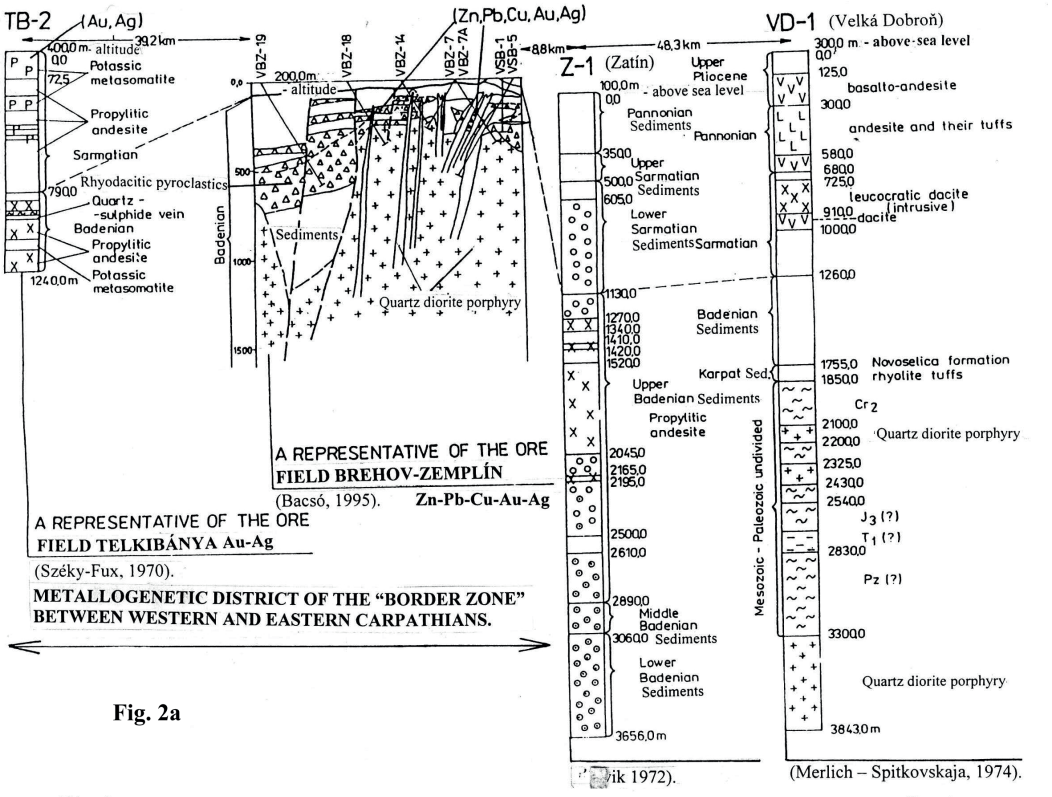

Fig. 2a

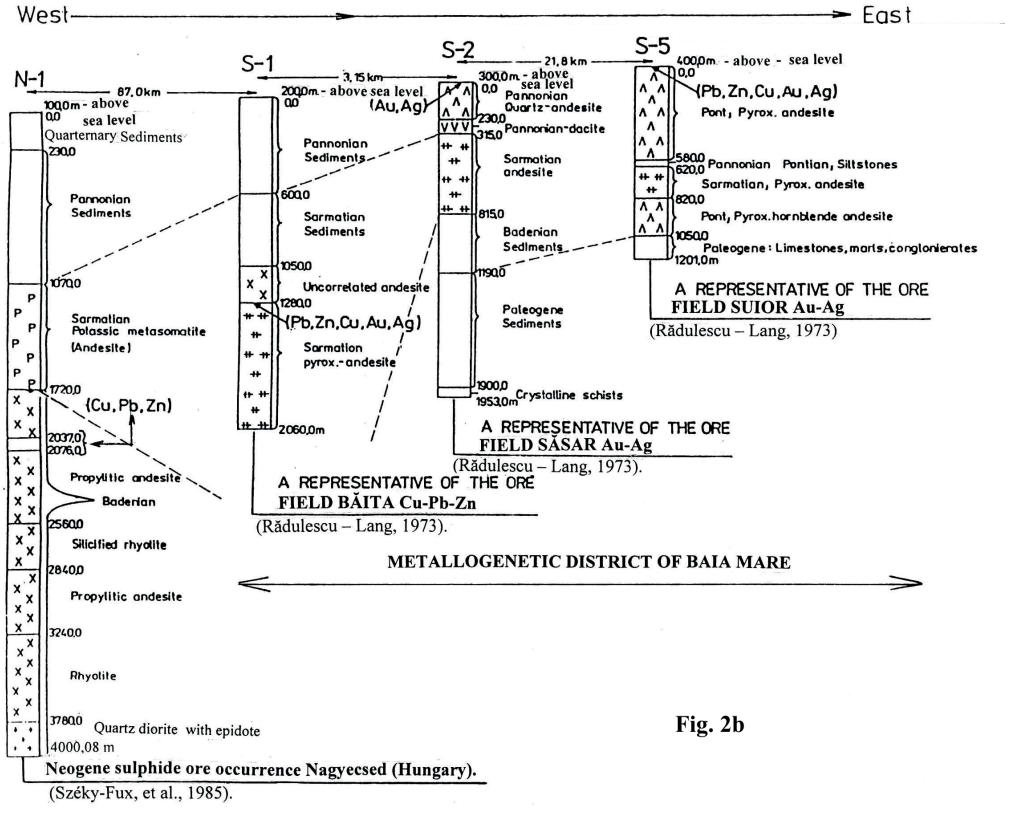

Fig. 2b

Fig. 2a, b. Geological and metallogenetic representative deep drillhole profiles: a) along the eastern part of the Komárovce–Brehov lineament within the "Border Zone" segment between Western and Eastern Carpathians; b) along the eastern part of the Recsk–Baia Mare lineament within the Eastern Carpathian segment.

Deep faults constitute the global network on the whole "Border Zone" between W. Carpathians and E. Carpathians and lineaments facilitated the magma penetration. The Mesozoic ophiolite rocks are connected with deep faults, similarly to Neogene magmatics (Soták et al., 1993; Faryad, 1999; Savu, H., 2009). First of all, concerning plate tectonics the ultramafic rocks are considered as an undeniable indicator of deep faults (Franklin et al., 1981; Sato, 1991; Ohmoto, 1996). Finally, the so-called small Neogene intrusions (for example in the deeper part of the Brehov ore deposit they are directly connected with the Komárovce–Brehov subequatorial lineament, which is in agreement with their subvolcanic character (Fig. 2a). In the "Border Zone" of the W. Carpathians and E. Carpathians it is possible to define orthogonal pattern of deep faults (E–W; N–S). The main deep faults divide the basement of the "Border Zone" into following blocks with different geological structures and development: The Iňačovce–Krichevo area block, the Zemplinicum elevated block, the Slanské vrchy Mts. block, the Baia Mare ore district block and the Beregovo elevated block.

Ophiolites in the "Border Zone" between the W. Carpathians and E. Carpathians represent tectonically transported assemblages of ultramafic rocks, gabbro, basalt pillow lavas, commonly capped by chert or other pelagic sedimentary rocks. Their occur in linear deep tectonic zones of Eastern Slovakia and are generally interpreted as fragments of oceanic crust and mantle that have been thrust (obducted) on the adjacent continental margin. By this way some lineaments, or at least some their segments, represent the geosuture zones.

In the "Border Zone" of the W. Carpathians and E. Carpathians we have distinguished six subequatorial deep faults (from the south to the north):

The **Recsk–Baia Mare lineament** (Figs. 2 and 2b) as the master subequatorial deep fault, representing a backbone of the Internal Carpathian–Alpine Cenozoic metallogenetic belt, with rich porphyry copper deposit near the village of Recsk (Hungary) and large ophiolite bodies on Darnó and Szarvaskő hills. In the eastern part of the lineament a group of big epithermal, low-sulfidation base metal and gold deposits is developed at the Baia Mare town. The ore-bearing Neogene quartz diorite porphyry subvolcanic bodies crop out along the deep faults (Fig 2b; Széky-Fux et al., 1985).

The **Rudabánya–Beregovo subequatorial lineament** is indicated by the Rudabánya Fe and base metal deposit (Szakáll & Kovács, 1995; Földessy et al., 2009), by lacustrine hydrothermal exhalative mineralizations near Háromhuta and Mogyoróska villages in the Tokaj Mts. (Gyarmati, 1977), by buried volcanoes in Tokaj Mts. and gold-silver and base metal deposits near Beregovo settlement. Along the Rudabánya–Beregovo subequatorial deep fault also other ore-bearing Neogene subvolcanic bodies are buried (Fig. 2; Vityk et al., 1994; Biruk & Skakun, 2000).

The **Komárovce–Brehov subequatorial lineament** is indicated by large bodies of ophiolites near village of Komárovce, by gold-silver deposit Telkibánya, by the base metal-gold deposit Brehov, by Neogene subvolcanic bodies near village of Veľká Dobroň (Ukraine). (Figs. 2 and 2a; Merlich & Spitkovskaja, 1974; Hovorka et al., 1977; Bacsó, 2000). The continuation of the Komárovce–Brehov lineament to the west is traced by occurrences of ophiolites near villages of Komjáti (Hungary) and Bohúňovo (Slovakia).

The **Štítnik–Sečovce subequatorial lineament** traced along the Rožňava discontinuity zone (the Meliata unit s.s.), which represents the southern border of the Gemericum and is characterized by the presence of blueschist, serpentinites, as well as very low grade sediment, that partly thrust on Paleozoic sequences of Gemericum (Faryad et al., 1998). On the east, near villages of Pavlovce, Blatná Polianka, Rebrín and Senné (Slovakia), the Štítnik–Sečovce lineament is traced by the deep drillholes intersecting the ophiolites. (Mořkovsky & Cverčko, 1987; Gnojek et al., 1991; Faryad, 1999).

The **Dobšiná–Zbudza subequatorial lineament zone** in its western segment follows the crustal discontinuity related to earlier Paleozoic Rakovec suture zone (Németh, 2002). In earlier interpretation it was supposed that serpentinized peridotites at the village of Jaklovce were exhumed along this lineament, representing the northern branch of Meliata Ocean (Faryad et al., 1998), but later their displaced position as Paleo-Alpine nappe outlier was proved (Németh et al., 2021). The eastern continuation of this lineament was intersected by deep drilling hole near village of Zbudza, revealing a large body of serpentinized peridotite (Mořkovsky & Cverčko, 1987; Kozur & Mock, 1997).

Fig. 3. Detail of the deep fault structural and metallogenic scheme for region around the Zemplín Paleozoic-Mesozoic elevation (Bacsó, 2014, compiled using own geological data and geophysical data from Pospíšil & Bodoky, 1981–1990). 1 – principal ore deposit; ore, occurrence; 2 – hydrothermal veins; 3 – lacustrine siliceous deposit; 4 – centre of Cenozoic hot-spring activity; 5 – mostly subaerial andesitic volcanics, Upper Badenian–Pannonian; 6 – mostly submarine rhyodacite and andesite volcanics, Upper Badenian–Sarmatian; 7 – gravimetric anomalies produced by Neogene magmatics; 8 – Klippen Belt, Mesozoic–Paleogene; 9 – submarine caldera: a) without central elevation, b) with central elevation; 10 –Prešov–Kráľovský Chlmec graben; 11 – Paleozoic-Mesozoic elevation of "Zemplín Island"; 12 – subaerial central volcanic zone; 13 – interpreted deep lineaments; 14 – buried Neogene volcanic structure; 15 – geological cross section; 16 – deep drillhole.

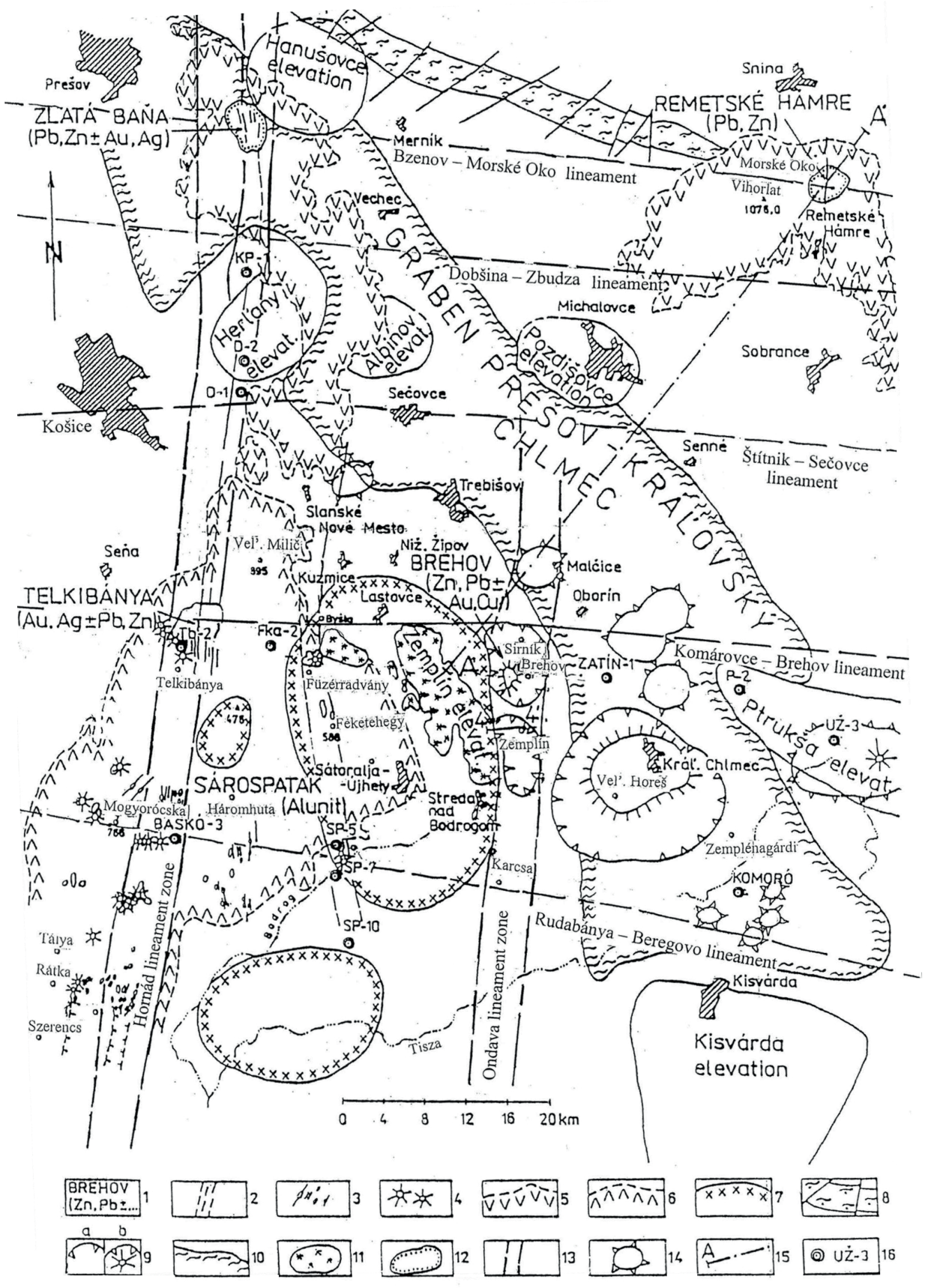
Prešov
ZLATÁ BAŇA
(Pb,Zn±Au,Ag)
Hanušovce elevation
Snina
REMETSKÉ HÁMRE
(Pb, Zn)
A
A'
Mernik
Bzenov – Morské Oko lineament
Morské Oko
Vihorlat
1076,0
Remetské Hámre
Vechec
KP-1
N
Dobšina – Zbudza lineament
Michalovce
Herľany
D-2
elevat.
Albínov elevat.
GRABEN PREŠOV-CHLMEC-KRÁĽOVSKÝ
Pozdišovce elevation
Sobrance
D-1
Sečovce
Košice
Senné
Štítnik – Sečovce lineament
Trebišov
Slanské Nové Mesto
Veľ. Milič
Niž. Žipov
BREHOV
(Zn, Pb±Au,Cu)
Malčice
Seňa
Kuzmice
Lastovce
Oborín
TELKIBÁNYA
(Au, Ag±Pb, Zn)
Tb-2
Fka-2
Sírnik
Brehov
ZATÍN-1
Komárovce – Brehov lineament
P-2
Telkibánya
Füzérradvány
Feketehegy
Zemplín
Ptruksa elevat.
UŽ-3
Kráľ. Chlmec
Veľ. Horeš
SÁROSPATAK
(Alunit)
Sátoralja-Újhely
Mogyorócska
Háromhuta
Streda nad Bodrogom
BASKÓ-3
SP-5
SP-7
Karcsa
Zemplénagárdi
KOMORÓ
Tálya
Rátka
Hornád lineament zone
SP-10
Rudabánya – Beregovo lineament
Kisvárda
Szerencs
Tisza
Ondava lineament zone
Kisvárda elevation
0 4 8 12 16 20 km
BREHOV (Zn, Pb±...
1
2
3
4
5
6
7
8
a b
9
10
11
12
13
14
15
UŽ-3
16

The **Bzenov–Morské oko subequatorial lineament** on the west is traced by a large magnetic "ophiolite" anomaly near the village of Bzenov, by the drillhole V-1, intersecting the serpentinite body in the southern periphery of the city of Prešov (Slávik, 1974), by the base metal and gold ore deposit Zlatá Baňa in the Slanské vrchy Mts., and by the base metal ore field near Morské oko in the Vihorlat Mts. Along the Bzenov–Morské oko subequatorial lineament the ore-bearing Neogene subvolcanic diorite porphyry bodies occur (the Zlatá Baňa and Morské oko ore fields; Figs. 2, 3 and 4; Tözsér, 1972; Slávik, 1974; Kaličiak & Ďuďa, 1980; Gnojek, 1987; Bacsó & Ďuďa, 1988; Divinec et al., 1988).

The complementary submeridional lineament to the above mentioned set of subequatorial lineaments in the "Border Zone" between W. Carpathians and E. Carpathians is represented by the **Hornád lineament zone** among the Zlatá Baňa base and gold metal deposit, the Telkibánya precious metal deposit and the lacustrine hydrothermal-exhalative mineral occurrences near villages of Háromhuta and Mogyoróska in the Tokaj Mts. (Hungary – Gyarmati, 1977).

The Ondava submeridional lineament zone is developed app. 25–35 kilometers east from the Hornád submeridional lineament zone. That lineament zone is traced from north to south by the Malčice buried volcanoes, by the Brehov–Sirník interpreted caldera and by Neogene ore deposit near village of Brehov, by the Zemplín–Somotor interpreted caldera and by the submarine ore field near the village of Zemplín, as well as by the buried volcanics and subvolcanic bodies near the village of Somotor (Figs. 2, 3, 5a and 5b).

3 Local Geology – the Brehov–Zemplín ore sector

The Brehov–Zemplín ore sector is located 16–22 km to SSE of the town of Trebišov. It forms a N–S oriented, 15 km long zone, wide 6–8 km, along the Ondava interpreted submeridional lineament zone. The submarine, hydrothermal mineralization of the Brehov–Zemplín metallogenetic sector is located in the immediate transition zone between the Zemplín Paleozoic elevation in the western side, and the Neogene Prešov–Kráľovský Chlmec graben on the eastern side (Figs. 2, 3, 4, 5a and 5b). In the northern part of this structure is located the Brehov–Sirník interpreted, buried submarine caldera with the Brehov volcanogenic, stratabound base and gold metal deposit. In the southern part of this structure the Zemplín–Somotor interpreted buried caldera is developed, with the Zemplín volcanogenic, andesitic, stockwork-feeder zone base metal ore occurrences.

Both ore mineralizations, near the Brehov village, as well as near the Zemplín village were formed within a resurgent caldera horst structure in the submarine environment. In the case of the Brehov area, the caldera probably opened along outward dipping faults, which was promoted by magma degassing, seawater influx and high temperature leaching, resulting in origin of the metal rich hydrothermal fluids. The thick rhyodacitic pyroclastics and epiclastics accumulation within the caldera has disposed with increased permeability, being exploited by mineralizing solutions. The specific caldera processes were the key factors in the formation of possible mineral ore deposits (Franklin et al., 1981; Sato, 1990; Ohmoto, 1996).

3.1 The Brehov ore field

3.1.1 Ore resources of the Brehov submarine hydrothermal deposit

As revealed by extended deposit survey (Bacsó, 1995a, b), before attenuation of mining survey and ores exploitation in Slovakia, the Brehov volcanogenic, stratabound, base and gold metal deposit contained a total of known resources of mostly semi-massive, heterolithic, sulphide-matrix breccia ores: 11.965 million metric tons (MT); grading: 0.821 wt. percent Pb; 1.466 wt. percent Zn; 0.212 wt. percent Cu; 0.424 g/t Au.

The total tonnage of ore at the end of the most extensive survey in the middle 1990s:

a) 8.392 million metric tons (MT) represent Pb, Zn, Cu ore, grading:

a_1) 0.943 wt. % Pb;

a_2) 1.86 wt. % Zn;

a_3) 0.119 wt. % Cu;

a_4) 0.017 g/t Au;

b) 0.837 million metric tons (MT) represent Pb, Zn, Cu, Au ore, grading:

b_1) 2.206 wt. % Pb;

b_2) 2.100 wt. % Zn;

b_3) 0.113 wt. % Cu;

b_4) 0.646 g/t Au;

c) 1.177 million metric tons (MT) represent Cu ore, grading:

c_1) 0.034 wt. % Pb;

c_2) 0.125 wt. % Zn;

c_3) 1.150 wt. % Cu;

c_4) 0.024 g/t Au;

d) 1.558 million metric tons (MT) represent Au ore, grading:

d_1) 0.014 wt. % Pb;

d_2) 0.018 wt. % Zn;

d_3) 0.664 wt. % Cu;

d_4) 2.804 g/t Au.

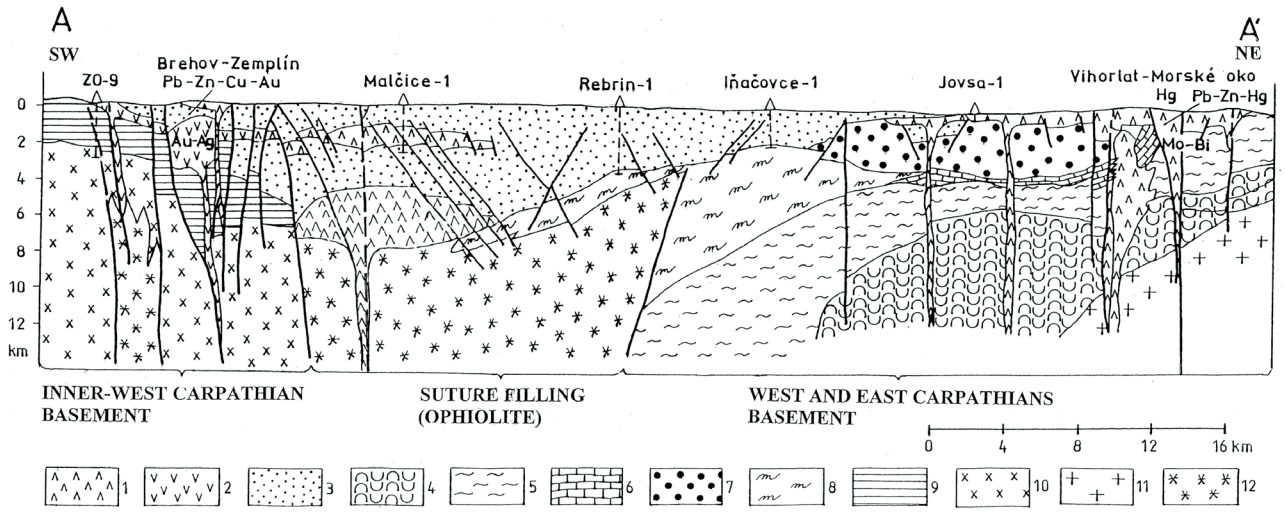

Fig. 4. Cross section through Pannonian basin ("Zemplín Island" ridge) to outer flysch Carpathians (Vihorlat Mts.) (Bacsó, 2014). 1 – Neogene andesite volcanics; 2 – Neogene rhyodacite magmatics; 3 – sediments of the Transcarpathian depression; 4 – Dukla flysch belt; 5 – Magura flysch belt; 6 – Klippen Belt; 7 – Humenné Mesozoic – Krížna nappe; 8 – Iňačovce–Kričeva unit; 9 – Late Paleozoic Zemplín Group; 10 – Zemplinicum; 11 – crystalline basement of Eastern Europe; 12 – ophiolite (serpentinized peridotite).

3.1.2 Paleontology and stratigraphy of the Brehov ore deposit

Based on stratigraphic results from the drillholes VBZ-1A, VSB-6, VSB-9 and VBZ-18, Zlinská in 1993 stated that the prospecting area of Brehov and its surroundings (drillhole VS-17 near the village of Cejkov) is built of sediments extending from Lower Badenian to Lower Sarmatian. These, taking into account the lithology, represent an equivalent of the Nižný Hrabovec Formation, the Vranov Fm., the Lastomír Fm. and the Stretava Fm.

In the Brehov ore deposit, the ore-bearing inner-caldera volcanic sedimentary sequence was dated by the fauna of *Spiroplectinella carinata* and *Bullimino-bolivino* zones to Wieliczkan and marine Kosovian, representing the transition of Middle and Upper Badenian. The ore-bearing volcanic-sedimentary sequence of calcareous claystone, alternating with hydrothermally altered rhyodacite explosive breccias and rhyodacite lapilli pumice tuffs as well as rhyolite epiclastics, is developed in the whole deposit area from surface down to 100–400 m depth (Zlinská, 1993; Bacsó, 1995a, b).

The total depth of the submarine emplacement of the volcanic-sedimentary ore-bearing sequence and of the sulphide mineralization still remains an open question. The presence also of subaerial Sarmatian andesite in this region, sedimentary facies and structures, typical for littoral environment, the presence of a neritic fauna in the Upper Badenian pelites in the hanging wall of mineralization and the mechanical constrains on stockwork fracturing favour the interpretation of genesis in a shallow-water environment (Bacsó, 2014).

3.1.3 Geological setting of the Brehov ore deposit

The Brehov ore deposit, located in the immediate western neighbourhood of the Brehov village, was developed in the center of the southern part of buried-submarine caldera Brehov–Sirník (Figs. 2, 3, 5a, b and 6). The vertical lithostratigraphic column of the Brehov ore deposit and diagrammatic presentation of the tectonic setting is in Fig. 7.

Available knowledge about the geological setting of the Brehov ore deposit extends from the surface to a depth of 650 m to the upper part of the quartz diorite porphyry stock body, representing a deepest part, reached by our drilling works. The direct known level of the Brehov ore deposit in the footwall encompasses a stockwork feeder zone of the subaqueous ores. It probably contains the former conduits, through which the metal bearing fluids were ascending and presumably spread on the seafloor. The Brehov feeder zone was located adjacent to quartz diorite porphyry rocks. The footwall mineralization is represented by pyrite-chalcopyrite stockwork veinlets and ore disseminations. The discrete veins are not present.

Within the quartz diorite porphyry footwall feeder zone of the Brehov ore deposit our drillholes intersected also sill and dike bodies of altered fine-grained quartz diorite porphyry, broadly contemporary with the pyrite, chalcopyrite + (pyrrhotine) hydrothermal mineralization. We interpret the quartz diorite porphyry intrusion as a "heater", driving the hydrothermal convective system.

The Brehov ore deposit sulphide mineralization represents distinct geochemically and mineralogically zoned Zn-Pb-Cu system. Cu (in chalcopyrite) dominates in

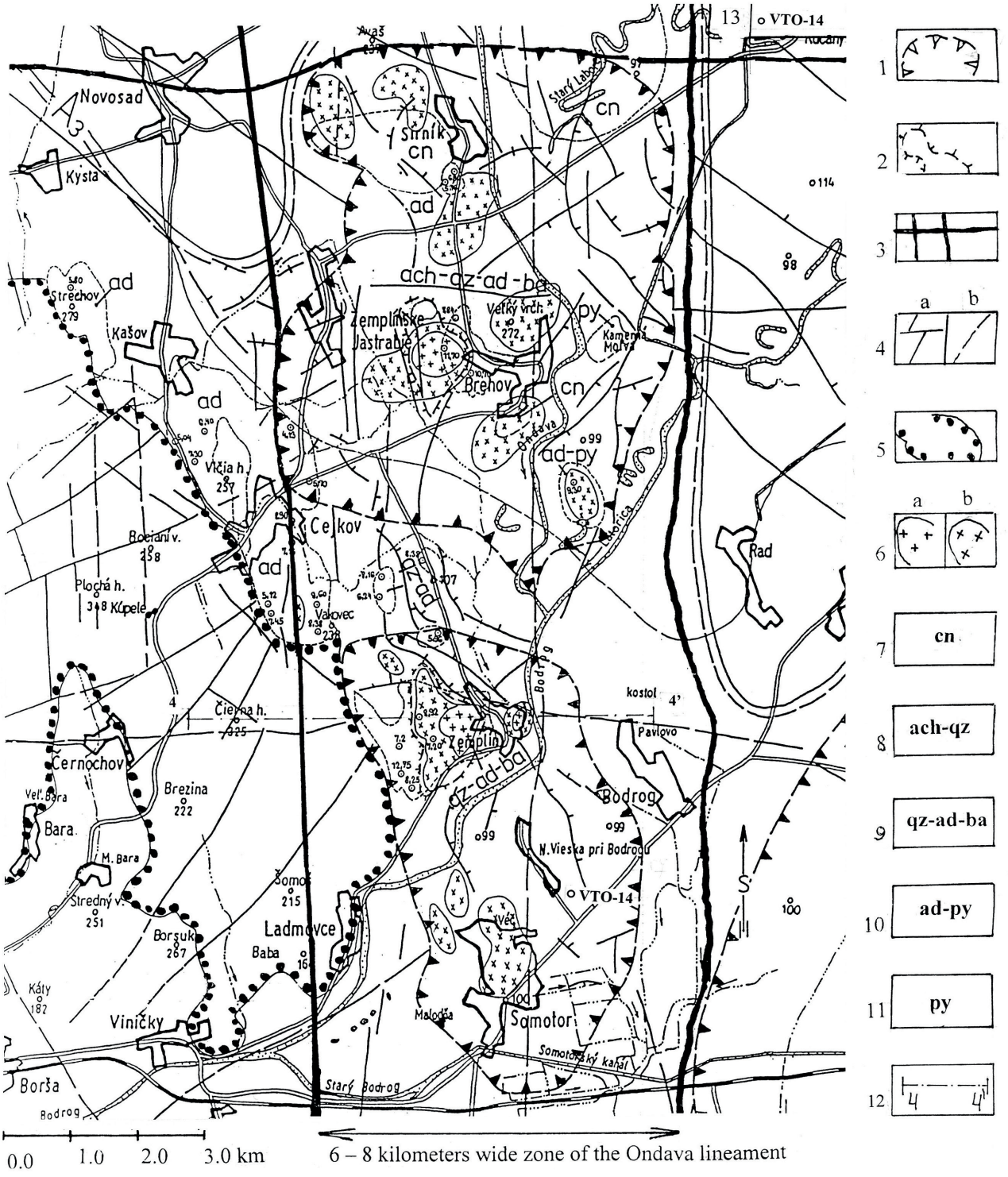

Fig. 5a. Interpreted calderas Brehov–Sirník and Zemplín–Somotor; Neogene magmatic bodies and products of alteration (on surface) (Bacsó, 2014; interpreted and compiled using own geological data and according geophysical data from Velich, Husák & Stránska, 1988–1991).

1 – interpreted fault boundaries of fossil submarine calderas; 2 – interpreted boundaries of elevation inside of caldera; 3 – deep fault; 4 – shallow fault: a) interpreted, b) assumed; 5 – Late Paleozoic-Mesozoic units of Internal Carpathians ("Zemplín Island"); 6 – ore-bearing subvolcanic intrusions: a) proved, b) interpreted. Surface products of hydrothermal alteration: 7 – chalcedony; 8 – agate – jasper – quartz; 9 – quartz – adularia – barite; 10 – adularia – pyrite; 11 – pyrite, 12 – line of cross-section.

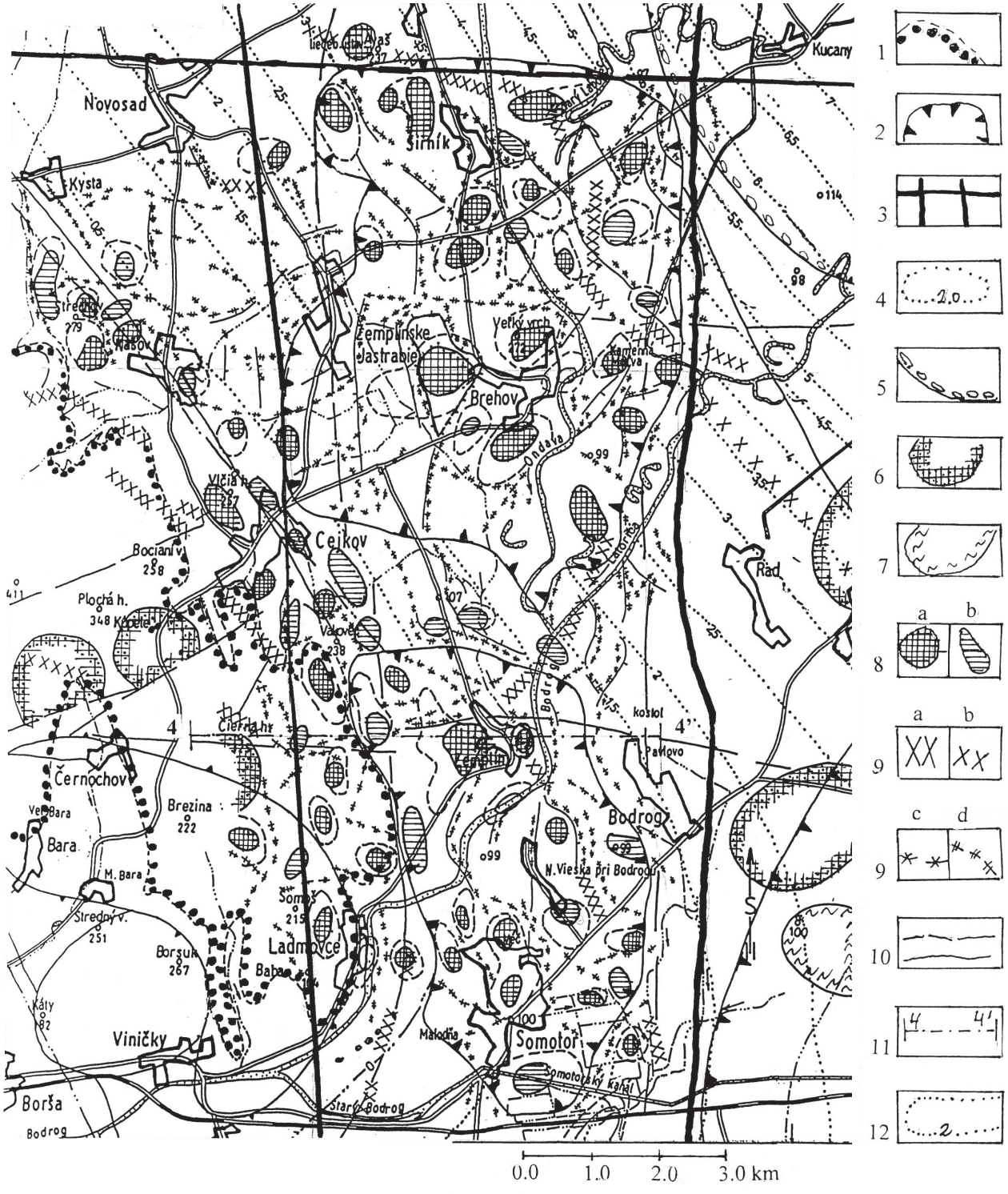

Fig. 5b. Geological and gravimetric schematic map of Brehov–Zemplín area. Interpreted calderas (Bacsó, 2014; interpreted and compiled according own geological data and geophysical data from Velich, Husák & Stránska, 1988–1991). 1 – Late Paleozoic, Mesozoic of Internal Carpathians ("Zemplín Island"); 2 – boundaries of interpreted caldera structures; 3 – deep faults; 4 – outline of Pre-Cenozoic basement surface in East Slovakian depression (based on seismic and gravimetric data – depth in kilometers); 5 – boundaries of Prešov–Kráľovský Chlmec graben structure with negative polarity; 6 – positive density anomalies from regional gravimetrical measurements; 7 – negative density anomalies from regional measurements; 8 – contours of local gravity anomalies: a) positive polarity, b) negative polarity; 9 – density boundaries: a) highly expressive, b) expressive, c) highly distinct, d) distinct; 10 – normal faults, 11 – line of cross-section; 12 – isolines of Pre-Cenozoic basement in kilometers.

the footwall stockwork rocks and the bottom part of the semi-massive sulphide lenses, while Zn-Pb minerals prevail in the center and upper part of the stratabound ore lenses.

Bimodal volcanic rock associations system (rhyodacite volcaniclastics, rhyodacite extrusive bodies, and quartz diorite porphyry bodies) occur near Brehov Fe-Zn-Cu sulphides.

The ore associations of the Brehov volcanogenic ore deposit consist of subhorizontal, stratabound-concordant ore lenses and discordant stockwork ores, members which are formed in a continuous set. The concordant semi-massive lenses of Zn-Pb-Cu-Fe ores are usually underlain by a discordant feeder (pipe) stockwork Fe + Cu + Au zone of ore. The ore twins represent two close contemporary and genetically related, but discordant ore bodies. Semi-massive upper concordant ore bodies consist at least by 40–65 % of fine- to coarse crystalline stratabound metallic minerals, the rest being represented by gangue and rock minerals.

The Brehov submarine base and gold metal deposit manifests similarities to the Kuroko deposits of Japan. The majority of ore mineralization is hosted by rhyodacite pyroclastics and epiclastics, by breccias and partly by calcareous claystone. The Middle Badenian sedimentary calcareous claystone is partly thermally metamorphosed near the contacts with the Late Badenian quartz diorite porphyry bodies. Semi-massive fine-grained sphalerite, galena, chalcopyrite and pyrite are located here with smaller amount of tetrahedrite and quartz, calcite, sericite and chlorite gangue. They form conformable lenses, distributed around former volcanic centre (for example near the summit of Travnický kopec hill west of the Brehov village). Stockwork veinlets and disseminated mineralization contain the same Zn-Pb-Cu minerals as the footwall of the semi-massive stratabound ore bodies.

The moderate to intensive silicification and chloritization of the host rocks of ore mineralization indicates that at least a portion of the stockwork ore predated the emplacement of the semi-massive stratabound ores.

In the Brehov ore deposit the calcareous claystone sedimentary facies occur in association with rhyodacite amygdaloidal flows, coarse-grained epiclastics, rhyodacite breccias to fine laminated tuffs, péperite breccias and tuffs. Many breccias are polymictic, composed of fragments ranging in composition from rhyodacite to quartz diorite porphyry. The clasts are usually present in a fine-grained chlorite matrix. The amygdules and spaces between the rock fragments are often filled with calcite, quartz and pyrite.

The Brehov ore deposit is a part of a resurgent caldera horst, submeridional oriented structure long 2200–2600 m and wide 850–1000 m in east-west direction, located in the center of the southern part of the Brehov–Sirník buried submarine caldera (Fig. 6).

The central gold-bearing zone of the Brehov ore deposit was penetrated by drillholes, VBZ-3, VBZ-7, VBZ-7A, VBZ-14 and VBZ-20. Beside a common type of main and minor ore minerals as sphalerite, galena, chalcopyrite and pyrite, there are present mostly trace minerals – gold, gold with bismuth, native silver, synchysite-Ce, ferberite, wolframite, adularia, brunsvigite, ripidolite, pycnochlorite and Mg-siderite. These trace minerals are typical only for the central part of the Brehov ore deposit (Figs. 6, 7, 8 and 9; Tabs. 1, 2 and 3).

The peripheral part of the Brehov ore deposit extends around the drillholes VBZ-4, VBZ-1A, VBZ-15, VBZ-18, VSB-1, VSB-5, which intersected Zn-Pb-Cu-Fe main ore mineralization with its typical accessoric hydrothermal minerals of tetrahedrite, freibergite, acanthite, bournonite, pearceite, Fe-smithsonite, stibnite, polybasite, Mn-siderite and Zn-ankerite.

3.2 The Zemplín ore field

The Zemplín submarine ore structure is located approximately 6 km south from the Brehov ore field, in the immediate western neighbourhood of the village of Zemplín. The Zemplín ore field is located in the southern continuation of the submeridional Ondava lineament zone in the northern part of the Zemplín–Somotor interpreted submarine buried caldera (Figs. 2–5a, 5b and 11).

The Zemplín ore field was verified by a detail geological, geochemical and geophysical survey, followed by trenching and a set of 300 m and 650 m deep drillholes. As a result of detailed and realized drilling program, below a shallow cover of rhyodacite volcanics (less than 150 m) a big laccolithic, hydrothermally altered body of Middle Badenian extrusive-intrusive pyroxene andesite and microdiorite rock complex was ascertained, with numerous small (thick 1–2 m) chimney polymetallic sulphidic Pb, Zn, Cu ore bodies (Fig. 11).

This strongly altered laccolithic Middle Badenian andesite-microdiorite body represents the host-rock environment for the sulphidic galena, sphalerite, pyrite and chalcopyrite mineralization. On the other side, in the Zemplín ore field the small rhyodacite extrusive bodies of Upper Badenian age represent the ore-bearing substance of the base metal mineralization.

The comprehensive geological interpretation of the ore mineralization in the Zemplín ore field shows that it represents the lower discordant feeder zone of the Kuroko type submarine Neogene sulphide base metal mineralization. The upper submarine concordant – stratabound semi-massive ore zone of the hydrothermal deposit was very probably removed by denudation and erosion in the past.

3.3 The ore-bearing intrusion of the Brehov ore deposit

Due to the strong hydrothermal alteration of the Brehov ore-bearing intrusion, the generally accepted naming

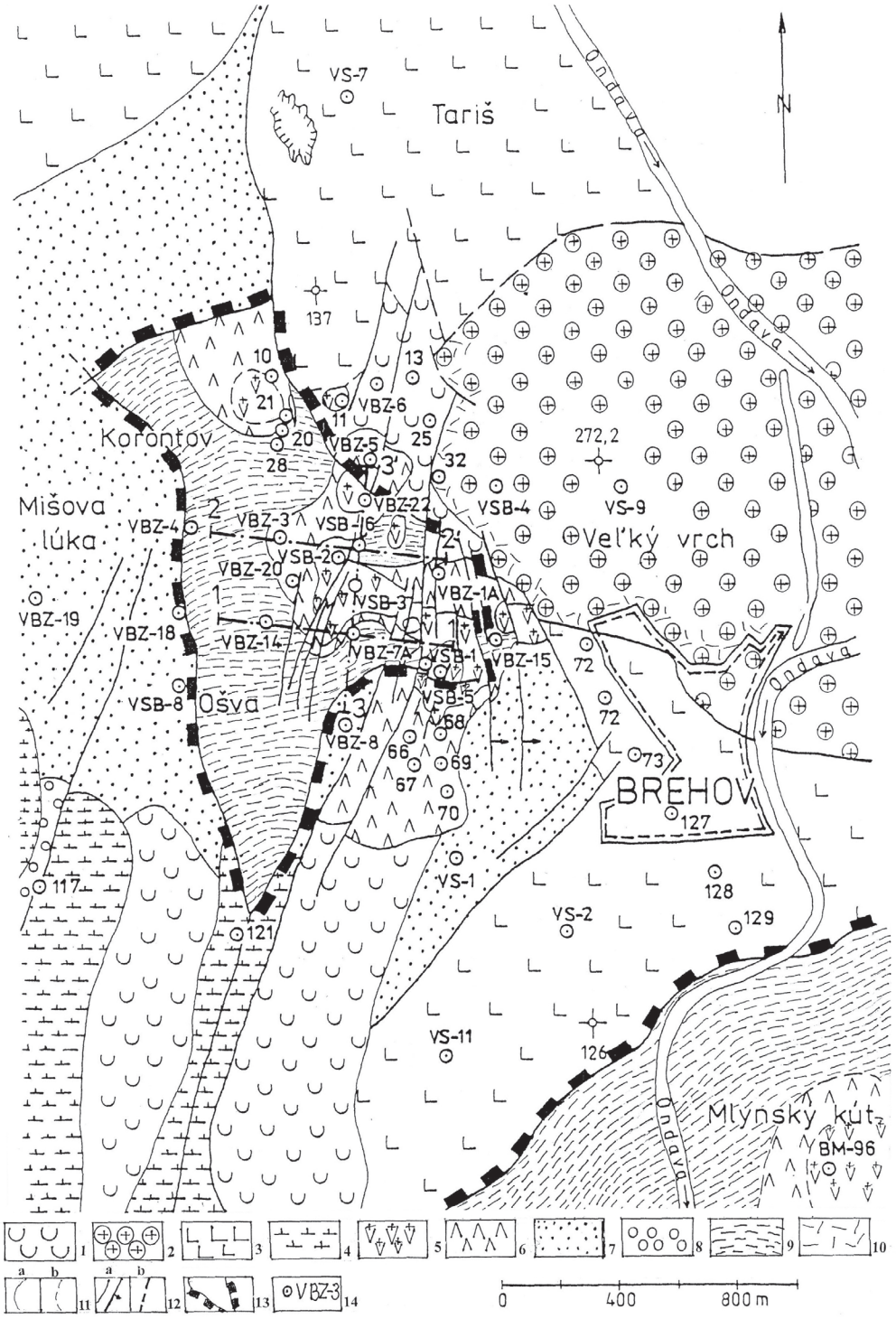

Fig. 6. Schematic geological map of the Brehov submarine hydrothermal ore deposit. 1 – Stretava Fm.: calcareous clays with beds of sand and rhyolite tuff and tuffite, Lower and Middle Sarmatian; 2 – extrusive bodies of pyroxene andesite; 3 – fresh lava flows of pyroxene andesite; 4 – strongly argillized lava flows of pyroxene andesite; 2–4 – Lower Sarmatian; 5 – silicified and adularized rhyodacite extrusions and lava flows; 6 – argillized rhyodacite extrusions and lava flows; 7 – calcareous clays – claystones with beds of siltstone, subsidiary tuffs and tuffites; 8 – Lastomír Fm.: redeposited fine-grained argillized volcaniclastics with pumice; 5–8 – Upper Badenian; 9 – sedimentary rocks of ore bearing volcanosedimentary sequence (claystone, sandstone, mudstone) of the Brehov resurgent caldera, transition sequence of Middle and Upper Badenian; 10 – brecciated rocks; 11 – geological boundaries: a) proved, b) assumed; 12 – faults: a) proved, b) assumed; 13 – ascertained boundaries of the Brehov ore deposit horst structure in the geological map; 14 – drillhole.

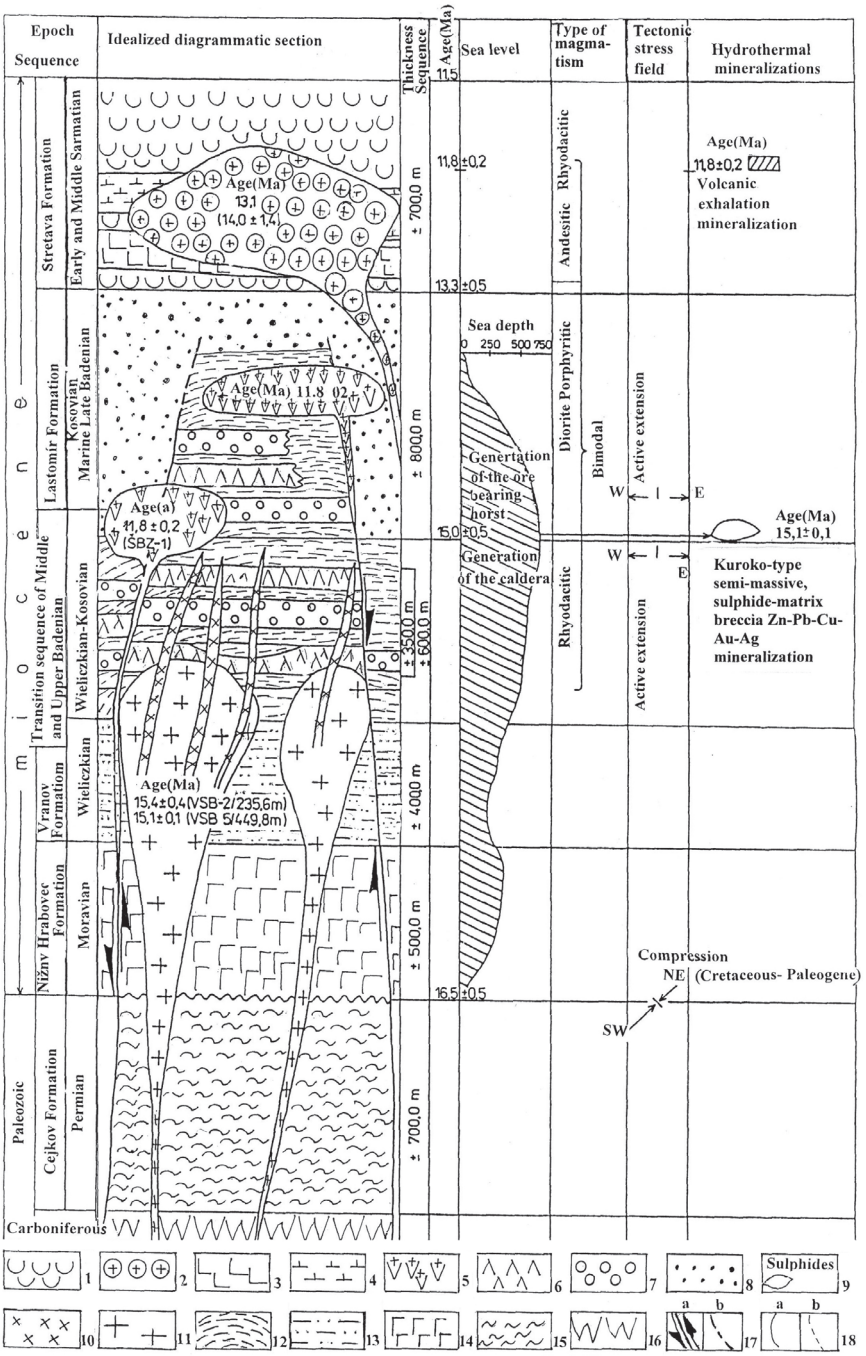

Fig. 7. Lithostratigraphic column of the Brehov ore deposit and diagrammatic presentation of the tectonic setting. 1 – Stretava Fm.: calcareous clays with beds of sand and rhyolite tuff and tuffite, Lower and Middle Sarmatian; 2 – extrusive bodies of pyroxene andesite; 3 – fresh lava flows of pyroxene andesite; 4 – strongly argillized lava flows of pyroxene andesite; 2–4 – Lower Sarmatian; 5 – silicified and adularized rhyodacite extrusions and lava flows; 6 – argillized rhyodacite extrusions and lava flows; 7 – Lastomír Fm.: calcareous clays – claystones with beds of siltstone, subsidiary tuffs and tuffites; 8 – redeposited fine-grained argillized volcaniclastics with pumice; 5–8 – Upper Badenian; 9 – polymetallic Fe-Zn-Pb-Cu-Au-Ag sulphide mineralization of the Brehov deposit; 10 – altered quartz diorite porphyry, sills, dikes; 11 – stock bodies of altered quartz diorite porphyry; 12 – sedimentary part of the ore bearing volcanosedimentary sequence (claystone, sandstone, mudstone) of the Brehov–Sirník resurgent caldera; 9–12 – transition sequence of Middle and Upper Badenian (Wieliczkian–Kosovian); 13 – Vranov Fm.: Grey calcareous claystone and sandstone, Middle Badenian–Wieliczkian; 14 – Nižný Hrabovec Fm.: calcareous sandstone alternating with beds of calcareous siltstone and claystone, Lower Badenian; 15 – Cejkov Fm.: redbrown sandstone, conglomerate, intercalations of sandy shale and rhyodacite tuff, Lower Permian; 16 – Kašov Fm.: green-grey sandstone with pebbles, sandy shale, products of rhyolite-dacite volcanism, Carboniferous; 17 – faults, generation of ore bearing horst: a) interpreted, b) assumed; 18 – geological boundaries: a) interpreted, b) assumed.

conventions for intrusive rocks on the basis of mineralogy and texture cannot be used. Therefore we have applied nomenclature based on chemical composition.

Traditional diagrams use the immobile elements (Floyd & Winchester, 1975, 1978; Winchester & Floyd, 1976, 1977). Actually, these diagrams, particularly the Nb/Y-Zr/TiO_2 diagram of Winchester and Floyd (1977) are in wide use even today. Regarding the Brehov–Zemplín metallogenetic sector (Fig. 12), for classification of altered rocks this diagram seems to work precisely.

Geochemically, the Neogene magmatic rocks in the "Border Zone" segment between W. Carpathians and E. Carpathians are very similar and can be all positioned to the same family of diorite, quartz-diorite and granodiorite magmas.

4 Mineralogical characteristic of the Brehov–Zemplín ore sector

4.1 The Brehov ore field

The Brehov deposit, correspondingly with other classical Kuroko type volcanogenic ore deposits, has two ore-bearing zones: The upper subhorizontal, stratabound, concordant ore-bearing zone of the ore bearing volcanic-sedimentary sequence (containing approximately 65 wt. % of the Kuroko type ore mineralization). The lower discordant, stockwork and feeder zone ore-bearing zone consists of veinlets of polymetallic mineralization in the altered quartz diorite porphyry stock body, containing app. 5 wt. % of the Kuroko ore mineralization. Between the upper and lower ore-bearing zones of the Brehov ore deposit a zone of quartz diorite porphyry sill and dike bodies occurs, with characteristic polymetallic mineralization, similar to hydrothermal veinlets mineralization in the lower ore-bearing zone of the deposit (containing approximately 30 wt. % of ore mineralization).

1. The stratabound, subhorizontal and concordant upper zone of ore mineralization, mostly in the rhyodacite epiclastics and pyroclastics horizons, dominantly in the form of semimassive Kuroko type sulphide matrix-breccia, Fe-Zn-Pb-Cu + Au, + Ag mineralization (Figs. 9 and 10; Tab. 2):

   Main minerals: Sphalerite, pyrite, galena, chalcopyrite, quartz, carbonate;

   Minor minerals: Barite, marcasite, specularite, Mg-siderite, amethyst, Fe-smithsonite, Zn-ankerite, Mn-siderite;

   Trace minerals: Tetrahedrite, pearceite, wolframite, scheelite, acanthite, bournonite, arsenopyrite, Ag-tetrahedrite, polybasite, stibnite, chalkosine, carbonate Ca + TR, monazite.
2. The hydrothermal veinlet minerals of sill and dike bodies of the altered quartz diorite porphyry transition zone, from subhorizontal, concordant, stratabound part of the deposit to discordant veinlet ore of the feeder zone intrusive (Figs. 9 and 10; Tab. 3):

   Main minerals: Pyrite, sphalerite, galena, chalcopyrite, quartz, carbonate;

   Minor minerals: Marcasite, specularite, gold, siderite, barite, Mg-siderite;

   Trace minerals: Scheelite, wolframite, native silver, acanthite, synchysite-Ce, greenockite (hawleyite?), ferberite, chalkosine, pearceite, cinnabar.

   Though the precious metals represent an important commodity in many Kuroko type deposits (Hannington et al., 1999), in the case of Brehov ore deposit they occur as volumetrically minor minerals (mostly in form of native gold). Visible gold is generally present as inclusions of native gold in major sulphide minerals, whereas silver occurs in Ag-sulphides and sulfosalt minerals such as tetrahedrite and freibergite.
3. The hydrothermal minerals of the discordant stockwork-feeder zone intrusive, from the altered quartz diorite porphyry stock body, mostly in form of veinlets (Figs. 9 and 10; Tab. 1):

   Main minerals: Pyrite, chalcopyrite, quartz, carbonate, chlorite;

   Minor minerals: Galena, sphalerite, adularia, Ca-siderite, marcasite, hematite, pycnochlorite, brunsvigite, ripidolite, Mn-siderite, specularite;

   Trace minerals: Tetrahedrite, native silver, acanthite, gold, gold with bismuth, scheelite, antimonite, barite, Fe-dolomite, carbonate Ce, carbonate.

In altered quartz diorite porphyry stock body, the Mg-chlorite mineralization, forming the fissure filling was intersected by the drillholes in the deeper part of the Brehov ore deposit. The Mg-chlorite mineralization indicates the presence of ophiolites in the near basement of the Brehov ore deposit (Tab. 1; Fig. 10). Similar Mg-rich chlorite was described by Herzig and Friedrich (1987) from the famous ophiolite locality Agrokipia on the Cyprus island.

A few kilometers north of Brehov ore deposit, the deep-oil drillholes Rebrín 1, Blatná Polianka 1, Senné 2, Senné 8, Pavlovce 1, Zbudza 1, located in the Pozdišovce–Krichevo geological unit in Paleogene–Mesozoic basement, have intersected the ophiolite body, mostly of serpentinized peridotites (Mořkovsky & Cverčko, 1987; Gnojek, 1987; Gnojek et al., 1991).

Caverns and fissures in the volcano-sedimentary ore-bearing sequences are partly filled with crystals of pure quartz, honey yellow sphalerite with dodecahedron crystals, crystals of galena and pyrite, sometimes with chalcopyrite. Within 1 centimeter wide caverns the pure slices of younger barite and in places also kaolinite are frequently visible. Synsedimentary polymetallic mineralization in the environment of sedimentary rocks presents sporadically in thin interbeds.

In the intrusive quartz diorite porphyry bodies (stocks, sills and dikes), the polymetallic ore mineralization has a character of veinlets, first of all pyrite and chalcopyrite, rarely with presence of sphalerite, galena, and in some places marcasite. Microscopic study has ascertained tetrahedrite, bournonite, scarce galenobismutite and pyrrhotite. In some grains of galena is present rare matildite (with increased content of silver, up to 2 %).

The bodies of quartz diorite porphyry with strong chloritization are bearing mostly carbonate and hematite mineralization in the form of veinlets, nests, and pods. In some places, in small fissures the bigger concentrations of chalcopyrite, pyrite, marcasite and relicts of pyrrhotite occur. From carbonate the Fe-dolomite is more often frequent, having the FeO content of 10.4–39.6 %, MgO 11.5–18.9 %, CaO 1.1–28.0 %. The hematite contains increased contents of vanadium, up to 0.046 %. The druses of crystallic light-violet amethyst were found, too.

1. The most frequent associations of hydrothermal minerals in the Brehov ore deposit are as follows: 1. The barite-quartz-pyrite + marcasite, hematite, rutile (so-called barite "ores");
2. Polymetallic ore with predominance of sphalerite, galena + chalcopyrite, barite, carbonate, tetrahedrite, bournonite, pyrite, marcasite (black ores);
3. Polymetallic ore with predominance of chalcopyrite, less marcasite, sphalerite, galena, tetrahedrite, bournonite, galenobismutite, pyrrhotite, pyrite (yellow ores);
4. Carbonates, quartz, hematite + chalcopyrite, pyrite, marcasite, pyrrhotite.

There can be summed up that polymetallic mineralization of the Brehov ore deposit consists of sphalerite, galena, pyrite, chalcopyrite, barite with hematite as main minerals. Quartz is present in the entire section of the ore deposit.

The most widespread ore mineral is sphalerite. The colour of sphalerite is from honey-yellow to brown (in the deeper part of the deposit). In sphalerite grains the rare inclusions of chalcopyrite or pyrrhotite occur. From the trace elements in sphalerite there were ascertained Sn (10–30 g/t), Ag (20–105 g/t), and Cd (0.27–0.37 g/t). The Fe contents in sphalerite are very low, mostly 0.3–1.0 %. In some sphalerites (in the center and deeper parts of the deposit), the very high contents of Ga (3.8–4.0 %) were ascertained. The contents of Ag in galena are around 5.0 g/t. The contents of Ag in chalcopyrite are only around 40 g/t. In barite in trace amounts there are present PbO (0.134–0.176 %) and SrO (1.23–2.52 %). Hematites contain low amount of TiO_2 (around 150 g/t).

4.2 The Zemplín ore field

Main minerals: Galena, sphalerite, pyrite, marcasite, quartz, amethyst, chalcedony calcite, dolomite and barite;

Minor minerals: Hematite, chalcopyrite, arsenic-pyrite, siderite;

Trace minerals: Tetrahedrite, chalkosine, Ag-tennantite, native silver, As-polybasite, acanthite, greenockite, (hawleyte?), mckinstryite, pearceite, scheelite.

Ore minerals are mostly connected with quartz-carbonate veinlets and occur in fissures and small caverns of the extrusive-intrusive altered pyroxene andesite body. Only very rare ore minerals are present in form of impregnations, mostly as cement between breccia fragments of andesite. Many times small crystals of galena, or sphalerite are in association with druses of quartz and kaolinite-illite, fulfilling small cavities.

From the hydrothermal alterations the hematitization, argillization, silicification and chloritization are the most widespread (Fig. 11).

Remark: Electron microprobe analyses of monomineralic multigrain aggregates were conducted with CAMSCAN LINK-AN 10 000 system, at the Research Institute ČSVP, in Stráž pod Ralskem, Czech Republic. Analyst: M. Scharmová and P. Súlovský. A total of 500 sulphide and gangue minerals were analysed, in order to obtain quantitative chemical data from mineral grains of the Brehov and Zemplín ore fields.

5 The Brehov submarine volcanogenic sulphide ore deposit – position within the Internal Carpathian–Alpine Cenozoic metallogenetic belt

Within the Internal Carpathian–Alpine Cenozoic metallogenetic belt, the Brehov ore deposit is located in the "Border Zone" segment between W. Carpathians and E. Carpathians, which is bearing a number of fully and partly submarine volcanogenic base metal and gold-silver ore deposits.

The first essential difference between the "Border Zone" segment of the W. Carpathians and E. Carpathians ore fields and those in other five large segments of the Internal Carpathian–Alpine Cenozoic metallogenetic belt is that the "Border Zone" segment ore fields are volcanogenetically and metallogenetically partly or fully developed in submarine environment, while the other five large segments of the Internal Carpathian–Alpine Cenozoic metallogenetic belt are developed mostly or exclusively in subaerial environment. Second principal difference between the "Border Zone" segment ore fields on one side and the subaerial ones in other segments of Internal Carpathian–Alpine Cenozoic metallogenetic belt on the other side is that in the "Border Zoner" segment the classical large epithermal, low-sulfidation vein deposits are not present, being so typical for all fully subaerial Neogene ore deposits of the Internal Carpathian–Alpine Cenozoic metallogenetic belt, first of all for the Western Carpathians segment, Eastern Carpathians segment and the Apuseni Mts segment.

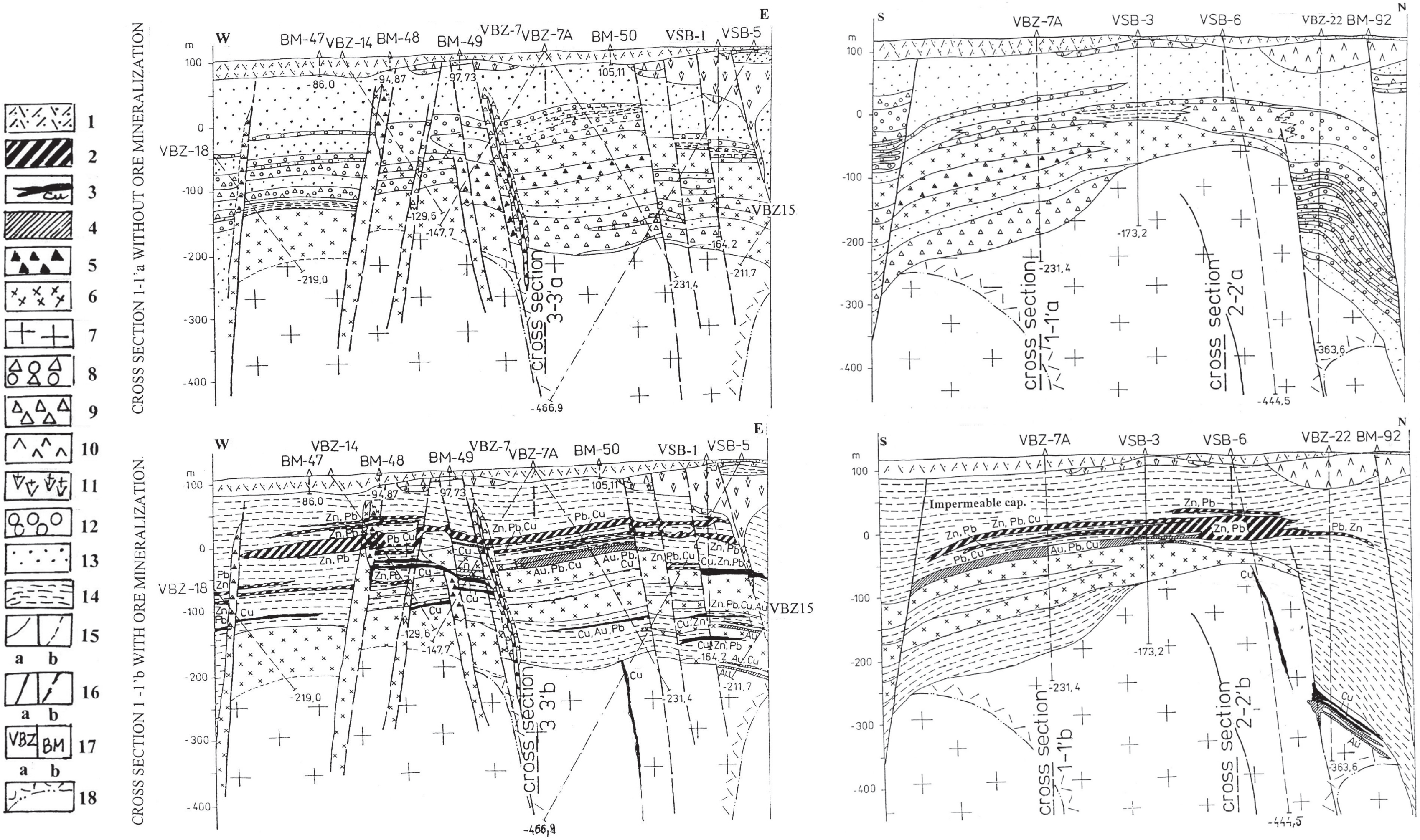

Fig. 8. Evidence of stratabound character of the Neogene ore mineralization in the volcanosedimentary sequence of the Brehov–Sirník interpreted resurgent caldera: ore mineralization is restricted to the volcanic part of the sequence. 1 – Quaternary clay, loam, sand; 2 – heterolithic semi-massive sulphide matrix-breccia Zn-Pb-Fe ore of claystone, sandstone, rhyodacite and its tuff, quartz diorite porphyry; 3 – magmatic hydrothermal semi-massive sulphide matrix-breccia Cu-Fe ore; 4 – siliceous stringer and disseminated Fe-Cu-Au ore of quartz diorite porphyry stock body of sills and dikes of quartz diorite porphyry; 5 – magmatic hydrothermal breccia of quartz diorite dikes; 6 – altered quartz diorite porphyry sills and dikes; 7 – stock body of altered quartz diorite porphyry; 8 – altered breccia of rhyodacite and its tuff; 9 – altered rhyodacite tuff and tuffite; 10 – argillized rhyodacite extrusions and lava flows; 11 – silicified and adularized rhyodacite extrusions and lava flows; 2–11 – Upper Badenian; 12 – hydrothermal explosive rhyodacite breccia; 13 – sedimentary part of the ore bearing volcanosedimentary sequence (claystone, sandstone, mudstone); 14 – undivided ore bearing volcanosedimentary sequence – transition from Middle to Upper Badenian (Wieliczkian–Kosovian); 15 – geological boundaries: a) proved, b) assumed; 16 – faults: a) proved, b) assumed; 17 – drillholes: a) deep 300–600 m; b) deep 10–100 m; 18 – brecciated hydrothermal vent (conduit) boundaries.

Ore bearing and altered volcanic sedimentary sequence.
Drillhole and depths : VBZ14/155.5 m, 158.0 m.
Present are hydrothermal minerals :
siderite, Mg-siderite, polybasite, tetrahedrite, pyrite, pearceite, galena, chalcopyrite, wolframite, scheelite, specularite, marcasite, monazite, carbonate Ca+TR, quartz.

VBZ14/158.3 – 160.3 m./
Contents of elements :
Pb(wt%)=0.01,
Zn(wt%)=0.01,
Cu(wt%)=1.53,
Au(g/t)=0.04,
Ag(g/t)=28.8.

Top part of altered quartz diorite porphyry subvolcanic body;(to depth 100 m).
Drillhole and depths : VBZ7A/147.7 m, 157.8 m, 357.2 m.
Present are hydrothermal minerals : scheelite, pyrite, ferberite, wolframite, specularite, sphalerite, galena, gold, barite, Mg-siderite, synchisite – Ce.

Drillhole and depth :
VBZ7A/162.6 – 163.6 m,
Contents of elements :
Pb(wt%)=0.005,
Zn(wt%)=0.03,
Cu(wt%)=0.002,
Au(g/t)=2.20,
Ag(g/t)=0.80.

Sill and dike bodies of altered quartz diorite porphyry.
Drillhole and depths : VBZ7A/162.2 m, 231.8 m.
Present are hydrothermal minerals :
sphalerite, galena, chalcopyrite, quartz, pyrite, marcasite, wolframite, scheelite, gold, native silver, acanthite, synchysite – Ce,greenockite (hawleyite?), specularite, siderite, Mg-siderite.

Drillhole and depth :
VBZ7A/167.4 – 168.9.
Contents of elements :
Pb(wt%)=2.36,
Zn(wt%)=0.01,
Cu(wt%)=0.09,
Au(g/t)=1.06,
Ag(g/t)=23.80.

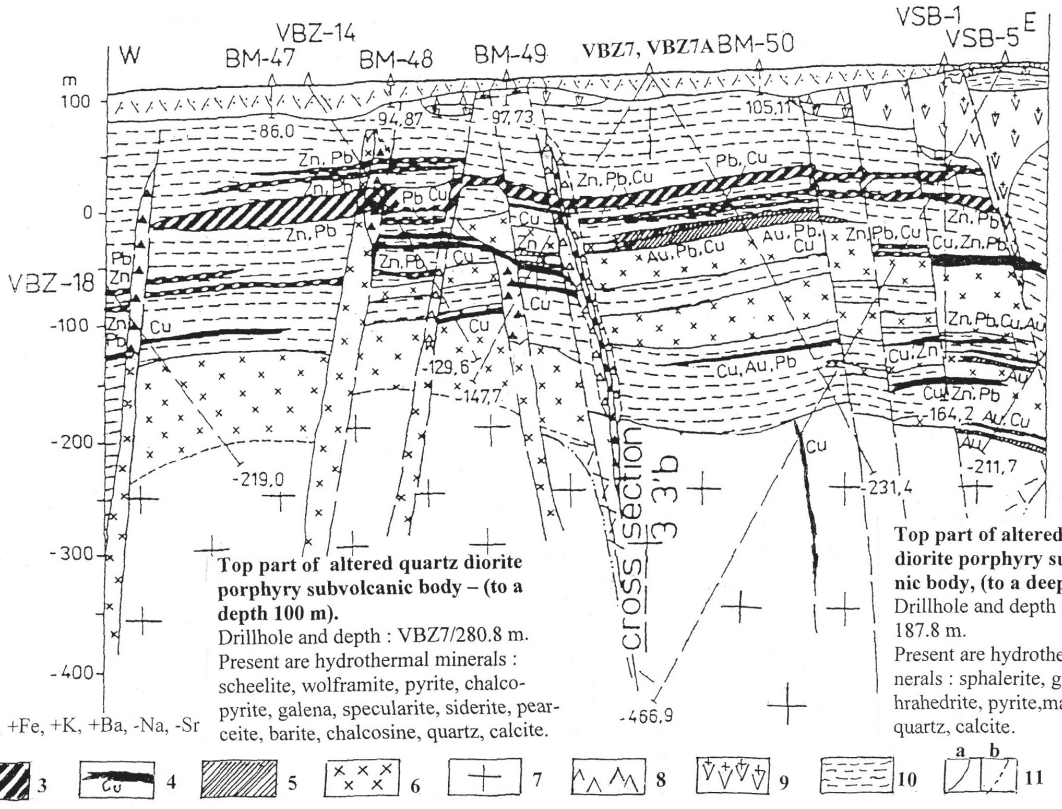

Ore-bearing and altered volcanic sedimentary sequence.
Drillhole and depth :
VBZ18/225.0 m.
Present are minerals :
sphalerite, pyrite,
galena, Ag-tetrahedrite,
monazite, carbonate Ca+TR,
tetrahedrite.
Drillhole and depth :
VBZ18/231.0 – 232,.3 m/
Pb(wt%)=0.65,
Zn(wt%)=2.74,
Cu(wt%)=0.02,
Au(g/t=0.01,
Ag(g/t)=343.18

Top part of altered quartz diorite porphyry subvolcanic body – (to a depth 100 m).
Drillhole and depth : VBZ7/280.8 m.
Present are hydrothermal minerals : scheelite, wolframite, pyrite, chalcopyrite, galena, specularite, siderite, pearceite, barite, chalcosine, quartz, calcite.

Top part of altered quartz diorite porphyry subvolcanic body, (to a deep 100 m).
Drillhole and depth : VBZ15/187.8 m.
Present are hydrothermal minerals : sphalerite, galena, tetrahedrite, pyrite,marcasite, quartz, calcite.

Ore-bearing and altered volcanic sedimentary sequence.
Drillhole and depth :
VSB5/106.6 m, 111,05 m.
Present are hydrothermal minerals :
sphalerite, smithsonite, pyrite, galena, acanthite, chalcopyrite, bournonite, tetrahedrite, barite, chalcosine, marcasite.
Drillhole and depth :
VSB5/117.0 – 119.0 m.
Contents of elements :
Pb(wt%)=1,86,
Zn(wt%)=0,78,
Cu(wt%)=1,02,
Au(g/t)=0,01,
Ag(g/t)=39,6.

Drillhole and depth :
VBZ15/321.0 – 323.0 m/
Contents of elements :
Pb(wt%)=1.17,
Zn(wt%)=1.43,
Cu(wt%)=0.06,
Au(g/t)=0.10,
Ag(g/t)=11.35.

Changes in rock chemistry : +Mg, +Fe, +K, +Ba, -Na, -Sr

Fig. 9. Representative hydrothermal mineral assemblage from the Brehov ore deposit, cross-section 1–1`: 1 – Quaternary clay, loam and sand; 2 – Early Sarmatian dike body of pyroxene andesite; 3 – heterolithic semi-massive sulphide matrix breccia Zn-Pb-Fe ore in claystone, sandstone, rhyodacite and rhyodacite tuff; 4 – magmatic hydrothermal semi-massive sulphide matrix breccia Cu-Fe ore; 5 – siliceous stringer and disseminated Fe-Cu-Au ore; 6 – altered quartz diorite porphyry sills and dikes; 7 – stock body of altered quartz diorite porphyry; 8 – argillized rhyodacite extrusions and lava flows; 9 – silicified and adularized rhyodacite extrusions and lava flows; 3–9 – Late Badenian; 10 – undivided ore bearing volcanosedimentary sequence – transition from Middle to Upper Badenian; 11 – geological boundaries: a) proved, b) assumed; 12 – faults: a) proved, b) assumed; 13 – drillholes: a) deep 300–650 m; b) deep 10–100 m; 14 – brecciated hydrothermal vent (conduit) boundaries; 15 – magmatic hydrothermal breccia of quartz diorite porphyry dikes; 16 – heterolithic breccia of altered claystone, sandstone, rhyodacite tuff, rhyodacite, quartz diorite porphyry.

Top-part of the altered diorite porphyry subvolcanic body,(to a depth 100 m).
Drillhole and depth : VBZ20/184,9 m/.
Present are hydrothermal minerals : hematite, chalcopyrite, siderite, galena, acanthite, monazite, carbonate Ca+REE, carbonate Ce, gold, gold with Bi, native silver.

Drillhole and depth : VBZ20/222.40 – 228.4 m/.
Contents of elements : Pb(wt%)=0.002, Zn(wt%)=0.013, Cu(wt%)=0.738, Au(g/t) = 1.3 Ag(g/t) = 1.27

Deeper part of the diorite porphyry subvolcanic body, (more than 100 m).
Drillholes and depths : VSB2/223.6 m, 265.5 m. VSB6/601.5 m,.
Present are hydrothermal minerals: pyrite, marcasite, quartz, carbonate, specularite, pycnochlorite, brunsvigite, ripidolite, adularia, Mg-siderite, dolomite, apatite, zircon, REE-carbonate.

Drillhole and depth : VSB2/190.6 – 191.7 m/. Contents of elements : Pb(wt%)=0.01, Zn(wt%)=0.03, Cu(wt%)=8.54, Au(g/t)=0.01, Ag(g/t)=10.29,

Drillhole and depth : VSB6/150.7 – 151.7 m. Contents of elements : Pb(wt%)=1.39, Zn(wt%)=2.14, Cu(wt%)=0.02, Au(g/t)=1.10, Ag(g/t)=5.8.

Deeper part of the diorite porphyry subvolcanic body, (more than 100 m).
Drillhole and depths : VBZ3/205.0 m, 253.5 m.
Present are hydrothermal minerals : pyrite, marcasite, galena, sphalerite, chalcopyrite, tetrahedrite, Ca-siderite, native silver,acanthite. calcite, monazite, quartz.
Drillhole and depth : VBZ3/134.0 – 135.5 m/. Contents of elements : Pb(wt%)=0.04, Zn(wt%)=0.04, Cu(wt%)=0.02, Au(g/t)=8.07, Ag(g/t)=2.49,

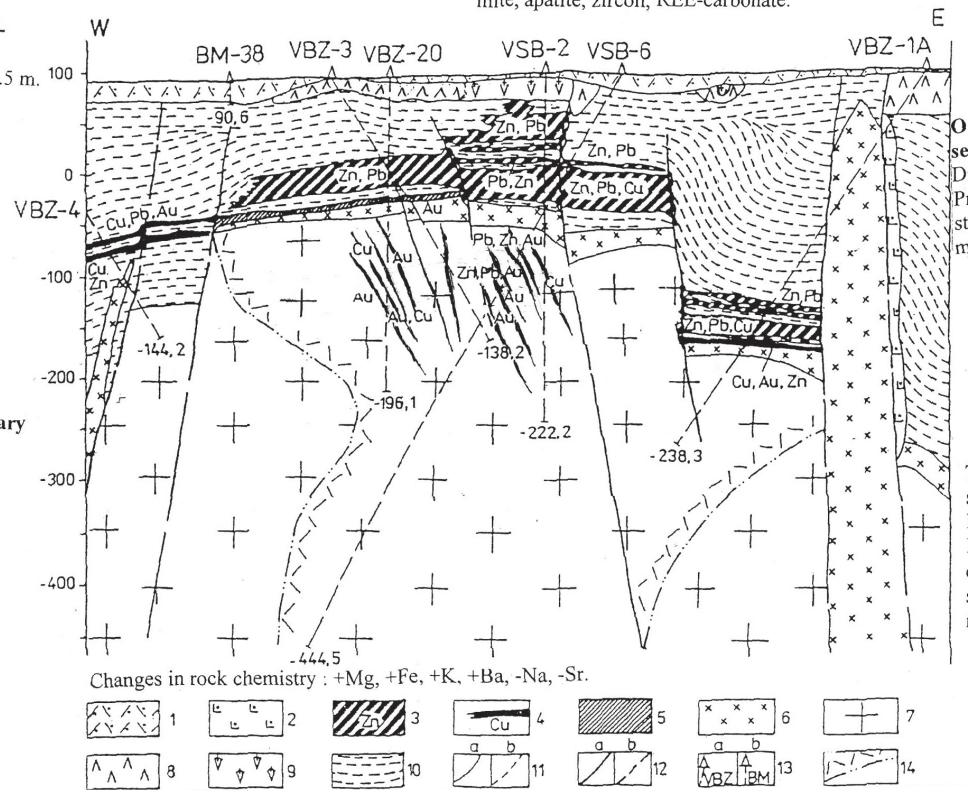

Ore-bearing, altered volcanic-sedimentary sequence.
Drillhole and depth :VBZ4/180.6 m.
Present are hydrothermal minerals : tetrahedrite, pearceite, galena, chalcopyrite, pyrite, marcasite, barite, amethyst, arsenopyrite, quartz, calcite.
Drillhole and depth : VBZ4/193.0 – 195.0 m/. Contents of elememts : Pb(wt%)=0.40, Zn(wt%)=0.90, Cu(wt%)=0.59, Ag(wt%)=12.3,

Ore-bearing, altered volcanic-sedimentary sequence.
Drillhole and depth : VBZ1A/288.0 m.
Present are hydrothermal minerals : stibnite, barite, scheelite, Mn-siderite, monazite, quartz.
Drillhole and depth : VBZ1A/291,2 – 293,2 m/. Pb(wt%)=1,33, Zn(wt%)=4,24, Cu(wt%)=0,06, Au(g/t)=0,06, Ag(g/t)=27,2.

Top part of the altered diorite porphyry subvolcanic body, (less than 100 m).
Drillhole and depth : VBZ1A/315.75 m.
Present are hydrothermal minerals : quartz, carbonate, pyrite, marcasite, sphalerite, chalcopyrite, galena, antimonite, barite,scheelite,, Mn-siderite,
Drillhole and depth : VBZ1A/326.0 – 327.0 m. Contents of elements : Cu(wt%)=0.85, Au(g/t)=0.07, Ag(g/t)=48.

Fig. 10. Representative hydrothermal mineral assemblage from the Brehov ore deposit, cross-section 2–2`. Explanations see in Fig. 9.

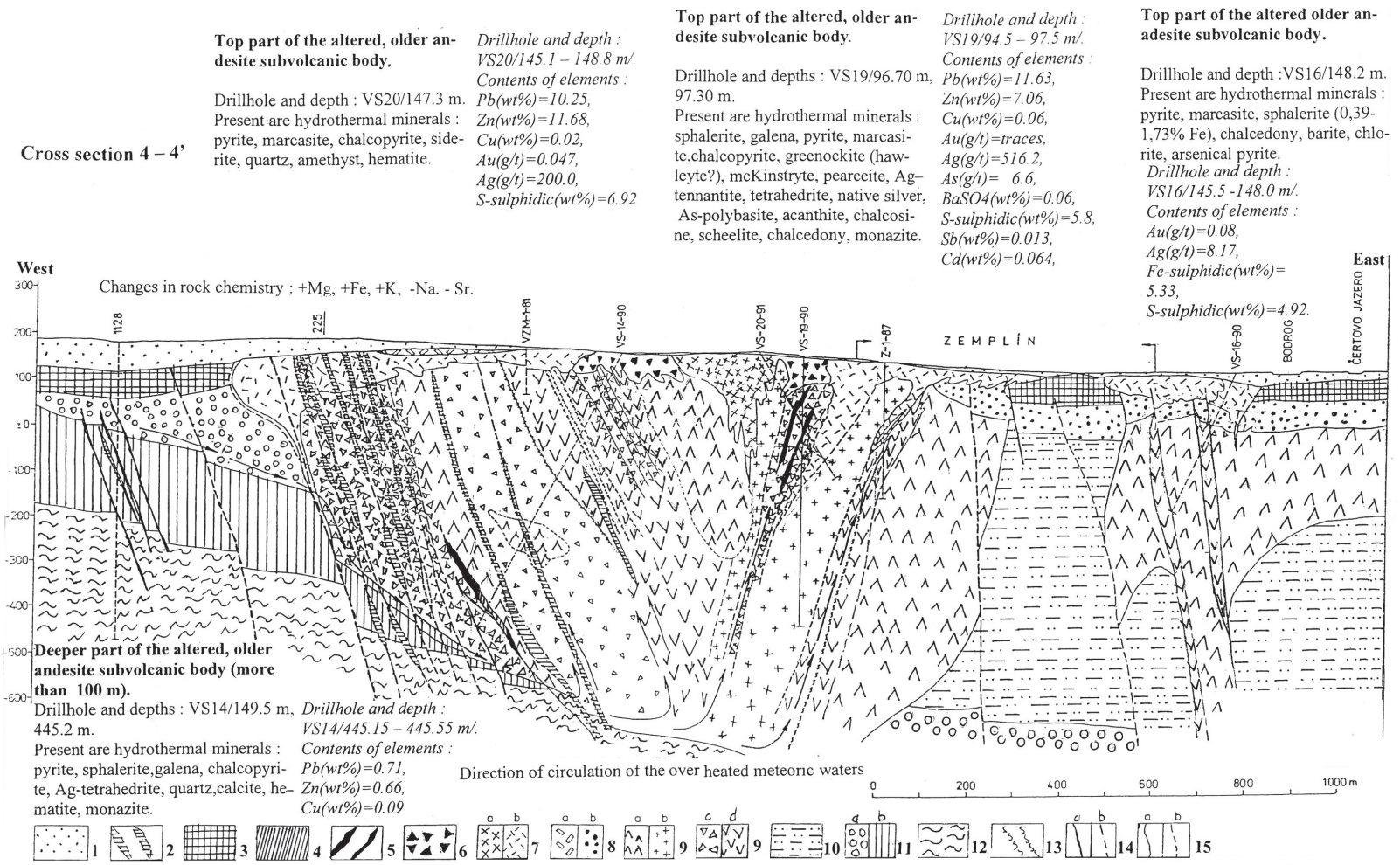

Fig. 11. Representative hydrothermal mineral assemblages and their relationship to ore geology. Submarine hydrothermal center near village of Zemplín in eastern Slovakia. 1 – Quaternary alluvial deposits; 2 – dike bodies of basaltic andesite, Upper Sarmatian; 3 – Kochanovce Fm.: calcareous clays, lignite seams, rhyodacitic tuffs, tuffites, Middle Sarmatian; 4 – zone of veinlets, impregnations, poor hydrothermal Zn-Pb-Fe-Ag mineralization in andesitic environment; 5 – rich Zn-Pb-Ag-Fe ore in andesitic chimneys; 6 – altered, brecciated rhyodacite with amethyst–quartz veinlets in vesicles; 4–6 – Upper Badenian–Lower Sarmatian; 7 – rhyodacite extrusions, irregularly fractured, with quartz, chalcedony (jasper) veinlets and zones of K-metasomatism: a) massive rock with adularization, silicification and argillization, b) brecciated, altered rhyodacite; 8a – redeposited, altered volcaniclastics of rhyodacite, mostly brecciated and with silicification; 8b – weakly altered, redeposited volcaniclastics of rhyodacite; 9 – altered subvolcanic bodies: a) coarse-grained intrusive andesites with vesicles, b) fine-grained intrusive altered andesite, both near sulphidic Zn-Pb-Ag-Fe mineralization with adularia, sporadically with barite, c) autoclastic breccia of strongly altered intrusive andesite, d) zones of weakly altered, brecciated intrusive andesite; 7–9 – Upper Badenian; 10 – Vranov Fm.: calcareous claystones, sandstones, Middle Badenian; 11 – Lúžna Fm.: a) conglomerates, b) sandstones, Lower Triassic; 12 – Cejkov Fm.: sandstones, conglomerates, Lower Permian; 13 – linear zones of brecciation, 14 – faults: a) inferred, b) interpreted; 15 – geological boundaries: a) inferred, b) interpreted.

Inside the "Border Zone" segment between W. Carpathians and E. Carpathians, the nearest (app. 39 km west) of Brehov submarine ore deposit is located the Telkibánya "subaerial" ore deposit with several differences:

A) The Brehov ore structure is located on the proximal eastern flank of the Paleozoic–Mesozoic Zemplín elevation, the Telkibánya ore structure is located on the distal western flank of the Zemplín elevation.

B) The Brehov ore deposit is fully a product of submarine development, the Telkibánya gold-silver ore deposit represents an epithermal, fully subaerial, low-sulfidation, vein metallogenetic structure and only volcanogenetically it has developed partly in submarine magmatic conditions.

The evidences of partly submarine character of the volcanogenic environment of Telkibánya ore field ("Telkibánya stratovolcano") are as follows:

1. In the Telkibánya deposit area, the drillhole Telkibánya-2 demonstrates below 790 m thick Sarmatian andesite volcanic sequence the volcanic and sedimentary rocks of Badenian age (proven by microfossils in the sediments).
2. The submarine dacitic-andesitic lavas and péperitic breccias, interbedded with shallow marine sediments in the Füzérkajata-2 drillhole indicate the contemporaneous subsidence of the Tokaj Mts. volcano-tectonic graben with volcanic activity (the Telkibánya ore deposit area).
3. Towards the end of the Badenian time, volcanic activity was represented by dacite domes, tuffs of dacite-rhyolite composition and tuff breccia deposited in a shallow marine environment.
4. An accumulation of rhyolite pyroclastics, alternating with shallow marine clays and marls in the Upper Badenian–Lower Sarmatian reflects the repeated sinking of the Tokaj Mts. graben, which is proved also by recent recognition of occurrences of péperites and hyaloclastite breccias in the cores of Telkibánya-1, Telkibánya-2 and Telkibány-9 drillholes, which indicates that part of the Early Sarmatian volcanism, producing the Lower Sarmatian andesites indeed took place under subaquaeous conditions (Molnár et al., 2000).

The conformity between the rift (lineament) settings of subaerial low-sulfidation epithermal Telkibánya deposit and the submarine Kuroko type Brehov deposit raises the possibility that transitional deposit types may exist with prevailing shallow water conditions. Indeed the Zlatá Baňa ore deposit in the Slanské vrchy Mts., which formed during bimodal volcanism and rifting of an andesitic arc, has character of partly submarine, and partly subaerial structure.

The Zlatá Baňa stratovolcano, bearing the base metal and gold mineralization deposit, in the central volcanic zone has two spatially and timely complicated zones. The lower zone of volcanosedimentary rhyolitic-acidic composition of Eggenburgian–Badenian age and the upper andesitic, diorite porphyric zone with the age from Sarmatian to Lower Pannonian (12.2–10.0 Ma age; Repčok et al., 1988). The demonstration, that in Sarmatian time the volcanogenetic and metallogenetic processes also had partly submarine, and partly subaerial nature in the Zlatá Baňa ore structure represent the situation that base and gold metal mineralizations are developed only in the form of **mineralized tectonic zones** and not in the form of epithermal veins, occurring e.g. in typical Neogene subaerial epithermal vein deposits in the Banská Štiavnica ore district (Slovakia), in the Baia Mare ore district and the Apuseni Mts (both in Romania).

The position of the Zlatá Baňa ore deposit in the northwestern deep centre of the Prešov–Kráľovský Chlmec graben (Fig. 3) indicates that with high probability this ore structure – at least partly – developed in submarine conditions.

According to Gessel (1878), the precious opal mineralization in the Dubník (Libanka) deposit is concentrated in two concordant, subhorizontal beds of so called "opal bearing" country rocks, and not in discordant vein type epithermal structures, which means, with high probability that the Dubník precious opal deposit and the whole Zlatá Baňa base metal and gold deposit developed, at least partly, also in submarine environment. The first precious opal-bearing layer is 30–80 m thick and its known extent is about one kilometer; the second precious opal-bearing bed situated westly is 10–30 meters thick, and has of about 70 meters strike length.

In the "Border Zone" segment between W. Carpathians and E. Carpathians within the Internal Carpathian–Alpine Cenozoic metallogenetic belt, another subtype of transitional – from submarine to subaerial – ore deposits is represented by the Begaň–Beregovo–Kvasovo metallogenetic sector in Transcarpathian part of Ukraine (Fig. 2).

Our new geological and metallogenetic interpretation (Bacsó, 2014) of the gold, silver and base metal mineralization in Begaň–Beregovo–Kvasovo ore sector, based on data and descriptions from Lazarenko et al. (1968), Skakun et al. (1992), Gozhik (1993), Biruk and Skakun (2000) and Emetz (2001) is as follows:

In the Begaň–Beregovo–Kvasovo ore sector a special subtype of Kuroko Sarmatian shallow submarine ore deposit (Muzievo) has developed, having two genetic-morphological features of economically important Au-Ag-base metal mineralizations:

1. The Sarmatian upper concordant, subhorizontal stratabound shallow zone of mushroom shaped gold-rich hydrothermal quartz-barite irregular

lenses (Au-ore shoot veinlets) in the "Upper Tuffs" horizon, usually very close to the contact with the underlying subhorizontal clayey sediments. Until now six Au-rich lenses were discovered. The ore bodies are irregular, funnel, or mushroom shaped, with diameters usually not exceeding 50 m. The ores consist of quartz, barite, clay minerals, gold, silver, as well as minor amount of pyrite. The average contents of gold in the lenses are 31 g/t Au, and 21 g/t Ag.

2. The lower discordant part of the Muzievo ore deposit is mostly in the "Middle Tuffs" horizon in the form of steep dipping Au-bearing veins and Au-bearing vein zones. The vein-form Au mineralization is represented by 17 veins, also of Sarmatian age, which are concentrated in a 1200 m wide zone. The length of veins varies from 300 to 1000 m.

Both parts (concordant and discordant) of the special Kuroko type shallow submarine Muzievo gold-silver-base metal mineralizations are exclusively developed only in the host volcanosedimentary sequence of Eggenburgian–Pannonian age.

6 Conclusions

The Kuroko type submarine, volcanogenic, stratabound, sulphide ore deposit near village of Brehov and ore occurrence near village of Zemplín in the Eastern Slovakia represent a new type of hydrothermal mineralization in the Internal Carpathian–Alpine Cenozoic metallogenetic belt, being characterized geologically, mineralogically and metallogenetically in this publication. The Brehov ore deposit manifests a complex stratabound submarine development with concordant main sulphide upper deposit part and less important discordant veinlets and disseminated impregnations of feeder zone in its lower part.

Our knowledge about Brehov volcanogenic stratabound base metal and gold deposit we gained by geological mapping, geochemical and geophysical regional and detail survey, by trenching and from drillholes. The field survey was followed by geological and metallogenetic interpretations.

In the Internal Carpathian–Alpine Cenozoic metallogenetic belt preferably in the "Border Zone" segment of this belt between W. Carpathians and E. Carpathians, there are geological conditions for discovery of more 2–4 similar submarine base metal and gold deposits – with the higher probability in the areas of interpreted submarine Sirník–Brehov and Zemplín–Somotor calderas.

The Internal Carpathian–Alpine Cenozoic metallogenetic belt consists of six naturally individualized regional segments, from west to east they are as follows:

1. The Western Alps Brusson segment;
2. The Eastern Alps Hohe Tauern segment;
3. The Western Carpathians segment;
4. The "Border Zone" segment between Western and Eastern Carpathians;
5. The Eastern Carpathians segment;
6. The Apuseni Mountains segment.

Within the Internal Carpathian–Alpine Cenozoic metallogenetic belt the **"Border Zone"** segment between Western and Eastern Carpathians has four principal metallogenetic sectors:

a) The Brehov–Zemplín metallogenetic sector; with two ore fields;
b) The Telkibánya metallogenetic sector; with one ore field;
c) The Zlatá Baňa metallogenetic sector; with two ore fields and one precious opal field;
d) The Begaň–Beregovo–Kvasovo metallogenetic sector; with three ore fields.

In the "Border Zone" segment and in the Western Carpathian segment of the Internal Carpathian–Alpine Cenozoic metallogenetic belt the discontinuous bodies of **exhumed ophiolites** indicate the course of suture zones, representing crustal discontinuities, being preferably used for establishing younger subequatorial lineament zones.

Complementary submeridional oriented Hornád and Ondava lineament zones are accompanied with the Miocene ore-hosted volcanic structures (submarine and subaerial) with the ore fields of Brehov, Zemplín, Zlatá Baňa, Dubník and Telkibánya.

Miocene gold mineralization in the "Border Zone" segment between W. Carpathians and E. Carpathians is richest in the Muzievo (Beregovo) ore field (4–8 g/t) and in the Brehov ore field (2–3 g/t).

The most favourable conditions for Miocene rhyolite-rhyodacite **volcanosedimentary** Au-Ag-base metal ore host-rock sequences development in the near surface beds were in the Brehov–Zemplín and Begaň–Beregovo–Kvasovo metallogenetic ore sectors. In these sectors the ore-bearing Miocene intrusive-extrusive complexes are represented by quartz diorite porphyry, intrusive andesite and extrusive–intrusive rhyodacite bodies.

Only the "Border Zone" segment between W. Carpathians and E. Carpathians has fully or partly submarine origin of Miocene volcanogenic base and precious metal deposit in the region.

The geological, mineralogical and metallogenetic findings and revealed regional relations in the case of Brehov base metal and gold deposit indicate that the geological aspects of Neogene ore deposits in the Carpathians can be interpreted taking into account the theory of lineaments origin based on crustal discontinuities being indicated by the linear ophiolite zones occurrences on the surface or revealed in boreholes.

Acknowledgement

Author is grateful for extended ore exploration in Eastern Slovakian Neogene volcanic fields held in the 1970s–1990s, providing valuable primary data, being summed up in this article. Constructive comments and suggetions by Zoltán Németh (ŠGÚDŠ) and anonymous reviewer are greatly appreciated.

Samples of magmatic rocks, from boreholes in depth:	Mineralogical composition. ("Phenocrysts").					
	Holocrystalline altered-transformed groundmass	K-feldspar	Quartz	Carbonate	Sericite	Chlorite
VSB-1/178.5 m	87.9	9.1	3.0	–	–	–
VSB-2/153.5 m	70.8	8.5	15.3	5.4	–	–
VSB-2/247.5 m	79.9	11.6	5.1	3.4	–	–
VSB-2/333.2 m	74.9	11.3	3.7	0.4	–	9.7
VSB-2/340.5 m	75.4	18.9	2.2	3.5	–	–
VSB-5/438.0 m	71.7	3.6	–	2.9	15.2	6.6
VSB-5/611.0 m	78.3	3.5	–	7.1	6.6	4.5
VSB-5/647.5 m	78.2	4.5	–	7.9	9.4	–
VSB-6/158.5 m	78.4	14.7	3.3	–	–	3.6
VSB-6/370.5 m	78.2	2.5	–	2.1	11.9	5.3
VSB-6/606.5 m	76.8	8.2	–	4.8	–	10.2
VSB-6/649.0 m	80.3	13.1	–	4.1	2.5	–
VSB-3/219.0 m	75.5	–	–	10.9	–	13.6
VSB-3/140.0 m	79.9	–	4.8	5.6	–	9.7
VSB-3/135.5 m	80.0	–	6.4	13.6	–	–

Nb/Y–Zr/TiO$_2$ diagram for volcanic rocks. (Winchester & Floyd, 1977)

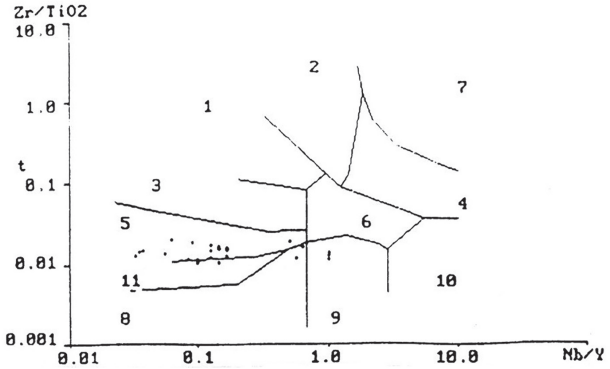

Extrusive – intrusive altered, ore-host andesite and microdiorite; Middle Badenian age; Zemplín ore field (29 samples).

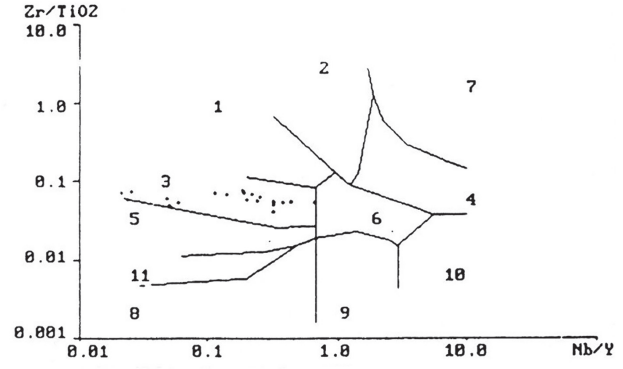

Ore-bearing quartz diorite porphyry; Brehov ore field; Upper Badenian age (24 samples).

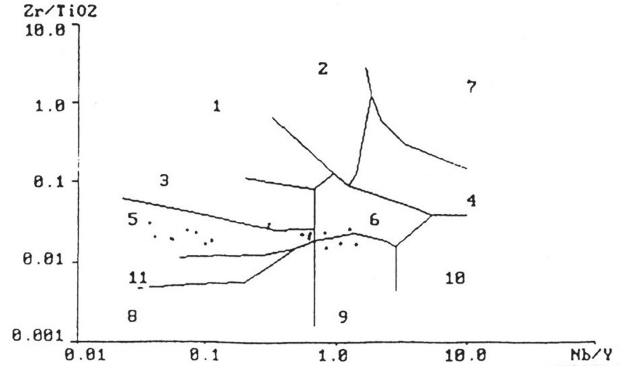

Post ore andesite and dacite; Brehov, Veľký vrch (272), Lower Sarmatian age; Brehov ore field (22 samples).

1 – rhyolite; 2 – comendite pantelerite; 3 – rhyodacite, dacite; 4 – trachyte; 5 – andesite; 6 – trachyandesite; 7 – phonolite; 8 – subalvalinc basalt; 9 – alcaline basalt; 10 basanite; 11 – andesite/basalt.

Fig. 12. Basic petrographic and planimetric evaluation (in wt. %) of the altered submarine ore bearing Brehov intrusion – altered quartz diorite porphyry (Bacsó, 2014) and classification of altered Neogene magmatic rocks from individual levels of the Zemplín ore field after Winchester & Floyd (1977).

References

Bacsó, Z. & Ďuďa, R., 1988: Metalogenéza a rudné formácie rudného poľa Remetské Hámre. *Miner. Slov., 20, 3, 193–220.*

Bacsó, Z., 1995a: Subvulkanické telesá Východného Slovenska, polymetalické, drahokovové, vzácnekovové a ortuťové rudy. Vyhľadávací prieskum. Stav k 1. 9. 1995. Záverečná správa. *Manuscript. Bratislava, archive. St. Geol. Inst. D. Štúr, 171 p.*

Bacsó, Z., 1995b: Brehov západ, polymetalické rudy; Vyhľadávací prieskum. Stav k 15. 4. 1995. Záverečná správa. *Manuscript. Bratislava, archive. St. Geol. Inst. D. Štúr, 206 p.*

Bacsó, Z., 2000: Geology, mineralogy of the submarine volcanogenic sulphide deposit near Brehov in Eastern Slovakia: A genetic ore formation model. *Miner. Slov., 32, 265–267.*

Bacsó, Z., 2014: The Brehov volcanogenic and stratabound base metal and gold deposit (Eastern Slovakia). *Manuscript. Bratislava, archive St. Geol. Inst. D. Štúr, 1–38.*

Biruk, S. & Skakun, L. Z., 2000: Bismuth minerals of the Beregovo ore field: Mineral assemblages and spatial zonation (Transcarpathian Ukraine). *Geol. Quart., 44, 1, 39–46.*

Burian, J., Slavkay, M., Štohl, J. & Tőzsér, J., 1985: Metallogenesis of neovolcanites in Slovakia. *Bratislava, Alfa, 269 p.*

Dilek, Y. & Furnes, H., 2014: Ophiolites and their origins. *Elements, 10, 93–100.*

Divinec, Ľ., Kotuľák, P., Repčiak, M., Kaličiaková, E. & Ďuďa, R., 1988: Ložisko Zlatá Baňa vo svetle nových údajov geologického prieskumu. *Miner. Slov., 20, 3, 221–238.*

Emetz, A. V., 2001: Beregovo Au-Ag-Pb-Zn ore filed (Intercarpathian): ore review and genesis. In: Piestrzyński et al. (eds.): Mineral deposits at the beginning of the 21st century. *Lisse, Swets Zeitlinger Publ., 523–526.*

Faryad, S. W., Spišiak, J., Horváth, P., Hovorka, D., Dianiška, I. & Sándor, J., 1998: Meliata unit – petrology, geochemistry and geotectonic position of metabasites. Western Carpathians, Slovakia. *J. metamorphic Geol., 13, 701–714.*

Faryad, S. W., 1999: Exhumation of the Meliata high pressure rocks (Western Carpathians): Petrological and structural records in blueschists. *Acta Montan. Slov., 4, 2, 137–144.*

Floyd, P. A. & Winchester, J. A., 1975: Magma type and tectonic setting discrimination using inmobile elements. *Earth planet. Sci. Lett., 27, 211–218.*

Földessy, J., Németh, N., Gerges, A., Kupi, L. & Tóth, Sz., 2009: Re-discovery of a mining district – the Rudabánya (Hungary) base metal mineralization. Securing the Future 2009 International scientific conference. *8th ICARD, June 22–26, 2009, Skelleftea, Sweden.*

Franklin, J. M., Lyndon, W. & Sangster, D. F., 1981: Volcanic associated massive sulfide deposit. *Econ. Geol., 75th Anniv. Vol., 485–627.*

Gessel, S., 1878: A vörösvágási, Dubniki opálbányák földtani viszonyai. *Mathem. Természett. Közl. (Budapest), 15, 213–222.*

Gilmour, P., 1977: Mineralized intrusive breccias as guides to concealed porphyry copper systems. *Econ. Geol., 72, 290–298.*

Gnojek, I., 1987: Magnetická anomálie u Bzenova, jz. od Prešova. *Miner. Slov. 19, 2, 169–173.*

Gnojek, I., Hovorka, D. & Pospíšil, L., 1991: Sources of magnetic anomalies in the pre-Tertiary basement of Eastern Slovakia. *Geol. Carpath., 42, 3, 169–180.*

Gozhik, M. F., 1993: The Beregovo gold – polymetallic district. *Fieldtrip guide, IUGS/UNESCO – Modeling workshop, Budapest, 35–49.*

Gyarmati, P., 1977: A Tokaji hegység intermediár vulkanizmusa. *Magy. áll. Földt. Intéz. Évk., 58, 1–225.*

Hannington, M. D., Poulsen, K., H., Thompson, J., F., H. & Sillitoe, R. H., 1999: Volcanogenic gold in the massive sulfide environment. *Econ. Geol. Rev., 8, 325–356.*

Heinrich, Ch. & Neubauer, F., 2002: Cu-Au-Pb-Zn-Ag metallogeny of the Alpine – Balkan – Carpathian – Dinaride geodynamic province. *Mineral. Depos., 37, 533–540.*

Herzig, P. M. & Friedrich, G. H., 1987: Sulphide mineralization, hydrothermal alteration and chemistry in the drillhole CY-2a, Agrokipia, Cyprus. Cyprus Crustal Study project: Initial Report, Holes Cy – 2, CY – 2a. *Energy, Mines Res., Canada, 103–138.*

Hovorka, D., Snopko, L. & Zlocha, J., 1977: Gabropegmatit z ultrabazického telesa pri Komárovciach. *Miner. Slov., 9, 1, 11–20.*

Ishiwatari, A., 1985: Alpine ophiolites: product of low-degree mantle melting in a Mesozoic transcurrent rift zone. *Earth Planet. Sci. Lett., 76, 1–2, 93–108.*

Kaličiak, M. & Ďuďa, R., 1980: Development in time and formational subdivision of the mineralization in the Zlatá Baňa area (Slanské vrchy Mts.). *Miner. Slov., 13, 1, 1–23.*

Kaličiak, M., Lexa, J. & Határ, J., 1985: Hydrothermal mineralization at the village Zemplín. *Geol. Zbor. Geol. carpath., 36, 216–229.*

Kozur, H. & Mock, R., 1997: New paleographic and tectonic interpretations in Slovakian Carpathians and their implications for correlations with the Eastern Alps and other parts of the Western Tethys, Part 2: Inner Western Carpathians. *Miner. Slov. 29, 3, 164–209.*

Kutina, J., 1980: Are lineaments ineffective guides to ore deposits? *Glob. Tecton. Metallog., 1, 2, 200–205.*

Lang, B., 1979: The base metal-gold hydrothermal ore deposits of Baia Mare, Romania. *Econ. Geol., 74, 1336–1351.*

Lazarenko, E. A., Gnilko, M.. K. & Zayceva, V. N., 1968: Metallogeny of the Transcarpathians. *Lviv Univ. press, 178 p.*

Lexa, J. & Kaličiak, M., 2000: Geotectonic aspects of the Neogene volcanism in Eastern Slovakia. *Miner. Slov., 32, 205–210.*

Mayo, E. B., 1958: Lineaments tectonics and some ore districts of the Southwest. *Min. Engng, 10, 11, 1169–1175.*

Merlich, B. V. & Spitkovskaja, S. M., 1974: Deep faults, Neogene magmatism and ore deposition of the Transcarpathians. *Vyšča škola, 172 p.*

Molnár, F., Zelenka, T. & Pécskay, Z., 2000: Geology, styles of mineralization and spatial temporal characteristics of the hydrothermal system in the low-sulfidation type epithermal gold-silver deposit at Telkibánya. *Geol. Carpath., 46, 205–215.*

Mořkovsky, M. & Cverčko, J., 1987: Magnetic anomalies in the Neogene basement of East Slovakia lowland. *Miner. Slov., 19, 3, 255–260.*

Németh, Z., 2002: Variscan suture zone in Gemericum: Contribution to reconstruction of geodynamic evolution and

metallogenetic events of Inner Western Carpathians. *Slovak Geol. Mag., 8, 3–4, 247–257.*

Németh, Z., Radvanec, M., Kobulský, J., Gazdačko, Ľ., Putiš, M. & Zákršmidová, B., 2012: Allochthonous position of the Meliaticum in the North-Gemeric zone (Inner Western Carpathians) as demonstrated by paleopiezometric data. *Miner. Slov., 44, 57–64.*

Neubauer, F., 2002: Contrasting Late Cretaceous with Neogene ore provinces in the Alpine-Balkan-Carpathian-Dinaride collision belt. *Geol. Soc. London, Spec. Publ.*

Neubauer, F. & Heinrich, Ch., 2003: Late Cretaceous and Tertiary geodynamics and ore deposit evolution of the Alpine--Balkan-Carpathian-Dinaride orogen. Mineral Exploration and Sustainable Development. *In: Eliopoulos et al. (eds.): Millpress, Rotterdam.*

O`Driscoll, E. S. T., 1981: Structural corridors in Landsat lineament interpretation. *Mineral. Depos., 16, 85–101.*

O`Driscoll, E. S. T., 1985: The application of lineament tectonics in the discovery of the Olympic Dam Cu-Au-U deposit at Roxby Downs, South Australia. *Glob. Tecton. Metallog., 3, 43–57.*

Q`Driscoll, E. S. T., 1986: Observation of the lineament-ore relation. *Phil. Trans. Royal. Soc. London, 317, 195–218.*

Ohmoto, H., 1996: Formation of volcanogenic massive sulphide deposits: The Kuroko perspective. *Ore geol. Rew., 10, 135–177.*

Pécskay, Z. & Molnár, F., 2002: Relationships between volcanism and hydrothermal activity in the Tokaj Mountains, Northeast Hungary, based on K-Ar ages. *Geol. Carpath., 53, 5, 303–314.*

Quadt, A. (ed.), 2002: The Timing and Location of Major Ore Deposits in an Evolving Orogen. *Geol. Soc. London, Spec. Publ., 204, 81–102.*

Popescu, C. Gh. & Neascu, A., 2010: Metallogeny of east Carpathians with special view to the metallogenetic district of Baia Mare, Bucuresti. *Ser. geol., XLIII, 19–26.*

Pospíšil, L. & Bodoky, T., 1981: Deep structure and magmatism of Neogene age in the Transcarpathian depression (Eastern Slovakia and NE Hungary). *Miner. Slov., 13, 4, 289–306.*

Rădulescu, D. & Lang, B., 1973: Sugesti privind intrpretarea structurii geologice a părtii de nord a muntiloir Gutii. *Bucuresti, D. S. Inst. Geol., LIX.*

Repčok, I., Kaličiak, M. & Bacsó, Z., 1988: Age of some volcanics of Eastern Slovakia. *Západ. Karpaty, Sér. Mineral. Petrogr. Gechém. Metalogen., 11, 75–88.*

Richards, J. P., 2000: Lineaments Revisited. *Soc. Econ. Geol., 14–20.*

Richards, J. P., Boyce, A. J. & Pringle, M. S., 2001: Geological evolution of the Escondida area, northern Chile. A model for spatial and temporal localization of porphyry Cu mineralization. *Econ. Geol., 96, 2.*

Sato, T., 1990: Volcanogenic massive sulfide deposits – with special reference to Kuroko type Deposits. *Manuscript. Geol. Surv. Japan, 1–36.*

Savu, H., 2009: Genesis of the Carpathian ophiolitic suture and origin of its varied magmatic rocks, Romania. *Proc. Rom. Acad. Sci., Ser. B, 2–3, 141–150.*

Skakun, L. Z., Matkovsky, O. I. & Gohzik, M. F., 1992: Au ores of Beregovo ore field. *Vest. Lvov Univ. Scr. Geol., 11, 128–145.*

Slávik, J., 1972: Pochované vulkanické pohorie na juhu východného Slovenska. *Geol. Práce, Spr., 58, 45–56.*

Slávik, J., 1974: Vulkanizmus, tektonika a nerastné suroviny neogénu východného Slovenska a pozícia tejto oblasti v Neoeurope. *Manuscript. Bratislava, archive St. Geol. Inst. D. Štúr, 1–341.*

Soták, J., Spišiak, J. & Biroň, A., 1993: Metamorphic sequences with "Bündnerschiefer" lithology in the Pre-Neogene basement of the Eastern Slovakian basin. *Mitt. Österr. geol. Gesell. (Wien), 111–120.*

Soták, J., Szakáll, S. & Kovács, Á., 1995: Silver minerals from Rudabánya (N. Hungary). *Acta mineral. petrogr. (Szeged), XXXVI, 5–15.*

Szakáll, S. & Kovács, Á., 1995: Silver minerals from Rudabánya (N. Hungary). *Acta mineral. petrogr. (Szeged), 36, 5–15.*

Széky-Fux, V., 1970: The Telkibánya mineralization and its Intra-Carpathian connections. *Budapest, Academic Press, 1–266.*

Széky-Fux, V., Pap, S. & Barta, I., 1985: Geological results of the boreholes Nagyecsed – 1 and Komoró 1 from the Nyírség, NE Hungary. *Bull. Hung. Geol. Soc., 115, 63–77.*

Sillitoe, R. H. & Hedenquest, J., 2003: Linkages between volcanotectonic settings, ore-fluid compositions, and epithermal precious metal deposits. *Soc. Econ. Geol., Spec. publ., 10, 1–29.*

Tőzsér, J., 1972: Záverečná správa z vyhľadávacieho prieskumu v Prešovsko-Tokajskom pohorí. *Manuscript. Bratislava, archive St. Geol. Inst. D. Štúr, 1–239.*

Velich, R., Husák, L. & Stránska, M., 1991: Veľký Brehov – gravimetria. Záverečná správa. *Manuscript. Bratislava, archive St. Geol. Inst. D. Štúr, 1–42.*

Velich, R., 1993: Interpretácia významnych anomálií tiažového poľa v širšom okolí Brehova; *Manuscript. Bratislava, archive St. Geol. Inst. D. Štúr, 1–23.*

Vityk, O., M. & Krouse, R. H., 1994: Fluid evolution and mineral formation in the Beregovo gold-base metal deposit, Transcarpathia, Ukraine. *Econ. Geol., 89, 547–565.*

Winchester, J. A. & Floyd, P. A., 1976: Geochemical magma type discrimination application to altered and metamorphosed basic igneous rocks. *Earth planet. Sci. Lett., 28, 459–469.*

Winchester, J. A. & Floyd, P. A., 1977: Geochemical discrimination of different magma series and differentiation products, using immobile elements. *Chem. Geol., 20, 325–343.*

Zlinská, A., 1992: Zur biostratigraphischen Gliederung des Neogens des Ostslowakischen Becken. *Geol. Práce, Spr., 96, 51–57.*

Zlinská, A., 1993: Biostratigrafické a paleoekologické hodnotenie horninových vzoriek v rámci úlohy Subvulkanické telesá Východného Slovenska a Brehov. *Manuscript. Bratislava, archive St. Geol. Inst. D. Štúr, 1–21.*

Zlinská, A., 2004: Charakteristika litostratigrafických jednotiek neogénu Východoslovenskej panvy na základe foraminifer. *Geol. Práce, Spr., 109, 131–141.*

Vulkanogénne stratiformné polymetalické a zlatorudné ložisko Brehov (východné Slovensko): jeho pozícia a genetické vzťahy v rámci vnútrokarpatsko-alpínskej kenozoickej metalogenetickej zóny

Submarinné vulkanogénne stratiformné sulfidické ložisko typu Kuroko v oblasti obce Brehov a rudné výskyty v oblasti obce Zemplín na východnom Slovensku reprezentujú nový typ hydrotermálnej mineralizácie vo vnútrokarpatsko-alpínskej kenozoickej metalogenetickej zóne. Ložisko Brehov reprezentuje komplexný stratiformný submarinný vývoj s konkordantne vystupujúcou hlavnou sulfidickou mineralizáciou vo vrchnej časti ložiska. Žilná mineralizácia sprevádzaná sulfidickými impregnáciami sa nachádza v spodnej časti mineralizovaného horizontu.

Vnútrokarpatsko-alpínsku kenozoickú metalogenetickú zónu tvorí šesť segmentov (zo západu na východ; obr. 1): 1. západoalpský segment oblasti Brusson; 2. východoalpský segment pohoria Taury; 3. západokarpatský segment; 4. segment „hraničnej zóny“ medzi Západnými Karpatmi a Východnými Karpatmi; 5. východoalpský segment; 6. segment Apusenských vrchov.

Segment „hraničnej zóny“ medzi Západnými Karpatmi a Východnými Karpatmi (obr. 2, 2a) pozostáva zo štyroch hlavných metalogenetických sektorov: a) brehovsko-zemplínsky metalogenetický sektor s dvomi doteraz známymi rudnými poľami (obr. 3 – 12), b) metalogenetický sektor v oblasti obce Telkibánya s jedným rudným poľom, c) metalogenetický sektor v oblasti obce Zlatá Baňa s dvomi rudnými poľami a výskytmi vzácneho opálu, d) metalogenetický sektor v oblasti Begaň – Beregovo – Kvasovo s tromi rudnými poľami. V tomto segmente „hraničnej zóny“ a tiež v segmente Západných Karpát sa výskyty kenozoickej mineralizácie viažu na priebeh transkrustálnych diskontinuít zo skorších orogénnych procesov, resp. sú spojením viacerých segmentov takýchto oslabených zón buď s ekvatoriálnym, alebo meridionálnym priebehom vytvárajúcim kontinuálne extenzné štruktúry, tzv. lineamenty. Napríklad submeridionálny hornádsky a ondavský lineament je zónou miocénnej vulkanickej aktivity a s ňou spätej mineralizácie (submarinnej alebo subaerickej): rudných polí Brehov, Zemplín, Zlatá Baňa, Dubník a Telkibánya. Medzi najbohatšie miocénne zlatorudné mineralizácie v „hraničnej zóne“ medzi Západnými Karpatmi a Východnými Karpatmi patria rudné polia Muzievo (Beregovo; 4 – 8 g/t) a Brehov (2 – 3 g/t).

Najpriaznivejšie podmienky na vývoj miocénnej ryolitovo-ryodacitovej vulkanosedimentárnej Au-Ag polymetalickej mineralizácie v hostiteľských horninových sekvenciách v plytko uložených vrstvách boli v rudných sektoroch Brehov – Zemplín a Begaň – Beregovo – Kvasovo. Rudonosné miocénne intruzívno-extruzívne komplexy v týchto rudných sektoroch sú vytvárané kremenitými dioritovými porfýrmi a extruzívno-intruzívnymi ryodacitovými telesami.

V rámci vnútrokarpatsko-alpínskej kenozoickej metalogenetickej zóny v nami skúmanom segmente „hraničnej zóny“ medzi Západnými Karpatmi a Východnými Karpatmi dokladáme, že miocénna vulkanogénna polymetalická a vzácnokovová mineralizácia má úplne alebo čiastočne submarinný pôvod. Predpokladá sa, že predovšetkým segment „hraničnej zóny“ medzi Západnými Karpatmi a Východnými Karpatmi disponuje geologickými predpokladmi na výskyt ďalších 2 – 4 podobných submarinných polymetalických a zlatorudných ložísk – s najväčšou pravdepodobnosťou v oblastiach interpretovaných submarinných kalder Sirník – Brehov a Zemplín – Somotor.

Regionálne súvislosti vychádzajúce z geologických, mineralogických a metalogenetických zistení v prípade polymetalického a zlatorudného ložiska Brehov indikujú, že vznik neogénnych rudných ložísk v zóne Karpát môže byť interpretovaný aj teóriou lineamentov ako celokôrových diskontinuít, ktoré sa vygenerovali pozdĺž priebehu skorších sutúrnych zón indikovaných ofiolitmi, prípadne s príspevkom viacerých ďalších oslabených zón korešpondujúceho smeru.

Doručené / Received: 6. 7. 2014
Doručenie aktualizovanej verzie / Received updated version: 31. 1. 2023
Prijaté na publikovanie / Accepted: 30. 6. 2023

Mineralia Slovaca, Web ISSN 1338-3523, ISSN 0369-2086, https://doi.org/10.56623/ms.2023.55.1.4
55, 1 (2023), 53 – 70, © Authors 2022. CC BY 4.0

Stratiform U-Cu mineralization in the Lopejské Čelno valley near Podbrezová (Veporic Unit, Western Carpathians)

RICHARD KOPÁČIK[1*], ŠTEFAN FERENC[1], TOMÁŠ MIKUŠ[2], ŠIMON BUDZÁK[3], JURAJ BUTEK[1] and EVA HOPPANOVÁ[1]

[1]Department of Geography and Geology, Faculty of Natural Sciences, Matej Bel University, Tajovského 40, 974 01 Banská Bystrica, Slovak Republic; *e-mail: kopacikrichard95@gmail.com
[2]Earth Science Institute, Slovak Academy of Sciences, Ďumbierska 1, 974 01 Banská Bystrica, Slovak Republic
[3]Department of Chemistry, Faculty of Natural Sciences, Matej Bel University, Tajovského 40, 974 01 Banská Bystrica, Slovak Republic

Abstract: The studied mineralization is located on the eastern slopes of Lopejské Čelno valley, south of the Lopej village (cadastral area of Podbrezová village, Central Slovakia). The U occurrence was described and classified as U-Cu stratiform mineralization. The mineralization is located in the Ľubietová Zone of Veporic Unit, and is bound to the arkosic sandstones containing Permian volcanoclastic material. The host rock of mineralization underwent low-grade metamorphism and limonitization. Lens shaped ore bodies are characterized by disseminated pyrite, rutile, chalcopyrite, leucoxene and metatorbernite. Small cavities and cracks in rock are also filled and/or coated by goethite, Mn oxides and malachite. Uranium is irregularly distributed within the host rock and is bound to the U-Ti oxides, brannerite and torbernite/metatorbernite. Brannerite and leucoxenized U-Ti oxides are the only one primary uranium U^{4+} minerals, for the first time identified in studied occurrence. Brannerite forms clusters of needle-like crystals (up to 100 μm in size). It occurs in close spatial and genetic association with U-Ti oxides, rutile, leucoxene and clay minerals. Chemical composition of brannerite and U-Ti oxides differs in ratio of U/(U + Ti): from 0.22 to 0.29 apfu for brannerite and from 0.09 to 0.22 apfu for U-Ti oxides. Metatorbernite forms light green crystals, typically occurs in small cavities and fractures in rock. It shows an unusual light green luminescence under UV radiation. The average chemical composition of metatorbernite can be expressed by empiric formula $(Cu_{0.75}Ba_{0.06}Ca_{0.03}K_{0.04}Al_{0.02}Mg_{0.01}Fe_{0.01})_{\Sigma 0.94}$ $(UO_2)_{\Sigma 2.00}$ $(PO_4)_{\Sigma 2.01}$ $(H_2O)_8$. Occasionally torbernite/metatorbernite directly replaces single crystals of apatite.

Key words: U-Cu mineralization, U-Ti oxides, brannerite, metatorbernite, Veporic Unit, Western Carpathians

Graphical abstract

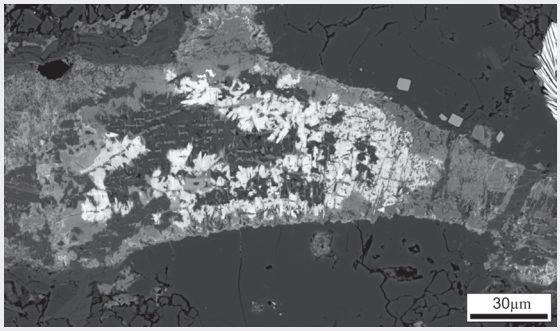

Highlights

- Mineralized grains of U-Cu mineralization near Podbrezová in Lopejské Čelno valley are composed of brannerite, U-Ti oxides, rutile, leucoxene and clay minerals
- Mineralization was created during alteration (chloritization) of biotite connected with hydrothermal processes and the subsequent *"Pronto-reaction"* – adsorption of uranium onto the formed Ti oxides
- Mineralization forming correlates with the temperature generated during the Alpine orogeny, or by its fading

Introduction

Primary ores processed in the nuclear industry mostly include uraninite and coffinite. Unconventional target ores include brannerite (UTi_2O_6) and U-Ti oxides (uranoferous leucoxene), because of its high U content of up to 55 wt % U (Patchett & Nuffield, 1960). Brannerite (UTi_2O_6) is found among the major uranium-bearing minerals in many ore deposits and variety of geological environments including hydrothermal and pegmatitic, which represent the most frequent occurrences. In the Western Carpathians, brannerite and U-Ti oxides were studied in Košice-Kurišková and Novoveská Huta U-Mo deposits, also at several mineralogical, resp. deposit occurrences such as Gemerská Poloma-Peklisko, Prakovce-Zimná voda, Kálnica, Krompachy, etc. (Rojkovič, 1997).

Brannerite and U-Ti oxides were also uniquely identified during the revision research of U-Cu mineralization in the Lopejské Čelno site near Podbrezová. The main goal of this study is to clarify the genesis of the primary U^{4+} mineralization, represented by brannerite and U-Ti oxides.

Geological setting

In the 1960s, in the vicinity of the villages of Podbrezová, Ľubietová and Osrblie, the geological survey focused on U ores was carried out, for the purpose of searching for industrial uranium concentrations. The studied occurrence of U-Cu mineralization is located about 1.5 km south of the Lopej village center (cadastre of the Podbrezová village) in the Lopejské Čelno valley, on the west-facing slopes of the Belohrad elevation (764 m a.s.l.). The geographic coordinates of the central part of the occurrence are N 48.8042° and E 19.5085°. Geological survey took place here in 1964–1965. Mineralization was verified by three boreholes (in 1964) and by a narrow-profile adit. After the excavation of the tunnel was completed, two exploratory wells were drilled from its face. Additional exploratory wells with a depth of 300 m were drilled in the valley in 1965. However, the survey work did not confirm economic concentrations of uranium and the geological survey was terminated in the same year (Daniel, 2006).

Mineralization is developed in the Ľubietová Zone of the Veporic tectonic unit (Fig. 1a). The crystalline complexes of the Ľubietová Zone (Fig. 1b) are characterized with three basic zones. The northernmost part consists of orthogneisses to migmatites (also bodies of paragneisses, leucocratic granites, amphibolites). Zones of mylonitization are abundant. The more southerly zone is built by paragneisses, micaschists and amphibolites (frequently diaphtorized). Phyllites and diaphtorites (phyllonites) mainly form the southernmost zone. Bodies of granitic and granodioritic porphyres are less frequent (Slavkay et al., 2004). Orthogneisses are considered to be either a product of paragneiss anatexis (Maheľ et al., 1967), or represent a product of regional metamorphism of granitoids (Kamenický, 1977), rhyolites, dacites and their pyroclastics, respectively (Kamenický, 1982). Granitic porphyres represent younger element of crystalline complexes. According to older opinions (e.g., Zoubek, 1958), the bodies of granite porphyry are inlet channels of Permian volcanism, emerging in the Permian sediments of the Ľubietová Group (Harnobis horizon, Brusno Formation). The Lower Permian age of granite porphyries is evidenced by finds of their fragments in the Upper Permian Predajná Formation (Vozárová, 1979). Chemical U-Th-Pb dating of the monazite from the granite porphyries at Osrblie gave an age of 265 ± 9 Ma (Bezák et al., 2008), SHRIMP dating of zircons from them (Predajnianske Čelno valley) indicates an age of 273 ± 4 Ma (Vozárová et al., 2016). The younger age of 184 ± 9 million years determined by the Rb/Sr method (Spišiak & Siman, 2014) can probably be justified by the reactivation of the primary age of the granite porphyries, which was caused by a tectonothermal event related to the development of the Meliata Ocean. In the wider vicinity of the studied locality, the crystalline shell is represented by the Permian Ľubietová Group (Vozárová, 1979), formed by Brusno (lower) and Predajná (upper) formations. Both consist of clastic sedimentary rocks (arkosic shales, sandstones), accompanied by quartz porphyry bodies. Sedimentary rocks of Brusno Formations are divided by the volcanogenic Harnobis horizon (dacite, tuffs, ignimbrites). The Permian age of the sediments was evidenced by the palynomorph community (Planderová & Vozárová, 1982), SHRIMP dating of magmatic zircons of Harnobis volcanics yielded ages of 273–279 Ma ± 4 Ma (Upper Cisuralian – Lower Guadalupian; Vozárová et al., 2016). The boundary between the complex of the Early Paleozoic metamorphics and the Permian rocks form a 200 m thick thrust line, along which the Early Paleozoic rocks of the Ľubietová Zone were thrust onto the Late Paleozoic rocks. Its general direction is NE–SW and dip 40–45° to the SW. Lower-order tectonic faults course in the NW-SE direction (Daniel, 2006).

U-Cu mineralization in the Lopejské Čelno occurrence is bound to Permian, limonitized, altered arkosic sandstones containing bodies of acid volcanics.

Mineralogy of the Lopejské Čelno site was previously studied by Rojkovič and Novotný (1993), who described it as a stratiform accumulation of poor U-Cu ores. Rojkovič (1997) revealed the contents of some elements at this occurrence as follows: U 40–460 ppm, Cu 30–300 ppm, Ti 1 600–3 000 ppm, Mo < 3 ppm, Pb 20–210 ppm, V 40–140 ppm, Ni 10–20 ppm, Zr 120–260 ppm, Co 4–7 ppm, Y 10–40 ppm and C_{org} 400–4500 ppm. Mineralization was traced in the zone with length of 200 m (NW-SW direction), dipping 40–60° to the SE. Pyrite, rutile, leucoxene, chalcopyrite, goethite and torbernite were identified in ore lenses (up to 1 m in size; Rojkovič & Novotný, 1993).

Methods used

Samples with increased radioactivity were searched in the outcrops along the forest road (Fig. 2), using a SGR – Scintillation Gamma Radiometer detector (sample activity measured in cps), with a measuring range of 400–3 000 keV and a measurement step of 0.2 s.

Polished thin sections were observed in both, reflected and transmitted light applying a Nikon ECLIPSE LV 100 POL polarising microscope (Faculty of Natural Sciences UMB, Banská Bystrica).

Photo documentation of the minerals was done using binocular magnifier Nikon SMZ1500 with camera SD-Fi2. Luminescence of minerals under UV radiation was observed using Raytech R5-FLS-2V lamp at wavelength of 400–315 nm (Faculty of Natural Sciences UMB, Banská Bystrica).

X-ray diffraction analysis (PXRD) was performed on a Bruker D8 Advance equipment (Earth Science Institute of Slovak Academy of Sciences – SAS, Banská Bystrica;

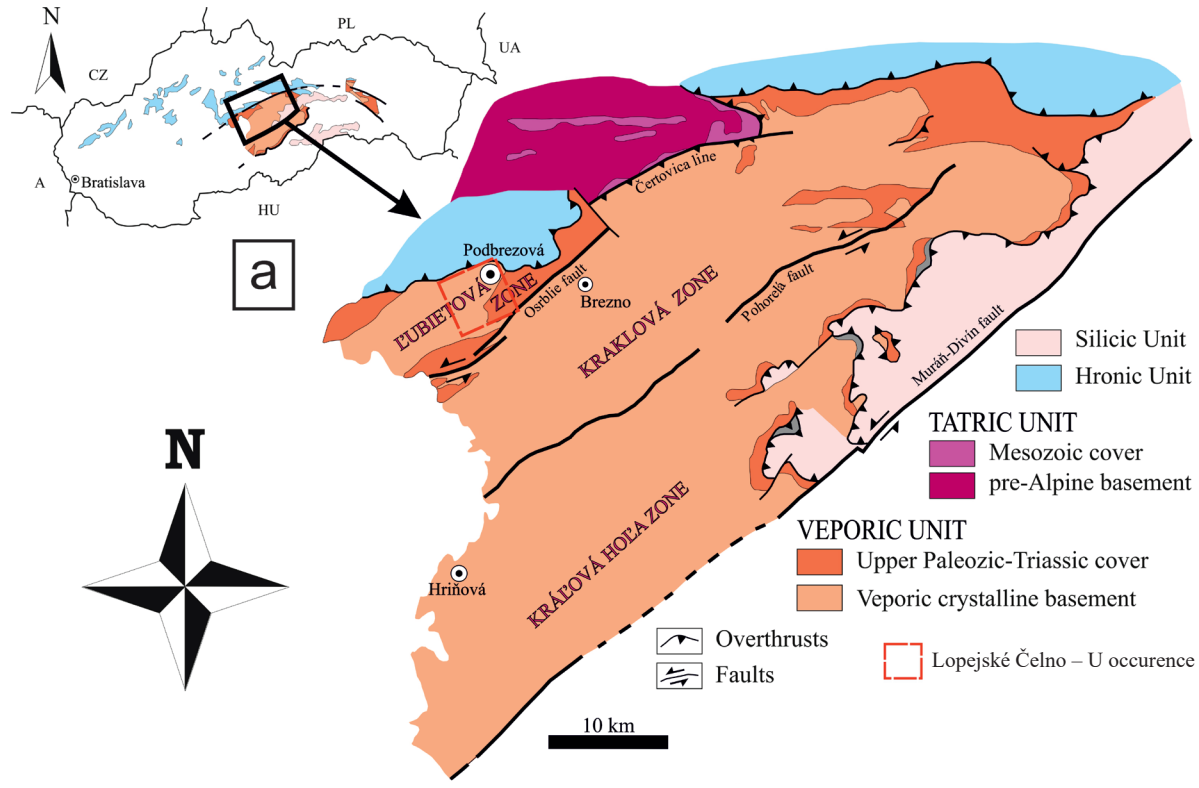

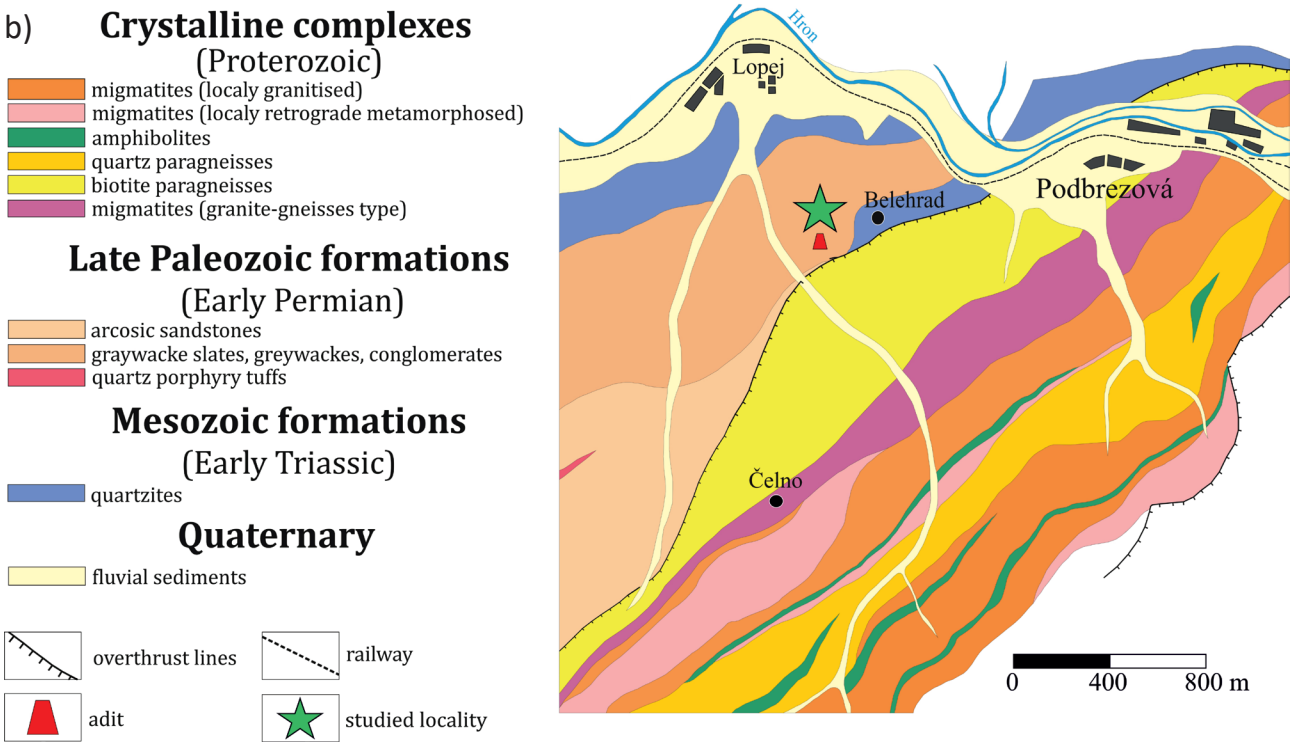

Fig. 1. a – Geological map of the wider surroundings of the studied locality (according to Zoubek, 1936, 1958). b – Detailed geological map of the U-Cu mineralization occurrence in Lopejské Čelno (according to Drnzík, 1963).

analysed by RNDr. Adrián Biroň, PhD.) using CuK_α (1.5418 Å) radiation generated at a voltage of 40 kV and a current of 30 mA. The powder mount was placed in an ethanol suspension onto a Si single crystal. Subsequently, diffraction data were obtained under the following conditions: apertures 0.3° – 6 mm – 0.3° – 0.2 mm, primary and secondary Soller aperture 2.5°, step 0.02° 2Θ/1.25 s, measuring range 2.0–65.0° 2Θ, EDS detector Sol-XE. Diffraction patterns were evaluated using the ZDS software (Ondruš, 1993). Individual reflections were indexed according to structure data available in Downs and Hall-Wallace (2003).

The chemical composition of minerals was determined using an electron microanalyser Jeol-JXA-8530F (Institute of Earth Sciences SAS, Banská Bystrica). The microanalyser was used to determine chemical composition of minerals using energy-dispersive spectrum (EDS) and wave-dispersion microanalysis (WDS).

WDS microanalyses of metatorbernites were performed under the following conditions: accelerating voltage 15 kV, measuring current 15 nA. The diameter of the electron beam ranged from 5 to 10 μm. The ZAF matrix correction was used. The following elements (standard, X-ray line) were measured: orthoclase (KKα), diopside (CaKα), UO_2 (UMß), crocoite (PbMß), baryte (SKα), apatite (PKα), fluorite (FKα), albite (Na Kα), celestite (SrLα), albite (Si Kα), corundum (AlKα), $GaAs_2$ (AsLα), olivine (MgKα), willemite (ZnKα), cuprite (CuKα), Co (CoKα), Bi_2S_3 (BiLα), olivine (FeKα), baryte (BaLα). Silicates were analysed under the following conditions: accelerating voltage 15 kV and measuring current 20 nA. The diameter of the electron beam ranged 5–10 μm The following elements (standard, X-ray line) were measured: quartz (SiKα), orthoclase (KKα), rutile (TiKα), albite (AlKα, NaKα), hematite (FeKα), rhodonite (MnKα), diopside (MgKα, CaKα), $ScVO_4$ (VKα), Cr_2O_3 (CrKα), fluorite (FKα) and NaCl (ClKα). Chemical analysis of brannerites and U-Ti oxides were acquired at 15 kV of accelerating voltage, 20 nA current and 2 μm beam diameter. The following lines and standards were used: diopside (CaKα), orthoclase (KKα), uranium oxide (UMß), thorianite

Fig. 2. Sampling site with U mineralization in the Lopejské Čelno – ore lenses in the forest road cut and directly in the road (photo Š. Ferenc, 2017).

(ThMα), crocoite (PbMß), $LiNbO_3$ (NbLα), cubic zirconia (ZrLα), apatite (PKα), YPO_4 (YLα), fluorite (FKα), albite (NaKα), celestite (SrLα), orthoclase (SiKα), albite (AlKα), diopside (MgKα), $HoPO_4$ (HoLß), $YbPO_4$ (YbLα), $GdPO_4$ (GdLß), $DyPO_4$ (DyLα), $TbPO_4$ (TbLα), $EuPO_4$ (EuLα), $NdPO_4$ (NdLα), $CePO_4$ (CeLα), $LaPO_4$ (LaLα), willemite (ZnKα), hematite (FeKα), rhodonite (MnKα),vanadinite (VKα), rutile (TiKα) and $ScVO_4$ (ScKα).

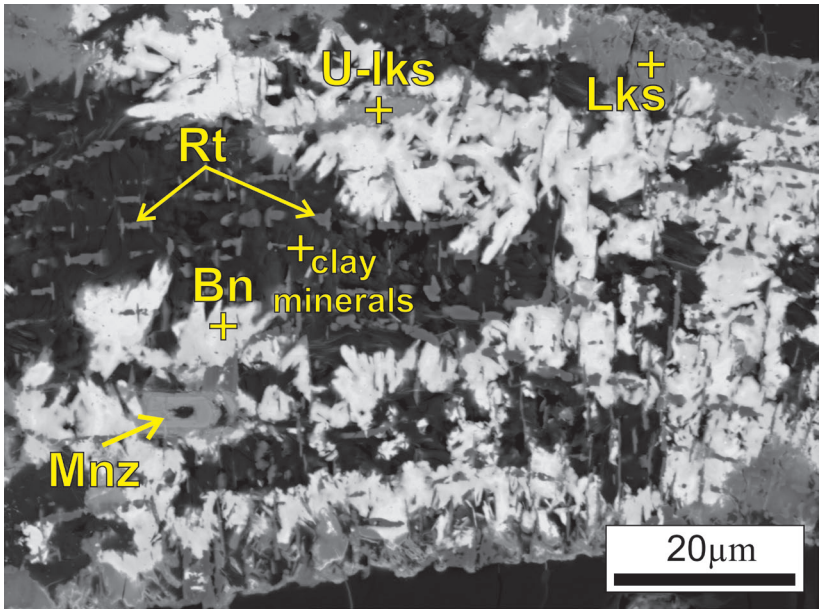

Fig. 3. Grain formed by brannerite (*Bn*), rutile (*Rt*), U-Ti oxides (*U-lks*) and leucoxene (*Lks*). BSE image (photo T. Mikuš).

The detection limit for individual elements ranged from 0.01 to 0.03 wt. %. Elements whose content values are below the detection limit are not included in the tables below. X-ray element distribution maps were obtained (the same device) with an accelerating voltage of 15 kV and probe current of 15 nA.

Raman spectral analysis (Institute of Earth Sciences SAS, Banská Bystrica; analysed by RNDr. Stanislava Milovská, PhD.) was performed on a LabRAM-HR 800 (Horiba Jobin Yvon). The instrument consists of an Olympus BX 41 microscope, a Czerny-Turner type spectrometer. Calibration of the instrument was performed using a laser line (0 cm^{-1}) and Si standard (520,6 cm^{-1}). Raman spectra were taken in two acquisitions, for a period of 20 to 60 seconds per spectral window, in the range of 60 to 4 000 cm^{-1}, using lasers with λ 532 and 633 nm and a source power of 60 respectively 17 mW, with a diffraction grating of 600 streaks/mm and a confocal slit of 100 µm. Laser beam diameter on sample is 2 µm. Spectra were corrected for background subtraction using the math function by LabSpec 5 software. The results were compared with the LabSpec databases and RRUFF (Lafuente et al., 2015).

Infrared spectroscopic analyses (IR) in the spectral range from 4 000 to 400 cm^{-1} were performed on a Nicolet iS50 instrument (Matej Bel University, Banská Bystrica), using a conventional attenuated total refraction (ATR) technique with synthetic diamond as a measuring crystal. For each measurement, 32 scans were performed in steps of 4 cm^{-1}. The detected infrared spectra were compared with several internet databases (RRUFF; lisa.chem.ut.ee) and published works.

Chemical composition of chlorite group mineral phases was calculated applying software WinCac (Yavuz et al., 2015).

Results

Petrography of the host rocks

The host Permian arcosic sandstones are mainly formed by clasts of mono- and polycrystalline, subangular, undulose quenching quartz (up to 1 cm in size), muscovite aggregates (up to 0.2 mm) and

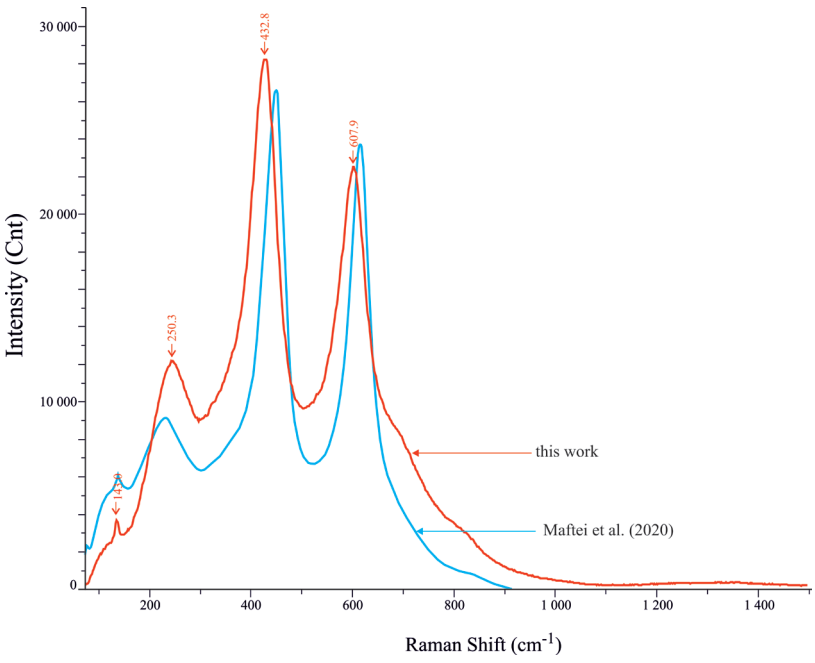

Fig. 4. Raman spectrum of rutile from the Lopejské Čelno (red colour) compared with previously published spectrum (Maftei et al., 2020; blue colour).

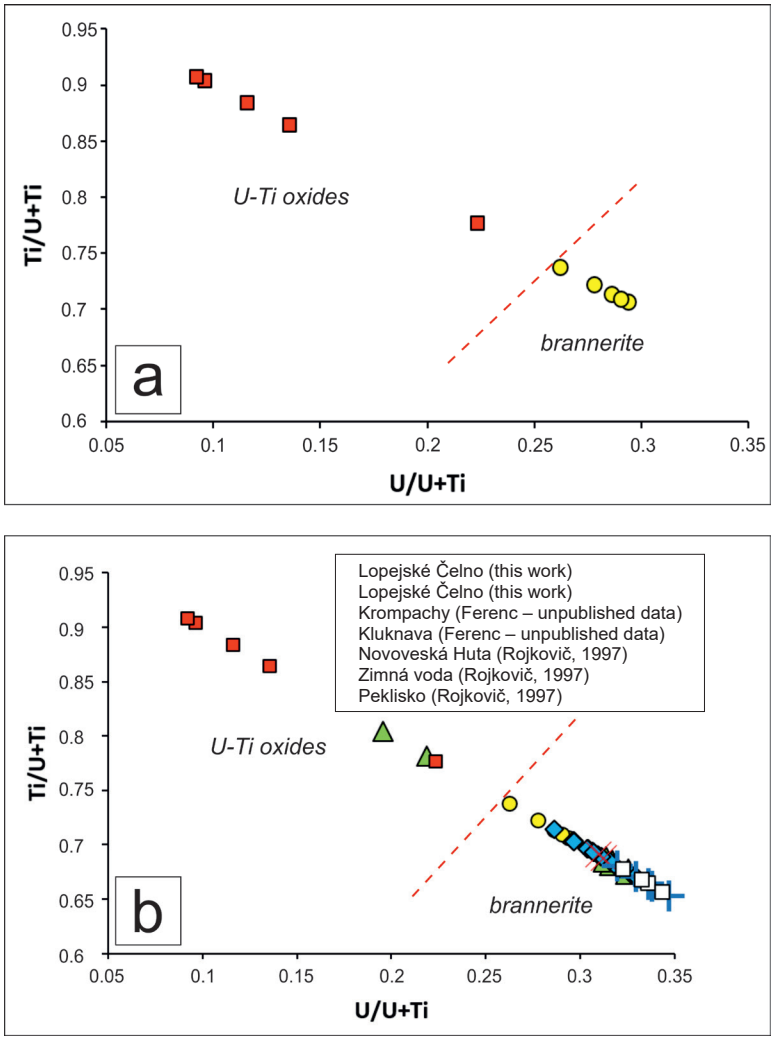

Fig. 5. Differences in the chemical compositon of brannerite and U-Ti oxides from the Lopejské Čelno (a) compared with composition in other occurrences in the Western Carpathians (b). Border line between brannerite and U-Ti oxides constructed according to Lumpkin et al. (2012).

chlorite. Rarely were found biotite and K-feldspars, which, however, are often chloritized and sericitized. Rock matrix is microcrystalline, quartz-sericitic to sericitic. Mineralized (U-Cu) rock is, in addition, in a great extent limonitized. It shows obscure tectonic directing and foliation, indicating weak Alpine metamorphic reworking. Small cavities and fissures in the rock have goethite and unspecified black Mn oxides fill. Uranium is distributed irregularly in the rock and is bound to the U-Ti oxides, brannerite and uranyl phosphate metatorbernite.

Mineralogical characteristic

Primary mineralization

Primary mineralization was detected only rarely in mineralized grains with a size of up to 120 µm (Fig. 3).

Rutile was identified in close association with brannerite, leucoxene, U-Ti oxides a clay minerals. Cationic position in dominantly occupied by Ti (81.29–86.10 wt. %; up to 0.86 apfu Ti), increased contents of Si (6.92–8.20 wt. %; up to 0.11 apfu Si) and Al (3.01–3.94 wt. %; max. 0.06 apfu Al) were also detected. Rutile (like polymorph TiO_2) was confirmed also by Raman spectroscopy (Fig. 4).

Brannerite is the only identified primary (U^{4+}) uranium mineral at the occurrence, observed only very rarely. It forms clusters of needle-like crystals (length up to 100 µm). It occurs in close spatial association with U-Ti oxides (*uranoferous leucoxene*), rutile and clay minerals. Uranium is dominant in the cationic position (47.43–43.79 wt. % UO_2; up to 0.68 apfu U), Ti (37.76–31.60 wt. % TiO_2; max. 1.76 apfu Ti). Trace elements are represented by Si (max. 5.82 wt. % SiO_2; 0.37 apfu Si), Ca (max. 2.68 wt. % CaO; 0.18 apfu Ca), Fe (up to 2.64 wt. % FeO; 0.14 apfu Fe), also by weakly increased content of Y, Al, K, Mg, Mn, Pb, Zr, As and REE.

U-Ti oxides, also known as *uranoferous leucoxene*, were identified in association with brannerite and rutile. Unlike brannerite, their chemical composition is characteristic mainly by decreased U content (16.80–41.95 wt. % UO_2; max. 0.55 apfu U) and, vice versa – increased contents of P (up to 5.92 wt. % P_2O_5; 0.26 apfu P) and Si (max. 7.80 wt. % SiO_2; 0.40 apfu Si).

The differences in the chemical composition of brannerite and U-Ti oxides (ab. 1), can be expressed by their content ratio (in apfu, or in atomic %) U/(U + Ti): 0.22-0.29 in brannerite and 0.09–0.14 for U-Ti oxides (Fig. 5a). Both studied mineral phases were compared with their occurrences in other sites in the Western Carpathians (Fig. 5b).

Supergene minerals

Metatorbernite (spontaneously dehydrated torbernite to a more stable phase) forms light green, tabular crystals up to 2 mm in size (Fig. 6a). Their aggregates fill fissures in the rock, or small cavities after leached rock-forming minerals (Fig. 6b, c). Occasionaly replaces fluorapatite crystals (Fig. 12). As for metatorbernite chemical composition (Tab. 3), cationic position is dominantly occupied by Cu (3.37–7.77 wt. % CuO; up to 0.93 apfu Cu; Fig. 7) and U (57.22–66.66 wt. % UO_3; max. 2.10 apfu U). K (max. 0.36 wt. % K_2O; 0.72 apfu K), Ca (up to 0.64 wt. % CaO; 0.10 apfu Ca) and Mg (up to 0.11 wt. % MgO; 0.03 apfu Mg) are less abundant. For anionic position there is characteristic dominant P (13.27–16.72 wt. % P_2O_5; up to 2.08 apfu P), only weakly increased contents of As and Si

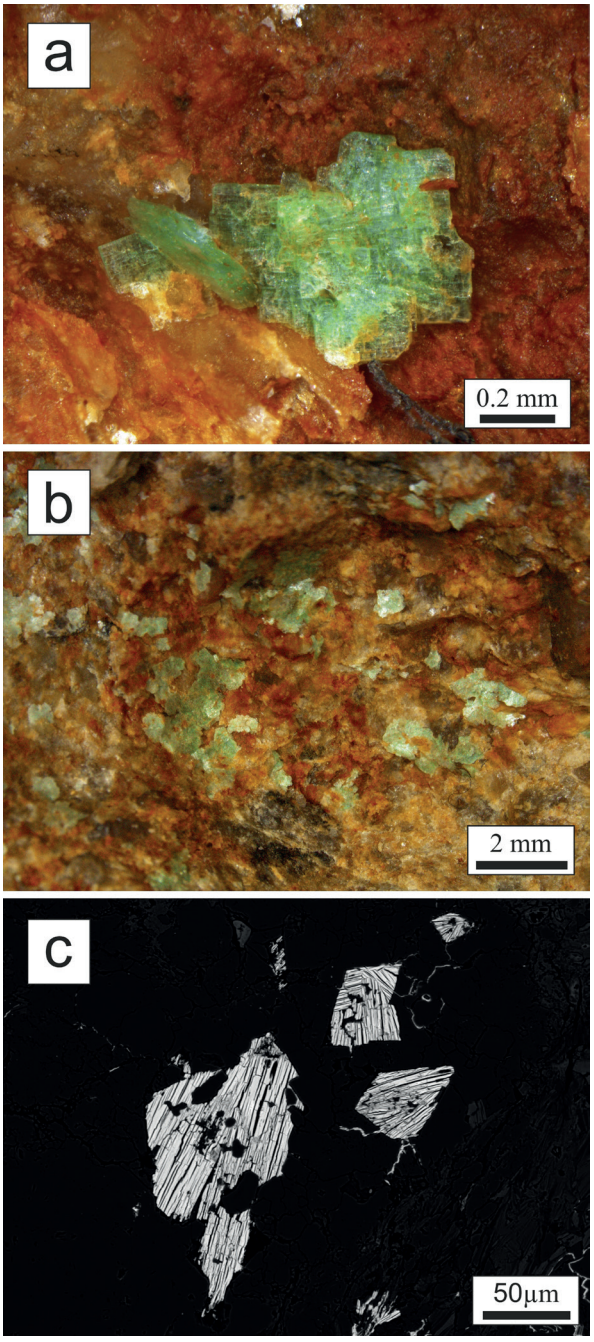

Fig. 6. Aggregates of light green, tabular metatorbernite crystals (**a**, **b**; photo R. Kopáčik) often form filling of cavities and cracks in the rock (**c**; BSE image; photo T. Mikuš).

were found. Average empirical formula (6 WDS analyses) of metatorbernite from Lopejské Čelno occurrence is $(Cu_{0.75}Ba_{0.06}Ca_{0.03}K_{0.04}Al_{0.02}Mg_{0.01}Fe_{0.01})_{\Sigma 0.94}(UO_2)_{\Sigma 2.00}(PO_4)_{\Sigma 2.01}(H_2O)_8$.

Several bands were detected in the IR spectrum of the studied metatorbernite (Fig. 8). The band at 902 cm^{-1} can be assigned to the antisymmetric valence vibration ν_3 UO_2^{2+} and the bands at 843, 810 and 789 cm^{-1} to

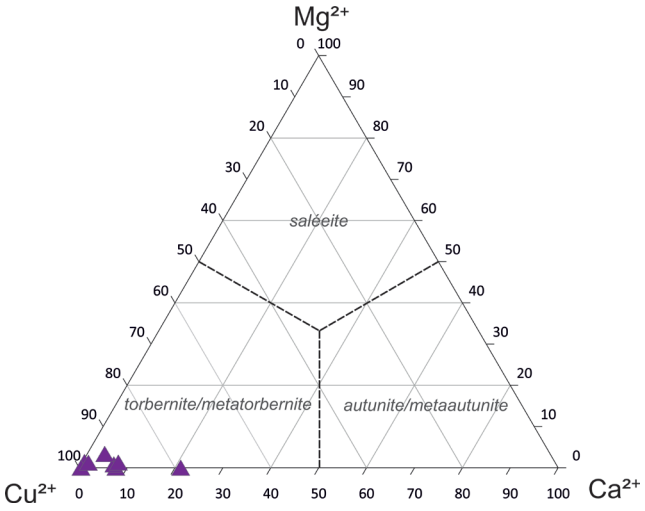

Fig. 7. Chemical composition of metatorbernite from Lopejské Čelno in the ternary diagram of the system Cu-Ca-Mg (according to Plášil et al., 2009).

the symmetric valence vibration ν_1 UO_2^{2+}. Bands 673, 607 cm^{-1} apparently correspond to the liberation modes of molecular water. Triple degenerate antisymmetric valence vibration ν_4 PO_4^{3-} is represented by bands at 461 and 539 cm^{-1}. Band at 987 cm^{-1} represents triple degenerated ν_3 PO_4^{3-} valence vibration. Band at 1 636 cm^{-1} is manifest of deformation vibration of H_2O. Valence vibration ν OH of water molecules corresponds with bands at 2 924, 3 341 and 3 403 cm^{-1}. The obtained spectrum corresponds very well with previously published data for torbernite / metatorbernite (Čejka et al., 1984; Čejka & Urbanec, 1990; Frost, 2004; Frost et al., 2005; Plášil et al., 2009).

Malachite is relatively rare. It forms thin crusts covering up to 3 cm on the rock debris or fillings of fissures and cavities in the rock. It was identified by PXRD analysis, while the measured diffractometric data agree well with the previously published data for this mineral phase (Süsse, 1967; Downs et al., 1993).

Discussion and conclusion

In the Western Carpathians, a similar type of mineralization occurs in the Malé Karpaty Mts. at Lošonec and Smolenice (Rojkovič, 1997), in the Nízke Tatry Mts. at Benkovský potok, Ipoltica and Nižný Chmelienec occurrences (Hronic Unit; Drzník, 1969; Rojkovič, 1998; Rojkovič & Vozár, 1972; Václav & Vozárová, 1978; Hoppanová et al., 2021). In the Northern Gemeric Unit U ± Cu mineralization in so-called copper sandstones, occurs near Novoveská Huta and Stratená villages (Ondrejkovič et al., 1964; Grecula et al., 1995; Števko, 2014; Ferenc et al., 2022).

Increased contents of uranium and accompanying elements is present in the Permian acid volcanics and these

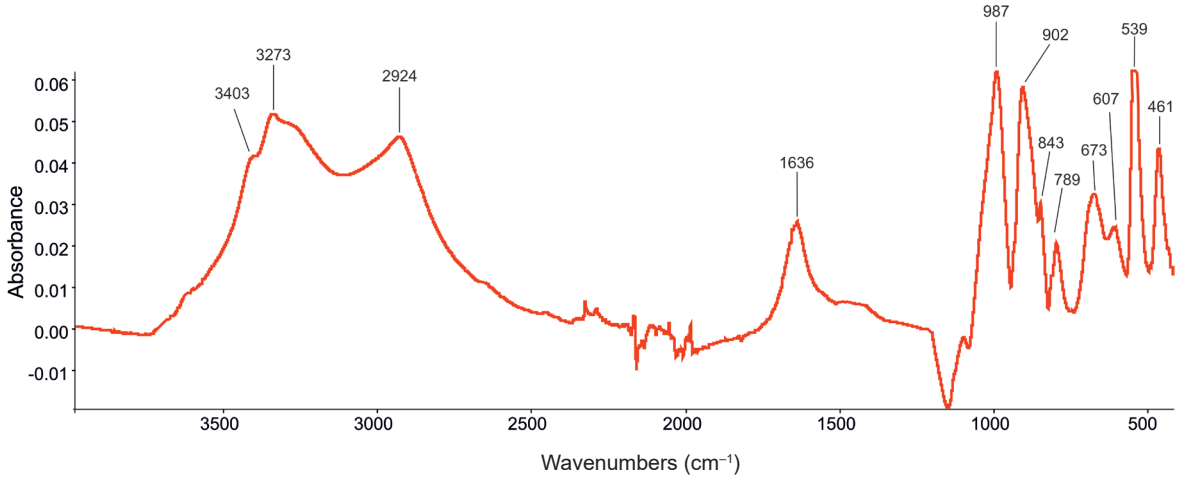

Fig. 8. Infrared spectrum of metatorbernite from Lopejské Čelno occurrence.

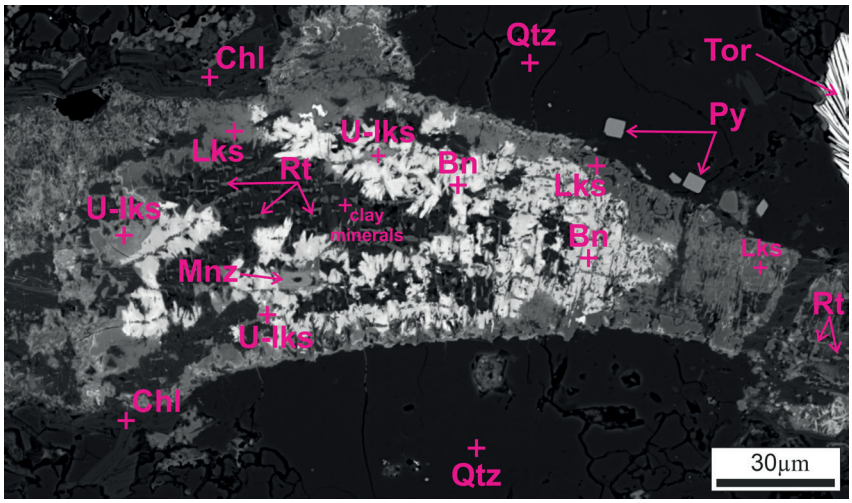

Fig. 9. Grain of altered biotite with U^{4+} minerals brannerite (*Bn*) and U-Ti oxides (*U-Lks*) and magmatic monazite-(Ce) (*Mnz*), in close space association with decay products of biotite hydrothermal alteration: rutile (*Rt*), leucoxene (*Lks*), *clay minerals* and chlorite (*Chl*). Surrounding of grain form quartz (*Qtz*) with pyrite (*Py*) and metatorbernite (*Tor*). BSE image (photo T. Mikuš).

Fig. 10. Chemical composition of brannerite and U-Ti oxides from Lopejské Čelno in ternary diagram of the system U-Ti-Si, compared with those from the other localities in the Western Carpathians.

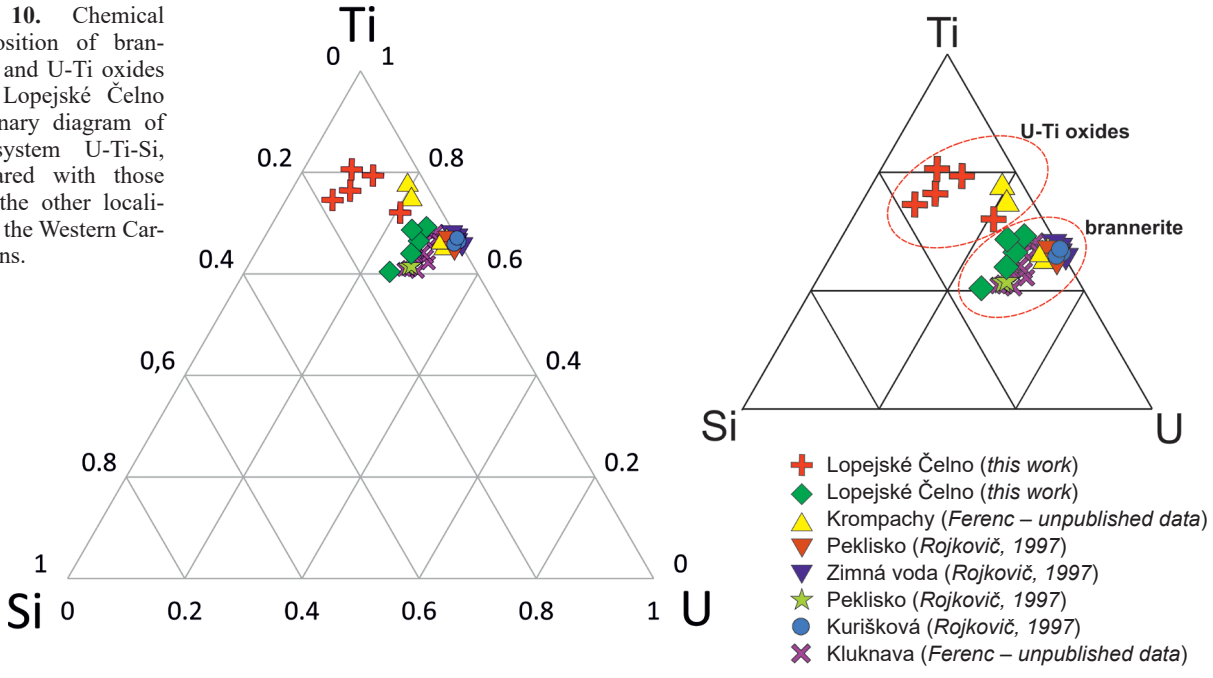

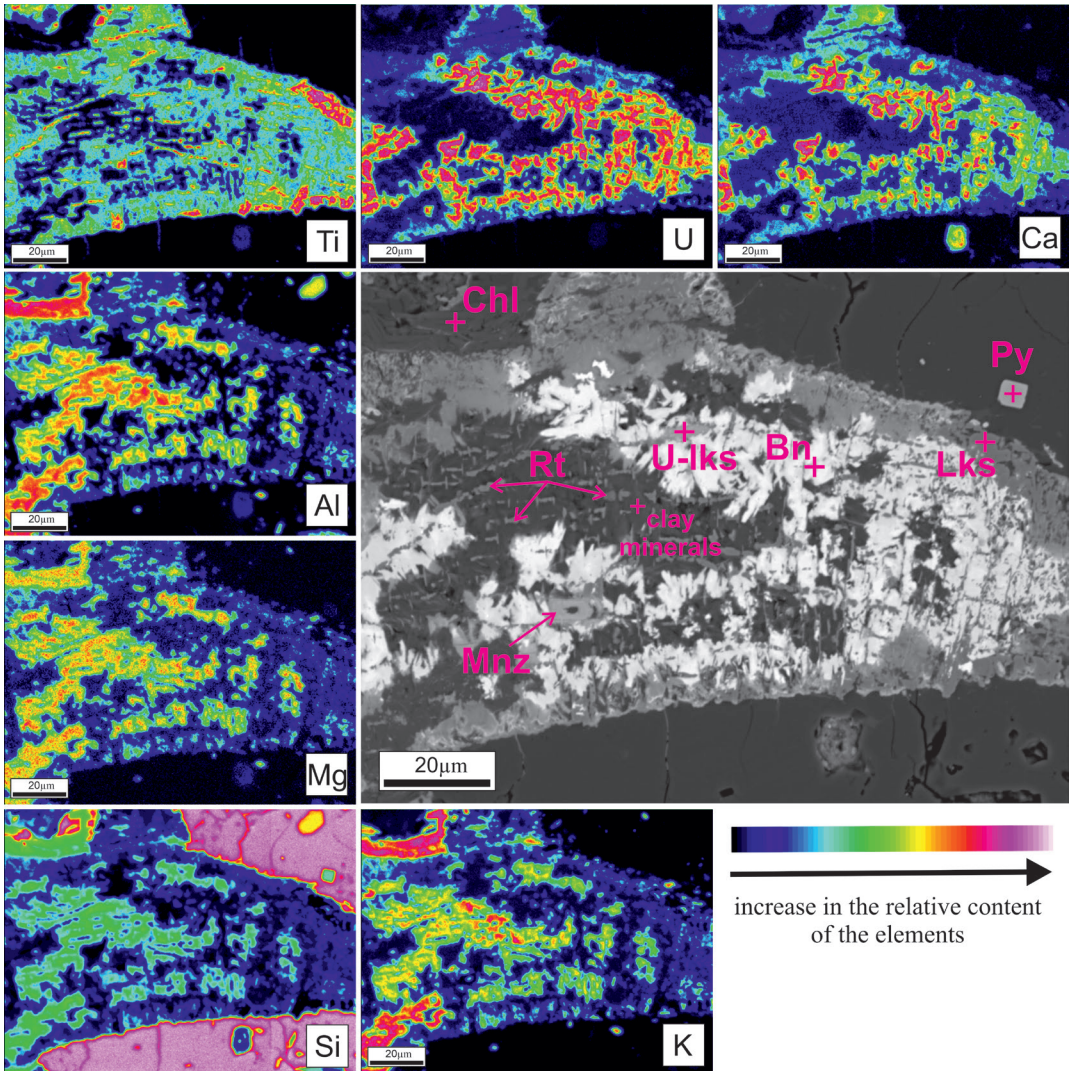

Fig. 11. Back-scattered electron (BSE) images and X-ray element distribution maps in uranium-bearing grain from Lopejské Čelno (photo and maps T. Mikuš).

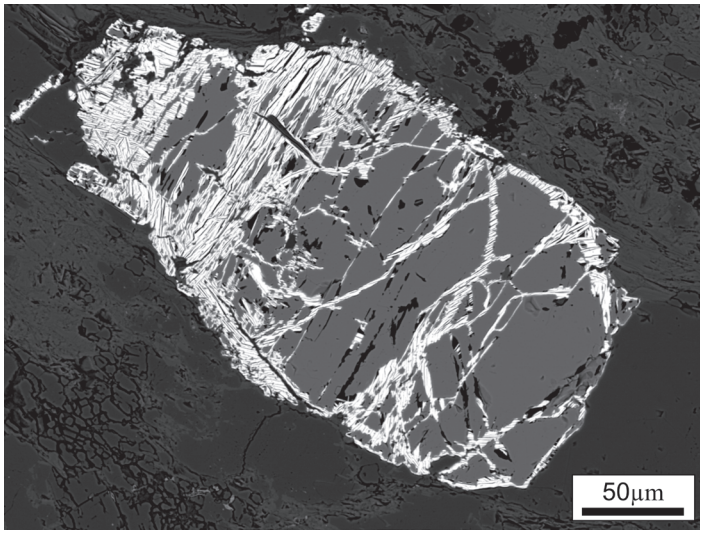

Fig. 12. Hypidiomorphic grain of fluorapatite (grey) replaced by metatorbernite (white). BSE image (photo T. Mikuš).

are therefore a potential source of uranium (Rojkovič et al., 1989). Uranium was released from devitrified acid volcanic glass. Subsequently, together with other ore elements, it precipitated in a reducing environment under the influence of the adsorption of some minerals (Ti oxides, Fe oxides, clay minerals). This process resulted in the formation of stratiform U ore accumulations in the continental Permian (poor grade ores) of the Western Carpathians (Rojkovič & Mihál', 1991). Remobilization and concentration of stratiform Hercynian ore mineralization during Alpine orogenesis caused formation of richer U mineralization (Rojkovič & Novotný, 1981).

Primary mineralization and its genesis

The revision study of mineralization in Lopejské Čelno brought new knowledge. Primary U^{4+} mineralization represented by brannerite and U-Ti oxides was identified here; accompanying

minerals are rutile, Ti oxides (leucoxene) and clay minerals (probably illite). Because primary mineralization occurs only rarely, even only in grains with a size of up to 120 μm (Fig. 9), its mineral phases are in close spatial association and often overgrow; it is complicated to clarify its genesis with certainty. The most probably explanation for its formation is the alteration (chloritization) of biotite connected with hydrothermal processes and the subsequent adsorption of uranium onto the formed Ti oxides, while the source of Ti was biotite. This sequence of geochemical processes could have been caused by the Alpine metamorphic processes with following p-T conditions: 300–700 MPa at 300–500 °C in the Permian sediments of the Ľubietová Zone (Kamenický, 1978; Slavkay et al., 2004); 500–1 100 MPa at of 430–620 °C in the crystalline basement of the Veporic Unit (Plašienka et al., 1999; Janák et al., 2001; Jeřábek et al.; 2008). Vozárová (1979) also describes completely altered biotite at the site.

Biotite easily decomposes during hydrothermal processes. The most common secondary products of its alteration are chlorite, muscovite, sericite, clay minerals, leucoxene, epidote-zoisite, rutile, recrystallized biotite accompanied with a number of minerals with small or no relation to the chemical composition of biotite (Schwartz, 1958). The release of titanium and the formation of Ti oxides represent one of the most characteristic features of biotite alteration (Lovering, 1949; Schwartz, 1958; Bisdom, 1967; Deer, 1992).

Adsorption of uranium onto newly formed Ti oxides closely relates to the so-called "*Pronto-reaction*". This process described Ramdohr (1957), who reported the formation of brannerite and U-Ti oxides in situ either by adsorption of uranium to Ti/Fe-Ti mineral phases, or by binding of titanium to uraninite to form uranotitanates, according to the chemical equation:

$$UO_2 + 2 - 3TiO_2 \rightarrow UTi_{2-3}O_{6-8}.$$

The "Pronto-reaction" takes place in hydrothermal systems that reach temperatures of around 225 °C (Schidlowski, 1996), which in the case of Lopejské Čelno, correlates with the temperature generated during the Alpine orogeny, or by its fading.

Most of natural brannerites are metamict (Smith, 1984). Metamictization is caused by damage of the brannerite crystal structure due bombardment with α-particles from the uranium decay (Lian et al., 2002). For this reason, the crystal structure parameters of naturally occurring brannerite are not certainly known. In addition, the uranium in brannerite is usually partially oxidized (presence U^{4+}, U^{5+} also U^{6+} valences), either, brannerite itself is often hydrated (Finch & Murakami, 1999). In hydrothermal brannerites, Ca, Th, Y, and REE replace uranium, while Si, Al and Fe replace titanium due to oxidation and partial hydration (Smith, 1984). Brannerite from Lopejské Čelno has an increased content of Si (max. 0.37 apfu), Ca (up to 0.18 apfu), Fe (max. 0.14 apfu) and Al (max. 0.14 apfu). U-Ti oxides also have higher values of Si (up to 0.30 apfu), Ca (up to 0.11 apfu), Fe (up to 0.16 apfu) and Al (up to 0.21 apfu), which confirms the hydrothermal nature of the mineralization. Compared to the data of Finch (1996), brannerites in the Veporic Unit could have formed already during the main phase of Alpine metamorphism at medium to high temperatures (temperatures close to 400–600 °C), by direct precipitation from solutions containing the uranyl ion UO_2^{2+}, while the source of uranium was devitrified volcanic glass. An important role play releasing of titanium from biotite during its alteration and the formation of Ti/Fe-Ti oxides. The subsequent fading of the Alpine orogeny (reduction of p-T conditions, mainly temperature) created conditions for the adsorption of the remaining uranium on U-Ti oxides, which can be evidenced by the lower concentration of uranium in U-Ti oxides. A similar mechanism of formation of U mineralization was observed at the deposits Zadní Chodov and Rožná (Czech Republic), where the Ti released during the biotite chloritization played an important role in the brannerite formation (René & Dolníček, 2017).

In samples from Lopejské Čelno, clay minerals fill the space between brannerite, rutile, leucoxene and U-Ti oxides (U-leucoxene). According to Bisdom (1967), titanium minerals in close spatial association with clay minerals in the places of fully or partially altered biotite often form a pattern that roughly coincides with the interlamellar positions in the altered biotite. Equivalent orientation of rutile was also found in mineralized grains from Lopejské Čelno, while rutile admixtures in mafic minerals here were observed by Vozárová (1979; Fig. 9). On the edge of the mineralized grains and in the host rock, chlorite and muscovite are abundantly represented (Tab. 3).

The distribution of individual elements is shown in Fig. 10 and correlates well with the described mineral phases. According to Schwartz (1958), the presence of several mineral phases with different chemical composition within one grain (phenocryst) indicates, that hydrothermal solutions are the decisive factors in biotite transformation. Another important factor is the variability of rock permeability, when in one part of the rock; biotites can be completely altered, while in another part they remain intact.

Oxidation zone

In the Lopejské Čelno occurrence, malachite, goethite and torbernite/metatorbernite represent the supergene alteration of mineralized rocks.

Precipitation of uranyl phosphates takes place in a low pH environment (Langmuir, 1978). The formation of

metatorbernite (and uranyl phosphates in general) in the oxidation zone is conditioned by the oxidation of U^{4+} to U^{6+}, forming the uranyl cation UO_2^{2+} (Civetta & Gasparini, 1972). If there is an active exchange of oxygen-rich waters, the destruction of primary uranium minerals and the formation of uranyl ions occurs:

$$UO_2 + H_2O + 1/2O_2 = UO_2^{2+} + 2OH^-.$$

The occurrence of sulphides (mainly pyrite) with the formation of sulphuric acid has a great influence on the destruction of uranium ore:

$$2FeS_2 + 7O_2 + 2H_2O = 2FeSO_4 + 2H_2SO_4.$$

The resulting acidic solutions intensify the decay of primary uranium minerals. Uranium is usually found in natural solutions in the form of complexes. The formation of stable soluble uranyl complexes enables the migration of U and the formation of secondary uranium minerals (Tripathi, 1983; Liu & Neretnieks, 1990). For the formation of metatorbernite, as well as other uranyl phosphates, the addition of phosphorus in the form of PO_4^{3-} anions is important. The dominant uranyl-phosphate complexes are $[UO_2H_2PO_4]^+$, $[UO_2HPO_4]^0$ and $[UO_2PO_4]^-$ (Langmuir, 1978). These are provided to the system as a product of the interaction of meteoric waters with the surrounding rocks, while there is an interaction with accessory apatite (and other rock-forming minerals containing P), which is unstable in acidic conditions and decomposes according to a chemical reaction (Vinogradov, 1963):

$$Ca_5(PO_4)_3F + 5H_2SO_4 \rightarrow 3H_3PO_4 + 5CaSO_4 + HF.$$

The subsequent fall in pH, together with changes of other chemical and physical factors (Eh, chemical composition of solutions, p-T conditions) in solutions causes destruction of uranyl-phosphate complexes and precipitation of metatorbernite (Chernikov, 1981; Baes & Mesmer, 1976; Langmuir, 1997). The source of Cu for metatorbernite at the Lopejské Čelno occurrence was mostly chalcopyrite. Rarely, hypidiomorphic fluorapatite crystals directly replaced by metatorbernite can be observed in sandstones from here (Fig. 12).

An unusual phenomenon in metatorbernite from Lopejské Čelno is a weak yellow-green luminescence. Luminescent torbernites were also identified at other localities in the Western Carpathians: Novoveská Huta, Peklisko, Zimná voda (Ferenc et al., 2003), Brezno-Skalka (our unpublished data) or in Bohemia (Medvědín; Plášil et al., 2009). Based on a comparison of the chemical composition with metatorbernite without luminescence ("normal" metatorbernite), it can be concluded, that luminescence is not caused by a change in chemical composition, i.e. the presence of a luminophores. Therefore, luminescence can be caused either by defects in the crystal lattice of luminescent metatorbernites, or by an admixture of nanoparticles of another mineral (Plášil et al., 2009).

Acknowledgements

This work was supported by the Ministry of Education, Slovak Republic VEGA-1/0563/22 project, as well as the Slovak Research and Development Agency under the contract APVV-19-0065. Authors express their thanks to J. Sejkora (National Museum Prague) and M. Števko (Slovak Academy of Science) for detailed reviews and improvement of the manuscript.

References

Baes, C. F. & Mesmer, R. E., 1976: The Hydrolysis of Cations. *New York, Wiley-Interscience, 489 p.*

Bezák, V., Broska, I., Konečný, P., Petrík, I. & Košler, J., 2008: Permský magmatický komplex v severnom veporiku: interpretácia z nových datovaní kyslých magmatitov. *Miner. Slov., 40, 127–134.*

Bisdom, E. B. A., 1967: Micromorphology of a weathered granite near the Ria de Arosa (NW Spain). *Leidse Geol. Mededel., 37, 1, 33–67.*

Civetta, L. & Gasparini, P., 1972: A review of U and Th distribution in recent volcanics from southern Italy: magmatological and geophysical implications. *In: Adams, J. A. S., Gaskell, T. S. & Lowder, W. M. (eds.): Natural radiation environment, vol. II. Houston, Rice Univ. Dep. Geol., 483–516.*

Čejka, J. & Urbanec, Z., 1990: Secondary uranium minerals. The mineralogy, geochemistry and crystal chemistry of the secondary uranium (VI) minerals. *Praha, Academia, 93 s.*

Čejka, J. JR, Muck, A. & Čejka, J., 1984: To the infrared spectroscopy of natural uranyl phosphates. *Phys. Chem. Miner., 11, 172–177.*

Daniel, J., 2006: Zhodnotenie geologických prác na U rudy vo vybraných oblastiach Západných Karpát na území Slovenska. Záverečná správa. *Manuscript. Spišská Nová Ves, URANPRES, 111 p.*

Deer, W. A., Howie, R. A. & Zussman, J., 1992: An introduction to the rock-forming minerals, 2nd ed. *London, Longman Scientific & Technical, 696 p.*

Downs, R. T., Bartelmehs, K. L., Gibbs, G. V. & Boisen, M. B. JR, 1993: Interactive software for calculating and displaying X-ray or neutron powder diffractometer patterns of crystalline materials. *Amer. Mineralogist, 78, 1104–1107.*

Downs, R. T. & Hall-Wallace, M., 2003: The American Mineralogist crystal structure database. *Amer. Mineralogist, 88, 1, 247–250.*

Drnzík, E., 1963: Zhodnotenie geologických prác na U rudy vo vybraných oblastiach Západných Karpát na území Slovenska. *In: Daniel, J., 2006. Manuscript. Spišská Nová Ves, URANPRES, 111 s.*

Drnzík, E., 1969: O zrudnení typu meďnatých pieskovcov v perme melafýrovej série na severovýchodných svahoch Nízkych Tatier. *Miner. Slov., 1, 7–37.*

Ferenc, Š., Mikuš, T., Kopáčik, R., Vlasáč, J. & Hoppanová, E., 2022: Cu-(U) mineralisation in the copper sandstones at Šafárka occurrence near Novoveská Huta (Spišská Nová Ves), Spišsko-gemerské Rudohorie Mts., Western Carpathians, Gemeric Unit, eastern Slovakia. *Acta Geol. Slov., 14, 2, 87–101.*

Ferenc, Š., Rojkovič, I. & Maťo, Ľ., 2003: Uranylové minerály Západných Karpát. *In: Zborník z konferencie Mineralogie Českého masivu a Západních Karpat. Olomouc a Horní Údolí, Univerzita Palackého, 17–23.*

Finch, R. J. & Murakami, T., 1999: Systematics and paragenesis of uranium minerals. *In: Burns, P. C., Finch, R. J. (eds.): Uranium: Mineralogy, Geochemistry and the Environment. Rev. Miner., 38, Washington, Miner. Soc. Amer., 673 s.*

Finch, W. I., 1996: Uranium provinces of North America-their definition, distribution, and models. *US Geol. Surv. Bull., 2141, 1–18.*

Frost, R. L., 2004: An infrared and Raman spectroscopic study of the uranyl micas. *Spectrochimica acta. Part A, Molecular and biomolecular spectroscopy, 60, 7, 80 –1469.*

Frost, R. L., Erickson, K., Carmody, O. & Weier, M. L., 2005: Near-infrared spectroscopy of torbernites and metatorbernites. *Spectrochim. Acta. Part A, Molecul. biomolecul. spectrosc., 61, 4, 749–54.*

Grecula, P., Abonyi, A., abonyiová, M., Antaš, J., Bartalský, B., Bartalský, J., Dianiška, I., Drnzík, E., Ďuďa, R., Gargulák, M., Gazdačko, Ľ., Hudáček, J., Kobulský, J., Lörincz, L., Macko, J., Návesňák, D., Németh, Z., Novotný, L., Radvanec, M., Rojkovič, I., Rozložník, L., Rozložník, O., Varček, C. & Zlocha, J., 1995: Mineral deposits of the Slovak Ore Mountains. *Bratislava, Geocomplex, 834 s.*

Holland, T. J. B. & Redfern, S. A. T., 1997: Unit cell refinement from powder diffraction data: the use of regression diagnostics. *Min. Mag., 61, 65–77.*

Hoppanová, E., Ferenc, Š., Kopáčik, R., Budzák, Š. & Mikuš, T., 2021: Supergénne minerály z U-Cu rudného výskytu Východná-Nižný Chmelienec v Nízkych Tatrách (hronikum, Slovensko). *Bull. Miner. Petrol., 29, 1, 77–89.*

Chernikov, A. A., 1981: Behaviour of Uranium in the Hypergene Zone (Povedenie Urana v Zone Gipergeneza). *Nedra, 207 p. (in Russian).*

Janák, M., Plašienka, D., Frey, M., Cosca, M., Schmith, S. Th., Lupták, B. & Méres, Š., 2001: Cretaceous evolution of a metamorphic core complex, the Veporic unit, 50 Western Carpathians (Slovakia): P-T conditions and in situ $^{40}Ar/^{39}Ar$ UV laser probe dating of metapelites. *J. Metamorph. Geol., 19, 197–216.*

Jeřábek, V., Janák, M., Faryad, S. W., Finger, F. & Konečný, P., 2008: Polymetamorphic evolution of pelitic schists and evidence for Permian low-pressure metamorphism in the Vepor Unit, West Carpathians. *J. Metmorph. Geol., 26, 465–485.*

Kamenický, J., 1982: Vývoj a podmienky metamorfózy v severozápadanej časti Slovenského rudohoria. *In: Krist, E. & Mihaliková, A. (eds.): Metamorfné procesy v Západných Karpatoch. Bratislava, Geol. Úst. D. Štúra, 23–37.*

Kamenický, J., 1977: Der geologische bau der nordwestlichen teiles der Vepor-erzgebirges. *Acta geol. geogr. Univ. Comen., Geol., 32, 5–43.*

Kamenický, J., 1978: Petrographie und geochemie der amphiboliter des NW-teiles der Vepor erzgebirges. *Acta geol. geogr. Univ. Comen., Geol. 33, 37–82.*

Lafuente, B., Downs, R. T., Yang, H. & Stone, N., 2015: The power of databases: the RRUFF project. *In: Armbruster, T. & Danisi, R. M., (eds.): Highlights in Mineralogical Crystallography. Berlin, De Gruyter, 1–30.*

Langmuir, D. A., 1997: Aqueous Environmental Geochemistry. *Upper Saddle River, Prentice-Hall, 600 s.*

Langmuir, D., 1978: Uranium Solution-Mineral Equilibria at Low Temperatures with Applications to Sedimentary Ore Deposits. *Geochim. cosmochim. Acta, 42, 547–569.*

Lian, J., Wang, L., Lumpkin, G. R. & Ewing, R. C., 2002: Heavy ion irradiation effects of brannerite-type ceramics. *Nuclear Instruments and Methods in Physics Research, 191, 565–570.*

Liu, L. & Neretnieks, I., 1990: Sensitivity Analysis of Uranium Solubility under Strongly Oxidizing Conditions. *In: Lee, J. H. & Wronkiewicz D. J.(eds.): Proceedings of Symposium on Science Base Nuclear Waste Managem-XXII (MRS, Warrendale, 1999). Cambridge Univ. Press, 556, 1001–1008.*

Lovering, T. S., Stoll., W. M., Wadsworth., Wagner, H. V., Stringham B. F., Morris, H. T., Lowell, S., Smith, J. F., Alberto, L., Terronest, Bonorino, F. G., Odell, J. W. & Mapes, V. E., 1949: Rock alteration as a guide to ore, East Tintic District, Utah. *USA, Econ. Geol., 64 p.*

Lovering, T. S., 1949: Origin of tungsten ores of Boulder County, Colorado. *Econ. Geol., 36, 229–279.*

Lumpkin, G. R., Leung, S. H. F. & Ferenczy, J., 2012: Chemistry, microstructure, and alpha decay damage of natural brannerite. *Chem. Geol., 291, 55–68.*

Maftei, A. E., Buzatu, A., Damian, G., Buzgar, N., Dill, H. G. & Apopei, A., 2020: Micro-Raman – a tool for the heavy mineral analysis of gold placer-type deposits (Pianu Valley, Romania). *Minerals, 10, 11, 988.*

Maheľ, M., Kamenický, J., Fusán, O. & Matějka, A., 1967: Regionální geologie ČSSR, 2. Západní Karpaty. *Praha, ČSAV, Ústř. Úst. geol., 496 p.*

Ondrejkovič, K., Macko, J., Kotras, J, Drnzíková, Ľ., Mandáková, K. & Kroupa, L., 1964: Záverečná správa a výpočet zásob Bindt- Novoveská Huta, Cu- pieskovce. *Manuscript. Bratislava, archive St. Geol. Inst. D. Štúr, 271 p.*

Ondruš, P., 1993: ZDS – A computer program for analysis of X-ray powder diffraction patterns. *Mater. Sci. Forum, 133–136, 297–300.*

Patchett, J. E. & Nuffield, E. W., 1960: Studies of radioactive compounds: X-The synthesis of crystallography of brannerite. *Canad. Mineralogist, 6, 483–490.*

Planderová, E. & Vozárová, A., 1982: Biostratigraphical correlation of the Late Paleozoic formations in the West Carpathians. *In: Sassi, F. P. & Varga, I. (eds.): Newsletter No. 4, IGCP Project No. 5., 61–71.*

Plašienka, D., Janák, M., Lupták, B., Milovský, R. & Frey, M., 1999: Kinematics and metamorphism of a Cretaceous core complex: the Veporic unit of the Western Carpathians. *Physics Chem. Earth (A), 24, 651–658.*

Plášil, J., Sejkora, J., Čejka, J., Škoda, R. & Goliáš, V., 2009: Supergene mineralization of the Medvědín uranium deposit, Krkonoše Mountains, Czech Republic. *J. Geosci., 54, 15–56.*

Ramdohr, P., 1957: Die "Pronto-Reaktion". *Neu Jb. Mineral., 10–11, 217–222.*

René, M. & Dolníček, Z., 2017: Uraninite, coffinite and brannerite from shear-zone hosted uranium deposits of the Bohemian massif (Central European Variscan belt). *Minerals, 7, 4, 50.*

Rojkovič, I. & Miháľ, F. 1991: Geological structure and uranium mineralization in the Permian rocks of the north-eastern part of the Slovenské Rudohorie Mts. *Miner. Slov., 23, 123–132.*

Rojkovič, I. & Novotný, L., 1981: Geologická stavba a uránové zrudnenie pri Novoveskej Hute. *Bratislava, IV. slovenská geologická konferencia, 2, 228–240.*

Rojkovič, I. & Novotný, L., 1993: Uranium mineralization in the Tatricum and Veporicum. *Miner. Slov., 25, 341–348.*

Rojkovič, I. & Vozár, J., 1972: Contribution to the relationship of the Permian volcanism in the Nortern gemerides and Choč u nit. *Geol. Zbor. Geol. carpath. 23, 7, 87–98.*

Rojkovič, I., 1997: Uranium Mineralization in Slovakia. *Bratislava, Univ. Komen., 117 p.*

Rojkovič, I., 1998: Stratiformná U-Cu mineralizácia v perme Nízkych Tatier. *Miner. Slov., 30, 66–71.*

Rojkovič, I., Šucha, V., Uher, P. & Franců J., 1989: Mineralogicko-geochemická charakteristika uránovej mineralizácie v perme gemerika. *Manuscript. Bratislava, archive Geol. Inst. Slov. Acad. Sci., 250 p.*

Schidlowski, M., 1966: Beiträge zur Kenntnis der radioaktiven Bestandteile der Witwatersrand-Konglomerate. II. Brannerit und "Uranpecherzgeister". *Neu. Jb. Mineral., Abh., 1105, 310–324.*

Schwartz, G. M., 1958: Alteration of biotite under mesothermal conditions. *Econ. Geol., 53, 164–177.*

Slavkay, M., Beňka, J., Bezák, V., Gargulák, M., Hraško, Ľ., Kováčik, M., Petro, M., Vozárová, A., Hrušković, S., Knésl, J., Knéslová, A., Kusein, M., Maťová, V. & Tulis, J., 2004: Ložiská nerastných surovín Slovenského rudohoria. *Bratislava, Št. Geol. Úst. D. Štúra, 286 s.*

Smith JR., D. K., 1984: Uranium mineralogy. *In: deViv, B., Ippolito, F., Capaldi, G. & Simpson, P. R. (eds.): Uranium Geochemistry, Mineralogy, Geology, Exploration and Resources. London, The Inst. Mining Metallurgy, London, 43–88.*

Spišiak, J. & Siman, P., 2014: Geochemistry of the granite porphyry from Ľubietová crystalline complexes (Western Carpathians). *Zbor. Konf. CEMC 2014 (Skalský Dvůr), 132–133.*

Števko, M., 2014: Mineralogická charakteristika supergénnych arzeničnanov medi z lokalít Novoveská Huta, Poniky a Špania Dolina. *Dizertačná práca. Manuscript. Bratislava, archive St. Geol. Inst. D. Štúr, 134 p.*

Süsse, P., 1967: Verfeinerung der kristallstruktur des malachits, $Cu_2(OH)_2CO_3$. *Acta Crystallogr., 22, 146–151.*

Tripathi, V. S., 1983: Uranium (VI) transport modeling: geochemical data and sub-models. *PhD thesis. Stanford (California), Stanford Univ., 297 p.*

Václav, J. & Vozárová, A., 1978: Characteristic of the Northern Gemeric Permian in the Košická Belá area. *Západ. Karpaty., Sér. Mineral. Petrogr. Geochém. Metalogen., 5, 83–108.*

Vinogradov, A. P., 1963: Osnovnie čerty geochimii urana. *Moskva, Akad. nauk SSSR, 351 p.*

Vozárová, A., 1979: Litofaciálna charakteristika permu v severozápadnej časti veporika. *Západ. Karpaty, Sér. Mineral. Petrogr. Geochém. Metalogen., 8, 143–199.*

Vozárová, A., Rodionov, N., Vozár, J., Lepekhina, E. & Šarinová, K., 2016: In n situ U-Pb (SHRIMP) zircon age dating from the Permian volcanites of the Northern Veporicum. *J. Geosci., 61, 221–237.*

Yavuz, F., Kumral, M., Karakaya, N., Karakaya, M. Ç. & Yildirim, D. K., 2015: A Windows program for chlorite calculation and classification. *Comput. Geosci., 81, 101–113.*

Zoubek, V., 1936. Poznámky o krystaliniku Západních Karpat. *Věst. St. geol. Úst. Čs. Republ., 12, 207–239.*

Zoubek, V., 1958: Postkinematické granitoidy tatro-veporského intruzívneho komplexu. *Manuscript. Bratislava, archive St. Geol. Inst. D. Štúr.*

Tab. 1

Chemical composition of brannerite and U-Ti oxides from Lopejské Čelno

	Bn	Bn	Bn	Bn	Bn	U-Ti	U-Ti	U-Ti	U-Ti	U-Ti
UO_2	48.64	47.43	46.14	45.41	43.79	41.95	20.48	15.89	16.80	22.45
ThO_2	0.12	0.19	0.22	0.17	0.22	0.17	0.47	0.30	0.48	0.31
Na_2O	0.03	0.04	0.02	0.01	0.05	0.03	0.00	0.02	0.12	0.01
K_2O	0.08	0.45	0.35	0.34	0.62	0.13	0.42	0.59	0.49	0.34
MgO	0.00	0.02	0.07	0.12	0.20	0.00	0.16	0.25	0.18	0.04
CaO	2.68	2.37	2.23	2.44	1.84	1.71	1.19	0.53	0.74	0.52
SrO	0.14	0.00	0.05	0.03	0.08	0.09	0.00	0.03	0.00	0.00
MnO	0.20	0.06	0.08	0.06	0.16	0.10	0.04	0.12	0.03	0.00
FeO	2.64	2.41	2.25	2.55	1.56	1.56	3.87	2.42	2.09	1.68
PbO	0.37	0.35	0.26	0.65	0.25	0.88	4.61	4.24	4.55	4.13
Al_2O_3	0.22	0.61	0.79	1.35	1.80	0.30	3.52	3.41	3.11	2.34
V_2O_3	0.17	0.00	0.00	0.19	0.00	0.26	0.26	0.00	0.00	0.00
Y_2O_3	0.67	0.41	0.41	0.41	0.34	0.51	0.09	0.15	0.12	0.06
Ce_2O_3	0.13	0.09	0.06	0.07	0.00	0.15	0.18	0.24	0.21	0.15
Nd_2O_3	0.22	0.14	0.15	0.10	0.20	0.14	0.14	0.11	0.10	0.15
Sm_2O_3	0.39	0.00	0.00	0.15	0.00	0.20	0.01	0.00	0.00	0.00
Eu_2O_3	0.14	0.00	0.00	0.05	0.00	0.13	0.04	0.00	0.00	0.00
Gd_2O_3	0.29	0.31	0.13	0.24	0.33	0.25	0.17	0.08	0.10	0.08
Tb_2O_3	0.15	0.00	0.00	0.19	0.00	0.25	0.12	0.00	0.00	0.00
Dy_2O_3	0.23	0.00	0.00	0.08	0.00	0.16	0.09	0.02	0.03	0.00
Ho_2O_3	0.00	0.00	0.00	0.05	0.00	0.13	0.14	0.00	0.00	0.00
Yb_2O_3	0.25	0.00	0.00	0.14	0.00	0.06	0.02	0.00	0.00	0.00
SiO_2	1.67	2.69	3.62	2.85	5.82	3.23	6.17	7.80	5.12	3.29
TiO_2	37.37	34.95	32.80	37.76	31.60	43.14	46.19	44.18	48.92	42.42
ZrO_2	0.34	0.32	0.34	0.43	0.43	0.42	0.93	0.60	0.62	0.48
P_2O_5	0.04	0.15	0.05	0.26	0.01	0.06	4.61	4.85	5.92	5.24
As_2O_5	0.00	0.78	0.70	0.00	0.57	0.00	0.00	0.00	0.00	0.19
Nb_2O_5	0.12	0.00	0.00	0.13	0.00	0.34	0.16	0.00	0.00	0.00
Total	97.28	93.77	90.70	96.21	89.87	96.34	94.04	85.83	89.69	83.86
Brannerite and U-Ti oxides [apfu] – based on 3 cations										
U	0.68	0.68	0.68	0.61	0.62	0.55	0.22	0.18	0.19	0.29
Th	0.00	0.00	0.00	0.00	0.00	0.00	0.01	0.00	0.01	0.00
Na	0.00	0.01	0.00	0.00	0.01	0.00	0.00	0.00	0.01	0.00
K	0.01	0.04	0.03	0.03	0.05	0.01	0.03	0.04	0.03	0.03
Mg	0.00	0.00	0.01	0.01	0.02	0.00	0.01	0.02	0.01	0.00

Tab. 1 – continuation

	Bn	Bn	Bn	Bn	Bn	U-Ti	U-Ti	U-Ti	U-Ti	U-Ti
Ca	0.18	0.16	0.16	0.16	0.13	0.11	0.06	0.03	0.04	0.03
Sr	0.00	0.00	0.00	0.00	0.00	0.00	0.00	0.00	0.00	0.00
Mn	0.01	0.00	0.00	0.00	0.01	0.00	0.00	0.01	0.00	0.00
Fe	0.14	0.13	0.12	0.13	0.08	0.08	0.16	0.10	0.09	0.08
Pb	0.01	0.01	0.00	0.01	0.00	0.01	0.06	0.06	0.06	0.06
Al	0.02	0.05	0.06	0.10	0.14	0.02	0.20	0.21	0.18	0.16
V	0.01	0.00	0.00	0.01	0.00	0.01	0.01	0.00	0.00	0.00
Y	0.02	0.01	0.01	0.01	0.01	0.02	0.00	0.00	0.00	0.00
Ce	0.00	0.00	0.00	0.00	0.00	0.00	0.00	0.00	0.00	0.00
Nd	0.00	0.00	0.00	0.00	0.00	0.00	0.00	0.00	0.00	0.00
Sm	0.01	0.00	0.00	0.00	0.00	0.00	0.00	0.00	0.00	0.00
Eu	0.00	0.00	0.00	0.00	0.00	0.00	0.00	0.00	0.00	0.00
Gd	0.01	0.01	0.00	0.00	0.01	0.00	0.00	0.00	0.00	0.00
Tb	0.00	0.00	0.00	0.00	0.00	0.00	0.00	0.00	0.00	0.00
Dy	0.00	0.00	0.00	0.00	0.00	0.00	0.00	0.00	0.00	0.00
Ho	0.00	0.00	0.00	0.00	0.00	0.00	0.00	0.00	0.00	0.00
Yb	0.00	0.00	0.00	0.00	0.00	0.00	0.00	0.00	0.00	0.00
Si	0.10	0.17	0.24	0.17	0.37	0.19	0.30	0.40	0.26	0.19
Ti	1.76	1.69	1.63	1.71	1.51	1.93	1.70	1.71	1.84	1.86
Zr	0.01	0.01	0.01	0.01	0.01	0.01	0.02	0.02	0.02	0.01
P	0.00	0.01	0.00	0.01	0.00	0.00	0.19	0.21	0.25	0.26
As	0.00	0.03	0.02	0.00	0.02	0.00	0.00	0.00	0.00	0.01
Nb	0.00	0.00	0.00	0.00	0.00	0.01	0.00	0.00	0.00	0.00
	0.89	0.89	0.88	0.81	0.84	0.69	0.33	0.28	0.29	0.36
	0.06	0.03	0.02	0.03	0.02	0.05	0.02	0.01	0.01	0.01
	0.01	0.01	0.00	0.01	0.00	0.01	0.06	0.06	0.06	0.06
Σ A site	0.95	0.92	0.91	0.85	0.86	0.75	0.41	0.35	0.36	0.43
	1.88	1.90	1.90	1.91	1.92	2.14	2.22	2.34	2.37	2.33
	0.16	0.18	0.19	0.23	0.22	0.11	0.37	0.31	0.27	0.24
Σ B site	2.05	2.08	2.09	2.15	2.14	2.25	2.59	2.65	2.64	2.57
Σ CAT	3.00	3.00	3.00	3.00	3.00	3.00	3.00	3.00	3.00	3.00
O	5.60	5.61	5.62	5.59	5.60	5.74	5.65	5.72	5.76	5.83
OH^-	0.40	0.39	0.38	0.41	0.40	0.26	0.35	0.28	0.24	0.17
Σ AN	6.00	6.00	6.00	6.00	6.00	6.00	6.00	6.00	6.00	6.00

Tab. 2

Representative WDS microanalyses of metatorbernite from Lopejské Čelno. H_2O* – H_2O content calculated assuming 8 H_2O molecules in ideal metatorbernite formula.

	1	2	3	4	5	6
K_2O	0.19	0.21	0.13	0.18	0.27	0.21
MgO	0.05	0.00	0.05	0.00	0.03	0.11
CaO	0.02	0.02	0.07	0.35	0.31	0.17
BaO	0.00	0.00	0.08	2.42	2.23	1.72
FeO	0.00	0.00	0.10	0.00	0.07	0.05
CuO	7.12	5.82	7.77	5.96	5.89	6.21
Al_2O_3	0.02	0.05	0.04	0.06	0.08	0.50
SiO_2	0.01	0.04	0.03	0.08	0.04	0.69
P_2O_5	13.27	16.72	15.58	15.67	15.93	15.69
As_2O_5	0.00	0.02	0.09	0.12	0.10	0.00
UO_3	57.22	66.01	62.84	62.59	61.70	62.06
H_2O	17.92	18.39	18.22	18.07	18.21	18.41
Total	77.91	88.87	86.76	87.42	86.65	87.42
Total*	95.83	107.26	104.98	105.49	104.86	105.83
Based on 12 O						
K	0.04	0.04	0.02	0.04	0.05	0.04
Mg	0.01	0.00	0.01	0.00	0.01	0.03
Ca	0.00	0.00	0.01	0.06	0.05	0.03
Ba	0.00	0.00	0.00	0.14	0.13	0.10
Fe	0.00	0.00	0.01	0.00	0.01	0.01
Cu	0.92	0.65	0.89	0.68	0.68	0.70
Al	0.00	0.01	0.01	0.01	0.01	0.09
ΣA site	0.99	0.70	0.96	0.93	0.94	0.99
Si	0.00	0.01	0.00	0.01	0.01	0.10
P	1.93	2.08	2.00	2.02	2.05	1.98
As	0.00	0.00	0.01	0.01	0.01	0.00
ΣT site	1.93	2.09	2.01	2.04	2.07	2.08
U	2.06	2.03	2.00	2.00	1.97	1.94
H_2O	8.00	8.00	8.00	8.00	8.00	8.00

Tab. 3

Representative WDS microanalyses of chlorite and muscovite

	Chlorites						**Muscovites**						
SiO_2	27.08	24.71	23.95	23.77	24.31	23.67	50.07	46.06	46.92	46.86	45.12	49.29	46.85
TiO_2	0.05	0.12	0.11	0.03	0.07	0.10	0.10	0.23	0.29	0.37	0.26	0.06	0.30
Al_2O_3	23.93	22.99	22.53	22.12	22.54	22.02	26.11	34.94	32.50	31.56	32.98	26.13	29.95
Cr_2O_3	0.01	0.03	0.05	0.00	0.01	0.02	0.04	0.00	0.00	0.00	0.00	0.00	0.03
FeO	25.63	28.15	29.03	28.09	27.31	27.85	3.14	1.17	2.41	1.97	1.53	3.26	2.62
MnO	0.44	0.67	0.54	0.49	0.43	0.46	0.05	0.06	0.00	0.00	0.05	0.03	0.02
MgO	8.42	9.04	9.61	9.43	9.71	9.59	3.48	0.70	1.34	1.89	1.20	3.47	1.82
CaO	0.02	0.03	0.03	0.03	0.04	0.04	0.00	0.00	0.00	0.02	0.01	0.02	0.05
BaO	0.17	0.13	0.13	0.18	0.05	0.12	0.25	0.29	0.21	0.23	0.36	0.09	0.19
Na_2O	0.03	0.02	0.02	0.03	0.03	0.05	0.06	0.81	0.43	0.35	0.54	0.14	0.34
K_2O	1.12	0.26	0.11	0.06	0.15	0.08	11.43	10.35	10.46	10.86	10.88	11.11	10.34
F	0.00	0.00	0.37	0.00	0.37	0.00							
Cl	0.01	0.00	0.01	0.01	0.01	0.00							
O = F	0.00	0.00	0.16	0.00	0.16	0.00							
O = Cl	0.00	0.00	0.00	0.00	0.00	0.00							
Total	86.90	86.14	86.33	84.23	84.87	84.00	94.74	94.61	94.56	94.12	92.93	93.59	92.51
H_2O	11.28	10.97	10.72	10.69	10.65	10.67							
Total*	98.18	97.11	97.04	94.92	95.52	94.67							
Based on 10 O and 8 OH							Based on 11 O						
Si	2.88	2.70	2.64	2.67	2.69	2.66	3.40	3.09	3.17	3.18	3.11	3.39	3.24
Ti	0.00	0.01	0.01	0.00	0.01	0.01	0.01	0.01	0.01	0.02	0.01	0.00	0.02
Al^{4+}							0.60	0.91	0.83	0.82	0.89	0.61	0.76
Al^{6+}	3.00	2.96	2.92	2.92	2.94	2.92	1.50	1.86	1.75	1.71	1.79	1.50	1.68
Cr	0.00	0.00	0.00	0.00	0.00	0.00	0.00	0.00	0.00	0.00	0.00	0.00	0.00
Fe^{2+}	2.28	2.57	2.67	2.63	2.53	2.62	0.18	0.07	0.14	0.11	0.09	0.19	0.15
Mn	0.04	0.06	0.05	0.05	0.04	0.04	0.00	0.00	0.00	0.00	0.00	0.00	0.00
Mg	1.33	1.47	1.58	1.58	1.60	1.61	0.35	0.07	0.13	0.19	0.12	0.36	0.19
Ca	0.00	0.00	0.00	0.00	0.00	0.00	0.00	0.00	0.00	0.00	0.00	0.00	0.00
Ba	0.01	0.01	0.01	0.01	0.00	0.01	0.01	0.01	0.01	0.01	0.01	0.01	0.01
Na	0.01	0.00	0.01	0.01	0.01	0.01	0.01	0.10	0.06	0.05	0.07	0.02	0.05
K	0.15	0.04	0.02	0.01	0.02	0.01	0.99	0.89	0.90	0.94	0.96	0.97	0.91
F	0.00	0.00	0.13	0.00	0.13	0.00							
Cl	0.00	0.00	0.00	0.00	0.00	0.00							

Stratiformná U-Cu mineralizácia v Lopejskom Čelne pri Podbrezovej (veporikum, Západné Karpaty)

Lokalita sa nachádza približne 1,5 km južne od centra bývalej obce Lopej (dnes kataster obce Podbrezová) v doline Lopejské Čelno. Je vyvinutá v ľubietovskom pásme tektonickej superjednotky veporika (obr. 1, 2), pričom je viazaná na limonitizované alterované arkózové pieskovce s polohami acidných vulkanitov permského veku. Mineralogické pomery na lokalite v minulosti študovali Rojkovič a Novotný (1993). Mineralizáciu opisujú ako U-Cu stratiformnú, kde v zrudnených šošovkách bol opísaný pyrit, rutil, leukoxén, chalkopyrit, goethit a torbernit (Rojkovič a Novotný, 1993). Revíznym štúdiom mineralizácie v Lopejskom Čelne bola identifikovaná primárna mineralizácia.

Primárna U mineralizácia sa v doline Lopejské Čelno vyskytuje len veľmi ojedinele v zrnách s veľkosťou do 120 μm (obr. 3). Z U^{4+} minerálov bol identifikovaný brannerit a U-Ti oxidy (obr. 5, 10; tab. 1) v úzkej priestorovej a genetickej asociácii s rutilom (obr. 4), Ti oxidmi (leukoxénom) a ílovými minerálmi (obr. 9, 11). Mineralizácia s najväčšou pravdepodobnosťou vznikala počas procesu alterácie biotitu spätého s hydrotermálnymi procesmi a adsorpciou uránu na Ti oxidy, pričom za zdroj Ti sa považuje práve biotit. Adsorpcia uránu na Ti oxidy, tzv. *Pronto-reakcia*, prebieha v hydrotermálnych systémoch pri teplote, ktorá koreluje s teplotou generovanou počas alpínskej orogenézy, resp. s jej doznievaním. Všetky spomínané minerálne fázy obsiahnuté v mineralizovaných zrnách sú typickými produktmi alterácie biotitu (Lovering et al., 1949; Schwartz, 1958; Bisdom, 1967; Deer et al., 1992; Finch, 1996; René a Dolníček, 2017). Na okraji mineralizovaných zŕn a v samotnej hornine sú hojne zastúpené chlority a muskovit (tab. 3).

Oxidačnú zónu zastupuje malachit, goethit a U^{6+} minerál metatorbernit (obr. 6, 7, 8). Vznik metatorbernitu (tab. 2) je spätý s deštrukciou primárnych U^{4+} minerálov v kyslých podmienkach a oxidáciou U^{4+} na U^{6+} za vzniku uranylového iónu UO_2^{2+}. Ostatné konštrukčné prvky (Cu, P) boli do metatorbernitov dodávané z minerálov obsiahnutých v hornine a z horninotvorných minerálov (chalkopyrit, apatit; obr. 12). Nezvyčajným javom pri metatorbernite z Lopejského Čelna je jeho luminiscencia, ktorá je pravdepodobne zapríčinená defektmi v kryštálovej štruktúre minerálu alebo vplyvom prímesí nanočastíc iného minerálu (Civetta a Gasparini, 1972; Langmuir, 1978; Plášil et al., 2009).

Doručené / Received: 17. 4. 2023
Prijaté na publikovanie / Accepted: 30. 6. 2023

Mineralia Slovaca, Web ISSN 1338-3523, ISSN 0369-2086, https://doi.org/10.56623/ms.2023.55.1.5
55, 1 (2023), 71 – 84, © Authors 2023. CC BY 4.0

Laboratory technological research of magnesium intermediates preparation from the dolomites raw materials suitable for magnesium metal production

ZUZANA DANKOVÁ[1], ALEXANDRA BEKÉNYIOVÁ[1], KATARÍNA ČECHOVSKÁ[1], ERIKA FEDOROVÁ[1], ZUZANA KOLLOVÁ[1], PAVEL BAČO[1], JARMILA NOVÁKOVÁ[2], TOMÁŠ ZACHER[2], VALÉRIA KANDRÍKOVÁ[2], EMÍLIA FABINYOVÁ[2] and JAROSLAV BRIANČIN[3]

[1]State Geological Institute of Dionýz Štúr, Regional centre Košice, Jesenského 8, Košice, Slovak Republic, zuzana.dankova@geology.sk
[2]State Geological Institute of Dionýz Štúr, Regional centre Spišská Nová Ves, Department of Geoanalytical Laboratories, Markušovská cesta 1, Spišská Nová Ves, Slovak Republic
[3]Institute of Geotechnics, Slovak Academy of Sciences, Watsonova 45, Košice, Slovak Republic

Abstract: Metallic magnesium has been included in the list of Critical Mineral Raw Materials (CRM) for European Union countries since 2010. The territory of the Slovak Republic has large reserves of mineral raw materials – magnesite and dolomite, which are the initial source of metal Mg. For technological research, the following raw materials (based on chemical analyses of samples) were chosen: dolomite ore from the Sedlice deposit (SED-1), Trebejov deposit (TR-1) and dolomite ore from the Kraľovany deposit (KRA-1). The second deposit is also located near the operation of a potential customer of laboratory results for the production of metal magnesium, OFZ a.s. The aim of the laboratory technological research was to determine the experimental conditions for obtaining suitable Mg intermediates for metal magnesium preparation. For this purpose, there were performed DTA/TG and XRD analyses to study its behaviour, total mass loss and amount of carbon dioxide after calcination process. By optimizing the annealing tests of dolomite, products were obtained that met two conditions for its subsequent use in the sillicothermal process, namely the molecular ratio of CaO/MgO, content of impurities and the content of CO_2. The optimization of calcination and repeated annealing pointed at the suitable conditions of dolomite raw sample processing (temperature of 1 050 °C for 2.5 hours, or 1 100 °C for 2 hours).

Key words: dolomite, annealing, calcinated dolomite

Graphical abstract

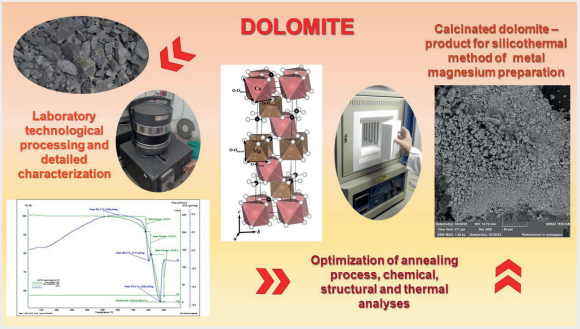

Highlights

- Domestic dolomite raw materials were technologically processed and characterized in detail.
- Calcinated dolomite samples exhibited changes of mineralogical phases, thermal and structural properties.
- Semi products prepared by optimization of annealing process possess the potentiality to be a suitable material for metal magnesium preparation.

1. Introduction

The topic of the availability of some metals or raw materials in the world, and especially in Europe, lasts for a decade. From 2010, when the first analysis of critical metals was prepared, further detailed analyses were elaborated, taking into account the greater need for the raw materials and their availability on world markets, as well as their cost. European countries remain a major importer of a large portion of metals and minerals, which are inevitable for the technologies used and for products necessary for economic growth and development. The European Commission has published the latest version of the study of Critical Raw Materials for EU countries with position of individual metals and raw materials regarding the import risk and economic importance in 2015 (Report of EC, 2015). The share of domestic production, as well as the presence of verified, but also estimated sources of these raw materials in the EU countries, are very small or possibly none. For this reason, the countries of the European Union are dependent on import of such raw materials.

Magnesium is the eighth most abundant element in the Earth's crust and it is also extractable from brine and seawater. The sources and raw materials from which

magnesium could be produced include also camallite, dolomite, serpentine and magnesite (Ramakrishnan & Koltun, 2004). Magnesium has a density two-thirds that of aluminium, one-quarter that of steel and only slightly higher than that of many polymers (Chen et al., 2015). It is also recycled easily compared with polymers, which makes it environmentally friendly (Prado & Cepeda-Jimeréz, 2015). Because of the substantial magnesium resources and the attractive magnesium products, magnesium metal is regarded as a potentially ideal substitute for aluminum metal- but the global annual production of magnesium metal is only 1.8 % that of aluminum metal (Zhang et al., 2022).

Magnesium is produced commercially either by electrolysing the magnesium chloride derived from raw materials, or by using a thermal reduction process, known as the Pidgeon process, using dolomite as the raw material. The process was invented and developed in Canada by Dr L. M. Pidgeon, in the early 1940s (Mehrabi et al., 2012), where a plant for magnesium production based on the ferrosilicon process was built to produce magnesium at the rate of ~4 500 kg per annum (or 10,000 lb per year) (Ramakrishnan & Koltun, 2004). The thermal reduction method is based on the chemical reduction between calcined dolomite (CaO · MgO) and ferrosilicon (Si-Fe) at high temperature (1 100–1 250 °C) and high vacuum (1.33–13.3 Pa) (Zhang et al., 2022).

The territory of the Slovak Republic has large reserves of mineral raw materials – magnesite and dolomite, which are the initial source of metal Mg. The supplies of these raw materials in Slovakia are immense in comparison to other European countries.

The dolomites in Slovakia occur in several Middle and Upper Triassic formations thick up to several 100 meters, or forming intercalations, interbeds, lenses in beds irregularly alternating with surrounding limestones. They are present in numerous geological units, their cover sequences and tectonic nappes. The most significant are the Middle- and Upper-Triassic dolomites of the Hronic unit, bearing the important dolomite deposits in the Choč nappe of the Strážovské vrchy Mts. (Fig. 1).

There are known some experimental works on magnesium metal production from raw magnesite (Tomášek & Špeťuch, 1995; Tomášek et al., 1997). There were even considerations on running its production in the Slovak Magnesite Works in Jelšava (Immer, 1998). The positive results of the production of intermediate products from dolomites and magnesites have been obtained recently. The own laboratory experiment of the production of metallic magnesium by the silicothermal method was carried out at the SGUDS, regional centre Košice. Under experimental conditions, it was possible to prepare separate reduced crystals of metallic magnesium (Bačo et al., 2016). The aim of this work is to prepare suitable intermediates for the Mg production by the calcination process with the molecular ratio of CaO : MgO in the range of 1.1 to 1.5 (close to the composition of the dolomite raw materials), with the maximum impurity content 2.5 % (R_2O_3 + SiO_2) and CO_2 content below 0.3 %, otherwise the magnesium yield drops sharply (Tomášek et al., 1997). From a mixture of CaO + MgO oxides in the above-mentioned ratio using ferrosilicon (FeSi75) and in the presence or absence of a catalyst (CaF2) it is possible to prepare metallic Mg by silicothermal reduction by condensation of its vapours in a vacuum or in an inert atmosphere (due to its reverse oxidation to MgO at normal pressure) (Tuček et al., 2016).

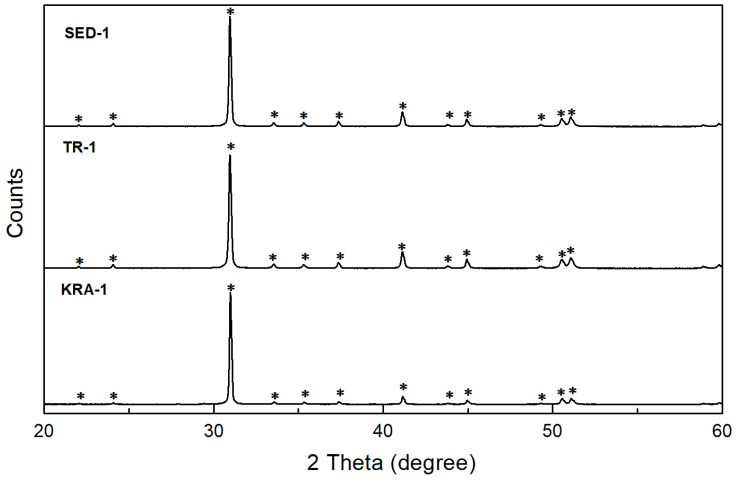

Fig. 1. Significant dolomite deposits in individual geological units of the Western Carpathians. Yellow pentagon and designations in bold in location indicate the deposits with reserves stated in the Balance of Reserves in Reserved Deposits with the state to 1. 1. 2018.

2. Materials and Methods

2.1. Raw materials

For experimental purposes, dolomite ores from the Sedlice (SED-1), Trebejov (TR-1) and Kraľovany (KRA-1) deposites were chosen as raw materials. Bulk samples of dolomites were freely air-dried and subjected to preparatory work – crushing in three stages in jaw crushers and sorting on sieves of different sizes: + 8.0; 4.0 – 8.0; 2.0 – 4.0; 1.0 – 2.0; –1.0 mm; whereas all samples, or the grain fractions prepared from them were subsequently homogenized and quartered. From each raw sample after these works and from the grain size classes, individual homogeneous parts were prepared for further laboratory processing, including their grain size characteristics.

2.2. X-ray diffraction analyses

Qualitative mineralogical analysis of input samples was carried out by the X-ray diffraction (XRD) method on the BRUKER D2 Phaser device: CuKα radiation, monochromatic Ni filter, accelerating voltage of the X-ray radiation generator 30 kV, current intensity 10 mA, range of detected angles 5 – 70° 2theta, step 0.01°, time 0.3 sec/step. Processing and evaluation of measured data were realized using the software DIFFRAC.EVA V3.1. Measurement, equipped with the PDF-2/2013 database.

2.3. Differential thermal analyses/Thermogravimetric analyses (DTA/TG)

NETZSCH STA 449 F3 Jupiter derivatograph (NETZSCH Gerätebau Gmbh., Selb, Germany) equipped with a Std SiC furnace and an Autovac MF Cs rotary pump was used for thermal DTA/TG analysis. Measurements were made under the following conditions: heating range: 24 – 1 000 °C, heating rate 10 °C · min^{-1}, reference material: powdered Al_2O_3, crucibles: ceramic Al_2O_3, furnace atmosphere: N_2, N_2 circulation: 20 ml . min^{-1}.

2.4. Annealing tests

Annealing tests of dolomite fractions were carried out in an electric laboratory furnace ELOP-1200/15 at temperatures of 1 000 °C and 1 050 °C with a holding time of 0.5; 1; 2 and 2.5 hours.

Input samples of raw materials and processed intermediates/products were subjected to chemical analysis using the Röntgen-fluorescence energodispersion spectrometer (XRF) X-LAB 2000, Spectro in the Geoanalytical laboratories of the SGUDS in Spišská Nová Ves.

3. Results

3.1. Mineralogical and thermic analyses of raw dolomites

Dolomite raw materials were characterized by high purity, in the case of the SED-1 sample, the presence of the monomineral phase of dolomite was confirmed. In addition to a high proportion of dolomite, sample TR-1 also contained an accessory proportion of quartz and sample KRA-1 accessory proportion of calcite (Fig. 2).

Dolomite is a mineral with a calcite superstructure, formed by both magnesite and calcite molecules, $CaMg(CO_3)_2$. During thermal decomposition, $MgCO_3$ molecules are less stable and release CO_2 earlier than the $CaCO_3$ compound.

The mineralogical analysis of the SED-1 dolomite sample pointed to the high purity of the raw material, without the detection of any impurities. Two significant endothermic decreases can be observed from the DTA curve, where at a temperature of 793 °C, CO_2 is released from $MgCO_3$ dolomite molecules and the corresponding weight loss represents 20.04 % of the sample weight. At a higher temperature, 852 °C, CO_2 is released from $CaCO_3$ molecules and this decomposition corresponds to a mass loss of 25.78 %. The total weight loss in the temperature range of 700 – 900 °C is 45.82 % and corresponds to the decomposition of dolomite (Fig. 3).

The composition of dolomite sample TR-1 is also characterized by high purity, with minimal participation of quartz admixture. DTA analysis of the sample has a characteristic curve for dolomite with two significant

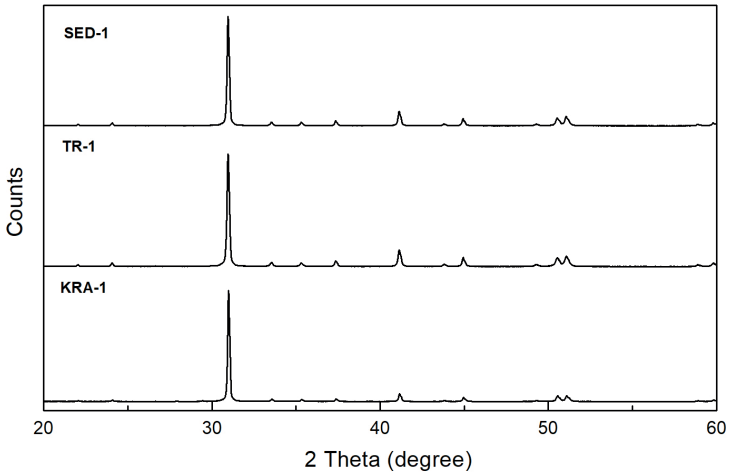

Fig. 2. XRD analyses of raw samples SED-1, TR-1 and KRA-1 (* – dolomite).

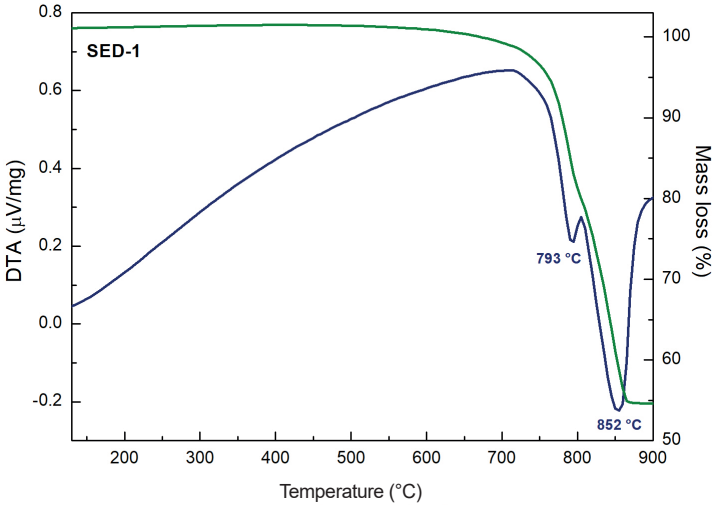

Fig. 3. DTA/TG analysis of raw sample SED-1.

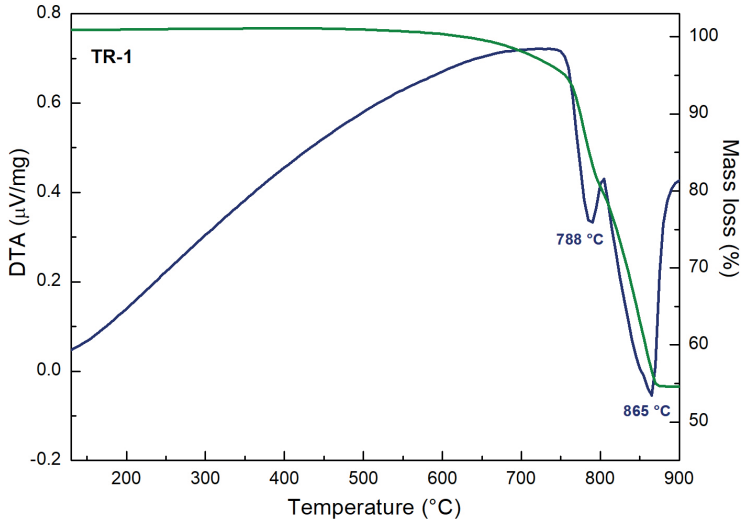

Fig. 4. DTA/TG analysis of raw sample TR-1.

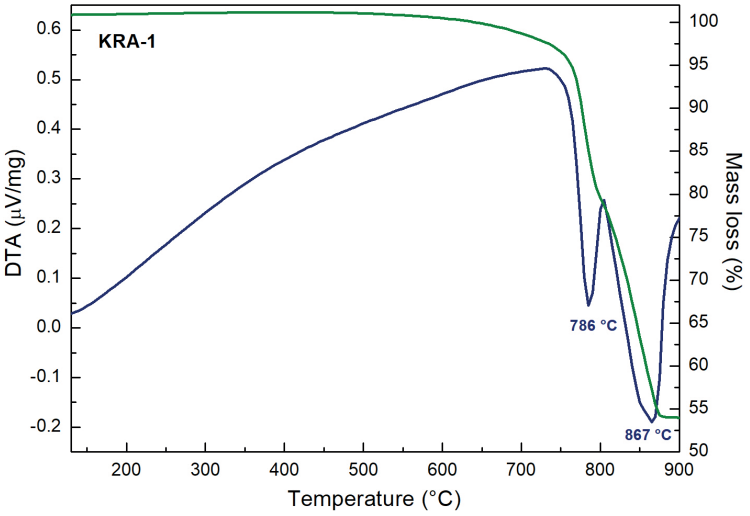

Fig. 5. DTA/TG analysis of raw sample KRA-1.

endothermic reactions at temperatures of 788 °C and 865 °C. The total weight loss represents 45.85 %, while the release of CO_2 from the decomposition of $MgCO_3$ of dolomite molecules corresponds to 20.11%, the CO_2 coming from the decomposition of $CaCO_3$ is 25.74 % of the sample weight (Fig. 4).

For the sample KRA-1 two endothermic decreases were observed at temperatures of 786 °C and 867 °C corresponding to weight loss of 20.32 % and 25.91 %, respectively (Fig. 5).

3.2. Chemical analyses

The separated and homogenized fractions of dolomite raw materials were subjected to chemical analysis for further laboratory processing. The results of chemical analyses of separated grain size classes are shown in Tab. 1.

3.2. Results of annealing tests of dolomite raw materials

Separated grain size fractions of the tested dolomite ores were evaluated after annealing tests in terms of annealing loss (Tab. 2).

From the Tab. 2 it can be observed that for the SED-1 sample, the required thermal decomposition (above 98 %) occurs in the coarse-grained fraction (4 – 8 mm) at both temperatures, regardless of the annealing time. On the contrary, the fraction below 1 mm is the most stable and the required dolomite decomposition occurs after annealing at 1 050 °C for more than 2 hours. For this sample, annealing of grain fractions above 1 mm was effective at the temperature of 1 050 °C with a holding time of minimal 0.5 hours.

For sample TR-1, only annealing of fractions over 2 mm at the temperature of 1 050 °C with a duration of over 2 hours was effective. On the contrary, the sample KRA-1 reached required decomposition for all studied grain fractions at both temperatures.

After initial annealing tests, optimization of the process was carried out. Individual fractions of all samples were combined and annealed at temperatures of 1 050 °C for 2.5 hours and 1 100 °C for 1 hour. The products after annealing and chemical analysis were evaluated with regard to the required conditions for calcined dolomite. The preparation of the product from the dolomite raw material into the mixture for the batch for the silicothermal production of Mg consists in the preparation of calcined dolomite (CaO . MgO) so that the molecular ratio of CaO : MgO is in the range of 1.1 to 1.5 : 1, the content of impurities together with SiO_2 is below 2.5 % and a maximum CO_2 content of 0.3 % (Blahút et al., 1994).

Products from input ore samples SED-1, TR-1 and KRA-1, annealed at both selected temperatures, met two of the three conditions, namely the molecular ratio of CaO: MgO and the content of impurities below 2.5 %. The SED-1 sample after the optimized annealing process showed a CO_2 content of 0.37 % (for t = 1 050 °C) and 0.44 % (for t = 1 100 °C), the TR-1 sample had contents of 0.33 % and 0.51 %, and KRA-1 0.40 and 0.44 %, respectively (Tab. 3).

The samples after calcination (1 050 °C/2.5 hours) were characterized by the X-ray diffraction and DTA/TG analyses with the aim to describe the structural changes

Tab. 1

Basic chemical composition of particular grain fractions of dolomite ore samples SED-1. TR-1 and KRA-1

Sample	Fraction [mm]	Mass yield [%]	SiO_2	Al_2O_3	Fe_2O_3	CaO	MgO	TiO_2	MnO	K_2O Na_2O [%]	P_2O_5	Chemical composition S_{tot}, SO_3 FeO	CO_2	A. l.	Hg	Sb	Cr	Ni As [mg/kg]		Pb	Cd	Sr
SED-1	input	100	1.07	0.16	0.20	30.3	20.9	< 0.01	0.01	< 0.05	< 0.2	< 0.01	< 0.02	< 0.05	0.14	46.7	47.3	0.10	< 2	< 5	< 4	< 1	< 5	< 1	79
	4–8	57.77	0.44	0.16	0.12	30.4	21.3	< 0.01	< 0.01	< 0.05	< 0.2	< 0.01	0.04	0.10	0.11	42.8	47.3	< 0.01	< 2	< 5	< 4	< 1	< 5	< 1	71
	2–4	25.31	0.28	0.15	0.11	30.4	21.3	< 0.01	< 0.01	< 0.05	< 0.2	< 0.01	0.02	0.05	0.10	41.4	47.5	< 0.01	< 2	< 5	< 4	< 1	< 5	< 1	73
	1–2	7.02	0.38	0.16	0.10	30.3	21.3	< 0.01	< 0.01	< 0.05	< 0.2	< 0.01	0.03	0.08	0.09	42.8	47.6	< 0.01	< 2	< 5	< 4	< 1	< 5	< 1	72
	–1	9.90	0.44	0.19	0.26	30.4	21.2	< 0.01	0.01	< 0.05	< 0.2	< 0.01	0.03	0.08	0.22	41.4	47.3	0.03	< 2	< 5	22	3	11	< 1	72
TR-1	input	100	1.02	0.42	0.24	30.4	21	0.02	< 0.01	0.05	< 0.2	0.01	0.02	0.05	0.22	46.8	46.8	< 0.01	< 2	< 5	5	< 1	< 5	< 1	72
	4–8	55.4	1.37	0.45	0.28	30	20.8	0.02	0.01	0.16	< 0.2	0.01	0.07	0.18	0.25	42.1	46.7	< 0.01	< 2	< 5	< 4	< 1	< 5	< 1	68
	2–4	24.4	1.06	0.40	0.25	30.1	21	0.02	0.01	0.13	< 0.2	0.01	0.03	0.08	0.22	42.5	46.9	< 0.01	< 2	< 5	< 4	2	< 5	< 1	68
	1–2	8.13	0.92	0.41	0.23	30	21	0.02	0.01	0.15	< 0.2	0.01	0.04	0.10	0.21	41	47.2	< 0.01	< 2	< 5	< 4	< 1	< 5	< 1	67
	–1	12.1	1.25	0.45	0.27	29.9	20.9	0.02	0.01	0.11	< 0.2	0.01	0.05	0.13	0.24	41	46.8	0.01	< 2	5	21	< 1	< 5	< 1	67
KRA-1	input	100	0.12	< 0.05	< 0.05	30.6	21.4	< 0.01	< 0.01	< 0.05	< 0.2	< 0.01	< 0.02	< 0.05	< 0.05	46.6	47.7	< 0.01	< 2	< 5	< 4	1	< 5	< 1	46
	4–8	51	< 0.05	< 0.05	< 0.05	30.4	21.4	< 0.01	< 0.01	< 0.05	< 0.2	< 0.01	0.13	0.33	< 0.05	43.2	47.7	< 0.01	< 2	< 5	< 4	< 1	< 5	< 1	46
	2–4	30.4	< 0.05	0.08	0.07	30.5	21.3	< 0.01	< 0.01	< 0.05	< 0.2	< 0.01	0.04	0.10	0.06	43.2	47.8	< 0.01	< 2	< 5	< 4	< 1	< 5	< 1	47
	1–2	8.36	< 0.05	< 0.05	< 0.05	30.7	21.4	< 0.01	< 0.01	< 0.05	< 0.2	< 0.01	< 0.02	< 0.05	< 0.05	42.1	47.8	< 0.01	< 2	< 5	< 4	< 1	< 5	< 1	47
	–1	10.3	0.07	< 0.05	< 0.05	31.3	21	< 0.01	< 0.01	< 0.05	< 0.2	< 0.01	0.02	0.05	< 0.05	43.2	47.5	< 0.01	v 2	< 5	9	< 1	< 5	< 1	45

A. l. – annealing loss

Tab. 2

Annealing loss depending on grain fractions. temperature and heating period for dolomite samples SED-1. TR-1 and KRA-1

Sample	**SED-1** (Sedlice)							
Temperature	1 000 °C					1 050 °C		
Time	0.5 h	1.0 h	2.0 h	2.5 h	0.5 h	1.0 h	2.0 h	2.5 h
Fraction [mm]	Annealing loss [%]							
4–8	46.85	46.89	47.15	46.90	47.16	47.09	47.24	47.10
2–4	46.72	46.92	47.08	46.79	46.91	46.97	47.20	47.10
1–2	46.70	46.75	46.99	46.92	46.96	46.96	47.10	47.01
Below 1	46.30	46.34	46.69	46.46	46.66	46.73	46.89	46.84
	Theoretical dolomite decomposition to loss by annealing [%]							
4–8	**98.16**	**98.24**	**98.78**	**98.26**	**98.81**	**98.66**	**98.97**	**98.68**
2–4	97.88	**98.30**	**98.64**	**98.03**	**98.28**	**98.41**	**98.89**	**98.68**
1–2	97.84	97.95	**98.45**	**98.30**	**98.39**	**98.39**	**98.68**	**98.49**
Below 1	97.00	97.09	97.82	97.34	97.76	97.90	**98.24**	**98.14**
Sample	**TR-1** (Trebejov)							
Temperature	1 000 °C					1 050 °C		
Time	0.5 h	1.0 h	2.0 h	2.5 h	0.5 h	1.0 h	2.0 h	2.5 h
Fraction [mm]	Annealing loss [%]							
4–8	46.31	46.32	46.71	46.66	46.48	46.56	46.79	46.91
2–4	46.24	46.38	46.55	46.67	46.47	46.47	46.73	46.88
1–2	46.10	46.19	46.32	46.44	46.27	46.40	46.69	46.73
Below 1	45.75	45.80	46.07	46.17	45.87	46.09	46.55	46.59
	Theoretical dolomite decomposition to loss by annealing [%]							
4–8	97.02	97.05	97.86	97.76	97.38	97.55	**98.03**	**98.28**
2–4	96.88	97.17	97.53	97.78	97.36	97.36	97.90	**98.22**
1–2	96.58	96.77	97.05	97.30	96.94	97.21	97.82	97.90
Below 1	95.85	95.96	96.52	96.73	96.10	96.56	97.53	97.61
Sample	**KRA-1** (Kraľovany)							
Temperature		1 000 °C				1 050 °C		
Time	0.5 h	1.0 h	2.0 h	2.5 h	0.5 h	1.0 h	2.0 h	2.5 h
Fraction [mm]	Annealing loss [%]							
4–8	47.36	47.35	47.38	47.33	47.36	47.47	47.47	47.40
2–4	47.29	47.30	47.30	47.26	47.30	47.41	47.37	47.34
1–2	47.19	47.30	47.31	47.22	47.28	47.33	47.37	47.29
Below 1	46.94	47.08	47.04	47.00	47.01	47.21	47.16	47.11
	Theoretical dolomite decomposition to loss by annealing [%]							
4–8	**99.22**	**99.20**	**99.27**	**99.16**	**99.22**	**99.46**	**99.46**	**99.31**
2–4	**99.08**	**99.10**	**99.10**	**99.02**	**99.10**	**99.33**	**99.25**	**99.18**
1–2	**98.87**	**99.10**	**99.12**	**98.93**	**99.06**	**99.16**	**99.25**	**99.08**
Below 1	**98.34**	**98.64**	**98.55**	**98.47**	**98.49**	**98.91**	**98.81**	**98.70**

Tab. 3

Products of calcination of crushed dolomite SED-1, TR-1 and KRA-1 below 8 mm

Sample Conditions of calcination	**SED-1** (Sedlice)												
	Chemical composition [%]												
	CaO	MgO	SiO_2	TiO_2	Al_2O_3	Fe_2O_3	MnO	Na_2O	K_2O	P_2O_5	CO_2	CaO : MgO	Σ $R2O_3$
1 050 °C; 2.5 hrs	30,60	21,70	0,24	<0.01	0,15	0,10	< 0.01	< 0.2	< 0.05	< 0.01	**0,37**	**1,41**	**0,86**
Conditions of	Chemical composition [%]												
calcination	CaO	MgO	SiO_2	TiO_2	Al_2O_3	Fe_2O_3	MnO	Na_2O	K_2O	P_2O_5	CO_2	CaO : MgO	Σ $R2O_3$
1 100 °C; 1 hr	30,60	21,70	0,21	< 0.01	0,14	0,07	< 0.01	< 0.2	< 0.05	< 0.01	**0,44**	**1,41**	**0,86**
Sample	**TR-1** (Trebejov)												
Conditions of	Chemical composition [%]												
calcination	CaO	MgO	SiO_2	TiO_2	Al_2O_3	Fe_2O_3	MnO	Na_2O	K_2O	P_2O_5	CO_2	CaO : MgO	Σ $R2O_3$
1 050 °C; 2.5 hrs	30,10	21,30	1,02	0,02	0,47	0,21	< 0.01	< 0.2	< 0.05	0,01	**0,33**	**1,41**	**2,06**
Conditions of	Chemical composition [%]												
calcination	CaO	MgO	SiO_2	TiO_2	Al_2O_3	Fe_2O_3	MnO	Na_2O	K_2O	P_2O_5	CO_2	CaO : MgO	Σ $R2O_3$
1 100 °C; 1 hr	30,10	21,30	0,88	0,02	0,41	0,23	< 0.01	< 0.2	< 0.05	0,01	**0,51**	**1,41**	**2,06**
Sample	KRA-1 (Kraľovany)												
Conditions of	Chemical composition [%]												
calcination	CaO	MgO	SiO_2	TiO_2	Al_2O_3	Fe_2O_3	MnO	Na_2O	K_2O	P_2O_5	CO_2	CaO : MgO	Σ $R2O_3$
1 050 °C; 2.5 hrs	30,70	21,60	< 0.05	< 0.01	< 0.05	< 0.05	< 0.01	< 0.2	< 0.05	0,01	**0,44**	**1,42**	**0,45**
Conditions of	Chemical composition [%]												
calcination	CaO	MgO	SiO_2	TiO_2	Al_2O_3	Fe_2O_3	MnO	Na_2O	K_2O	P_2O_5	CO_2	CaO : MgO	Σ $R2O_3$
1 100 °C; 1 hr	30,80	21,70	< 0.05	< 0.01	< 0.05	< 0.05	< 0.01	< 0.2	< 0.05	< 0.01	**0,40**	**1,42**	**0,40**

and changes of their thermal properties. The dolomite sample SED-1 after calcination showed two endothermic peaks on the DTA curve. Smaller one at a temperature of about 453 °C and more expressive at a temperature of 819 °C. The total weight loss for the SED-1 sample was 30 % (Fig. 6). A small endothermic peak at a temperature of 452 °C, probably corresponding to brucite $MgOH_2$ (thermal reaction of brucite appear at 350 – 450 °C), and a more expressive one at a temperature of 821 °C, corresponding to calcite, were also observed for the TR-1 sample. The total weight loss was about 28 % (Fig. 7). For the sample KRA-1 the first endothermic peak was appeared at about temperature 374 °C and the second one at 835 °C (Fig. 8). The total weight loss was 33 %. Difference between the theoretical weight loss and the mas loss on TG curve is not significant, is up to 1,5 % which can by caused by measurement or instrument deviation. The weight losses for samples TR-1, SED-1 and KRA-1 remained approximately constant.

Further experiments are planned to investigate differences in the calcination behaviour of dolomite samples, and in industrial use must be taken into account to ensure complete calcination according to selected temperatures.

The major mineralogical phases in all calcinated samples were calcite and periclase (Figs. 9 – 11). For samples SED-1 and TR-1, expressive content of vaterite and minor content of portlandite were also observed. In the samples SED-1 and KRA-1 the accessory proportion of aragonite was detected, too.

The presence of portlandite in the annealed samples is not desirable and is probably related to the analyzed higher content of CO_2.

The samples after annealing showed a typical calcite structure. The surface of the calcinated samples was rougher compared to the raw samples, with significant smaller agglomerated calcite particles (Fig. 12).

The reason of higher CO_2 contents in the prepared products could be caused by the manipulation of the samples. The reaction of calcinated samples with airy CO_2 is very fast and it can occur also during the preparation of samples for chemical analyses. The chemical analyses were crucial for further optimization of dolomite processing. They are also time-consuming to process. In addition, the analyses can be performed only in the other workplace than raw material processing were realized. From this reason the DTA/TG and XRD analyses presented above were made on samples that had been freely standing for a certain time since calcination. On the basis of all obtained results, the control annealing and characterization were performed using only the DTA/TG and XRD analyses.

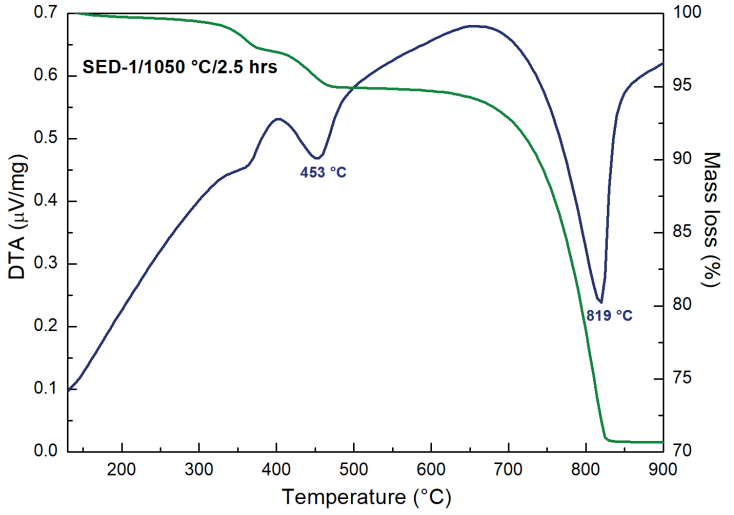

Fig. 6. DTA/TG analysis of calcinated sample SED-1; 1 050 °C/2.5 hours.

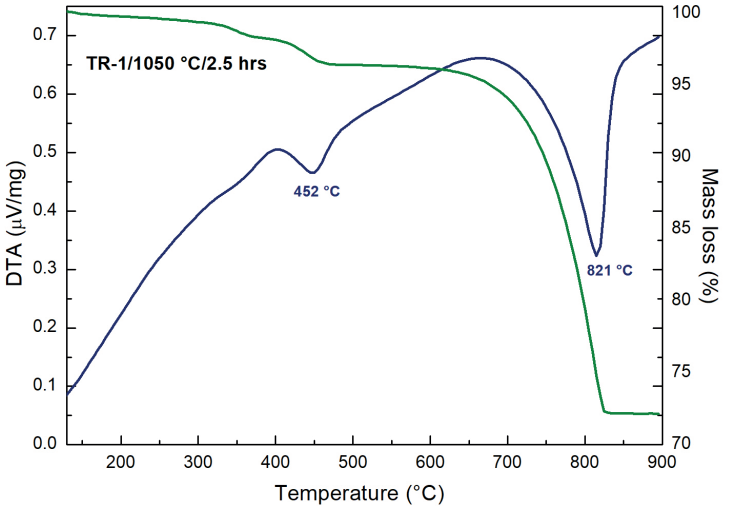

Fig. 7. DTA/TG analysis of calcinated sample TR-1; 1 050 °C/2.5 hours.

In order to exclude errors during the annealing process the raw dolomite samples were first annealed at higher temperature 1 100 °C for 2 hours. The thermogravimetric analyses were performed immediately. Almost non weight loss was observed for all studied samples, what pointed at the required decomposition of $CaCO_3$ (Figs. 13 – 15).

Also a control annealing of the KRA-1 sample at 1 050 °C for 2.5 hours was repeated. The sample was immediately characterized by X-ray diffraction measurement. The analysis showed total dolomite decomposition to required CaO and MgO compounds (Fig. 16).

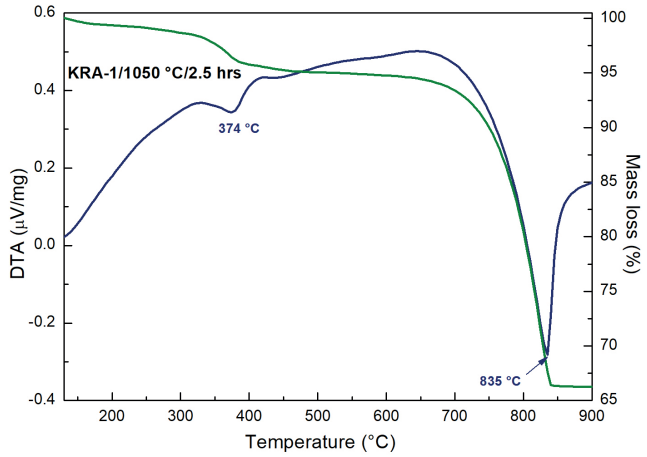

Fig. 8. DTA/TG analysis of calcinated sample KRA-1; 1 050 °C/2.5 hours.

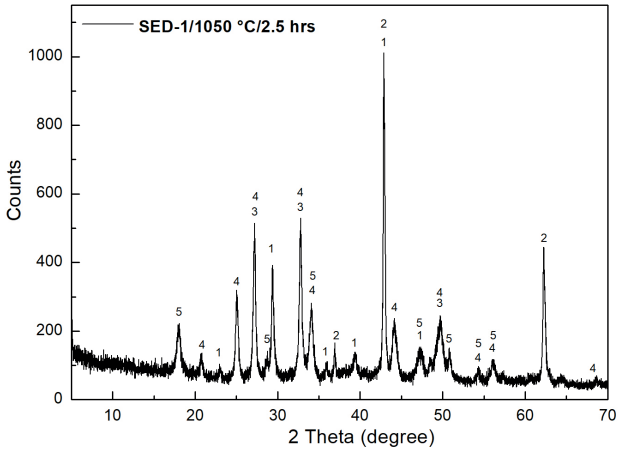

Fig. 9. XRD analysis of calcinated sample SED-1 (1 050 °C/2.5 hrs); 1 – calcite, 2 – periclase, 3 – aragonite, 4 – vaterite, 5 – portlandite.

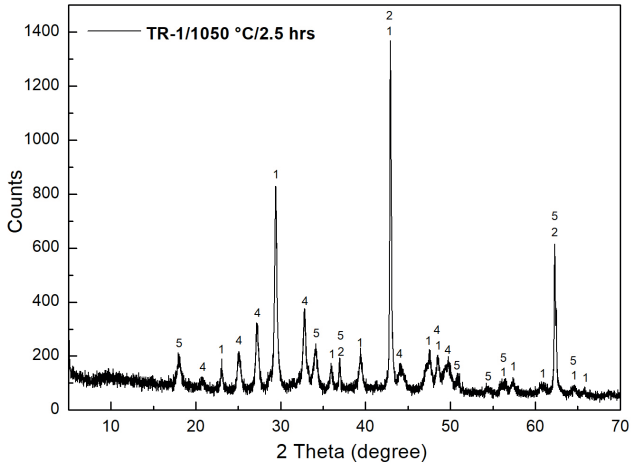

Fig. 10. XRD analysis of calcinated sample TR-1 (1 050 °C/2.5 hrs); 1 – calcite, 2 – periclase, 4 – vaterite, 5 – portlandite.

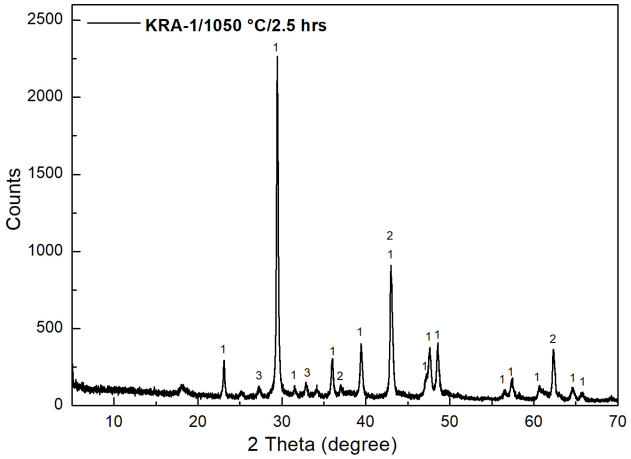

Fig. 11. XRD analysis of calcinated sample KRA-1 (1 050 °C/2.5 hrs); 1 – calcite, 2 – periclase, 3 – aragonite.

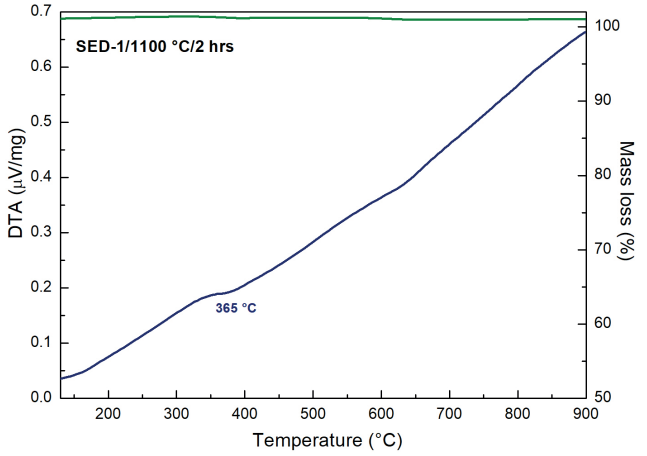

Fig. 13. DTA/TG analysis of calcinated sample SED-1; 1 100 °C/2 hours.

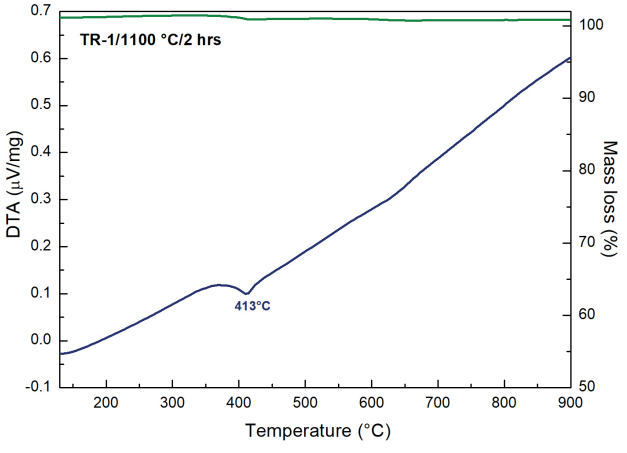

Fig. 14. DTA/TG analysis of calcinated sample TR-1; 1 100 °C/2 hours.

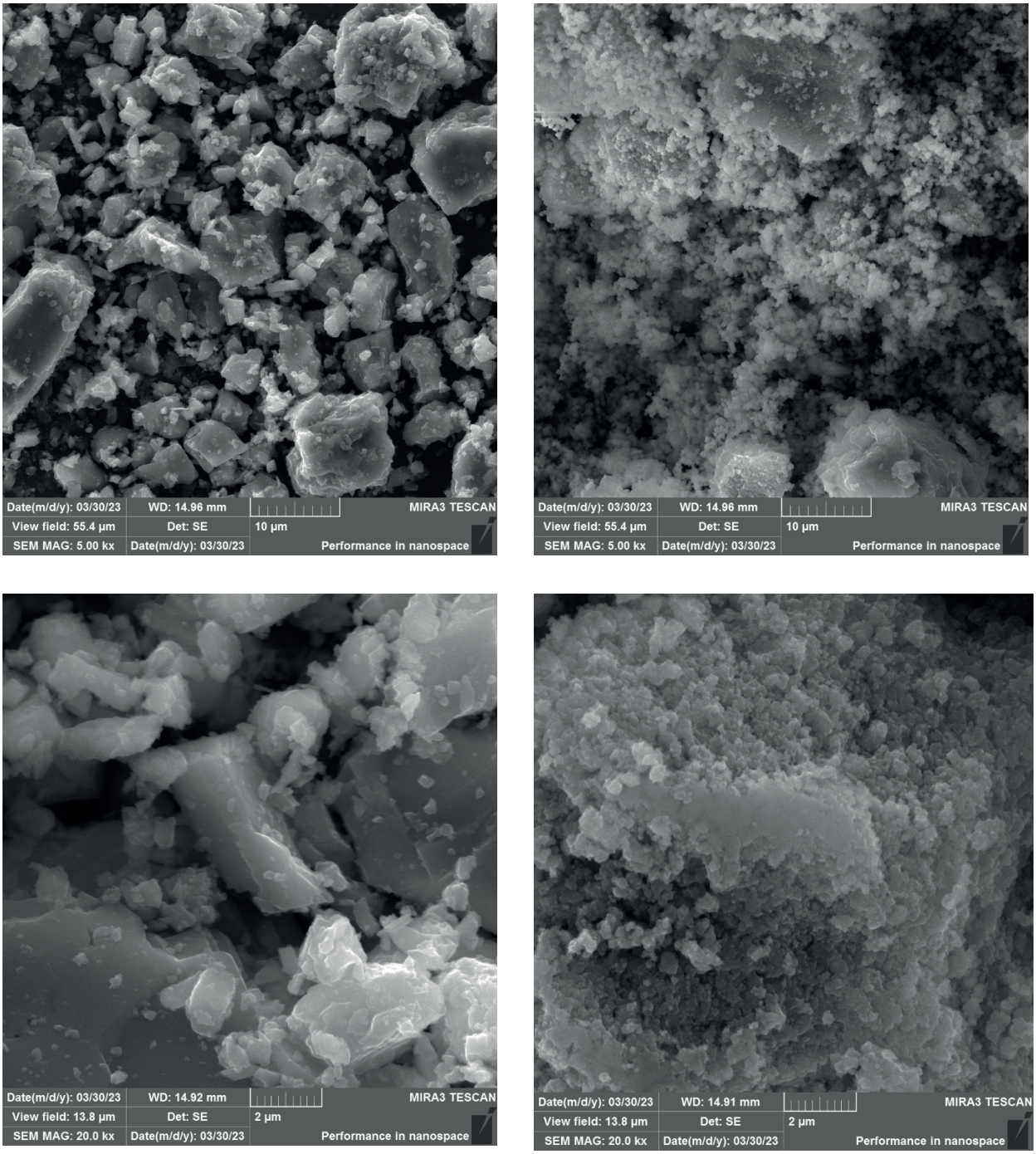

Fig. 12. Morphology of raw sample TR-1 (left up), TR-1 sample calcinated at 1 050 °C/2 hours (right up) and raw sample KRA-1 (left down), KRA-1 sample calcinated at 1 050 °C/2 hours (right down) observed by scanning electron microscope.

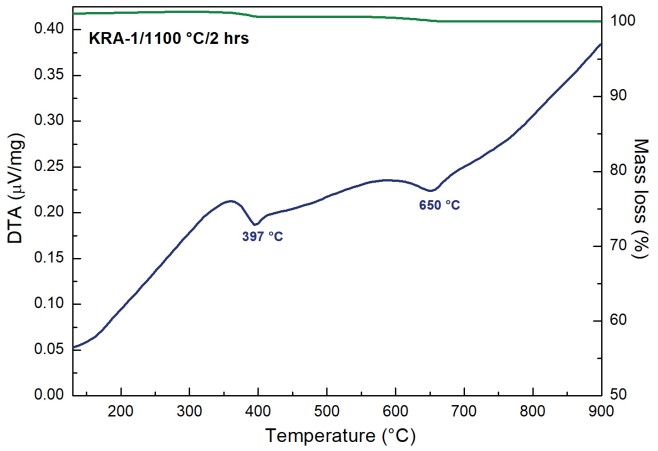

Fig. 15. DTA/TG analysis of calcinated sample KRA-1; 1 100 °C/2 hours.

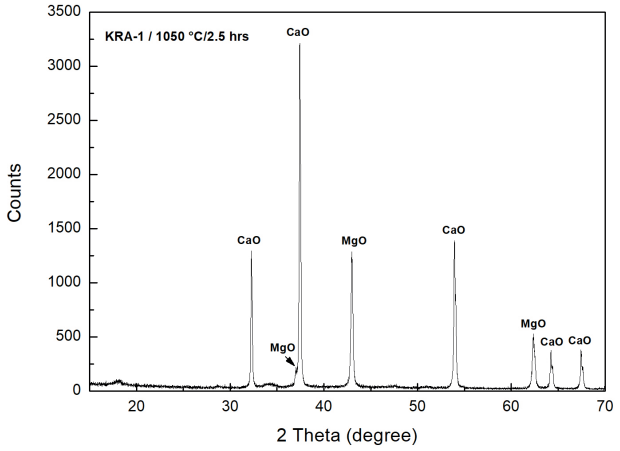

Fig. 16. XRD analysis of control calcination of sample KRA-1; 1 050 °C/2.5 hours.

The optimization of calcination and repeated annealing pointed at the suitable conditions of dolomite raw sample processing (temperature of 1 050 °C for 2.5 hours, or 1 100 °C for 2 hours) for magnesium metal production. The problematic are samples processing for chemical analyses, where the reaction with airy CO_2 should be prevented during the samples manipulation.

4. Conclusion

The aim of the study was the initial laboratory technological processing of selected domestic dolomite ores and their characterization. By annealing dolomites, according to chemical analyses, it is possible to obtain products that meet two conditions for their subsequent use as feedstocks in the silicothermal process for the preparation of metallic magnesium, namely the molecular ratio and the content of impurities. Control annealing of raw samples and their immediate characterization using DTA/TG and XRD pointed to the desired decomposition of dolomite, where the CO_2 content in the products should be at the required values. Furthermore, the conditions of chemical analyses of annealed samples will be studied in order to minimize the reaction of calcinated dolomites with atmospheric CO_2, which should be a suitable complement to structural and thermogravimetric analyses.

The knowledge obtained so far from the technological processing of dolomites will enable the development and testing of methods for the preparation of magnesium intermediates for semi-operational to operational conditions of their preparation. Given the current crisis situation caused by the lack of critical raw materials, the mentioned laboratory technological research is important also from the point of view of the use of high-quality domestic raw material resources, which can be interesting and beneficial especially for manufacturers operating in the Slovak Republic.

Acknowledgment

This work was supported by the Slovak Research and Development Agency under the Contract no. APVV-21-0176. Authors are also grateful to reviewers of primary manuscript Silvia Dolinská from Slovak Academy of Sciences and anonymous reviewer.

This material is a contribution to the EuroGeoSurveys HORIZON-CSA Geological Service for Europe project.

References

Bačo, P., Tuček, Ľ., Bačová, Z., Čechovská, K., Németh, Z., Košúth, M., Kovaničová, Ľ. & Repčiak, M., 2016: Potential sources of raw materials for the production of magnesium metal. Final report of Geological task No. 15 13. *Manuscript. Bratislava, archive St. Geol. Inst. D.* Štúr *(in Slovak).*

Bačo, P., Broska, I., Kollová, Z. & Németh, Z., 2022: Inventory of critical raw materials in Slovakia. In: Critical raw materials in the economies of the V4 countries. *Katowice, Glow. Inst. Górn., 61–77.*

Blahút, I., Rabatin, Ľ., Tomášek, K. & Kocúr, J., 1994: Possibilities for the production of metal magnesium from dolomites and waste magnesite raw materials. *Uhlí a Rudy – Geol. Průzk., 6, 207–210 (in Slovak).*

Chen, L.-Y., Xu, J.-Q., Choi, H., Pozuelo, M., Ma, X., Bhowmick, S., Yang, J.-M., Mathaudhu, S. & Li, X.-CH., 2015: Processing and properties of magnesium containing a dense uniform dispersion of nanoparticles. *Nature, 528, 539–543.*

Immer, J., 1998: Slovak magnesite plants Jelšava are increasing the export their products. *Týžd. Trend (in Slovak).*

Mehrabi, B., Abdellatif, M. & Masoudi, F., 2012: Evaluation of Zefreh dolomite (central Iran) for production of magnesium via the Pidgeon process. *Min. Proc. Ext. Met. Rev., 33, 316–326.*

Perez Prado, M. T. & Cepeda-Jimenez, C. M., 2015: Strength ceiling smashed for light metals. *Nature, 528, 486–487.*

Ramakrishnan, S. & Koltun, P., 2004: Global warming impact of the magnesium produced in China using the Pidgeon process. *Res. Conserv. Rec. 42, 49–64.*

REPORT ON CRITICAL RAW MATERIALS FOR THE EU, 2015: Report of the Ad hoc Working Group on defining critical raw materials. *Ref. Ares (2015)1819503 – 29/04/2015, 41 pp.*

Tomášek, K., Rabatín, R., Špeťuch, V., Ševičvička, O., Urban, Ľ. & Sitár, R., 1997: Patent Certificate Nr. 281 685: The method of production of magnesium from magnesite raw materials. *09 July 1997 (in Slovak).*

Tomášek, K. & Špeťuch, V, 1995: Laboratory verification of conditions for silicothermal reduction of dolomite. *Uhlí a Rudy – Geol. Průzk., 6, 184–185 (in Slovak).*

Tuček, Ľ., Čechovská, K., Kovaničová, Ľ., Košuth, M. & Marčeková, M., 2016: Potential sources of raw materials for the production of magnesium metal, Appendix No.1 – Technological part of Final report of Geological task No. 15 13, p. 9–10. *Manuscript. Bratislava, archive St. Geol. Inst. D.* Štúr *(in Slovak).*

Zhang, Z., Lu, X. & Yan, Y., 2022: A novel pathway for the preparation of Mg metal from magnesia. *J. Magnes. Alloy, 10, 2847–2856.*

Laboratórny technologický výskum prípravy medziproduktov z dolomitovej suroviny vhodných na výrobu kovového horčíka

Problematika dostupnosti niektorých kovov či surovín vo svete, a najmä v Európe, trvá už desaťročie. Od roku 2010, keď bola vypracovaná prvá analýza kritických kovov, boli vypracované ďalšie podrobné analýzy zohľadňujúce väčšiu spotrebu nerastných surovín a ich dostupnosť na svetových trhoch, ako aj ich cenu. Európske krajiny ostávajú významným dovozcom veľkej časti kovov a nerastov, ktoré sú nevyhnutné pri používaných technológiách a produktoch potrebných na ekonomický rast a rozvoj. Európska komisia zverejnila najnovšiu verziu štúdie *Kritické suroviny pre krajiny EÚ* s postavením jednotlivých kovov a surovín z hľadiska dovozného rizika a ekonomického významu v roku 2015 (Správa EK, 2015). Podiel domácej produkcie, ako aj prítomnosť overených, ale aj odhadovaných zdrojov týchto nerastných surovín v krajinách EÚ sú veľmi malé, prípadne žiadne. Preto sú krajiny Európskej únie závislé od dovozu týchto nerastných surovín.

Horčík je ôsmy najrozšírenejší prvok zemskej kôry a je aj extrahovateľný zo soľanky a morskej vody. Zdroje a suroviny, z ktorých by sa horčík mohol vyrábať, zahŕňajú aj kamallit, dolomit, serpentín a magnezit (Ramakrishnan a Koltun, 2004). Vzhľadom na možné surovinové zdroje horčíka a možnosti jeho využitia sa kovový horčík považuje za potenciálne ideálnu náhradu za kovový hliník, ale celosvetová ročná produkcia kovového horčíka tvorí len 1,8 % produkcie hliníka (Zhang et al., 2022).

Horčík sa komerčne vyrába buď elektrolýzou chloridu horečnatého získaného z nerastných surovín, alebo pomocou procesu tepelnej redukcie, známeho ako Pidgeonov proces, s použitím dolomitovej suroviny. Tento proces vyvinul v Kanade Dr. L. M. Pidgeon začiatkom štyridsiatych rokov minulého storočia (Mehrabi et al., 2012). Bol tam postavený aj závod na výrobu horčíka (Ramakrishnan a Koltun, 2004). Metóda tepelnej redukcie je založená na chemickej redukcii medzi kalcinovaným dolomitom (CaO . MgO) a ferosilíciom (Si-Fe) pri vysokej teplote (1 100 – 1 250 °C) a vysokom vákuu (1,33 – 13,3 Pa) (Zhang et al., 2022).

Územie Slovenskej republiky disponuje veľkými zásobami nerastných surovín – magnezity, serpentinity a dolomity, ktoré sú východiskovým zdrojom kovového Mg. V predchádzajúcich prácach sa tieto suroviny širšie hodnotili a skúmali z technologického hľadiska. Ako najvhodnejšie na prípravu kovového Mg sa javili dolomity (Bačo et al., 2016). Dolomity na Slovensku tvoria samostatné súvrstvia v strednom a vrchnom triase hrubé až niekoľko sto metrov alebo vystupujú ako vložky, polohy, šošovky alebo telesá, nepravidelne sa prelínajúce s okolitými vápencami. Sú zastúpené vo všetkých geologických jednotkách, tak v obalových sekvenciách, ako aj v tektonických príkrovoch. Najväčší význam majú stredno- až vrchnotriasové dolomity hronika. Významnejšie ložiská sa nachádzajú v chočskom príkrove v Strážovských vrchoch.

Laboratórny pokus výroby kovového horčíka silikotermickou metódou sa uskutočnil aj v ŠGÚDŠ, regionálnom centre Košice. V laboratórnych podmienkach sa podarilo pripraviť samostatné redukované kryštály kovového horčíka (Bačo et al., 2016).

Cieľom štúdie bolo prvotné laboratórne technologické spracovanie vybraných domácich dolomitových rúd a ich charakterizácia. Na experimentálne účely sa zvolili

ako vstupné suroviny dolomity z lokalít Sedlice (SED-1), Trebejov (TR-1) a Kraľovany (KRA-1). Kusové nerozpadavé vzorky dolomitov sa voľne presušili na vzduchu a podrobili prípravným prácam – zdrobňovaniu drvením a triedeniu na frakcie: +8,0; 4,0 – 8,0; 2,0 – 4,0; 1,0 – 2,0; –1,0 mm. Žíhacie skúšky jednotlivých frakcií dolomitov sa realizovali v elektrickej laboratórnej peci ELOP-1200/15 pri teplote 1 000 a 1 050 °C s časom výdrže 0,5; 1; 2 a 2,5 hod. Vstupné vzorky a produkty kalcinácie boli charakterizované pomocou chemických, röntgeno(rtg.)difrakčných, diferenciálnych termických a termogravimetrických (DTA/TG) analýz.

Na základe rtg. analýz dolomitová vzorka zo Sedlíc (SED-1) obsahovala len minerálnu fázu dolomit, kým vstupná vzorka z Trebejova (TR-1) akcesorický podiel kremeňa a vzorka z Kraľovian (KRA-1) akcesorický podiel kalcitu.

Jednotlivé frakcie po žíhacích skúškach boli vyhodnotené z hľadiska straty žíhaním. V prípade vzorky SED-1 dochádzalo k požadovanému tepelnému rozkladu (vyše 98 %) v hrubozrnnej frakcii (4 – 8 mm) pri oboch hodnotách teploty, bez ohľadu na čas žíhania. Naopak, frakcia menšia ako 1 mm bola najstabilnejšia. Požadovaný rozklad dolomitu nastal až po žíhaní pri 1 050 °C pri výdrži viac ako 2 hodiny. Pri tejto vzorke bolo efektívne žíhanie frakcií väčších ako 1 mm pri teplote 1 050 °C s časom výdrže minimálne 0,5 hodiny.

Pri vzorke TR-1 bolo účinné iba žíhanie frakcií väčších ako 2 mm pri teplote 1 050 °C s výdržou viac ako 2 hodiny. Naopak, vzorka KRA-1 dosiahla požadovaný rozklad pri všetkých študovaných frakciách a pri oboch vybraných hodnotách teploty.

Po počiatočných skúškach žíhania sa vykonala optimalizácia procesu. Jednotlivé frakcie dolomitových vzoriek menších ako 8,0 mm boli zlúčené a žíhané pri teplote 1 050 °C s výdržou 2,5 hodiny a 1 100 °C s výdržou 1 hodinu. Produkty po žíhaní a chemickej analýze sa vyhodnotili s ohľadom na požadované podmienky pre kalcinovaný dolomit do vsádzky na silikotermickú prípravu kovového Mg.

Príprava produktu z dolomitovej suroviny do vsádzky na silikotermickú výrobu Mg spočíva v príprave kalcinovaného dolomitu (CaO . MgO) tak, aby molekulárny pomer CaO : MgO bol v rozmedzí 1,1 až 1,5 : 1, obsah nečistôt spolu s SiO_2 menej ako 2,5 % a obsah CO_2 maximálne 0,3 % (Blahút et al., 1994).

Produkty zo vstupných vzoriek žíhaných pri oboch vybraných hodnotách teploty spĺňali dve z troch podmienok, a to molekulárny pomer CaO : MgO a obsah nečistôt menej ako 2,5 %.

Vzorka SED-1 po optimalizovanom žíhacom procese vykazovala obsah CO_2 0,37 % (pri t = 1 050 °C) a 0,44 % (pri t = 1 100 °C), vzorka TR-1 obsah 0,33 a 0,51 %. Röntgenodifrakčná analýza poukázala na prítomnosť kalcitu a periklasu, ale aj menších podielov portlanditu, vateritu a aragonitu v kalcinovaných vzorkách. Prítomnosť portlanditu v produktoch po kalcinácii nie je žiaduca a súvisí s vyšším obsahom CO_2 stanoveným chemickou analýzou.

Príčina vyššieho obsahu CO_2 v pripravovaných produktoch môže byť spôsobená aj manipuláciou so vzorkami. Reakcia kalcinovaných vzoriek so vzdušným CO_2 je veľmi rýchla a môže nastať aj pri príprave vzoriek na chemické analýzy (mletie vzorky, príprava tablety na prvkovú rtg. analýzu). Pretože chemické analýzy boli kľúčové pre ďalšie laboratórne technologické spracovanie dolomitových vzoriek, uvedené rtg. a DTA/TG analýzy produktov sa realizovali až po získaní výsledkov z chemických analýz, teda v dôsledku „státia“ mohla nastať aj čiastočná degradácia vzoriek. Navyše, realizácia chemických analýz je časovo náročná a je možné vykonávať ich len na pracovisku GAL SNV, teda nie v mieste technologickej úpravy dolomitov. Vykonalo sa teda niekoľko ďalších žíhacích skúšok a kontrolných DTA/TG meraní bez chemických analýz a na základe získaných výsledkov sa realizovalo kontrolné žíhanie a charakterizácia produktov len pomocou DTA/TG a rtg. difrakčných analýz.

Aby sa vylúčili chyby počas procesu žíhania s cieľom získať požadovaný žíhaný produkt, vstupné vzorky dolomitov so zrnitosťou menej ako 8,0 mm sa najskôr 2 hodiny žíhali pri vyššej teplote, 1 100 °C. DTA/TG analýzy sa uskutočnili okamžite po vychladnutí vzorky. Pri všetkých študovaných vzorkách sa nepozoroval takmer žiadny úbytok hmotnosti, čo poukazovalo na požadovaný rozklad $CaCO_3$.

Zopakovalo sa aj žíhanie vzorky KRA-1 pri teplote 1 050 °C s výdržou 2,5 hod. Okamžite po vychladnutí bol produkt charakterizovaný pomocou rtg. difrakčnej analýzy, ktorá potvrdila rozklad dolomitu na požadované minerálne fázy CaO a MgO.

Optimalizácia kalcinácie a opakovaného žíhania overila vhodné podmienky spracovania dolomitovej suroviny (teplota 1 050 °C počas 2,5 hodiny, resp. 1 100 °C počas 2 hodín) na výrobu kovového horčíka. Problematickým sa javí spracovanie vzoriek na chemické analýzy, kde by sa malo pri manipulácii so vzorkami zabrániť reakcii so vzdušným CO_2. Ďalej sa teda budú študovať podmienky prípravy žíhaných vzoriek na chemické analýzy s cieľom minimalizovať reakciu kalcinovaných dolomitov

s atmosférickým CO_2, ktoré sa budú kontrolovať a doplnia sa výsledkami štruktúrnych a termogravimetrických analýz.

Doteraz získané poznatky z technologického spracovania dolomitov umožnia vývoj a testovanie metód prípravy horčíkových medziproduktov v poloprevádzkových až prevádzkových podmienkach ich prípravy. Vzhľadom na súčasnú krízovú situáciu spôsobenú nedostatkom kritických surovín je uvedený laboratórny technologický výskum dôležitý aj z hľadiska využívania kvalitných domácich surovinových zdrojov, ktorý môže byť zaujímavý a prínosný najmä pre výrobcov pôsobiacich v Slovenskej republike.

Doručené / Received: 9. 5. 2023
Prijaté na publikovanie / Accepted: 30. 7. 2023

Mineralia Slovaca, Web ISSN 1338-3523, ISSN 0369-2086, https://doi.org/10.56623/ms.2023.55.1.6
55, 1 (2023), 85 – 102, © Authors 2023. CC BY 4.0

Estimation of specific yield in bedrock near-surface zone of hilly watersheds by examining the relationship between base runoff, storage and groundwater level

PETER BAJTOŠ[1], PETER MALÍK[2] and RADOVAN ČERNÁK[2]

[1]State Geological Institute of Dionýz Štúr, Markušovská cesta 1, SK-052 01 Spišská Nová Ves, Slovak Republic; peter.bajtos@geology.sk
[2]State Geological Institute of Dionýz Štúr, Mlynská dolina 1, SK-817 04 Bratislava, Slovak Republic

Abstract: A catchment-scale method for estimation of specific yield (S_y) in the zone of groundwater level fluctuation is proposed. It is applicable to hilly watersheds, where deep groundwater discharge – not drained by local streams as baseflow – is small and can be neglected. Therefore, it is mostly employable for bedrock flow systems, dominated by shallow unconfined fractured rock aquifers. Method provides an estimate of specific yield (S_y) by combined analysis of streamflow recession, storage/runoff relationship and groundwater level fluctuation (Q-S-H). For groundwater storage (S) values evaluation, river discharge (Q) master recession curves are constructed and interpreted. The method produces as more reliable results as number of groundwater level observation sites increases. As example, it is demonstrated at the Levočský potok Brook watershed (Western Carpathians, Slovakia), built by fracture porosity dominated Paleogene sediments. Estimated characteristic S_y value is from the interval 0.001–0.002 and 0.002–0.005 for low and medium storage/runoff conditions – or bottom and middle part of GWL fluctuation zone – respectively.

Key words: specific yield, groundwater storage, groundwater table fluctuation, base runoff, bedrock flow systems

Graphical abstract

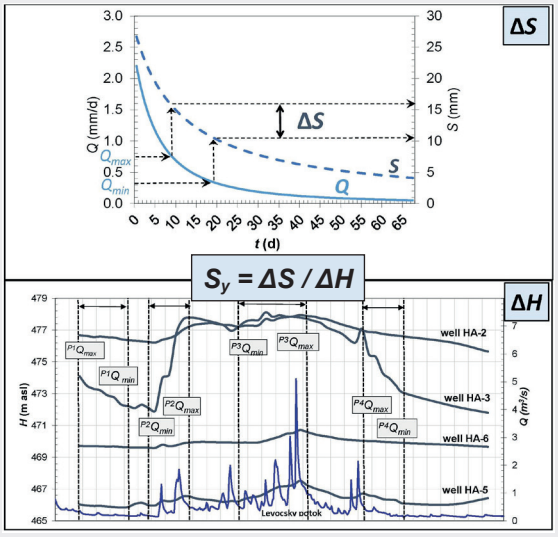

Highlights

- Regional estimation of specific yield ($S_y = \Delta S / \Delta H$) based on a combination of stream flow recession – storage/runoff – groundwater level fluctuation (Q-S-H) analysis is suggested. It is applicable to aquifers in hilly watersheds, where deep groundwater discharge (not drained by local streams as baseflow) is small and can be neglected.
- For watershed groundwater storage (S) evaluation, river discharge (Q) master recession curves are constructed and storage-discharge relationship $S = aQ^b$ for nonlinear reservoirs is accepted. Groundwater level (H) measurements are required to determine a representative ΔH value.
- Demonstration of the method at the Levočský potok Brook watershed (Western Carpathians, Slovakia), which is built by fracture porosity dominated Paleogene sediments, suggest that the characteristic S_y value at studied watershed is from the interval 0.001–0.002 and 0.002–0.005 for low and medium storage/runoff conditions (or bottom and middle part of GWL fluctuation zone), respectively.

1. Introduction

The specific yield (S_y) of a rock or soil, with respect to water is defined as ratio of the volume of water which, after being saturated, it will yield by gravity, to its own volume (Meinzer, 1923).

$$S_y = V_W / V_T \quad (1)$$

where V_W is the volume of drainable water and V_T is the total volume of porous rock or sediment.

Specific yield is part of the total porosity of a porous rock or sediment. Total porosity includes the fraction of pore space that is interconnected (called "effective porosity") and porosity of isolated pores. The effective porosity consists of specific retention and specific yield. Specific retention is the ratio of the volume of water that a given body of rock or soil will hold against the pull of gravity to the volume of body itself. Specific yield is the amount of water that is actually available for groundwater

pumping, when sediments or rocks are drained due to the lowering of the water table. The specific yield is used to determine how much water can be produced from an unconfined aquifer per a unit decline in the water table (Harter, 2019). Therefore, it is very important parameter, needed for evaluation and management of groundwater resources.

Methods commonly used to determine S_y are field methods (interpretation of aquifer hydrodynamic tests, water-budget methods, geophysical methods, methods based on recession curve analysis) and laboratory methods. A large variability exists in both laboratory and field- determined S_y values (Varni et al., 2013). Interpretation of aquifer tests in fractured-rock systems is often difficult because of ambiguity issues. Specific yield values determined from these tests are usually unreliable (Bardenhagen, 2000). Methods based on recession curve analysis derive hydraulic (including S_y) and geometric characteristic of aquifer from the recession curve shape. Their mathematical formulations represent various conceptual models developed from differential Boussinesq (1877) equation and they differ each other by ways of input data analysis (Brutsaert & Nieber, 1977; Brutsaert & Lopez, 1988; Parlange et al., 2001; Mendoza et al., 2003). Their applicability for S_y calculation in bedrock groundwater flow system is complicated by the need to know the aquifer thickness – however this aquifer datum is practically indeterminable in weathered fractured bedrock due to its vertical inhomogeneity of permeability. The water budget method is the most widely used technique for estimating specific yield in fractured-rock systems, probably because it does not require any assumptions of concerning flow processes (Healy & Cook, 2002). Several approaches, expressed by different forms of a simple water budget equation for basin

$$P + Q_{on} = ET + \Delta S + Q_{off} \quad (2)$$

and different ways of their members` determination (P – precipitation plus irrigation, Q_{on} and Q_{off} – surface and subsurface water flow into and out off the basin, ET – sum of bare soil and open water evaporation and plant transpiration, ΔS – change in water storage), were used (Walton, 1970; Gerhart, 1986; Hall & Risser, 1993; Rasmussen & Andreasen, 1959; Gburek & Folmar, 1999). However, given the current stage of the science, it is extremely difficult to assess the accuracy of any method. For this reason, it is highly beneficial to apply multiple methods of estimation and hope for some consistency in results.

This paper introduces a new method of regional estimation of specific yield based on a combination of stream flow recession – storage/runoff – groundwater level fluctuation (Q-S-H) analysis, which can be assigned to the group of field methods. It is applicable to aquifers in hilly watersheds, where deep groundwater discharge (not drained by local streams as baseflow) is small and can be neglected. Therefore, it is mostly employable for bedrock flow systems, dominated by shallow groundwater circulation. However, these aquifers often occupy the vast majority of mountain regions, which play a strategic role for water resources management at the regional and global scales (Aureli, 2002; Viviroli & Weingartner, 2004). Their study is difficult due to the complexities of the geology, the geomorphology and the climate patterns (Espinha Margues et al., 2013). Therefore, it entails challenges, concerning both input data collection and interpretation methods. The specific yield is a key parameter not only for groundwater resources evaluation, but also for estimation of recharge, using world-wide used water-table fluctuation (WTF) method (Schicht & Walton, 1961).

To demonstrate applicability of proposed method, here it is used to estimate average/representative value of S_y in the Levočský potok Brook watershed (the Hornádska kotlina basin / the Levočské vrchy Mts., Slovakia), which is built by fracture porosity dominated Paleogene sediments. Obtained results are compared to published values of S_y representing bedrock flow systems in hilly watersheds.

2. Method

Proposed method provides an estimate of specific yield (S_y) by combined analysis of stream flow recession – storage/runoff – groundwater level fluctuation (Q-S-H) at hilly watersheds. The method is based on the assumption that a rise in water-table elevation measured in shallow boreholes is caused by the addition of recharge across the water table at watershed and its following recession is caused by groundwater storage (S) loss due to baseflow (Q) generation. Supposing that storage loss (depletion) reflects baseflow recession, the recession curve extracted from the continuous multi-year hydrographs can be used to derive the storage loss value ΔS corresponding to average groundwater level decline ΔH in studied watershed. Thus, average Sy value in groundwater fluctuation zone is given as $S_y = \Delta S / \Delta H$.

Determination of the storage loss value ΔS is based on the construction of the master recession curve (MRC) for studied watershed, followed by specifying of recession coefficient a and recession exponent b from equation (1), by means of MRC interpretation.

MRC construction approach tries to find a solution to usual problem with application of individual recession curves, derived from selected time periods of recession – that in most cases they describe the process only partially, depending on the limiting water stages of these periods. To cover all possible solutions, different methods (Lamb & Beven, 1997; Rutledge, 1998; Posavec et al., 2006; Gregor & Malík, 2012b) of composing individual curves into a single master recession curve (with the longest

course and covering all documented water stages) were created. In this study, the approach developed by Gregor and Malík (2012a) supplemented by computational tool (the RC 4.0 module in the freely accessible HydroOffice software: http://www.hydrooffice.org) is used. It is based on genetic algorithm (main principles applied within the genetic algorithm procedures is explained by Hynek, 2008), which allows creation of the most probable natural, unaffected recessional discharge sequences in time, from which the master recession curves can be constructed. Such assembling of recessional discharge time series can help to avoid obstacles such as limited time-series datasets, incomplete recessions, too many segments in many recessional successions, complicated hydrograph shape, different time intervals of observations, short time-series intervals, imprecise measurements, different types of datasets (averaged or instantaneous data) or even rough (inaccurate) measurements of discharges.

Construction of MRC is based on extraction of recession periods from hydrograph. As a way to focus on the true natural storage-discharge relationship, the influence of the unknown factors as evapotranspiration (ET), snow melt and low permeability due to frozen soil, can be minimized by extraction only recessions occurring during appropriate seasons (for example, autumn months in temperate climatic range of northern hemisphere). To avoid the influence of overland flow, the beginning of the baseflow recession must be assumed not earlier than certain time interval, depending on watershed size and morphology. For example, Wittenberg (1999) starts baseflow recession two days after the inflection point of the MRC and Ye et al. (2014) record only 70 % of a falling limb as a recession period.

Constructed MRC is believed to represent the true natural storage-discharge relationship, which is unique for each watershed. It can be simulated using various model equations (recession functions) derived by many authors, which are incorporated in the RC 4.0 tool. The storage loss between two time points on MRC can be computed as sum of amounts discharged in chosen time steps using any of them. But only two have advantage of mathematically defined Q–S relationships. The exponential function (Maillet, 1905)

$$Q_t = Q_0 e^{-t/k} \tag{3}$$

is used to describe the recession of baseflow, where Q is discharge at time t, Q_0 the initial discharge and k the retention constant that supposedly represents storage lag-time (Wittenberg, 1999). This concept of single linear reservoir uses constant reaction factor, so storage is proportional to baseflow: $S = kQ$. Nonlinear reservoirs have reaction factors that increase with increasing storage, thus the storage-discharge relationship was modified by adding an exponent b (Wittenberg, 1999)

$$S = aQ^b \tag{4}$$

to define recession curve equation

$$Q_t = Q_0 \left[1 + \frac{(1-b)\, Q_0^{1-b}}{ab}\, t\right]^{1/(b-1)} \tag{5}$$

In this study, concept of nonlinear reservoir and the notional value of $b = 0.5$ is accepted. The notional value of b = 0.5 is suggested by Wittenberg (1999), based on recession curves from more than 80 gauging stations in Germany. It is also confirmed by other authors who, by adopting more theoretical approaches, found storage-outflow relationship corresponding to $S = aQ^{0.5}$ or $Q = S^2$ for discharge from springs (Drogue, 1972) and unconfined aquifers (Werner & Sundquist, 1951; Schoeller, 1962; Roche, 1963; Fukushima, 1988). Corresponding value of a is determined by fitting procedure, using the RC 4.0 module in HydroOffice software, customized for this purpose. Within this procedure, the a value together with initial discharge Q_0 value has been manually alternating until model curve – generated automatically according to equation (4) on the graph window – visually fitted to the section of MRC no influenced by overland flow (Fig. 4). The a value determined in this way makes it possible to calculate the actual storage for arbitrarily chosen datum of studied period, using equation (1). However, baseflow must be used as Q value in this calculation. This requirement may be met by selection of days when only baseflow occurs in the stream, or by correction of correspondent recorded Q values, influenced by surface runoff, onto baseflow values. An appropriate hydrogram separation method may be used for this correction. Among these, the envelope line method (*ELM*) for groundwater table-discharge (*H-Q*) relationships, proposed by Kliner and Kněžek (1974) for runoff separation from hydrograph, seems to be the most suitable for this study. The method is based on assumption that close relationship between groundwater and stream water level should exist, considering hydraulic connections between rivers and aquifers. The upper limit of the points in the *H-Q* graph usually makes it possible to draw an envelope line representing the flux formed by groundwater runoff (Fig. 7). This line can be used to calculate groundwater runoff for any measured groundwater table, in different types of natural conditions (Holko et al., 2002).

Finally, calculation of Sy is possible after selecting two $S – H$ value pairs, using equation (6). One represents a high (S_{max}, H_{max}) and the other a low (S_{min}, H_{min}) stage of storage / baseflow. The H_{max} and H_{min} values are calculated as the average of the time relevant data from available observation boreholes.

$$S_y = (S_{max} - S_{min}) / (H_{max} - H_{min}) \tag{6}$$

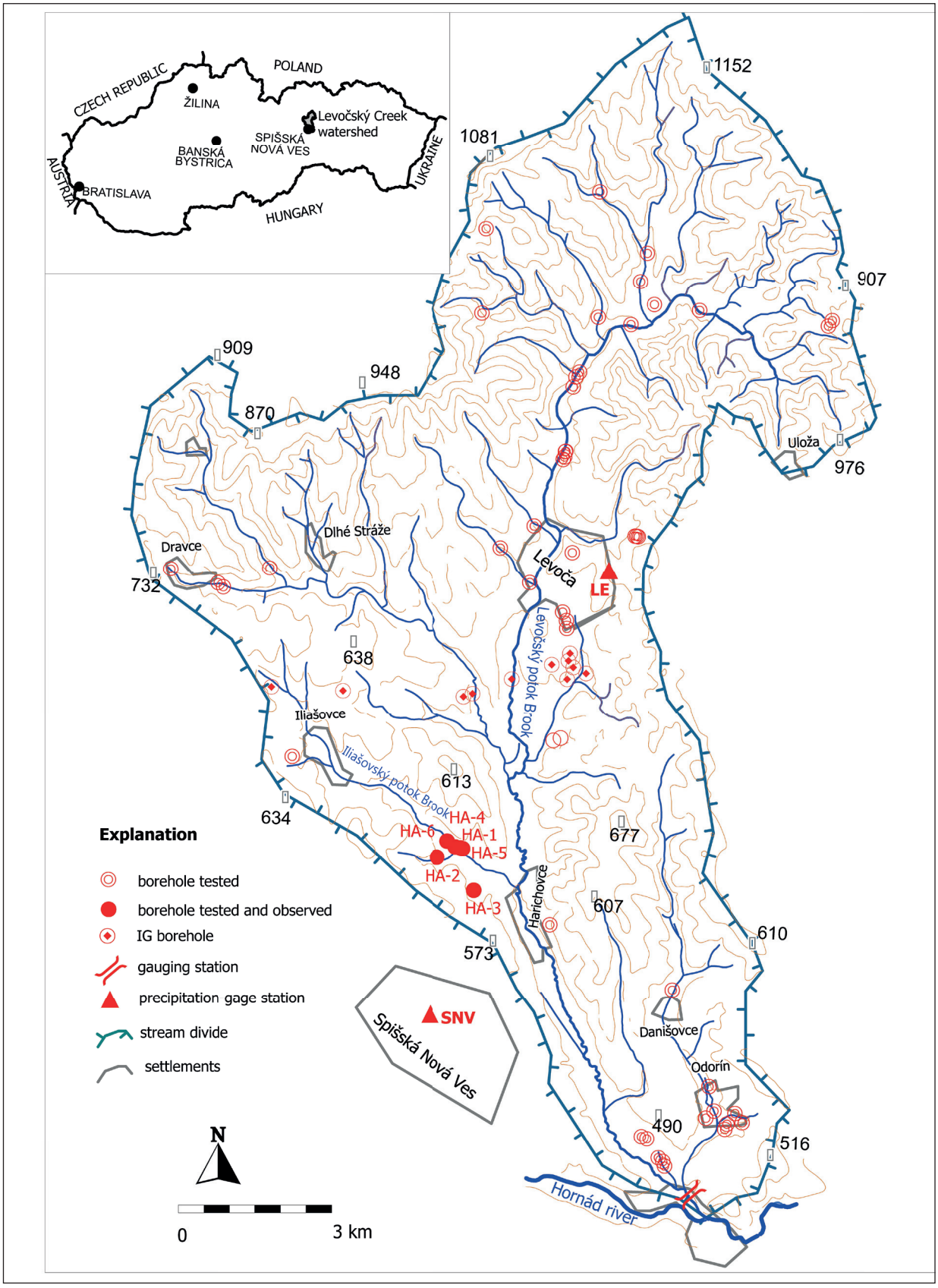

Fig. 1. Situation of the Levočský potok Brook watershed.

3. Example – S_y estimation for the Levočský potok Brook watershed

3.1. Study area

The study site shown in Fig. 1 is a 154.81 km^2 watershed located in central part of Slovakia. Hilly landscape lies in altitude of 422–1 215 m (656 m in average). Slopes are of variable length (0.5–1 km) and generally moderate (10.1 % in average) with local relief of 100–250 m. Density of channel network in watershed reaches 1.38 km/km^2. It is dewatered by 25.9 km long Levočský potok Brook into the Hornád river.

Hillslope soils are characterized as cambisols – mostly saturated (eutric, stagnieutric and calcaric) cambisols prevails in southern part of studied watershed, whereas oligobasic (dystric cambisoils, cambic umbrisoils and stagni-dystric cambisoils) occur in its northern part (Šály & Šurina, 2002). Average hydraulic conductivity of soil at studied watershed is $5.44.10^{-6}$ m.s^{-1} (Malík et al., 2007). It is covered by coniferous forest (39.9 %), prevailingly in higher altitudes. Lover parts of land are cultivated (27.1 %) or covered by meadows.

Bedrock is represented by flysch rocks with a predominance of layers fractured sandstones over silts and claystones of Paleogene age (Mello et al., 2000; Map server of SGIDŠ, 2016), belonging to geological unit of the Central-Carpathian Paleogene: Biely Potok Formation (55 % of the catchment area) and Zuberec formation (45 %). The regional hydrogeological research (Jetel, 2000) revealed that the permeability of the Central-Carpathian Paleogene flysch rocks is distinctly controlled by actual depth position below ground surface. Regular decrease of mean permeability in particular formations with depth can be described by exponential functions of the depth. The mean permeability in depths of 0–100 m decreases on average to 26–59 % of the initial value per every 10 m of depth increase. Primary differences in permeability between sandstones and argillaceous rocks fade away as a result of diagenetic changes, reducing intergranular permeability. Fissure permeability is of decisive importance. The maximum permeabilities and transmissivities are found in tectonically predisposed joint zones without any unequivocal relation with lithology. Consequently, hydrogeological function of stratiform aquifers and intergranular permeability in the flysch complex is of rather little importance. The main aquifer here is represented by the near-surface zone of increased permeability in first tens of meters below ground surface. Deeper circulation of groundwater occurs predominantly in subvertical joint zones.

After data selected from database containing pumping test reinterpretation results (Malík et al., 2016) of 48 boreholes (Fig. 1), hydraulic conductivity of flysch rock ranges between $2.59.10^{-8}$ and $3.57.10^{-4}$ m/s (geometric mean $4.87.10^{-6}$ m.s^{-1}) at the Levočský potok Brook watershed. Borehole depth is 5.7–150.2 m (52.78 m in average). Groundwater level (GWL) was recorded in the depth of 25.4–0.1 m below ground surface (3.74 m in average) and its areal distribution does not significantly depend on geomorphology. This fact can be demonstrated on graphs when recorded GWL depth H is plotted against vertical elevation of borehole head above regional drainage base (RDB), (Fig. 2a), or against local drainage base (LDB) (Fig. 2b). The H values usually don't exceed 10 m not only in valleys bottom, but also on slopes, what supports above mentioned opinion that near-surface zone represents

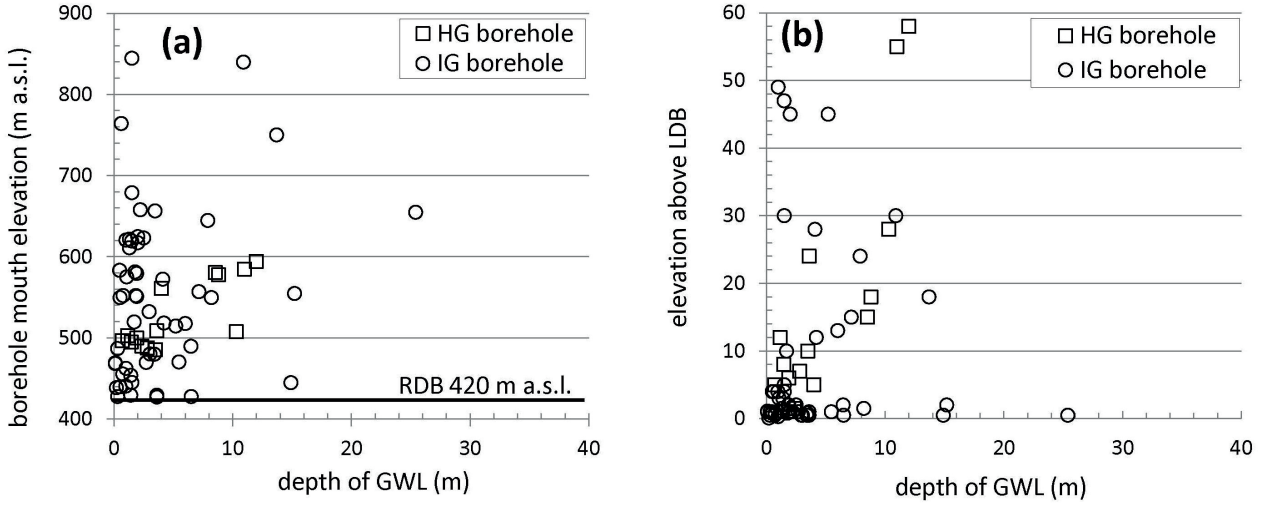

Fig. 2. Depth of groundwater level (GWL) in studied watershed recorded in boreholes versus: **a** – height of borehole mouths above sea level with the regional drainage level (RDB) marked; **b** – elevation of borehole heads above local drainage level (LDB); hydrogeological (HG) boreholes from database of Malík et al. (2016) and engineering geological (IG) boreholes from database of SGIDS are distinguished.

the main aquifer in flysch rocks of Central-Carpathian Paleogene. Therefore, this environment is dominated by bedrock groundwater flow system, in which baseflow forms substantial part of total groundwater discharge from watershed (Welch & Allen, 2014). Thus, cross-boundary groundwater flow is considered to be negligible.

Within the area of the Levočský potok Brook watershed, GWL fluctuation was observed on six boreholes, in frame of local hydrogeological research (Bajtoš & Michalko, 2003). HA-1, HA-4 and HA-6 boreholes are located 50–70 m from the Iliašovský potok Brook (tributary of the Levočský potok Brook). All three catch permeable fault zone, which is naturally dewatered by the Zimná Studňa Fissure Spring. Nearby situated HA-5 borehole is tectonically separated from this fault zone and it captures aquifer bound to near-surface zone. HA-2 and HA-3 boreholes are located in greater distance from the Iliašovský potok Brook (Fig. 1), their heads are 9.5 m and 16.7 m above local drainage base, respectively. Both boreholes are situated in a near-surface zone aquifer. GWL fluctuation on boreholes was measured during hydrological year 1995 (November 1994 – October 1995) on weekly frequency. Minimum GWL did not exceed depth of 7.1 m below ground surface in any borehole and range of GWL fluctuation ΔH (difference between minimal and maximal recorded GWL, $\Delta H = H_{min} - H_{max}$) reached values 0.491 – 6.170 m in individual boreholes (Tab. 1).

Rainfall precipitation events in studied area are distributed between March and October, whereas in period from November to February snow precipitations prevail. Highest monthly precipitation totals occur in June to August period, most dry conditions terms since January to March (Tab. 2). Annual precipitation total varies around 630 mm.

Discharge of the Levočský potok Brook is observed by SHMI on gauging station no. 8 424, situated close to

Tab. 1

Groundwater level fluctuation recorded at the Harichovce site during hydrological year 1995 (Bajtoš & Michalko, 2003)

Borehole	HA-1	HA-2	HA-3	HA-4	HA-5	HA-6
H_{avg}	–0.062	2.326	3.502	0.500	2.332	3.002
H_{max}	0.043	3.133	7.100	0.808	2.906	3.357
H_{min}	–0.448	1.408	0.930	-0.227	1.227	2.242
ΔH	0.491	1.725	6.170	1.035	1.679	1.115
Borehole depth	100	100	100	60	60	80
Borehole screen interval	7.5 – 59.0	6.6 – 54.3	9.4 – 45.0	10.0 – 55.2	10.0 – 55.6	10.0 – 54.0

Explanation: Havg, Hmin, Hmax – average, minimum and maximum GWL depth in meters below ground surface; ΔH = Hmax – Hmin

Tab. 2

Long term monthly and annual averages of precipitation total in mm recorded in period 1951–1980 by Slovak Hydrometeorological Institute on stations in Levoča (LE) and Spišská Nová Ves (SNV)

Station	I.	II.	III.	IV.	V.	VI.	VII.	VIII.	IX.	X.	XI.	XII.	Year
LE	26	25	26	43	70	97	90	82	50	42	41	32	624
SNV	23	25	27	46	73	99	90	79	48	46	46	31	633

Tab. 3

Long term monthly and annual averages (A), standard deviations (STD), minimum (MIN) and maximum values (MAX) of the Levočský potok Brook discharge in m^3/s recorded in period 1990–2012 by Slovak Hydrometeorological Institute on gauging station No. 8 424 in Markušovce

	I.	II.	III.	IV.	V.	VI.	VII.	VIII.	IX.	X.	XI.	XII.	Year
A	0.421	0.405	1.018	1.239	0.939	0.925	0.968	0.779	0.647	0.514	0.487	0.457	0.735
STD	0.424	0.313	1.259	1.098	0.738	1.229	1.328	0.753	0.840	0.360	0.436	0.458	0.893
MIN	0.131	0.101	0.072	0.152	0.150	0.168	0.098	0.105	0.119	0.135	0.144	0.075	0.075
MAX	5.723	2.383	13.313	8.212	9.272	19.488	15.823	7.011	11.900	3.486	4.448	4.501	19.488

its effluent into the Hornád river (Fig. 1). Highest average discharges connected with spring snow melting occur during March and April (Tab. 3). During winter season with little or no recharge, discharge is lowest. More than 80 % of observed time discharge not exceeded 1 m^3/s (Fig. 3), median value is 0.480 m^3/s.

3.2. Results

For S_y estimation at the Levočský potok Brook watershed, the record of stream discharge for period 1990–2012 and GWL data from 6 boreholes for hydrological year 1995 are disposable (Tab. 1). Based on recorded discharge Q, master recession curve (MRC) was constructed (Fig. 4). The use of MRC allows to simulate watershed groundwater storage (S) at different baseflow (Q) and corresponding GWL stages (H). Two different ways of S_y estimation are presented: 1) by comparing two hydrological stages selected on hydrograph (Fig. 6) and 2) by comparing two hydrological stages selected on Q-H graphs, using envelope line method (ELM; Kliner & Kněžek, 1974) (Fig. 7). Based on obtained S and H interdependent pairs of values, S_y is calculated in accordance with equation 6. Boreholes H-1 and H-4 was excluded from average H calculations because of their close distance to and their high hydraulic interconnection with H-6 borehole. Moreover, theirs GWL's are affected by the drainage effect of the Zimná studňa spring.

Master recession curve (MRC) for the Levočský potok Brook

MRC constructed for the Levočský potok Brook watershed through selection of 30 individual recessions from recharge record 1990–2012 and result of their automatic processing in genetic algorithm based procedure using RC 4.0 module in HydroOffice software is shown on Fig. 4. It is supposed that baseflow is exclusively present in discharge recession one day after inflection point or six days after its beginning (Fig. 4). This part of MRC was used for calibration of nonlinear model curve, in which the recession coefficient a = 15.5

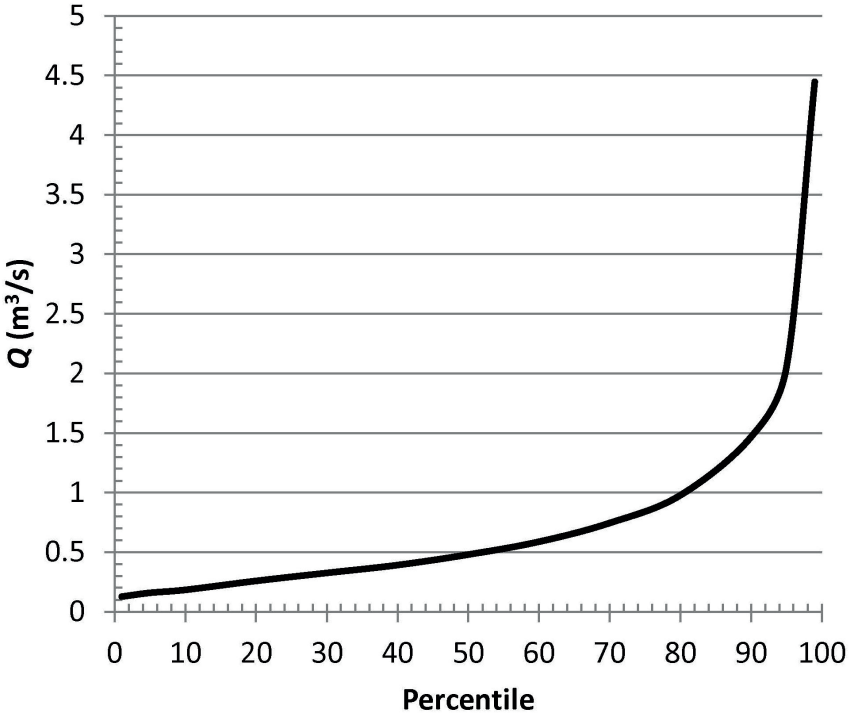

Fig. 3. Percentiles of the Levočský potok Brook discharge recorded in period 1990–2012 by Slovak Hydrometeorological Institute on gauging station No. 8 424 in Markušovce.

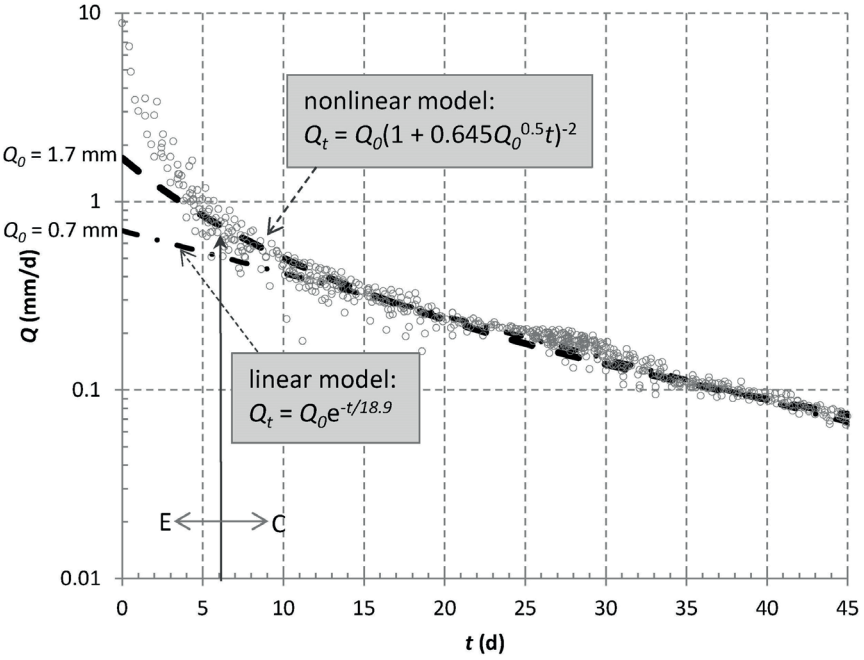

Fig. 4. Values of master recession curve (*circles*) generated using the RC 4.0 module in HydroOffice software by procedure based on genetic algorithm (Gregor & Malík, 2012a), with nonlinear model (dashed line) and linear model (dash-and-dot line) marked. Calibrated (*C*) and extrapolated (*E*) sections of nonlinear model line are distinguished.

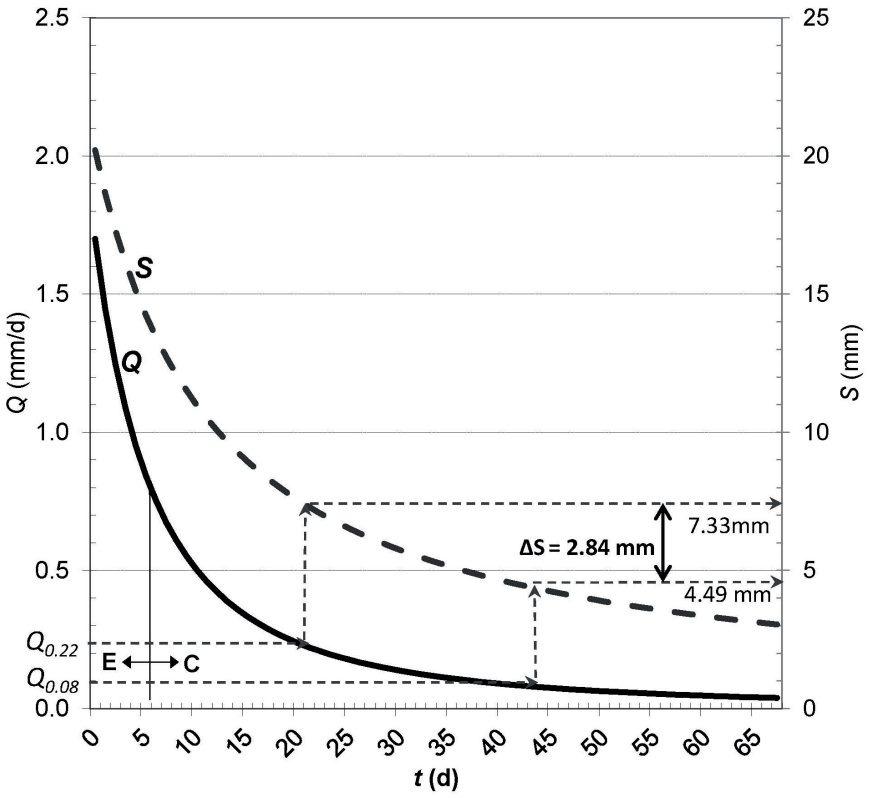

Fig. 5. Master recession curve (Q) and corresponding nonlinear changes of storage (S) for the Levočský potok Brook watershed. Calibrated (C) and extrapolated (E) sections of model MRC are distinguished. Further explanation in the text.

and initial discharge value Q_0 = 1.7 mm/d were found as fitted parameters. Therefore, storage-outflow relationship in studied watershed is described as $S = 15.5Q^{0,5}$. Both curves – model MRC with Q-values in mm/d and curve of corresponding S-values in mm – are depicted in Fig. 5, to illustrate their range and also to demonstrate the determination way of groundwater storage change for certain change of discharge. Expected maximum S value corresponding to Q_0 is 3.12 million m^3 (20.21 mm). Minimum S value corresponding to Q_{66} (Q in 66th day after Q_0 on MRC), and also equal to minimum recorded Q value, is 0.48 million m^3 (3.08 mm). Therefore, maximum amount of water being able to release from underground storage in given natural conditions is ΔS = 2.65 million m^3 (17.12 mm).

Estimation of S_y by comparing two hydrological stages selected on hydrograph

In the frame of this approach, the following procedure was applied: (a) One or more appropriate hydrologic periods are selected on the hydrograph. (b) For each period, two hydrological stages are selected, represented by river discharge values ${}^{Px}Q_{min}$ and ${}^{Px}Q_{max}$ together with their time relevant GWL values ${}^{Px}H_{min}$ and ${}^{Px}H_{max}$ for all disposable boreholes, whereby river discharge values are treated to represent baseflow (hydrological stages without surface flow were selected). (c) Using selected ${}^{Px}Q_{min}$ and ${}^{Px}Q_{max}$ values, ${}^{Px}S_{max}$ and ${}^{Px}S_{min}$ values are calculated (after storage-outflow equation $S = 15.5Q^{0,5}$ in this case, Fig. 5). (c) ${}^{Px}H_{max}$ and ${}^{Px}H_{min}$ are determined as average representatives of GWL in watershed for respective time. (d) S_y value is calculated following equation (5).

Five hydrological periods (P1–P5) are selected. Days bounding these periods are marked on hydrograph (Fig. 6). P1 period represents GWL decline with no or little recharge (winter time) and with low storage stage changed from 5.64 to 4.97 mm (Tab. 4). Period P2 is characterized by GWL rise and storage increase (from 5.01 to 7.96 mm) due to spring snow melting and soil thawing, combined with rain. During summer P3 period, GWL was rising due to repeated rains and storage increased from 7.07 to 8.71 mm. The decrease following this relatively high storage stage from 7.92 to 5.99 mm defines the P4 period. The autumn P5 period is characterized by low storage stage depletion from 1.37 to 0.69 m^3. Computed S_y values for selected hydrological periods vary from 0.0015 to 0.0045. Highest value belongs to high storage period P4, lowest one to winter dry period P1. Almost identical to the value for period P1 is the S_Y value of 0.0016 determined for spring period P2. For periods P3 and P5, mutually similar values of 0.0033 and 0.0027 was determined, respectively.

S_Y estimation based on comparison of two hydrological stages selected on Q-H graphs.

With this approach, Q-H graph is constructed for each disposable borehole (Fig. 7a–d) to obtain their characteristic H_{max} and H_{min} values corresponding to chosen low and high baseflow Q_{min} = 0.15 m^3/s and Q_{max} = 0.4 m^3/s (Tab. 5). In time of such hydrological stages, 0.69 or 1.13 million m^3 of groundwater is stored in watershed, respectively. Calculated value of S_Y = 0.0019 is very similar to those, obtained using previous approach (Tab. 4). Closest Q-H dependence was found for HA-3 borehole (Fig. 7b), suggesting that aquifer type observed by this borehole should represent the most important source of baseflow in studied watershed. Calculation of S_y using only GWT fluctuation in HA-3 borehole gives value of 0.0005.

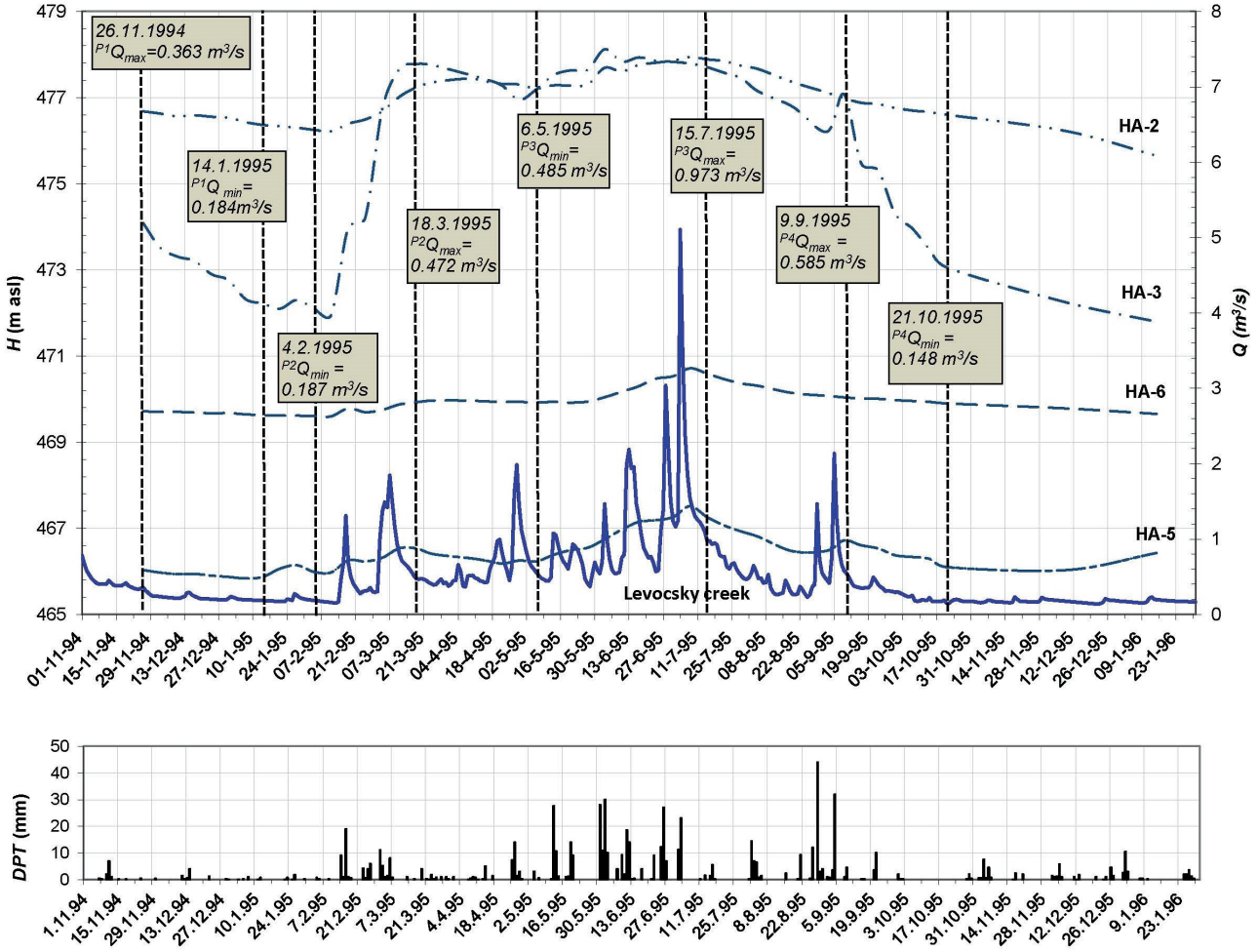

Fig. 6. Hydrograph of the Levočský potok Brook discharge, groundwater level in boreholes HA-2, HA-3, HA-5, HA-6 with selected hydrological stages chosen for specific yield calculation and daily precipitation totals measured at rainfall station Spišská Nová Ves.

Tab. 4

Altitude of groundwater level in boreholes and discharge of the Levočský potok Brook recorded with groundwater storage in watershed S_{LP} calculated and specific yield (*Sy*) values for selected time periods P1–P4

Period	GWL [m a. s. l.]					Discharge [m³/s]	Storage [m³]	Storage [mm]
		HA-2	HA-3	HA-5	HA-6	Q	S	S
P1	3. 12. 1994	476.630	473.520	465.972	469.706	0.237	872 384	5.64
	14. 1. 1995	476.365	472.220	465.872	469.626	0.184	768 675	4.97
	ΔH:	0.265	1.300	0.100	0.080	$\Delta^{P1}S$ =	103 710	0.67
			ΔH_{avg} = 0.436 m			$^{P1}S_y$ =	**0.001 5**	
P2	4. 2. 1995	476.252	472.100	465.989	469.606	0.187	774 916	5.01
	18. 3. 1995	477.240	477.780	466.532	469.928	0.472	1 231 132	7.96
	ΔH:	0.988	5.680	0.543	0.322	$\Delta^{P2}S$ =	456 216	2.95
			ΔH_{avg} 1.883 m			$^{P2}S_y$ =	**0.001 6**	

Tab. 4 – continuation

Period	GWL [m a. s. l.]					Discharge [m³/s]	Storage [m³]	Storage [mm]
P3	27. 5. 1995	477.608	477-643	466.248	469.942	0,372	1 092 962	7.07
	24. 6. 1995	477.855	477.705	467.188	470.474	0,565	1 346 970	8.71
	ΔH:	0,502	0,212	0,640	0,532	$\Delta^{P3}S$ =	254 008	1.64
			ΔH_{avg} = 0.472 m			**$^{P3}S_y$ =**	0.003 5	
P4	29. 7. 1995	477.737	477.448	466.926	470.362	0.267	925 954	5.99
	19. 8. 1964	477.360	476.787	466.49	470.141	0.467	1 224 594	7.92
	ΔH:	0.377	0.661	0.457	0.221	$\Delta^{P3}S$ =	298 640	1.93
			ΔH_{avg} = 0.429 m			**$^{P3}S_y$ =**	**0.004 5**	
P5	9. 9. 1995	476.988	477.077	466.718	470.041	0.585	1 370 603	8.86
	9. 12. 1995	476.222	472.245	466.030	469.783	0.176	689 389	4.46
	ΔH:	0.766	4.832	0.688	0.258	$\Delta^{P4}S$ =	681 214	4.40
			ΔH_{avg} = 1.636 m			**$^{P4}S_y$ =**	**0.002 7**	

Previous interpretation of *Q-H* graphs could be supported by documented relationship between local spring yield and GWL (Fig. 7e–h). The significant linear correlation is recorded for the Zimná studňa spring (ZSS) discharge and GWL in HA-6 borehole (R^2 = 0.955, R = 0.977, Fig. 7h), situated in the distance of 300 m from this spring. On the other hand, GWL in more closely located HA-5 borehole depend less significantly on spring discharge (R^2 = 0.863, R = 0.929, Fig. 7g), by reason that it do not intercepts the fault aquifer dewatered by ZSS. Dependency between ZSS discharge and GWL fluctuation in more remote boreholes HA-2 and HA-3 (Fig. 7e–f) is even more complex, comparing to HA-5 borehole. Slope of enveloping line changes from steep to sub-horizontal close to ground surface, suggesting the presence of upper vertical limit of GWL rise in given local conditions. This means that only steep section of enveloping line can be used for detection of baseflow in case of HA-2 and HA-3 boreholes (Fig. 7a–b). On the other hand, steeper sections of enveloping line in case of HA-5 and HA-6 boreholes can be regarded to shallow groundwater plus soil water (Kliner & Kněžek, 1974) or groundwater flow to shallow drains or ditches (Querner, 1997).

4. Discussion

Presented *Q-S-H* method of S_y estimation is based on comparison of groundwater storage change ΔS to respective difference of GWL ΔH (Eq. 5). Whereas values of ΔS are calculated by means of MRC constructed as unique one for studied watershed and therefore they characterize all watershed area, ΔH is averaged from as many site values as possible. In reality, the disposable number of observed

Tab. 5

Representative groundwater levels in boreholes determined for the Levočský potok Brook discharge Q_{LP} of 0.4 or 0.15 m³/s with calculated groundwater storage in watershed *S* and expected specific yield (S_y) value

GWL [m a. s. l.]					Discharge [m³/s]	Storage [m³]	Storage [mm]
Borehole	**HA-2**	**HA-3**	**HA-5**	**HA-6**	***Q***	***S***	***S***
$H_{0.40}$	477.35	477.28	466.74	470.19	0.400	1 133 349	7.33
$H_{0.15}$	476.30	472.08	466.16	469.72	0.150	694 032	4.49
ΔH:	1.05	5.20	0.58	0.47		ΔS = 439 317 m3	ΔS = 2.84 mm
		ΔH_{avg} = 1.46 m				**S_y = 0.001 9**	

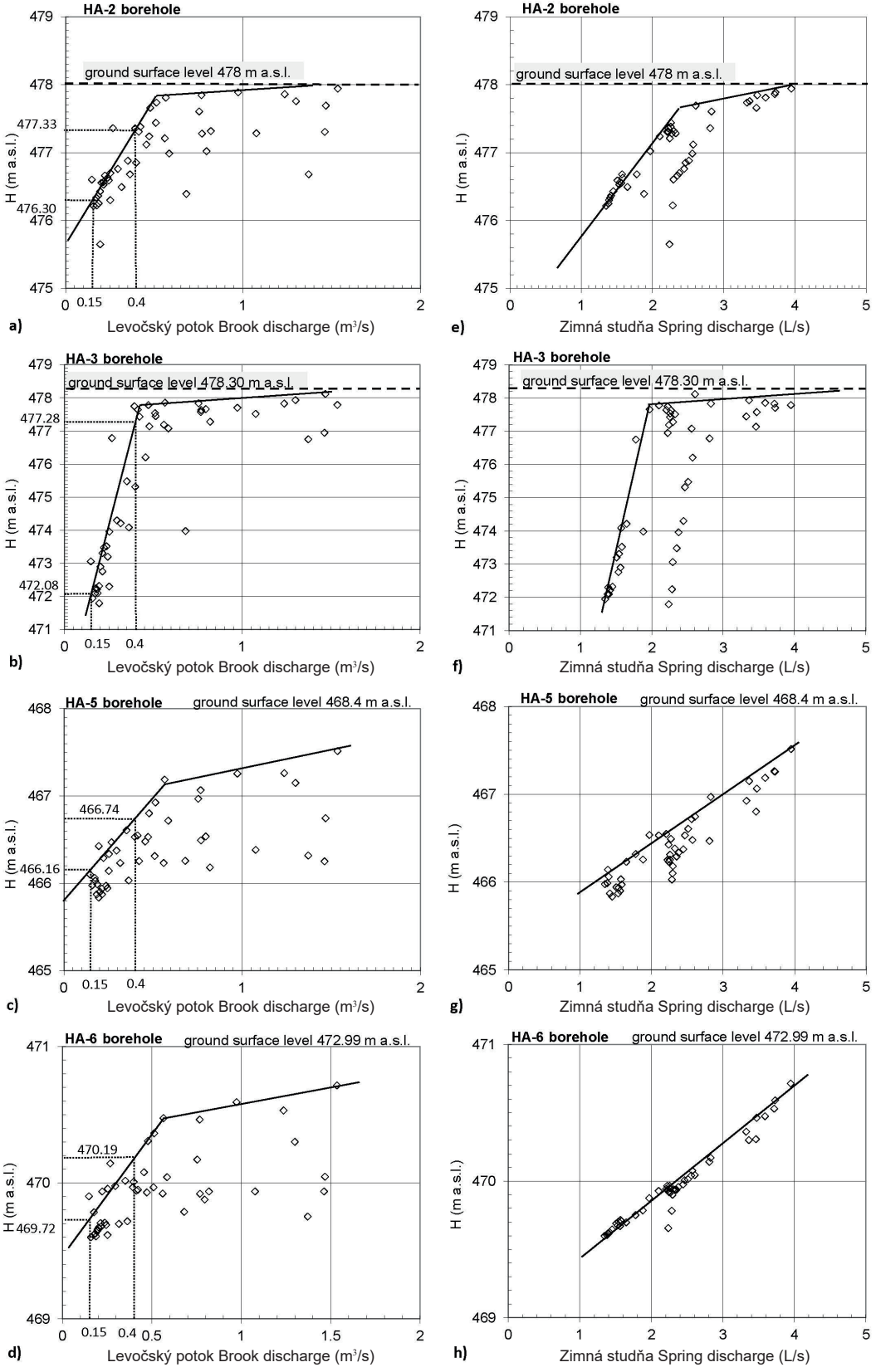

Fig. 7. Groundwater level *H* in observed boreholes versus the Levočský potok Brook discharge (a–d) and the Zimná studňa spring discharge (e–h). Explanation is given in the text.

boreholes (boreholes) usually is not very high therefore reliability of *ΔH* evaluation is crucial for the accuracy of S_y estimation.

In case of this study, four from six observed boreholes are usable for *ΔH* calculation – moreover they are situated within relatively small area comparing to overall watershed. The *ΔH* values recorded in them during hydrological year 1995 are from interval 1.04–6.17 m, giving average of 2.67 m. By comparing these values with Δ*H* values recorded on 11 boreholes situated in Paleogene sediments in the territory of Slovakia, which are observed by SHMI in frame of Slovak state monitoring program (0.72–4.28 m and 1.83 m in average, Tab. 6), it can be concluded that they are very alike in their range and also average values. The presented data suggest that difference of average *ΔH* value used for S_y estimation from real one

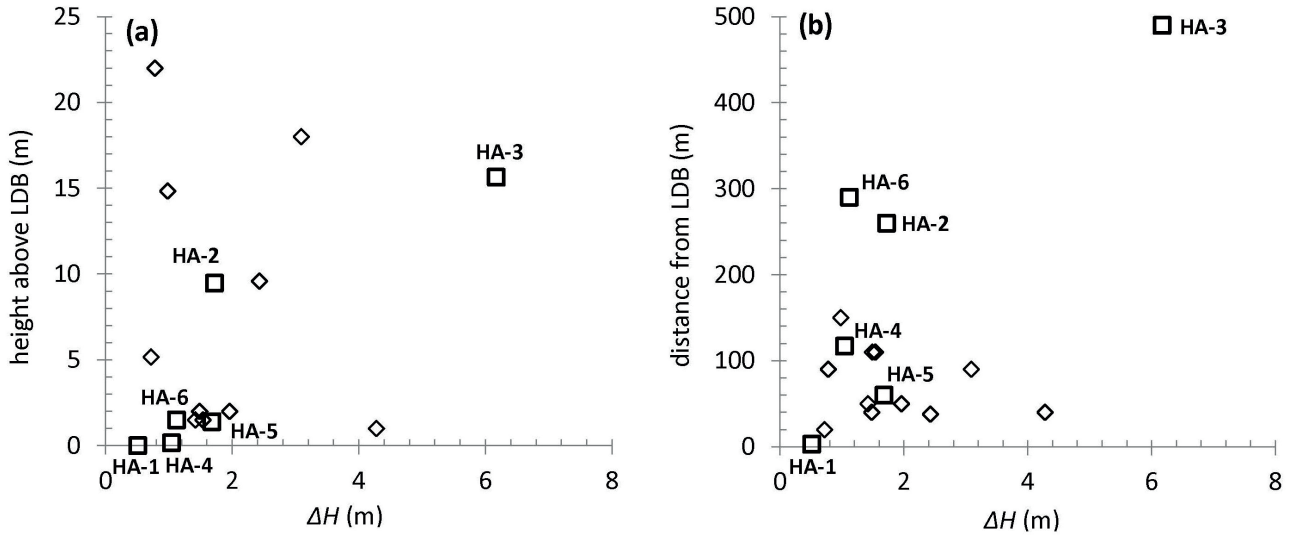

Fig. 8. Groundwater table fluctuation (*ΔH*) recorded in boreholes at the Harichovce site (squares) and in boreholes of state monitoring system (diamonds) versus: **a** – height of those borehole heads above local drainage base (LDB); **b** – distance of those boreholes from local drainage base (LDB).

Tab. 6

Groundwater level fluctuation on sites of state monitoring network situated in Paleogene sediments recorded by Slovak Hydrometeorological Institute (SHMI)

No.	Locality	Observed period	n	Elevation [m a. s. l.]	Hight above LDB [m]	H_{avg} [m]	H_{min} [m]	H_{max} [m]	ΔH [m]
5 211	Oravský Biely Potok	1991–2006	520	659.59	9.6	7.19	8.43	6	2.43
5 215	Jarabina	2004–2006	156	570.16	5.2	1.24	1.39	0.67	0.72
5 216	Ľubovnianske kúpele	2004–2006	156	566.18	22	5.32	5.58	4.8	0.78
5 219	Čirč	1982–2000	988	559.3	1.5	5.84	6.36	4.94	1.42
5 220	Livov	1982–2006	1 300	497.34	2	3.62	4.1	2.14	1.96
5 221	Olejníkov	1966–2006	2 132	514.21	1	5.23	6.5	2.22	4.28
5 222	Chminianske Jakubovany	1987–2005	988	401.21	1.5	1.53	2.22	0.68	1.54
5 223	Vyšné Raslavice	1983–2006	1 248	367.22	2	1.49	2.35	0.87	1.48
5 224	Dlhá Lúka	1989–2006	936	296.96	2	1.58	1.87	0.38	1.49
5 225	Hažlín	1989–2006	936	361.02	18	5.29	5.86	2.77	3.09
5 231	Zuberec	1990–2006	884	864.84	14.8	10.87	11.18	10.2	0.98

should be no higher than one meter in studied bedrock type. Underestimation of this calculated value is more likely than its overestimation.

Another question of *ΔH* values reliability is theirs possible affection by drainage effect and it relates to observation points located in zones of natural aquifer dewatering. Such kind of affection would cause underestimation of *ΔH*, compared to those observed in unaffected flow conditions on slope. In case of existence in regional scale, it could be revealed by positive correlation between *ΔH* recorded on individual boreholes and theirs height above local drainage base (LDB) – or theirs distance from LDB. However, existing data do not suggest existence of such correlation (Fig. 8a–b), so it can be supposed that *ΔH* estimation error due to drainage effect is not significant in this study.

The algorithm of the single nonlinear reservoir is used for the modeling of flow recession in this study, based on interpretation of MRC for the Levočský potok Brook. Although it does not fully correspond to the physical nature of ongoing processes, it describes the MRC more precisely as the algorithm for single linear reservoir (Fig. 4) and avoids the difficulty of dealing with multiple reservoirs. The problem of nonlinearity could also be solved using the assumption that baseflow is the outflow of two or more parallel linear reservoirs representing components of different response time (Moore, 1997; Schwarze et al., 1997). However, aquifers in the studied watershed are not linear reservoirs, as interpretation of the Zimná studňa spring recession curve reveals (Fig. 9). Depletion regime of local fault aquifer dewatered by this spring consists of two flow components. Simple groundwater flow component with laminar flow (described by exponential equation $Q_t = Q_0 e^{-\alpha(t-to)}$, Drogue 1967) is combined with turbulent flow component (linear equation $Q_t = Q_0[1 - \beta(t - t_0)]$, Mijatovič, 1972) occurring during highest recharge. Therefore, use of nonlinear model in this study is reasonable.

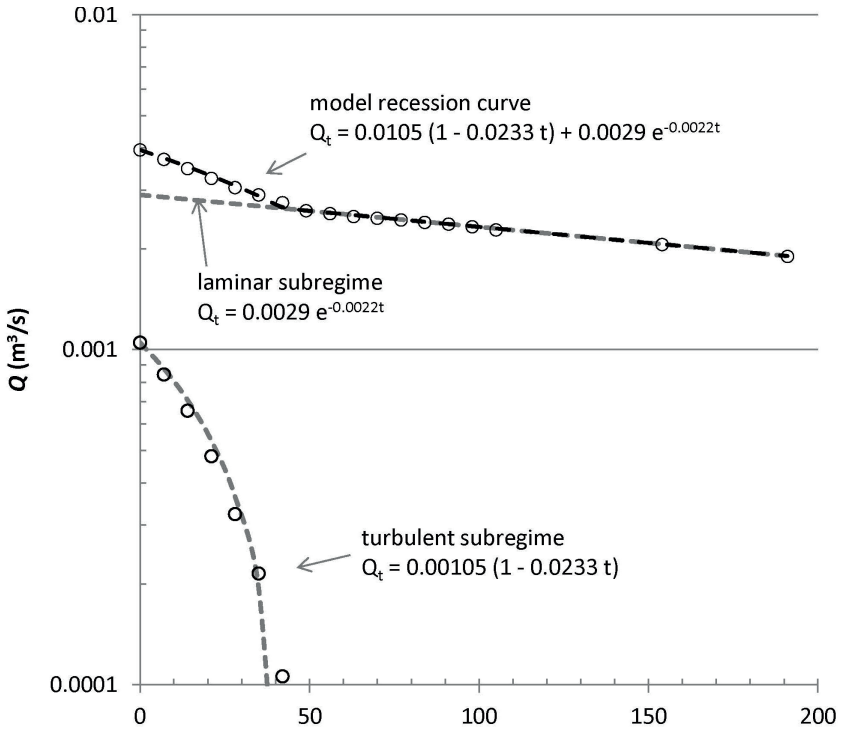

Fig. 9. Interpretation of the Zimná studňa spring recession curve.

The two presented ways of using the *Q-S-H* method give comparable results. Using the first one gives the option to estimate *Sy* for hydrological seasons chosen. Latter one – making use of *Q-H* graphs – represents conservative estimate as envelope line

Tab. 7

Results of S_y determination using five different methods based on recession curve analysis at the Odorica Brook watershed above gauging station no. 8 423 (Černák, 2016)

Considered aquifer thickness	LRM	KM	B [a1 – a3]	B [a2 – a3]	P
10	0.26	0.27	0.23	0.23	0.24
20	0.13	0.13	0.11	0.11	0.12
30	0.09	0.09	0.08	0.08	0.08
50	0.05	0.05	0.05	0.05	0.05
100	0.03	0.03	0.02	0.02	0.02

Explanation: Methods: LRM – linear reservoir model of Boussinesq (1877), KM – quadratic model of Boussinesq (1903), B(a1–a3) – method after Brutsaert, enveloping curves a1–a3, B(a2–a3) – method after Brutsaert – enveloping curves a2–a3, P – method after Parlange.

represents minimum baseflow that occurred for a particular measured groundwater table (Holko et al., 2002). Its advantage is given by ability to avoiding the error due to incorrect H data selection for calculation, which do not fully represent baseflow conditions. The S_y regional value obtained in this way for the Levočský potok Brook watershed of 0.0019 is very close to those, determined by pumping tests interpretation at the Harichovce site, where Bajtoš and Michalko (2003) states storativity coefficient of 0.0017 and 0.0014 for fissured fault zone captured in borehole HA-4 and HA-6, respectively (location of boreholes is shown on Fig. 1). As it is very probable that storativity in bedrock fissured/fault zones and in its weathered (near-surface) zone are very similar each other – like their permeability and transmissivity (Jetel, 2000) are – we can conclude here the consistency in results obtained by two independent methods.

The average computed from five S_Y values determined for different hydrological periods P1–P5 reaches 0.0028. More than this value, S_Y values computed for driest period P1 is similar to the value of 0.0019 determined using envelope line method. On the other hand, S_Y derived for wetter periods P3 and P4 are significantly higher (Fig. 10). These indications suggest that storativity of rocks forming upper parts of GWL fluctuation zone is significantly higher than those at its bottom. Based on data obtained the S_Y characteristic value at studied watershed is from the interval 0.001–0.002 and 0.002–0.005 for bottom and medium parts of GWL fluctuation zone, respectively. The existence of such vertical zonality of storativity is consistent with the previously described nature of studied bedrock aquifer.

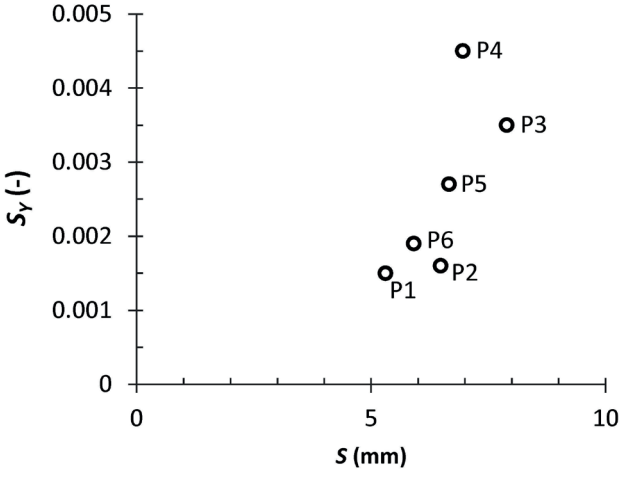

Fig. 10. Specific yield (S_y) versus average storage (S) determined for different hydrological periods (P1–P5) and using envelope line method (P6) at the Levočský potok Brook watershed.

Černák (2016) used 5 different methods to determine S_y for the Odorica Brook watershed (Tab. 7), which creates the SE part of the Levočský potok Brook watershed (Fig. 1). Among an alternative S_y estimates for different considered aquifer thickness (real aquifer thickness cannot be exactly determined in this environment due to its vertical inhomogeneity), the best match with Sy = 0.002 value characterizing entire studied watershed is reached for considered thickness of 100 m, for all used methods.

Size of S_y values estimated by this study for the Levočský potok Brook watershed is also similar to those, evaluated by hydrographs analysis for fractured sedimentary rock aquifers at different sites. For highly fractured zones in shales and interbedded shales, siltstones and sandstones from Pennsylvania, USA, Gburek et al. (1999) compared the recession of borehole hydrographs with the base flow recession curve over a 40-day period for a stream draining the aquifer. Through calibration of a groundwater flow model, S_y was estimated to be 0.01 in the overburden, 0.005 in the highly fractured rocks at shallow depths, and 0.0001 in poorly fractured material below 22-m depth. Gburek and Folmar (1999) used a water-budget method and estimated S_y to range from 0.007 to 0.01 for the highly fractured zone at the same site. Moore (1992) compared stream-flow hydrographs with groundwater hydrographs from shale and limestone aquifers on the Oak Ridge Reservation, Tennessee, USA, and estimated S_y of approximately 0.001 from slopes of the recession curves. Using an approach analogous to hydrograph separation, Shevenell (1996) estimated S_y of 0.003, 0.001 and 0.0001 for conduits, fractures, and matrix elements, respectively, of the limestone and dolomite Knox Aquifer at Oak Ridge, by apportioning segments of borehole recession curves to these different flow regimes.

5. Conclusion

Proposed *Q-S-H* method for S_y estimation at fracture rock watersheds is based on the comparison of different groundwater storage (S) stages in watershed to corresponding groundwater levels. It is based on the premise that a rise in water-table elevation measured in shallow boreholes is caused by the addition of recharge across the water table at watershed and its following recession is caused by groundwater storage loss due to baseflow generation. Another assumption is that deep groundwater discharge – not drained by local streams as baseflow – is as small as can be neglected. Not but what this assumption restrict applicability of the method almost exclusively for bedrock flow systems dominated by shallow fractured rock aquifers, it can be broadly used as they are worldwide abundant. This approach is a gross simplification of many complex phenomena, however it makes the method simply and ease of use. Demonstration of the method at the Levočský potok Brook watershed (Western Carpathians, Slovakia), which is built by fracture porosity dominated Paleogene sediments, suggest that the characteristic S_y value at studied watershed is from the interval 0.001–0.002

and 0.002–0.005 for low and medium storage/runoff conditions (or bottom and middle part of GWL fluctuation zone), respectively. These findings showed consistency of achieved representative estimate with S_y values previously stated by local aquifer tests and also with the range of published S_y values, determined worldwide by other methods for shallow fractured rock aquifers.

The method can be applied for watershed where runoff and GWL fluctuation is observed within the same time period. Whereas runoff daily recorded data are needed for long enough period to construct MRC (usually 2 or more years in moderate climate), GWL fluctuation data can be observed on lower frequency. Even two GWL measurement campaigns could be sufficient, being performed in appropriate time regarding hydrological regime. More than time frequency, number of observed objects and theirs appropriate location are important in case of GWL data.

S_y belongs to very important parameters characterizing hydraulic properties of rocks. Since its knowledge is necessary for non-steady state groundwater flow modeling and groundwater storage balance, correct S_y values lead to better quality of practical hydrogeological issues concerning proper management and protection of valuable groundwater resources. Despite of multitude of known S_y determination methods, there is still lack of characteristic values describing specific rock types in the literature. Another question is quality and reliability of S_y values obtained by different methods and its correlative consistency. Proposed *Q-S-H* method can estimate S_y on local or regional scale (it is average or characteristic value for entire watershed), so it is very useful for studies at such scales. Additionally, it could be valuable to use it in combination in other (laboratory or aquifer pumping test) methods in site scale studies.

Acknowledgment

The results of this study could be obtained thanks to the project support of European Union cohesion funds operational programme Research and Development, namely the project 'Integrated system of outflow processes simulation' (acronym ISSOP; ITMS code: 26220220066), co-financed from the European fund of regional development, what is gratefully acknowledged by the authors.

Authors express their thanks to Daniel Marcin (ŠGÚDŠ) and anonymous reviewer for careful review of the manuscript.

References

Aureli, A., 2002: What's ahead in UNESCO's International Hydrological Programme (IHP VI 2002-2007). *Hydrogeol. J., 10, 349–350, doi: 10.1007/s10040-002-0211-y.*

Bajtoš, P. & Michalko, J., 2003: Pilot hydrodynamic test of HA-1 borehole at the Harichovce site – in-depth hydrogeological survey (in Slovak). *Manuscript. Bratislava, archive St. Geol. Inst. D.* Štúr*, 64 p.*

Bardenhagen, I., 2000: Groundwater reservoir characterization based on pumping test curve diagnosis in fractured formation. In: Sililo, O. (ed.): Groundwater past achievement and future challenges. *Cape Town, South Africa – Balkema – Rotterdam, 81–86.*

Boussinesq, J., 1877: Essai sur la theories des eaux courantes. *Mem. present. div. sav. Acad. Sci. Inst, Nat. France, XXIII, 1.*

Boussinesq, J., 1903: Théorie Analytique de la Chaleur, Vol. II. *Paris, Gauthier-Villars.*

Brutsaert, W. & Lopez, J. P., 1988: Basic-scale geohydrologic drought flow features of riparian aquifers in the southern Great Plains. *Wat. Resour. Res., 34, 233–240.*

Brutsaert, W. & Nieber, J. L., 1977: Regionalized drought flow hydrographs from a mature glaciated plateau. *Wat. Resour. Res., 13, 3, 637–643.*

Černák, R., 2016: Storativity coefficient of flysch sediments and crystalline rock environments in mountain river basins [PhD. Thesis] (in Slovak). *Manuscript. Bratislava, archive Comen. Univ., Fac. Natur. Sci., Depart. Hydrogeol., 115 p.*

Drogue, C., 1967: Essai de détermination des composantes de l'écoulement des sources karstiques. Evaluation de la capacité de rétention par chenaux et fissures. *Chron. Hydrogeol., 10, Bureau Rech. Géol. Miniér., Paris, 43–47.*

Drogue, C., 1972: Analyse statistique des hydrogrammes de decrues des sources karstiques. *J. Hydrol., 15, 49–68.*

Espinha Marques, J., Marques, J., Chaminé, H. I., Carreira, P. M., Fonseca, P. E., Monteiro Santos, F. A., Moura, R., Samper, J., Pisani, B., Teixeira, J., Martins Carvalho, J., Rocha, F. & Borges, F. S., 2013: Conceptualising a mountain hydrogeologic system by using an integrated groundwater assessment (Serra de Estrela, Central Porugal): a review. *Geosci. J., 17,3, 371–386, doi: 10.1007/s12303-013-0019-x.*

Fukushima, I., 1988: A model of river flow forecasting for a small forested mountain catchment. *Hydrol. Process., 2, 167–185.*

Gerhart, J. M., 1986: Groundwater recharge and its effect on nitrate concentrations beneath a manured field site in Pennsylvania. *Groundwat., 24, 483–489.*

Gburek, W. J. & Folmar, G. J., 1999: A groundwater recharge field study site characterization and initial results. *Hydrol. Process., 13, 2813–2831.*

Gburek, W. J., Folmar, G. J. & Urban, J. B., 1999: Field data and groundwater modeling in a layered fractured aquifer. *Groundwat., 37, 175–184.*

Gregor, M. & Malík, P., 2012a: RC 4.0. User's manual. HydroOffice – Software for Water Science. www.hydrooffice.com.

Gregor, M. & Malík, P., 2012b: Construction of master recession curve using genetic algorithms. *J. Hydrol. Hydromech., 60, 1, 3–15, Doi: 10.2478/v10098-012-0001-8.*

Hall, D. W. & Risser, D. W., 1993: Effects of agricultural nutrient management on nitrogen fate and transport in Lancaster county, Pennsylvania. *Water Res. Bull., 29, 55–76.*

Harter, T., 2019: GW-1086 Specific Yield Storage Equation. *Wiley Encyclopedia of Water.* https://onlinelibrary.wiley.com/doi/book/10.1002/047147844X.

Healy, R. W. & Cook, P. G., 2002: Using groundwater levels to estimate recharge. *Hydrogeol. J., 10, 91–109.*

Holko, L., Herrmann, A., Uhlenbrook, S., Pfister, L. & Querner, E. P., 2002: Groundwater runoff separation – test of applicability of a simple separation method under varying natural conditions. In: FRIEND 2002 – Regional Hydrology: Bridging the Gap between Research and Practise (Proceedings of the Fourth International FRIEND Conference held at Cape Town, South Africa, March 2002). *IAHS Publ., 274, 265–272.*

Hynek, J., 2008: Genetické algoritmy a genetické programování (Genetic algorithms and genetic programming). *Praha, Grada Publ., 200 p. ISBN 978-80-247-2695-3.*

Jetel, J., 2000: New knowledge on hydrogeology of Cenozoic rocks in the Eastern Slovakia. *Miner. Slov., 32, 309–310.*

Kliner, K. & Kněžek, M., 1974: Metoda separace podzemního odtoku při využití pozorování hladiny podzemní vody (The underground runoff separation method making use of the observation of groundwater table). *J. Hydrol. Hydromech., XXII, 5, 457–466.*

Lamb, B. R. & Beven, K., 1997: Using interactive recession curve analysis to specify a general catchment storage model. *Hydrol. Earth Syst. Sci., 1, 1, 101–113.*

Maillet, E., 1905: Essai d'Hydraulique Souterraine et Fluviale. *Paris, Librairie Scientifique A. Hermann.*

Malík, P., Bačová, N., Hronček, S., Ivanič, B., Kočický, D., Maglay, J., Ondrášik, M., Šefčík, P., Černák, R., Švasta, J. & Lexa, J., 2007: Zostavovanie geologických máp v mierke 1 : 50 000 pre potreby integrovaného manažmentu krajiny (Composition of geological maps at a scale of 1 : 50 000 for the landscape management needs, in Slovak). *Manuscript. Bratislava, archive St. Geol. Inst. D.* Štúr *(No. 88158), 554 p.*

Malík, P., Švasta, J. & Bottlik, F., 2016: Hydrogeological boreholes and boreholes database and its use on regional rock permeability determination. *Slovak Geol. Mag., 16, 1, 67–93.*

Mello, J., Filo, I., Havrila, M., Ivanička, J., Madarás, J., Németh, Z., Polák, M., Pristaš, J., Vozár, J., Koša, E. & Jacko ml., S., 2000: Geological map of the Slovenský raj, Galmus Mts. and Hornád depression 1 : 50 000. *Bratislava, St. Geol. Inst. D.* Štúr.

Meinzer, O. E., 1923: The occurrence of groundwater in the United States with a discussion of principles. *US Geol. Surv. Water-Supp. Pap., 489, 321 pp.*

Mendoza, G. F., Steenhuis, T. S., Walter, M. T. & Parlange, J. Y., 2003: Estimating basin-wide hydraulic parameters of a semi-arid mountainous watershed by recession-flow analysis. *J. Hydrol., 279, 57–69, doi: 10.1016/S0022-169 4(03)00174-4.*

Mijatovič, B., 1972: Podzemna kraška akumulacija Poličnik kao najracionalniji način rešenja problema vodosnabdevanja Zadra i okoline (Karstic aquifer Poličnik as the most rational water supply solution in Zadra surroundings). *Zbor. Rad. Geol. Fak. (Beograd), 16, 97–128.*

Moore, G. K., 1992: Hydrograph analysis in a fractured rock terrane. *Groundwater, 30, 390–395.*

Moore, R. D., 1997: Storage-outflow modeling of streamflow recessions, with application to a shallow soil forested catchment. J. Hydrol., 198, 260–270.

Parlange, J. Y., Parlange, M. B., Steenhuis, T. S., Hogarth, W. L., Barry, D. A., Li, L., Stagnitti, F., Heilig, A. & Szilagyi, J., 2001: Sudden drawdown and drainage of a horizontal aquifer. *Water Resour. Res., 37, 2097–2101.*

Posavec, K., Bačani, A. & Nakič, Z., 2006: A visual basic spreadsheet macro for recession curve analysis. *Ground-Wat., 44, 5, 764–767.*

Querner, E. P., 1997: Description and application of the combined surface and groundwater flow model MOGROW. *J. Hydrol., 192, 158–188.*

Roche, M., 1963 : Hydrologie de Surface. *Paris, Gauthier – Villars Édit.*

Rasmussen, W. C. & Andreasen, G. E., 1959: Hydrologic budget of the Beaverdan Creek Basin, Maryland. *US Geol. Surv. Water-Supp. Pap, 1 472, 106 p.*

Rutledge, A. T., 1998: Computer Programs for Describing the Recession of Ground-Water discharge and for Estimating Mean Ground-Water Recharge and Discharge from Streamflow Records – Update. *U.S. Geol. Surv., Water-Res. Investig. Report 98-4148, 43 p.*

Schicht, R. J. & Walton, W. C., 1961 : Hydrologic budgets for three small watersheds in Illinois. Illinois State Water Survey report. *Survey Report of Investigation, 40.*

Schwarze, R., Dröge, W. & Opherden, K., 1997: Regional analysis and modelling of groundwater runoff components from small catchments in solid rock areas. *Landschaftsökol. Umweltforsch., 25, 59–62.*

Schoeller, H., 1962: Les Eaux Souterraines. *Paris, Masson* Édit.

Shevenell, L., 1996: Analysis of borehole hydrographs in a karst aquifer: estimates of specific yields and continuum transmissivities. *J. Hydrol., 174, 331–335.*

Šály, R. & Šurina, B., 2002: Soils. In: Landscape Atlas of the Slovak Republic. 1st ed. *Bratislava, Ministry Environ. Slovak Republic; Banská Bystrica, Slovak Environ. Agency, 344 p.*

Varni, M., Cornas, R., Weinzettel, P. & Dietrich, S., 2013: Application of water table fluctuation method to characterize groundwater recharge in the Pampa plain, Argentina. *Hydrol. Sci. J., 58, 7, 1446–1455.*

Viviroli, D. & Weingartner, R., 2004: "Water towers": a global view of the hydrological importance of mountains. In: Wiegandt, E. (ed.): Mountains: Sources of Water, Sources of Knowledge. *Adv. Glob. Change Res., 31, 15–20.*

Walton, W. C., 1970: Groundwater resources evaluation. *New York, McGraw – Hill, 664 p.*

Welch, L. A. & Allen, D. M., 2014: Hydraulic conductivity characteristics in mountains and implications for conceptualizing bedrock groundwater flow. *Hydrogeol. J., 22, 1003–1026. DOI 10.1007/s10040-014-1121-5.*

Werner, P. W. & Sundquist, K. J., 1951: On the groundwater recession curve for large watersheds. IAHS General Assembly. *Brusel, IAHS publ., 33, 202–212.*

Wittenberg, H., 1999: Baseflow recession and recharge as nonlinear storage processes. *Hydrol. Process., 13, 715–736.*

Wittenberg, H. & Sivapalan, M., 1999: Watershed groundwater balance estimation using streamflow recession analysis and baseflow separation. *J. Hydrol., 219, 20–33.*

Ye, S., Li, H. Y., Huang, M., Ali, M., Leng, G., Leung, L. R., Wang, S. & Sivapalan, M., 2014: Regionalization of subsurface stormflow parameters of hydrologic models: Derivation from regional analysis of streamflow recession curves. *J. Hydrol., 519, 670–682.*

Map server of the State Geological Institute of Dionýz Štúr, 2016: Digital geological map at a scale of 1 : 50 000. [Online]. Available from: http://apl.geology.sk/gm50js [Accesed on 29 January 2016].

Odhad vododajnosti pripovrchovej zóny skalných hornín v horských povodiach skúmaním vzťahu medzi základným odtokom, zásobou a úrovňou hladiny podzemnej vody

Vododajnosť (S_y) – schopnosť horniny nasýtenej vodou uvoľňovať ju voľným vytekaním pod vplyvom gravitácie – je dôležitý hydraulický parameter potrebný pri hodnotení a využívaní zdrojov podzemnej vody. Je aj kľúčovým parametrom pri odhade infiltrácie zo zrážok metódou WTF (Schicht a Walton, 1961). Na stanovenie vododajnosti sa používa viacero metód, či už terénnych alebo laboratórnych. Ich výsledkom sú však značne variabilné hodnoty S_y (Varni et al., 2013) a presnosť týchto metód sa hodnotí ťažko. Preto je veľmi prospešné aplikovať viacero metód stanovenia vododajnosti a sledovať konzistenciu dosiahnutých výsledkov.

Na regionálny odhad vododajnosti horninového prostredia v horských povodiach so zanedbateľným prestupom podzemnej vody do susedných povodí sa navrhuje aplikovať metódu založenú na kombinácii analýz výtokovej krivky povrchového odtoku, vzťahu zásoby vody v povodí k veľkosti podzemného odtoku a kolísania hladiny podzemnej vody (metóda *Q-S-H*). Za predpokladu, že pokles zásoby podzemnej vody odráža pokles základného odtoku v povodí podľa rovnice 4, reprezentatívna výtoková krivka (MRC; obr. 4) odtoku z povodia skonštruovaná z čiary prietoku z dostatočne dlhého obdobia môže byť využitá na určenie zmeny zásoby vody v povodí ΔS (obr. 5) zodpovedajúcej zmene úrovne hladiny podzemnej vody v povodí ΔH. Keďže hodnota ΔS zodpovedá množstvu odtečenej vody z povodia, môže sa určiť aj priamo z reálnej výtokovej čiary zaznamenanej vo zvolenom období neovplyvnenom rušivými vplyvmi ako súčet denných odtečených množstiev vo zvolenom časovom úseku. Priemerná vododajnosť v zóne kolísania hladiny podzemnej vody je potom daná vzťahom $S_y = \Delta S/\Delta H$.

Použitie metódy *Q-S-H* je demonštrované na povodí Levočského potoka, budovaného paleogénnymi sedimentmi s dominujúcou puklinovou priepustnosťou (obr. 1). Využili sa záznamy prietoku Levočského potoka zo stanice SHMÚ č. 8 424 v Markušovciach z rokov 1990 – 2012 a merania kolísania hladiny podzemnej vody v 6 vrtoch v hydrologickom roku 1995 (tab. 1). Na základe interpretácie zaznamenaných hodnôt prietoku bola skonštruovaná reprezentatívna výtoková krivka (MRC; obr. 4). Použila sa na kalibráciu nelineárnej modelovej krivky pri kalibračnom parametri získanom testovaním – koeficiente vyprázdňovania a = 15,5 (pri zvolenej hodnote parametra b = 0,5 reprezentujúcej nelineárny rezervoár). Jeho dosadením do rovnice 4 bol definovaný vzťah medzi zásobou podzemnej vody v študovanom povodí a jeho podzemným odtokom, vyjadrený rovnicou $S = 15{,}5Q^{0{,}5}$. To umožnilo simulovať zásobu podzemnej vody v povodí (S) pri rôznych úrovniach podzemného odtoku (Q) a korešpondujúcich úrovniach hladiny podzemnej vody (H). Prezentované sú dva odlišné spôsoby odhadu S_y: 1. porovnaním dvoch hydrologických stavov zvolených na hydrograme (obr. 6), 2. porovnaním dvoch hydrologických stavov zvolených na grafe *Q-H* s využitím metódy obalovej čiary (Kliner a Kněžek, 1974) (obr. 7). Na základe získaných časovo relevantných párov hodnôt S a H je hodnota S_y vypočítaná podľa rovnice 6. Prezentované dva prístupy dávajú porovnateľné výsledky. Použitie prvého z nich poskytuje možnosť výberu preferovaného hydrologického stavu v rámci sezónneho režimu, je však potrebné zvažovať rušivé vplyvy. Druhý z nich umožňuje konzervatívny odhad, keďže obalová čiara reprezentuje minimálny základný odtok pri určitej úrovni hladiny podzemnej vody.

Hodnoty S_y charakteristické pre pripovrchovú zónu hydrogeologického masívu v tomto povodí sú uvedeným postupom odhadnuté v intervale 0,001 – 0,002 pri nízkom základnom odtoku a v intervale 0,002 – 0,005 pri strednom základnom odtoku. Tieto hodnoty sú konzistentné s hodnotami koeficientu voľnej zásobnosti, zistenými v tomto povodí hydrodynamickými skúškami vrtov. Sú tiež v rozsahu hodnôt *Sy* určených inými terénnymi metódami v prostredí hydrogeologického masívu (Gburek, 1999; Gburek a Folmar, 1999; Moore, 1992; Shevenell, 1996). Pre potreby tejto štúdie bolo k dispozícii 6 vrtov s pozorovaním úrovne hladiny podzemnej vody (tab. 1). Len 4 z nich však bolo vhodné zaradiť do hodnotenia, a to

kvôli vylúčeniu vplyvu drenážneho účinku miestnej eróznej bázy. Hodnoty ΔH za hydrologický rok 1995 v nich dosahovali 1,04 – 6,17 m s priemerom 2,67 m. Porovnanie týchto hodnôt s hodnotami ΔH zaznamenanými v 11 vrtoch situovaných v paleogénnych sedimentoch na území Slovenska, ktoré pozoruje SHMÚ v rámci štátneho monitoringu podzemnej vody (0,72 – 4,28 m a priemer 1,83 m; tab. 6), ukazuje ich značnú podobnosť. Toto porovnanie naznačuje, že rozdiel priemernej hodnoty ΔH použitej na odhad Sy oproti reálnej hodnote by nemal byť väčší ako 1 m. Podhodnotenie použitej vstupnej hodnoty ΔH je pritom pravdepodobnejšie ako jej nadhodnotenie.

Použitie tejto metódy je limitované na povodia, v ktorých hlbší podzemný odtok do susedných povodí je taký nízky, že ho možno zanedbať. Ide najmä o povodia budované hydrogeologickým masívom – komplexmi spevnených hornín s puklinovou priepustnosťou bez významnejších súvislých vrstvových kolektorov, s obehom podzemnej vody sústredeným do pripovrchovej zóny, prípadne uzavreté hydrogeologické štruktúry. Údajová báza na použitie tejto metódy pozostáva z čiary prietokov toku zo záverečného profilu hodnoteného povodia a časovo korešpondujúcich údajov o kolísaní hladiny podzemnej vody v pozorovacích objektoch situovaných v tomto povodí. Na konštrukciu reprezentatívnej výtokovej krivky (MRC) sú potrebné denné záznamy prietoku z dostatočne dlhého obdobia (zvyčajne 2 roky a viac). Frekvencia meraní úrovne hladiny môže byť nižšia – pri vhodnom načasovaní vzhľadom na hydrologický režim postačuje niekoľko opakovaní merania. Najdôležitejší je počet vhodne situovaných pozorovacích objektov. Hoci tento prístup predpokladá značné zjednodušenie zložitých prírodných procesov prebiehajúcich pri tvorbe podzemného odtoku, je výhodný z hľadiska možnosti získania potrebných podkladových údajov a nenáročnosti ich vyhodnotenia.

Vododajnosť patrí k dôležitým parametrom charakterizujúcim hydraulické vlastnosti hornín. Keďže predstavuje vstupný parameter pri modelovaní neustáleného prúdenia podzemnej vody, korektné hodnoty S_y sú potrebné na kvalitné riešenia praktických hydrogeologických úloh týkajúcich sa správneho manažovania a ochrany zdrojov podzemnej vody. Napriek početným známym metódam ich určovania v odbornej literatúre pretrváva nedostatok dostupných charakteristických hodnôt S_y reprezentujúcich špecifické horninové typy. Kvalita a spoľahlivosť dostupných hodnôt S_y a ich konzistentnosť pri ich získavaní rôznymi metódami sú predmetom diskusií. Preto je potrebné rozširovať existujúcu údajovú bázu a testovať spoľahlivosť použitých metód. Navrhovanou metódou *Q-S-H* možno odhadovať S_y v lokálnej alebo regionálnej mierke ako hodnotu priemernú, resp. charakteristickú pre študované povodie. Pri regionálnych štúdiách a lokálnych prieskumoch je vhodné kombinovať ju s inými dostupnými metódami, najmä hydrodynamickými a laboratórnymi skúškami.

Doručené / Received: 27. 5. 2023
Prijaté na publikovanie / Accepted: 30. 6. 2023

Inštrukcie autorom

Etika publikovania, záväzná pri publikovaní v časopise Mineralia Slovaca: *www.geology.sk/mineralia položka* ***Publikačná etika***

1. Geovedný časopis Mineralia Slovaca publikuje scientometricky hodnotné recenzované pôvodné vedecké články s vysokým citačným potenciálom. V úvode príspevku musí autor jasne deklarovať, čím konkrétnym je jeho príspevok prínosný pre rozvoj geovied. Rešeršné štúdie sa publikujú len ojedinele.

2. Články na publikovanie (manuskripty) sa do redakcie zasielajú poštou (dva vytlačené exemplára a CD so všetkými súbormi v editovateľnej podobe) alebo e-mailom (editovateľné súbory a kompletná verzia vo formáte PDF).

3. Súčasne s článkom je potrebné redakcii poslať autorské vyhlásenie o originalite textu a obrázkov. Kópie obrázkov z iných publikácií musia byť legalizované získaním práva na publikovanie. Vyhlásenie musí obsahovať meno autora (autorov), akademický titul a trvalé bydlisko.

4. Rozsah manuskriptu na publikovanie je najviac 25 rukopisných strán (MS Word, Times New Roman, veľkosť písmen 12 bodov, riadkovanie 1,5) vrátane literatúry, obrázkov a vysvetliviek. V prípade veľkého odborného prínosu sú v ojedinelých prípadoch povolené aj dlhšie články.

5. Články sú publikované v angličtine so slovenským resumé v závere článku (za zoznamom citovanej literatúry).

Text

1. Abstrakt stručne sumarizuje článok. Môže mať najviac 200 slov a nemá obsahovať citácie. Počet kľúčových slov je maximálne 6. Text má mať úvod, charakteristiku (stav) skúmaného problému, použitú metodiku, nové zistenia, ich interpretáciu, diskusiu, záver a zoznam literatúry. Východiskové údaje musia byť zreteľne odlíšené od interpretácií. V texte musia byť odvolávky na všetky použité obrázky a tabuľky.

2. Hierarchiu nadpisov v texte je potrebné vyznačiť ceruzkou na ľavom okraji strany manuskriptu: 1 – najvyššia, 2 – nižšia, 3 – najnižšia.

3. V texte sa uprednostňuje citácia v zátvorke, napr. (Dubčák, 1987; Hrubý et al., 1988), pred formou ... podľa Dubčáka (1987).

4. Pozícia obrázkov a tabuliek v texte sa označí. Nie je vhodné, aby text v editore MS Word obsahoval vložené obrázky, ale náhľadová verzia v pdf ich má obsahovať.

5. Grécke písmená treba identifikovať na ľavom okraji slovom (napr. sigma). Potrebné je odlišovať pomlčku od spojovníka. Symboly, matematické značky, názvy skamenelín a pod., ktoré sa majú vysádzať kurzívou, autor v rukopise podčiarkne vlnovkou.

Obrázky a tabuľky

1. Ilustrácie a tabuľky vysokej kvality bývajú publikované buď **na šírku stĺpca (81 mm), alebo strany (170 mm).** Optimálna veľkosť písma a čísiel v publikovaných obrázkoch je 2 mm. Všetky texty v obrázkoch a tabuľkách, rovnako ako popisy k nim musia byť v angličtine. **Maximálny rozmer ilustrácie a tabuľky vytlačený v časopise je 170 x 230 mm.** Väčšie (skladané) ilustrácie sú publikované len v ojedinelých prípadoch.

2. Pri počítačovej tvorbe obrázkov odporúčame používať programy s vektorovým zobrazením (Corel Draw, Adobe Illustrator a pod.). Čiary tzv. vlasovej hrúbky, softvérová alebo rastrová výplň plôch (napr. v Corel Draw) nie sú prípustné. Výplne v obrázkoch musia pozostávať zo samostatne vysádzaných objektov.

3. Ilustrácie vrátane fotografií musia obsahovať **grafickú mierku** v centimetrovej či metrovej škále, prípadne sa rozmer zobrazených objektov vyjadrí v popise obrázka. Mapy a profily musia mať aj **azimutálnu orientáciu** a jednotné vysvetlivky, ktoré sa uvedú pri prvom obrázku. Zoskupené obrázky, napr. fotografie a diagramy, sa uvádzajú ako jeden obrázok s jednotlivými časťami označenými písmenami (a, b, c atď.).

4. Pri zasielaní fotografií vo forme počítačových súborov (formáty JPG alebo TIF) sa požaduje rozlíšenie minimálne 600 DPI. Publikovanie farebných ilustrácií môže byť spoplatnené.

Literatúra

1. Minimálne 50 % citácií musí reprezentovať publikácie od roku 2000. V zozname literatúry sa v abecednom poradí uvádza len literatúra citovaná v danom článku.

2. Spôsob uvádzania literatúry v zozname literatúry

Knižná publikácia: Gazda, L. & Čech, M., 1988: Paleozoikum medzevského príkrovu. *Bratislava, Alfa, 155 s.*

Článok v časopise: Vrba, P., 1989: Strižné zóny v metapelitoch. *Miner. Slov., 21, 135 – 142.*

Zborník: Návesný, D., 1987: Vysokodraselné ryolity. *In: Romanov, V. (ed.): Stratiformné ložiská gemerika. Špec. publ. Košice, Slov. geol. spol., 203 – 215.*

Manuskript: Radvanský, F., Slivka, B., Viktor, J. & Srnka, T., 1985: Žilné ložiská jedľoveckého príkrovu gemerika. Záverečná správa z úlohy SGR-geofyzika. *Manuskript. Spišská Nová Ves, archív Št. Geol. Úst. D. Štúra, 28 s.*

3. Pri článku viac ako dvoch autorov sa v texte cituje iba prvý autor s dodatkom et al., ale v zozname literatúry sa uvádzajú všetci.

Instructions to authors

Publication ethics, being obligatory for publishing in the journal Mineralia Slovaca: *www.geology.sk/mineralia item* ***Publication ethics***

1. Geoscientific journal Mineralia Slovaca publishes scientometrically valuable original peer-reviewed scientific articles with a high citation potential. In the introduction of each article the author(s) must clearly declare, which innovative data the paper brings for the development of geosciences. The retrieval studies are published only exceptionally.

2. The articles for publishing (manuscripts) must be sent to Editorial Office by post (two printed copies and CD with editable files), or by e-mail (editable files plus complete preview version in PDF format).

3. Simultaneously with the article the Editorial Office must receive the author´s proclamation that no part of the manuscript was already published and figures and tables are original as well. Copied illustrations from other publications must contain a copyright.

4. The extent of the manuscript for publishing is limited to 25 manuscript pages (MS Word, 12 points Times New Roman, line spacing 1.5) including figures, tables, explanations and references. In the case of contribution with a high scientific value, the longer manuscripts for publishing are exceptionally permitted.

5. Articles are published in English, with Slovak summary at their end. In a case of foreign authors not able to submit the article summary in Slovak, the Editorial Office translates their English summary to Slovak version.

Text

1. Abstract briefly summarizing the article is limited to 200 words, no references are allowed. The maximum number of key words is 6. Text of the article has to contain the introduction, characterization (state) of investigated problem, applied methodology, presented new data, discussion, conclusion and references. The obtained data must be distinctly separated from interpretations. All applied figures and tables must be referred in the text.

2. The hierarchy of headings in the manuscript must be clearly indicated.

3. The references in the text prefer parentheses, e.g. (Dubčák, 1987; Hrubý et al., 1988). The form "according to Dubčák (1987)" should be used only exceptionally.

4. Position of figures and tables must be indicated in the manuscript. Editable text of manuscript sent to editorial office must be without figures and tables, though the preview PDF has to contain them in a correct position.

5. Greek letter in the text must be identified at the left margin of the text (e.g. sigma). The text should strictly distinguish the dash from hyphen. Symbols, mathematic signs, names of fossils, etc., which should be printed in italics, must be underlined in the manuscript.

Figures and tables

1. The high quality figures and tables can be published either in **maximum width of column (81 mm) or page (170 mm).** The optimum size of letters and numbers in the camera-ready figure is 2 mm. All texts in figures and tables, as well as descriptions and notes to figures and tables must be in English. **Maximum dimension of figures and tables in the journal is 170 x 230 mm. Larger (fanfolded)** illustrations are published only exceptionally.

2. For figures drawing the editorial office recommends the vector graphics editors (Corel Draw, Adobe Illustrator, etc.). The very thin lines (hair lines), the pre-defined software or raster fillings of polygons (e.g. in Corel Draw) are not allowed. The filling must consist from separately set objects.

3. Each illustration including photographs must contain graphic (metric) scale, eventually the dimensions of visualized objects have to be stated in the describing text to figure. Maps and profiles must contain also the azimuth orientation, their detail explanations are stated at the first figure. Grouped figures, e.g. photographs and diagrams, are compiled as one figure with separate parts designated by letters (a, b, c, etc.).

4. The photographs sent as JPG of TIF files are required for having minimum 600 DPI resolution. Publishing of colour illustrations can be charged by a fee.

References

1. Minimum 50 % of referred works must represent contemporary publications after 2000. The references in alphanumeric order encompass only literature cited in the article.

2. Examples of referring:

Book: Gazda, L. & Čech, M., 1988: Paleozoic of the Medzev nappe. *Bratislava, Alfa, 155 p.*

Article in journal: Vrba, P., 1989: Shear zones in the metapelite complexes. *Miner. Slov., 21, 135–142.*

Anniversary volume: Návesný, D., 1987: High-potassium rhyolites. *In: Romanov, V. (ed.): Stratiform deposits of Gemericum. Spec. publ. Košice, Slov. geol. soc., 203–215.*

Manuscript: Radvanský, F., Slivka, B., Viktor, J. & Srnka, T., 1985: Vein deposits of the Jedľovec nappe of Gemericum. Final report from the project SGR-geophysics. *Manuscript. Spišská Nová Ves, Archive Št. Geol. Úst. D. Štúra, 28 p.*

3. The article with more than two authors is referred by the name of the first author with the amendment et al., but the list of references contains names of all authors.

Ďalšie informácie / Further information: mineralia.slovaca@geology.sk; zoltan.nemeth@geology.sk

OBSAH – CONTENT

PÔVODNÉ ČLÁNKY – ORIGINAL PAPERS

Indexed / Abstracted / Accessed by SCOPUS, WEB OF SCIENCE and EBSCO
Indexované / abstraktované / sprístupňované databázami SCOPUS, WEB OF SCIENCE a EBSCO

www.geology.sk/mineralia